Chapter 1

Intermolecular Interactions – The Essence of Crystal Engineering

Chapter 1

1.1 Crystal Engineering: An Outlook

The essential question of crystal engineering is "Given the molecular structure of an organic compound what is its crystal structure?"[1, pp-316] Though, the question looks trivial but is not easy to answer. During the crystallization process, molecules identify each other through intermolecular interactions.[2] Therefore, in-depth conceptualization of the intermolecular interactions and the recognition procedure of molecules is must, to answer the essential question of crystal engineering. Desiraju has defined crystal engineering as "the understanding of intermolecular interactions in the context of crystal packing, and the utilisation of such understanding in the design of new solids with desired physical and chemical properties".[2] In fact, the interest and investigations to find out the reasons for a particular molecular arrangement in the solid state has led to the emergence of this field.[3] New designing strategies are being explored and exploited in this field by studying the different packing modes in various crystal lattices. Then, by using these design principles, new crystals of desirable properties can be constructed.[4] This is because, many physical properties of the molecules like photochemical reactivity, optical and electronic properties, *etc*. depend on their arrangement in the solid state. So, these concepts could be applied for the designing of functional materials.[5]

The perception of crystal engineering has been started since 1921, when Bragg observed the similarities in the crystal structure of naphthalene and anthracene.[6] Robertson in 1951 was perhaps the first person to correlate the molecular structure with its crystal

structure.[7] He divided the structures of hydrocarbons in two parts. The first part of the structures was consisting of those hydrocarbons, whose thickness were comparable to the length and breadth of their molecules, and which were actually found to be the structures having a herringbone arrangement of molecules in their crystal lattices. The second part was consisting of those hydrocarbons, whose thickness were not comparable to the length and breadth of their molecules, which were essentially the structures containing a stacked arrangement of molecules in their crystal lattices.[7] This work was further extended by Gavezzotti and Desiraju in a more quantitative manner in the paper entitled "From molecular to crystal structure; polynuclear aromatic hydrocarbons".[8]

But, the term of crystal engineering was first introduced by Pepinsky[9] in 1955 though Schmidt[10] was the first to bring this concept into practice for studying photochemical reactions in the solid state for the first time in 1973. Later, the groups of Cohen,[11] Herbstein,[12] Lahav[13] and Leiserowitzits[14] made the field glorious in the following years. This field has been expanding for the last 30 years. A couple of books by Desiraju highlighted that the subject of crystal engineering is not just limited to the solid state photochemical reactions, rather goes far beyond that.[15] Its concepts can be applied to any field, that deals with the intermolecular interactions. Such type of fields covers the areas related to protein-ligand interactions, solid state photochemistry, and design of supramolecules, *etc*.[5]

1.1.1 Crystal Engineering and Supramolecular Chemistry

Crystals are being considered as supermolecules. It was first articulated by Jean-Marie Lehn in 1988 that both supramolecules and crystals are formed through molecules that interconnect among themselves through intermolecular interactions.[16] Dunitz[17] in one of his papers in 1991 has also considered crystal as a supramolecular entity. He has described it as "a super-molecule par excellence", an assembly of literally millions of molecules self-crafted by mutual recognition at an "amazing level of precision".[17] According to Desiraju, "construction of a crystal is a type of supramolecular solid state synthesis and crystallization becomes a supramolecular reaction and nucleation becomes its transition state".[3] Thus, the concepts of crystal engineering can be applied in supramolecular synthesis.

These supramolecules are found to consist of supramolecular synthons. The term synthon was first introduced by E. J. Corey in the context of retro synthesis and was defined

as “structural units within molecules which can be formed and/or assembled by known or conceivable synthetic operations”.[18] The definition of synthons given by Corey was quite broad, so this term gets readily adopted in the supramolecular chemistry. The supramolecular synthons are defined as “the structural units within supermolecules which can be formed and/or assembled by known or conceivable synthetic operations involving intermolecular interactions, and crystal engineering are the new organic synthesis”.[4] In organic synthesis, new molecules are designed through breaking and making of covalent bonds; in the similar way in the field of crystal engineering, novel crystal structures can be fashioned by the cleavage and creation of non-covalent interactions.[2,5,15] Thus, the role played by supramolecular synthons in crystal engineering is similar to the role played by conventional synthons in the organic synthesis.[15]

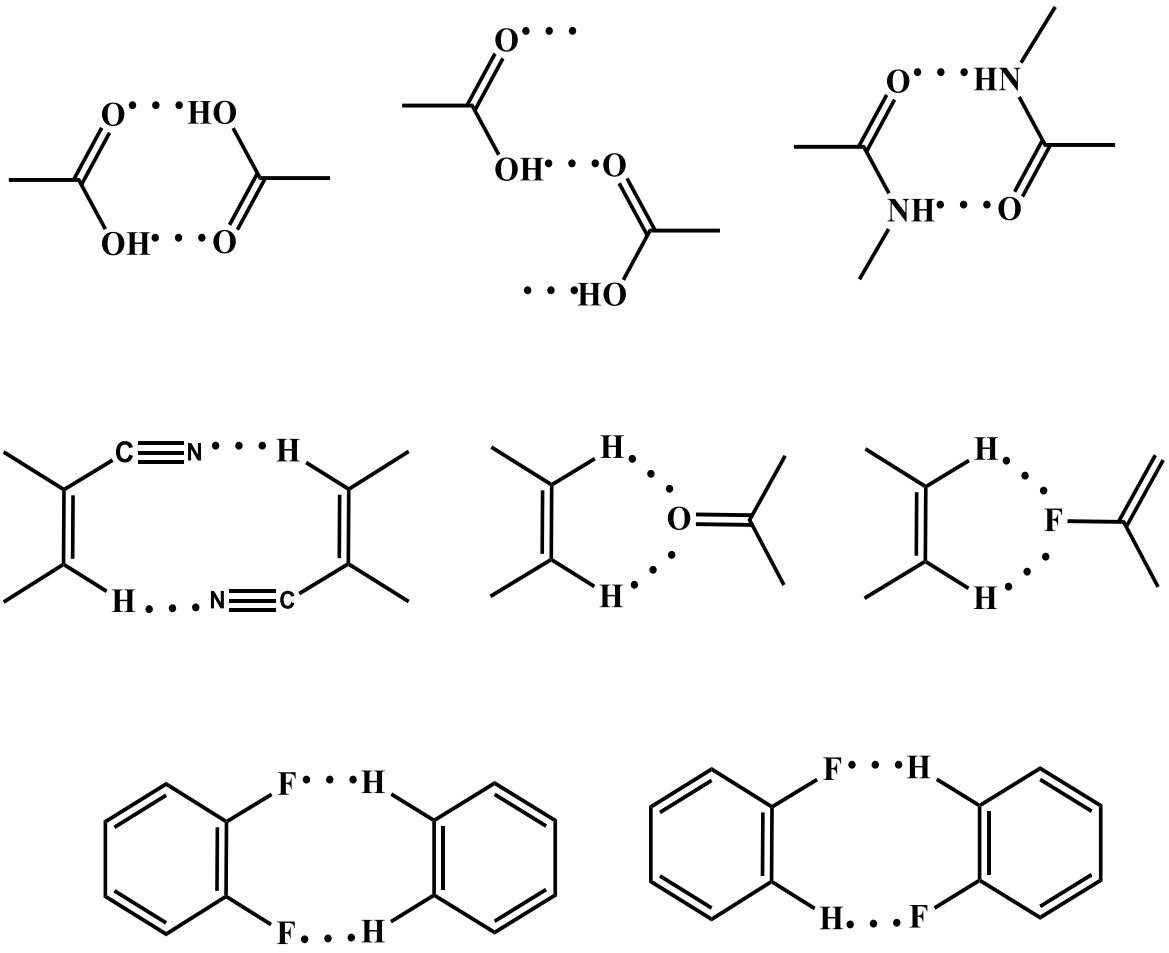

Scheme-1.1

These supramolecular synthons consist of entities, which interact through strong or weak hydrogen bonds. Designing of supramolecules through the recognition potential of molecules *via* strong hydrogen bonds is well known in the literature.[19] Weak hydrogen bonds despite their strength are directional enough to guide the molecules to pack in a definite direction. Based on the in-depth knowledge of the nature, directionality and strength of the intermolecular interactions, different supramolecular synthons have been conceived. Some of the examples of the supramolecular synthons formed through strong and weak hydrogen bonds have been taken from reference no. 3 and are given in the scheme 1.1.

For the aromatic molecules containing strong hydrogen bonding sites, the arrangement of molecules in two dimensions is easily predictable. But, the translation of molecules in the 3rd dimension is governed by other weaker interactions, and the control over those interactions is of paramount interest. Over and above, if a molecule does not have a strong hydrogen bonding site; it becomes more difficult to predict its structure even in one direction out of three-dimensional arrangements of molecules in the crystal lattice.[1] Thus, a lot more is there to explore about intermolecular interactions, which governs the crystallization and hence about crystal engineering as pointed out by Desiraju in one of his recent articles.[2]

1.2 Intermolecular Interactions in Crystal Engineering

The purpose of crystal engineering is to utilize the perception of intermolecular interactions to control the aggregation of molecules. The interactions regulate the assembly of organic molecules in the crystal lattice by providing high directional preferences to them, and these typically include hydrogen bonding interactions (strong or weak).[1] There exist some other types of interactions other than the hydrogen bonds, through which molecular recognition can also occur because of their directional characteristics, which involves halogens bonds[20] and also some other weak intermolecular interactions comprising of π–acceptors.[21] All these interactions are composite of electrostatic, polarization, charge transfer, dispersive and repulsive components with varying composition of each in different types of interactions.[22] These interactions are briefly discussed here.

1.2.1 The Hydrogen Bond: An Overview

The concept of hydrogen bonding was first initiated by Linus Pauling.[23] Out of several definitions[24], the most widely accepted definition of hydrogen bond by Pauling[25] is

"A hydrogen bond is an interaction that dictates association of a covalently bound hydrogen atom with one or more atoms, groups of atoms or molecules into an aggregate structure that is sufficiently stable to make it convenient for the chemist to consider it as an independent chemical species."

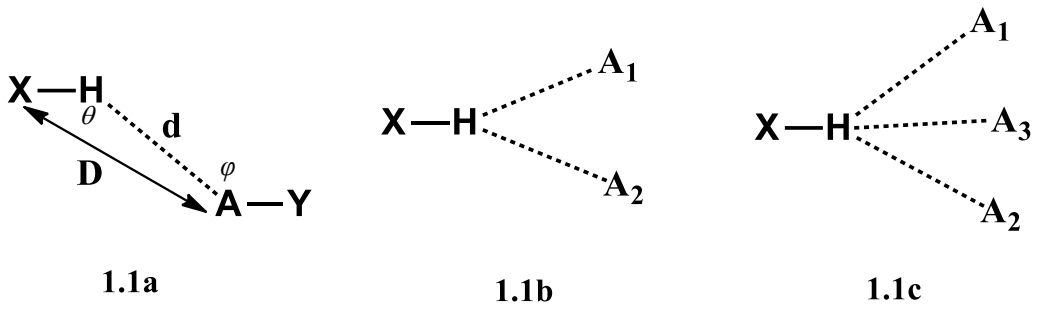

Figure 1.1: (a) Hydrogen bond with one acceptor. **(b)** Bifurcated hydrogen bond with two acceptors. **(c)** Trifurcated hydrogen bond with three acceptors.

In a hydrogen bond, the group X–H is called the hydrogen bond donor, and A is an acceptor atom. The parameters *D*, *d*, and θ determine the geometry of a hydrogen bond (figure 1.1). Earlier, when hydrogen atom position was not possible to locate by X-ray data, the parameter 'D' used to be emphasized. But, these days parameter *d* is more looked upon than *D*. The hydrogen bonds can be of the type of two, three or four center hydrogen bonds[26] as shown in figure 1.1. These are also called bifurcated and trifurcated hydrogen bonds. This bifurcation or trifurcation can be possible at the both acceptor and donor sites.

Pimentel and McClellan[27] have given another definition of the hydrogen bond, which does not put any restriction on the nature of the donor and acceptor groups. The definition is

"A hydrogen bond is said to exist when (1) there is evidence of a bond, and (2) there is evidence that this bond sterically involves a hydrogen atom already bonded to another atom."

A drawback of this definition was that it also involves van der Waals' contact in it, which is also a bond and may involve hydrogen in it.[28] Steiner and Saenger[29] gave another

definition in 1993 as a refinement of the above definition as "Any cohesive interaction where H carries a positive charge and A, a negative charge (partial or full) and the charge on H is more positive than on X".

The modern definition of the hydrogen bond[30] states that it is "an attractive interaction between a hydrogen atom from a molecule or a molecular fragment X–H in which X is more electronegative than H, and an atom or group of atoms in the same or different molecule, in which there is evidence of bond formation". This definition does not put any restriction on the nature of atoms involved, their strength and also on the indications of hydrogen bond formation. Thus, this definition becomes very broad, and it encompasses different kinds of hydrogen bonds within its limits.

Hydrogen bond can be categorized in different ways. But, from the point of view of crystal engineering these could be of the type of very strong, strong and weak hydrogen bonds. The table 1.5 reported in the book by Desiraju[1,pp 13] gives a condensed summary of the properties of different kinds of hydrogen bonds. Irrespective of the existence of any sharp boundaries between them, a general idea about these interactions can be drawn from that table.

1.2.1.1 Hydrogen Bond in Crystal Engineering

Designing of a self-assembled structure based on strong hydrogen bonds (O–H···O, N–H···O, N–H···N, O–H···N) is well known in the literature because of its highly directional characteristics and strength, which make them easily predictable.[19] These types of hydrogen bonds are considered "firm" because of their higher stabilization energies (4-15 kcal/mol). Different supramolecular synthons have been designed based on the strength and directionality of the strong hydrogen bonds.[31] Engineering of co-crystals based on the strong hydrogen bonds is clear indications of their utilization in crystal engineering.[32]

But, still tailoring of molecules in the crystals lattice through weak hydrogen bonds is non-trivial. This is because the molecules containing weak hydrogen bond donor and acceptors groups need not to associate in a particular fashion. The stabilization energy of weak hydrogen bond is generally < 4 kcal/mol. These bonds are electrostatic in nature and also directional to some extent. But because of their lower strength, their directionality can easily be altered by the presence of other interactions in the crystal lattice. Though the arguments for considering feeble hydrogen-bonded interactions may seem irrational, but there is an important aspect to reminisce that the cumulative contribution of a large number

of weak interactions in a crystalline solid cannot be ignored though the individual contribution of such interaction will be just a small amount of the stabilization energy. Thus, their broader influence on structures can be conceived. Therefore, lots of studies are being reported in the literature to explore more about their utilization in the field of crystal engineering, a brief description of which will be given subsequently. These can be categorized as the following:[33]

1. *Weak donor-strong acceptors* C–H···O, P–H···O, C–H···N
2. *Strong donor- weak acceptors* O–H···F–C, N–H···F–C, O–H···π, N–H···π
3. *Weak donor- weak acceptors* C–H···F–C, C–H···Cl–C

The C–H···O interactions were first recognized by Glasstone[34] in 1937 while studying the reasons for unusual physical properties of the mixture of haloforms with acetone. This uncommon behaviour of haloforms with acetone was explained by the directional electrostatic interactions of the type shown in figure 1.2.

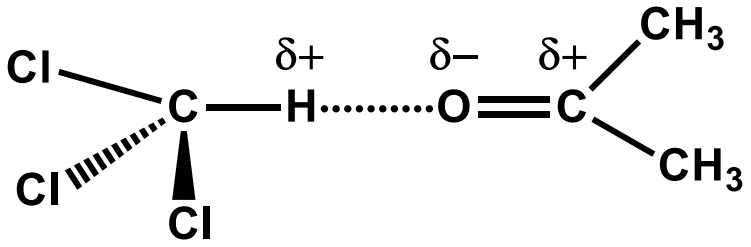

Figure 1.2: C–H···O interactions described by Glasstone. This figure has been re-drawn based on the figure from pp-30 of reference no. 1.

Then, Gordy[35] in 1939 termed these interactions as hydrogen bonds based on his IR experiments. He found that C–H stretching frequencies undergo bathochromic shifts in the presence of electronegative atoms, which is the indication of the formation of a hydrogen bond. He had also explained that the capability of a C–H group to donate its proton for the H-bond formation depends on the number of electron withdrawing groups attached to it as well as the carbon hybridization, C(*sp*)–H > C(sp^2)–H >C(sp^3)–H. In 1953, Dougill and Jeffrey[36] explained the high melting point of dimethyl oxalate due to bonding interactions between O atoms and C–H bonds, which they termed as 'polarization bonding'. Jones *et al.*,[37] in 1989 re-determined the structure of dimethyl oxalate and had found a network of C–H···O hydrogen bonds in its crystal lattice. Sutor[38] was the first to do a systematic study on a system of purines and pyrimidines, where C–H···O contacts were seen to occur and that too repeatedly. He had also determined the crystal structure of theophylline, caffeine,

uracil and a few other compounds to explain the importance of C–H···O hydrogen bonds. Taylor and Kennard[39(a)] in 1982 employed the technique of Cambridge Structural Database[39(b)] (CSD) to study weak hydrogen bonds based on 113 high-quality organic crystal structures determined by neutron diffraction. These studies had provided the shreds of evidence for the attractive nature of C–H···N, C–H···Cl, C–H···O and C–H···S contacts and termed these as hydrogen bonds. Desiraju[1,pp 40] has considered this study a proper scientific perspective and thus termed it as the end of the historical phase of the subject. Recent literature provide numerous examples of several packing motifs formed through C–H···X (X = O, N, S, Cl) hydrogen bonds to ascertain their role in crystal engineering.[40] Weak hydrogen bonds do form well defined and reproducible patterns in crystal structures, which can be rationalized based on the capabilities of the donor and acceptor groups.[1,pp 121] The prominence of these hydrogen bonds in supramolecular chemistry,[41] crystal engineering[15,42] and also in biological systems[43] has been well established in the literature.

1.2.2 A Short Note on the Interactions Involving π Acceptors

Weak hydrogen bonds involving strong donor (O–H, N–H, *etc*.) and weak acceptors primarily involving π acceptors (π = Ph, C=C, C≡C) have also been well studied in the literature.[44] If the donor is weak like C–H and on the acceptor side, there is a π electron cloud, then it becomes a debatable topic whether C–H···π interactions can be termed as hydrogen bond or not.[1,pp 155] C–H···π interactions do possess structure directing ability depending upon the acidity of the proton of the C–H group. These interactions are strong enough to control the conformation and packing modes of molecules in the organic solids. Nishio and Hirota have thoroughly reviewed the C–H···π interactions and have established its role in molecular recognition.[45] Nishio[46] has claimed that C–H···π interactions don't fall rapidly with distance, and their effect is visible even beyond the van der Waals' radii cut-off limit. These interact through the charge transfer from the π system to the antibonding orbital of the C–H group. The importance of intramolecular C–H···π interactions in controlling the shape of the molecule has been emphasized in a review written by Nishio.[47] Their crucial role in the stabilities of peptides is also well-known in the literature.[48] These interactions have a significant contribution in stabilizing the 3D structure of proteins.[49] The understanding of C–H···π interactions can have direct consequences in the field of optical and electronic devices,[50] supramolecular chemistry,[51] and drug designing.[52]

1.2.3 Interactions Involving Halogens: A Brief Sketch

Due to the high electronegativity of the halogens, C–X (X = F, Cl, Br or I) bonds are expected to be reasonably polar. Heavier halogens are known to form short intermolecular contacts with electron donors, as well as electron acceptors[53] due to the anisotropic distribution of electron density around the C–X bond. It has been concluded from theoretical calculations and experimental evidences that electrostatic potential around heavier halogen atoms (Cl, Br, I) is electropositive along the C–X bond and electronegative in its perpendicular direction, whereas for fluorine it remains negative overall around the C–F bond as is depicted in the figure 2 by Auffinger *et al.*[54]

Thus, an electron acceptor species will approach the halogen in a perpendicular direction to C–X bond, whereas an electron donor species will interact along the C–X bond. Therefore, halogen will interact with nucleophiles in a nearly linear geometry while interactions with electrophiles will occur in the side on manner (figure 1.3).[55]

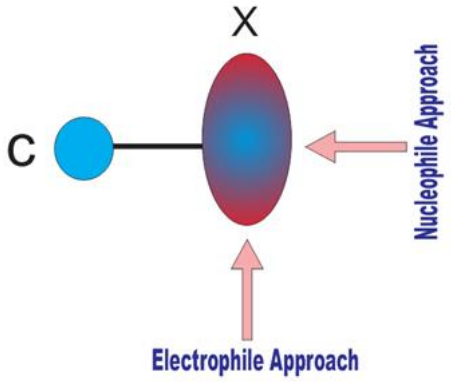

Figure 1.3: Direction of the approach of nucleophile and electrophile in a C–X bond. This figure has been re-drawn based on the figure from reference number 55(e).

In consequence of this, these should be excellent acceptors of hydrogen in a C–H···X–C hydrogen bond in the electrophilic direction of C–X bond. However, the formation of C–H···Cl hydrogen bonds has always been debated.[56] van den Berg and Seddon[57] through his systematic study on CSD have shown the role of C–H···X hydrogen bonds in the crystal packing. They have also proved that F and Cl are more prone to hydrogen bond formation than other heavier halogens due to their higher polarizability.

Moreover, because of the presence of both electron acceptor and donor sites over the halogens, interhalogen bonding also becomes possible. Geometrical categorization of Cl···Cl interactions has been done by Sakurai *et al.*,[58] in 1963. Ramasubbu *et al.*,[59] have

also characterized the interhalogen interactions of the type C–$X_1\cdots X_2$–C, into three types based on the two angles θ_1 and θ_2, where $\theta_1 = \angle C–X_1\cdots X_2$ and $\theta_2 = \angle X_1\cdots X_2–C$.

- *Type I* inter halogen interactions, θ_1 or $\theta_2 = 90°$,
- *Type II* inter halogen interactions, θ_1 or $\theta_2 = 180°$ and
- *Type III* interhalogen interactions, $\theta_1 = \theta_2$ and the two halogen atoms are related by the crystallographic center of inversion.

Later on, C–$X_1\cdots X_2$–C contacts were categorized in a more simplified manner into two types[60] (figure 1.4) as following.

- *Type I* (cis or trans geometry) and
- *Type II* (L geometry)

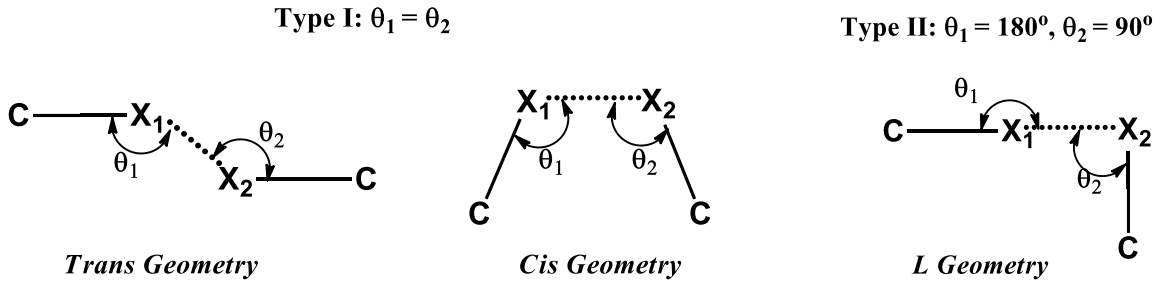

Figure 1.4: Different possible geometries through which halo⋯halo interactions are possible. The figure has been redrawn based on the figure from reference number 64(b).

Recently, in 2013, Desiraju has proposed homo halogen (X⋯X) contacts of three types based on his CSD analyses over these contacts.[61] The classification criterion is based on the difference between angles θ_1 and θ_2, which are described below

- $0° \leq |\theta_1 - \theta_2| \leq 15°$ -contacts will be classified as *type I*,
- $30° \leq |\theta_1 - \theta_2|$ -contacts will be classified as *type II*,
- $15° \leq |\theta_1 - \theta_2| \leq 30°$-contacts will be classified as *quasi type I/type II* interactions.

The role of $X_1\cdots X_2$ (X_1, X_2 = Cl, Br, I) interactions have been proven to be quite significant in crystal engineering.[62] Furthermore, halogens are also capable of interacting with a hetero atom containing a lone pair of electrons. Wulf *et al.*,[63] in 1936 have first discovered O–H⋯X–C hydrogen bonds through spectroscopic studies. But the shift in the stretching frequency of O–H bond was subtle because of their weak nature. Hence, these

bonds were not given attention until recently. The importance of X···O interactions has been recognized by designing a co-crystal through NO_2···X contacts in halogen and nitro substituted aromatic compounds.[64] These contacts were characterized as charge transfer or electron donor-acceptor interactions. But, nowadays the term 'halogen bonding' is used for such contacts. This term was introduced by Dumas *et al*.,[65] in 1983 and later was used by many authors.[66] Halogens bonds have been found to have number of similarities with the hydrogen bonds.[67] These are defined as "*A halogen bond occurs when there is evidence of a net attractive interaction between an electrophilic region associated with a halogen atom in a molecular entity and a nucleophilic region in another, or the same, molecular entity*".[68] The lists of features associated with the halogen bond have been described in detail by Desiraju *et al*., in the "Definition of the halogen bond, (IUPAC Recommendations 2013)".[69] A halogen bond is denoted as

R–X···Y

Where,

X is a halogen atom; R is a group that is covalently bonded to X; Y is a halogen bond acceptor and is a part of a molecule possessing a nucleophilic entity.

Now, it has been conceived that interactions involving halogens are significant in the crystal packing both in the absence as well as in the presence of other relatively stronger intermolecular interactions.[70] Recently, these were studied even in the solution state to understand their nature because most of the biological processes occur in the solution state.[71] Moreover, halogen bonds have also found applications in medicinal chemistry and chemical biology.[72]

Fluorine behaves differently amongst other halogens mainly because of its low polarizability and small size in comparison to the other halogens. Whereas other halogens were majorly found to interact through C–X_1···X_2–C interactions or R–X···Y halogen bond, but F *majorly* interacts through C–H···F hydrogen bond.[73] Therefore, interactions involving F are discussed separately and will be described in the following sections.

1.3 An Outline on Interactions Involving Fluorine

Fluorine is the most electronegative element in the periodic table. When F binds to the carbon, it forms the strongest bond (C–F) and its substitution in an organic compound brings enormous changes in its physical properties (melting and boiling points, refractive index, surface tension, lipophilicity, acidity, basicity, *etc*. to name a few) as well as its chemical reactivity.[74] Due to the nonconforming behaviour of F upon substitution to a compound, Schlosser[74(a)] has beautifully written about F in one of his articles:

"*Fluorine leaves nobody indifferent; it inflames emotions be that affections or aversions. As a substituent, it is rarely boring, always good for a surprise, but often completely unpredictable*."

This statement about F is also valid as far as the intermolecular interactions involving F are concerned. F bonded to a carbon is termed as 'Organic Fluorine', and the interactions comprising it has remained controversial in the literature.[73,75] But, it is crucial to understand them due to its important role not only in the crystal packing, but also in protein-ligand interactions.[76] Replacement of H by F is considered to be isosteric, through which conformational and electronic changes in a molecule can be brought with minor changes in its steric effect.[77] But, Smart[78] in one of his review articles has denied this generalized statement about the similar size of H and F in terms of their steric effects. To prove this, he has plotted the energies of non-bonding interactions *versus* the distance between two hydrogen atoms, a hydrogen and a fluorine atom and two fluorine atoms. It was shown that at an interatomic separation of 2.0 Å, the steric repulsion energy for two hydrogen and two fluorine atoms is 0.1 and 6.2 kcal/mol i.e. a "*significant fluorine steric effect*". Based on the values of van der Waals' radii given by Bondi,[79] Williams and Houpt,[80] F (1.35 and 1.44) and O (1.40 and 1.44); should be considered to be more isosteric than F and H. Due to similar size of F with O, high lipophilicity of F and the tendency for the formation of hydrogen bond, fluorinated molecules had been used to design suitable compounds, which can have enhanced biological applications in comparison to its non-fluorinated analogues. For example, for better transportation of 3F-Glu (figure 1.6) in red blood cells, its fluoro substituted analogue has been designed, named hexafluoroglucose (F_6-Glu) (figure 1.5). Both these molecules have similar shape and size. But, very high lipophilicity and low polarizability of F_6-Glu, makes it a better transporter than 3F-Glu.[81]

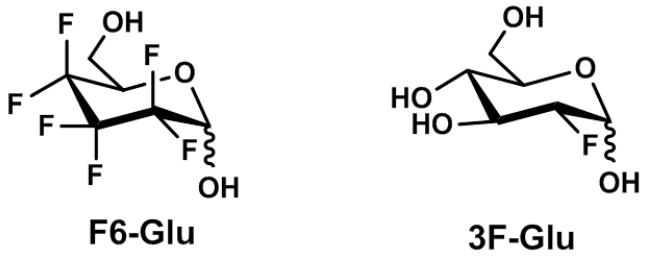

Figure 1.5: Chemical sketch of F_6-Glu and 3F-Glu. The figure has been redrawn based on the figure from reference number 81.

A debate regarding the significance of H···F hydrogen bonds came into picture, when the hydrogen bonds "paradigm" was questioned for DNA replication by Moran *et al*., in 1997.[82] They replaced thymine (**T**) by its non-polar isostere, which is difluorotoluene (**F**) (figure 1.6). Now because of the fluorination of the pairing edges, hydrogen bonds were believed to be absent. But, still difluorotoluene was coding efficiently for adenine during DNA replication. Thus, the importance of hydrogen bonds during DNA replication becomes spacious.

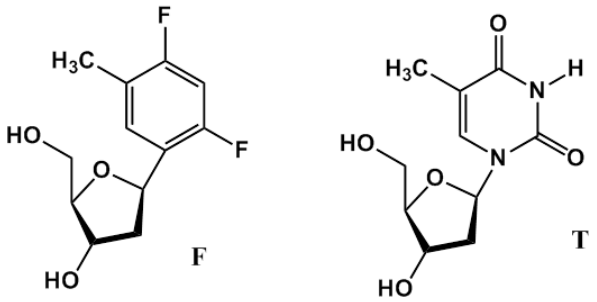

Figure 1.6: Molecular structure of adenine bonded to sugar and its non-polar analogue, difluorotoluene. This figure has been redrawn based on the figure from the reference number 82.

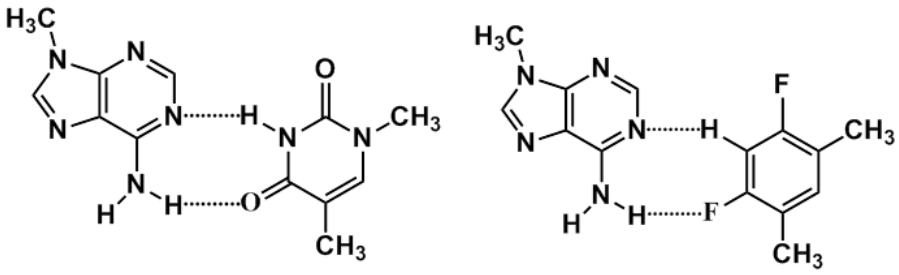

Figure 1.7: It describes the conventional and non-conventional hydrogen bonds between adenine and thymine in **(a)** and between adenine and difluorotoluene in **(b)** respectively. This figure has been redrawn based on the figure from the reference number 83.

But, later on Evans and Seddon[83] have proven that hydrogen bonds in DNA replications are vital because in the non-polar analogue of thymine non-conventional H···F hydrogen bonds has taken charge of conventional and strong N–H···O hydrogen bonds as described in figure 1.7. The importance of non-conventional hydrogen bonds for the high efficiency and fidelity of DNA syntheses was stressed upon by Seddon through this paper.

This argument was again interrogated by Kool *et al.*, who believed the fact that "shape complementarity and π stacking play more important role in fidelity during DNA syntheses than previously believed hydrogen bonds".[84] Thus, the debatable nature of X–H···F (X = C, N, O) hydrogen bond makes it important and interesting to explore further. Lots of studies have been done to signify the impact of interactions involving 'organic fluorine' in the crystal packing.[85] In 1994, it was inferred by Shimoni and Glusker through their database survey that X–H···F–C interactions are feeble when compared to C=O···H–X interactions.[86] The significance of these interactions was denied by Dunitz and Taylor in 1997 through their combined CSD and *ab-initio* studies, and they have concluded "Organic Fluorine Hardly Ever Accepts Hydrogen Bonds".[75(a)] Howard *et al*., by their CSD studies on limited number of structures, which were available within CSD at that time, has stated that "the predominant C–F···H–C contacts in the Database appear to have very little significance in energy terms and are essentially van der Waals' complexes".[87] Thalladi *et al*., through their systematic studies on fluorobenzenes have revealed the importance of 'organic fluorine' in the crystal packing.[88] They have shown that C–H···F interactions can be equally important as that of C–H···O or C–H···N hydrogen bonds in their guiding abilities of the packing of molecules in a particular array in its crystal structure. After this, a number of systematic studies have been done on different model systems like indole derivatives,[89] isoquinolines,[90] halogenated benzanilides,[91] trifluoromethyl substituted benzanilides,[92] aromatic azo compounds,[93] *etc*. and a lot more to unveil the hidden importance of fluorine mediated interactions. Through all these studies, it can be concluded that C–H···F interactions are weak hydrogen bonds, and these can be utilized for building the supramolecular architectures.

The question whether close F···F contacts are attractive in nature or these are just the results of close packing, has yet not been answered. Desiraju and Partasarathy[60] through a statistical survey have shown that X···X interactions are attractive in nature except the F···F interactions. In most of the cases, these contacts are assumed to be the consequence

of close packing.[94] But, some examples are also known in which they play an important role in the crystal packing or at least give some additional stability to the lattice along with the other interactions. Aloktra and Elguero[95] through their combined NMR and AIM studies, have found a bond critical point and bond path between the two fluorine atoms in the electron density map of the compounds that show a F···F coupling constant across the space. Choudhury *et al*. have also highlighted the influence of F···F interactions in a system of substituted Isoquinolines.[90(c)] F···F contacts have also been found in the liquid crystals composed of perfluorinated aromatic rings, which seems to direct their structures to some extent.[96] Mariaca *et al*.,[97] have found F···F interactions in the crystal structure of fluorine substituted stilbenes, which they have identified as subtle for the sidewise alignment of molecules in the crystallographic layer.

Furthermore, in the compounds containing one F atom and an aromatic ring, the possibility of C–F···π contacts is obvious. A database study has been reported by Prasanna and Guru Row[98] to establish the impact of C–F···π interactions in determining the molecular conformation and its role in the crystal packing. Generally, π electron cloud of an aromatic ring is an electron rich region. Hence, the interactions between an electronegative F atom and π electrons will become repulsive. However, if that aromatic ring contains electron withdrawing group, which can make its center electropositive, then C–F···π interaction will become stabilizing in nature. For numerous perfluorinated compounds, C–F···π interaction have been reported in the literature as one of the guiding tools for packing of molecules in the crystal lattice.[99] Hayashi *et al*., for the first time have reported the influence of C–F···π interactions not only in controlling the crystal packing, but also its thermal stability.[100] Moreover, through theoretical calculations also, C–F···π_F interactions (π_F center of a perfluorinated aromatic ring) have been proven to be quite stable with an interaction energy around ~ -2 kcal/mol.[98] At the same time C–F···π interactions, where π is the center of a unsubstituted benzene ring, have been found to be repulsive.[101] Thus, it is the electronic character of the aromatic ring, which determines the nature of C–F···π interactions.

1.4 Foreword

Crystal engineering has underlined the prominence of understanding intermolecular interactions. These non-covalent interactions have a direct influence on the crystal packing, molecular recognition, *etc*. Therefore, for designing of new crystal architecture, knowledge about these interactions is the utmost requirement. In spite of lots of studies, the role and function of weak hydrogen bonds have not reached a level, where one can have a control over these intermolecular interactions. To sum up, there is still a lot more to explore in this area. We are specifically interested in determining the guiding ability of fluorine to pack the molecules in the crystal lattice because of the importance of fluorine substituted molecules in pharmaceutical industries. As discussed above in detail, organic fluorine participates in the intermolecular interactions through various crystal-engineering motifs.[102] In spite of the different systematic studies on fluorine substituted organic molecules, clear understanding of the structure-directing role of fluorine has yet to be achieved.

In the following chapters, systematic studies have been performed on a model system of fluorine substituted *N*-benzylideneanilines to gain better understanding of fluorine mediated interactions. The selected model serve as an ideal model to gain insights into the fluorine mediated interactions because of the absence of any strong hydrogen bonding donor and acceptor sites in the molecular framework. Moreover, this system also enables us to study the effect of other halogens in place of F on the crystal packing. Thus, the concept of robustness of the synthons involving C–H···F hydrogen bonds can also be established, which remain unaltered by the replacement of one of the F in difluoro *N*-benzylideneanilines by Cl or Br. The interactions involving halogens have been found to be of prime importance in this system. In order to explicitly establish the directional influence of C–H···F hydrogen bonds, the stabilization energies of the dimers, interacting through these hydrogen bonds have also been evaluated. These energy values lie in the range of 1-4 kcal/mole. Furthermore, topological analyses of the concerned dimers have also been done to ascertain the hydrogen bond type nature of C–H···F interactions.

In this thesis, the role of fluorine in directing the packing motifs will be illustrated in chapter 2. The robustness of the motifs formed through C–H···F hydrogen bonds by the replacement of one of the F atoms by Cl or Br and by the addition of more F atoms to the system of difluoro substituted *N*-benzylideneanilines will be examined in Chapter 3 and 4

respectively. Chapter 5 deals with the theoretical and experimental charge density studies on the *mono*- and *tetra*- fluoro substituted isoquiniolines to gain better insight of these interactions.

Chapter 2 describes the different packing motifs, which were found to form through C–H···F hydrogen bonds in the structures of thirteen different mono/difluorinated substituted *N*-benzylideneanilines. The structural descriptions of all these compounds have been given in detail to reveal the importance of C–H···F hydrogen bonds. C–H···π interactions have also been found to be present in the crystal lattice of these compounds other than C–H···F hydrogen bonds. But, special emphasis has been given to the packing motifs designed through fluorine mediated interactions only. These short contacts that are generally found to be attractive in nature, with roughly one-third of the energy of conventional O–H···O hydrogen bond are termed as weak hydrogen bonds. However, if there are a large number of such interactions, their collective contribution to the stability of a system could be substantial**.**

Chapter 3 comprises of the structures of 36 different compounds. In this chapter, one of the F atoms of the compounds discussed in the 2nd chapter was replaced by its heavier halogen analogues and its effect has been analysed on the crystal packing. This study has clearly brought us to a conclusion that when the F, which has been found to be involved in the formation of C–H···F hydrogen bonds, has been replaced by Cl or Br, then those compounds were found to pack through entirely different packing motifs. But the replacement of the F, which has not been found to form C–H···F hydrogen bonds, keeps the packing motifs unaltered.

Chapter 4 deals with the study of the effect of more number of fluorine atoms on the packing motifs, which were found in the chapter 2. In this chapter, emphasis have been given on the study of robustness of synthons offered by organic fluorine. This study provides further proof of the importance of C–H···F hydrogen bonds in crystal engineering.

Chapter 5 deals with the theoretical and experimental charge density analysis on the *mono*- and *tetra*- fluorinated isoquinolines derivatives, which involves C–H···F hydrogen bonds and C–F···F–C interactions in their crystal lattices. The experimental analysis is done on high-resolution X-ray diffraction data while the theoretical analysis is done by the periodic calculation in the CRYSTAL14 program at the DFT (B3LYP/6-31G**) level. Based on all

eight of Koch and Popelier's criteria, defined using the theory of “Atoms in Molecules”, the hydrogen bond type nature of C–H···F interactions has been established. Moreover, the nature of type I C–F···F–C interactions have also been revealed in this study. The quantification of the strength of these interactions has also been done through these studies.

Chapter 2

Role of Organic Fluorine in Crystal Packing: Insights from Structural Investigation of a Series of Fluorine Substituted *N*-benzylideneanilines

Chapter 2

2.1 Introduction

The C–F group, which is found in a large number of small organic molecules and drugs available in the market, has still not been fully understood in terms of the strength and directionality of the interactions offered by this group in guiding the formation of crystal lattices. Understanding the relevance of C–F group in the crystal packing has been a major theme of the contemporary research.[73-75] Fluorine mediated interactions play an important role in the fields of chemistry and biology.[103] So, it becomes necessary to recognise the influence C–F group in governing the supramolecular assemblies. Moreover, it is also crucial to study the strength and directionality of the interactions offered by this group. A detailed crystallographic study has recently been done on a system of fluorine substituted benzanilides, where a strong hydrogen bond donor (N–H) and acceptor (C=O) groups were present.[91(a),104] But, the strength, directionality and the reproducibility of various supramolecular synthons formed by the C–F group in those molecules were not highlighted. In this system, it was realized that even in the presence of well-known N−H···O=C and C−H···O=C hydrogen bonds, the role of C−H···F−C along with C−F···π, C−F···F−C, and C−H···π intermolecular contacts were of substantial importance in guiding the crystal packing. We are interested to study and analyse the role of weak interactions offered by the organic fluorine in the absence of strong hydrogen bond. This is aimed to estimate the strength, identify the directionality, and to establish the reproducibility of supramolecular synthons involving organic fluorine in crystal lattices. Therefore, we have chosen *N*-benzylideneaniline as our model system for our study as this system does not

have any strong hydrogen bonding functional group. Moreover, many derivatives of *N*-benzylideneanilines are used as coordinating ligands in inorganic complexes, which show high catalytic activity.[105(a)] This class of compounds are important from biological perspective also, mainly because of their antifungal[105(b)] and antibacterial effects[105(c)] and for inhibiting enzyme activities.[105(d)] There are a few patents, which have highlighted the importance of this class of compounds in the protection of skin against the harmful effects of sunlight (erythema) on human skin[105(e)] and warm-blooded animals.[105(f)] All these properties make this moiety an interesting system to study. Other than this, the synthesis of various *N*-benzylideneanilines being simple and most of the compounds being solid and stable at room temperature, a large number of compounds belonging to *N*-benzylideneaniline family have been reported in the literature and Cambridge Structural Database (CSD). These structures contain $–CH_3$, –CN, $-NO_2$, -OH, -COOH, -Cl, -Br, $-OCH_3$, *etc*. group as substituents and are well studied from the structural point of view. The structures of the compounds, which have different substituents on the same molecular framework will be discussed and compared with our structures in the discussion section. These molecules being generally non-planar in comparison to the stillbenes and azobenzenes, show significantly different UV spectra.[106]

Our aim is to synthesize and structurally characterize a number of *mono*-, *di*-, and *tetra*- fluorinated derivatives of *N*-benzylideneaniline (scheme-2.1). In addition, we intend to compare the influences of C−F group with the influences of C−Cl and C−Br groups in the same molecular framework by synthesizing and analysing the structures of fluoro-chloro, fluoro-bromo and chloro-bromo substituted *N*-benzylideneaniline. The relationship between molecular conformation and structural aspects resulting from different halogen substitutions would enable us to understand the influence of organic fluorine in directing crystal lattices. Different conformers of a molecule, belonging to this system, can be trapped due to the conformational flexibility associated with C−C and C−N bond rotation connected to the two phenyl rings. This may lead to the existence of conformational polymorphs, which have been found in the current system studied. In the literature also, such polymorphs have been found as is the case of *N*-(*p*-methylbenzylidene)-*p*-methylaniline which exhibits trimorphic behavior in the solid state (concomitant polymorphism wherein crystals are obtained from ethanol), wherein both planar and nonplanar conformations have been observed.[107]

Furthermore, it is also known in the literature that the fluorine present at the *ortho* or *meta* position of different aromatic molecules generates positional disorder due to their involvement in different intermolecular interactions, thus provides stability to the crystal lattice.[108] The overall stability of the crystal lattice could be the result of entropic gain and also the increase in the number of intermolecular interactions. In the current series also, there are possibilities to find disorder in the molecules, in which fluorine will be substituted at the *ortho*- or *meta*- position. This may result in different intermolecular interactions and finally in the creation of different molecular and crystal structures. Our purpose is to access the different independent conformations of a given molecule by exploring the possibility of different conformational polymorphism, which can be possible for a given molecule and to understand the nature of disorder (static or dynamic) present in different fluorine substituted compounds. Thus, in this chapter, we present our structural investigation on a series of fluorine substituted *N*-benzylideneanilines (Scheme 2.1) to recognise the importance of the interactions offered by C−F group not only in crystal packing, but also for the generation of new polymorphs and in the stabilization of a disordered structure.

Scheme 2.1:

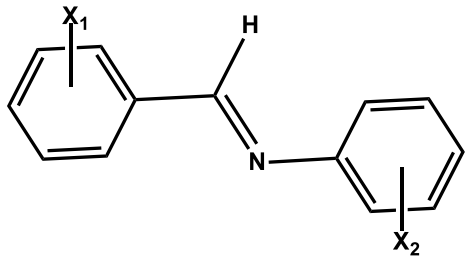

Where X_1, X_2 = F/H

Table 2.1: Compound Identification Table

Code	X_1	X_2
1	*p*-F	*p*-F
2	*p*-F	*m*-F
3	*p*-F	*o*-F

Code	X_1	X_2
4	*m*-F	*p*-F
5*	*m*-F	*m*-F
6	*m*-F	*o*-F

Code	X_1	X_2
7	*o*-F	*p*-F
8*	*o*-F	*m*-F
9	*o*-F	*o*-F

Code	X_1	X_2
10	H	*p*-F
11*	H	*m*-F
12	H	*o*-F

Code	X_1	X_2
13	*p*-F	H
14*,#	*m*-F	H
15*,#	*o*-F	H

* indicates the compounds, which were found to be liquid at room temperature. *,# indicates the compounds, which exist as liquid at room temperature, but could not be crystallized using *in situ* crystallization technique.

2.2 Experimental

2.2.1 Synthesis and Characterization

All the starting materials, were purchased from Sigma-Aldrich and were used without further purification. All the compounds were synthesized by taking an equimolar mixture of respective benzaldehyde (or fluorobenzaldehyde) and aniline (or fluoroaniline) and refluxing them in toluene in the presence of 4 Å activated molecular sieves for three hours. The crude product, obtained after filtration and subsequent evaporation of toluene under vacuum, was purified by neutral column. The pure materials were characterized by FTIR and ^{1}H NMR spectroscopy. Melting points (Table S1.1) were recorded and the DSC traces of all the solid compounds (figure S2.4:1 to S2.4:15) including other characterization details (NMR and IR) are given in the enclosed CD as electronic supporting information (ESI) (figure S2.1:1 to S2.1: 15; figure S2.2:1 to S2.2:15).

Fifteen new compounds were synthesized and characterized by the above procedure (Scheme 2.2). Five of these compounds (**5**, **8**, **11**, **14** and **15**) were found to be liquid at 25 °C. Three of these (**5**, **8**, and **11**) five liquids could be crystallized using *in situ* crystallization technique.[73(a),109] Among these 13 compounds, one compound (**9**) have been found to exhibit polymorphism. The crystal structures of 13 compounds have been systematically studied for the identification of unique supramolecular motifs involving fluorine in addition to other weak interactions that contribute toward the stability of the crystal packing. The method of their nomenclature has been given in table 2.1.

Scheme 2.2:

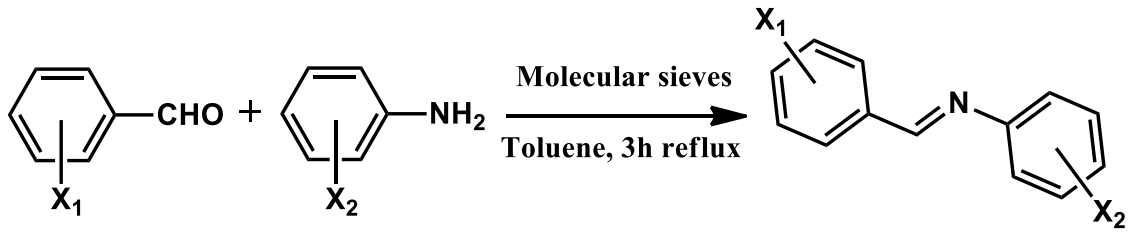

Where X_1, X_2 = F/H

2.3 Crystallography

2.3.1 Powder X-ray Diffraction Studies

PXRD patterns were recorded on a Rigaku Ultima IV diffractometer using parallel beam geometry equipped with a Cu – Kα radiation, 2.5° Primary and secondary soller slits, 0.5° divergence slit with 10 mm height limit slit, sample rotation stage (120 rpm)

attachment and DTex Ultra detector. The tube voltage and current applied were 40 kV and 40 mA. The data were collected over an angle range 5 to 50° with a scanning speed of 5° per minute with 0.02° step. The observed PXRD patterns have been compared (using WINPLOTR[110]) with the simulated PXRD patterns generated from the crystal coordinates using Mercury.[111] These are given in the ESI enclosed in a CD (ESI, figure S2.3:1 to S2.3:13).

2.3.2 Crystal Growth, Single Crystal Data Collection, Structure Solution and Refinement

Single crystals of desired size and quality were grown by slow evaporation by dissolving compound in different solvents or solvent mixtures such as DCM/hexane, chloroform/hexane, ethyl acetate/hexane, methanol/hexane and acetone/hexane.

Single Crystal X-ray data for all the compounds were collected using Bruker AXS KAPPA APEX-II CCD diffractometer (monochromatic Mo Kα radiation) equipped with an Oxford Cryostream 700 Plus at 100.0 (1) K. Data collection and unit cell refinements for the data sets were done using Bruker APEX2 suite,[112] data reduction and integration were performed by SAINT V7.685A12 (Bruker AXS, 2009) and absorption corrections and scaling was done using SADABS V2008/112 (Bruker AXS). The crystal structures were solved by using Olex2[113] or WinGx[114] packages using SHELXS97[115] and the structures were refined using SHELXL97. All the hydrogen atoms have been geometrically fixed and refined using the riding model. Table 2.15 lists the crystal and refinement data for all the compounds. All the packing and interaction diagrams have been generated using Mercury 3.1.1. Geometric calculations have been done using PARST[116] and PLATON.[117]

2.3.3 Crystal Growth and Data Collection for Liquids

Compounds **5**, **8**, **11**, **14** and **15** exist in the liquid state at ambient conditions. Therefore, these were tried to crystallize using *in situ* crystallization, which is a technique that helps in the crystallization of low melting compounds for their structure determination. In all the cases the compound was taken in 0.3 mm Lindemann quartz capillary. The capillary is sealed at both the ends with glue, mounted on Bruker AXS KAPPA APEX-II CCD diffractometer and was aligned vertically by setting the κ angle of the goniometer to 0^o. After alignment of the capillary, different strategies were applied to the crystallization of various compounds based on their DSC traces.

For Compound **5**, the capillary was first cooled to 200K at the rate of 360K/hr. But, the liquid was not solidified by itself. Then, a region of the capillary was heated by the CO_2

LASER of the OHCD[109(a)] and suddenly the heat was removed to give a cold shock to the compound inside the capillary. This process was repeated few times to trigger crystallization in the capillary. Then the capillary was heated up to 220K and a few cycles of zone melting scans using the CO_2 LASER of the OHCD were repeated for 3 hours to grow single crystal in the capillary. After the formation of suitable single crystal, single ϕ scan (scan width 0.3°, 1200 frames) data were collected by keeping ω and κ fixed at 0° and by positioning the detector at a fixed 2θ value of 30° and at a distance of 6.0 cm.

For Compound **8**, the capillary was cooled to 250K, which resulted in the formation of a polycrystalline mass on cooling. Numerous zone melting scans using the CO_2 LASER were accomplished for about 12-13 hours to get single crystals of the compound in the capillary. A similar ϕ scan data were collected as that for compound **5** with the scan width being 0.5° (720 frames).

Compound **11**, was initially cooled down to 140K at the rate of 360K/hr, which resulted in the transformation of the liquid to a glassy material. Then this glassy material was heated to 240K at the rate of 200K/hr. Zone melting scans using the CO_2 LASER from bottom to top always ended with the formation of a glassy material. After that, zone melting scans were performed from top to bottom for 3 hours, which has successfully resulted in the crystallization of the material, though very good quality crystals could not be grown. Similar ϕ scan data were collected with a scan width of 0.3° (1200 frames).

Different attempts for the crystallization of compound **14** and **15**, have always resulted into the glassy materials. Thus, these compounds could not be crystallized using *in situ* crystallization technique.

2.3.4 Crystallographic Modelling of Disorder

The compounds **1**, **4**, **5**, **7**, **9** (both Form **I** and Form **II**) and **11** were found to be disordered. In case of compounds **1**, **5** ($Z' = 0.5$) and both the forms of **9**, the positional disorder has been found around C=N bond due to in-plane flipping of the molecule. These compounds were refined with 0.5 occupancy using PART command in SHELXL97. Thermal parameters of the atoms of the two parts, which belong to the same chemical environment, were constrained to be equal by EADP command in SHELXL 97. In case of the compound **4** ($Z' = 2$), both the molecules in the asymmetric unit were disordered due to rotation of the phenyl rings around C_{Ar}–C/N bond with the occupancy ratio of 0.941(2):0.059(2) for molecule **A** and 0.935(2):0.065(2) for molecule **B** at 100K data. The corresponding values for 200K data are 0.946(3):0.054(3) and 0.936(3):0.064(3), and for

298K data are 0.960(3):0.040(3) and 0.951(3):0.049(3) respectively indicating the presence of static disorder in the crystal structure. The disorder for this compound too, was analyzed in the similar manner as was done earlier. Refinement of this compound was done for two independent positions, namely A and B ('A' for higher occupancy). For the purpose of refinement, the positions of carbon atom in benzene ring for A and B were kept fixed using EXYZ command in SHELXL97. For the atoms at the same position, thermal parameters were also constrained to be equal using EADP command in SHELXL97. All hydrogen atoms were then positioned geometrically and refined using a riding model with U_{iso}(H) = 1.2 U_{eq}(C,N). In case of the compound **7** (refined with Z′ = 0.5), the true molecule (possessing fluorine substitution at *para-* on the aniline side, while *ortho-* at the benzaldehyde side) does not have any symmetry. The requirement of Z′ = 0.5 intends the presence of crystallographic disorder around C=N bond, which generates the second half of the molecule around the center of inversion as shown in figure 2.7(a). Careful refinements were done with equal occupancy of both the parts (namely A and B for benzene ring) with similar refinement strategy as mentioned previously for compound **4**. The compound **11** (liquid at RT) was found to exhibit pedal motion in its crystal structure. Therefore, its pedal motion was accounted for by performing the disorder refinement as described earlier with the final population ratio in the two conformer being 0.850(6):0.150(6) (figure 2.11a). Except fluorine all other atoms in the minor conformer were refined isotropically and the thermal parameter of all the carbon atoms was constrained to the same value using EADP command in SHELXL97. Furthermore, constraint was also applied to the benzene rings of minor conformer to be a regular hexagon using FLAT command and also C–C bond lengths were restrained to 1.39Å using DFIX in SHELXL97. The C–C–C bond angles in the benzene ring were also restrained to be same value using SADI command in SHELXL97. The remaining molecules **2, 3, 6, 8, 10, 12, 13** do not exhibit any disorder in their crystal lattice.

2.4 Theoretical Calculations

(a) Stabilization Energy Calculations in Gas Phase

The intermolecular interactions observed in these compounds are of the type of C–H···F and C–H···π [table 1.1a/b to 13a/b]. The sum of the van der Waals' radii[83] has been considered as the limiting distance for the evaluation of the different interactions present in these compounds. Out of all these interactions observed in the crystal structures

studies by us, our primary interest was to look at the role played by the C–H···F hydrogen bonds in the crystal packing of these compounds. Therefore, the stabilization energies (**SE_{G09}**) of only those dimers, which interact through these interactions, have been computed using Gaussian 09.[118] Gauss View[119] has been used as a graphical interface for Gaussian 09. All the calculations were performed by using Gaussian09 at the second order Møller–Plesset perturbation method (MP2)[120] with the 6-31+G(*) basis set. The energies obtained for these dimers were corrected for the basis set superposition error (BSSE) by using counterpoise method.[121] It is to be noted that all the stabilization energy calculations are done in the gas phase because we are more interested in comparing the relative energies of the dimers that interact through various kinds of C–H···F hydrogen bonds rather than their absolute values. The coordinates of such dimers were taken from their respective experimentally determined crystal structures (at 100K) and were used for the calculation of the stabilization energies provided by them without further optimization. In the disorder structures, the coordinates of only the interacting conformer were used for the stabilization energy calculation. The energy of the monomers ($E_{monomer}$) or dimers (E_{dimer}) were calculated at the same level of theory. Then, the stabilization energy (**SE_{G09}**, ΔE_{dimer}) of the dimer motifs was calculated using the formula $\Delta E_{dimer} = E_{dimer} - (2 \times E_{monomer})$. Table 1.1a to 1.13a lists all these intermolecular interactions metrics along with their stabilization energies.

(b) AIM Calculations

To study the topological properties of the electron density, the wavefunction files (.wfn) for all the dimers were also generated by giving a command (output = wfn) in the input file for the single point energy calculation. From these wavefunction files, the topology of electron density distribution can be analyzed by Bader's quantum theory[122] of atoms in molecule. AIM2000[123] was used to compute the bond paths and bond critical points between the interacting atoms. (3, -1) Bond critical points were found for each C–H···F short contacts encountered in the various structures reported here. The topological properties, namely electron density (ρ), and the Laplacian of the electron density ($\nabla^2\rho$) at the (3, -1) bond critical points (BCPs) are listed in the tables containing the geometrical parameters of the intermolecular interactions.

Table 2.2: Crystallographic data for the compounds **1-13**.

DATA	**1**	**2**	**3**	**4**	**5**
Formula	$C_{13}H_9F_2N$	$C_{13}H_9F_2N$	$C_{13}H_9F_2N$	$C_{13}H_9F_2N$	$C_{13}H_9F_2N$
FW	217.21	217.21	217.21	217.21	217.21
CCDC No.	884979	884984	884985	884986	884987
Solvent system	C_2H_5OH	$CH_2Cl_2 + C_6H_{12}$	CH_3OH	CH_2Cl_2	*In situ*
Morphology	Plate	Block	Needle	Plate	Block
Crystal System	Triclinic	Monoclinic	Monoclinic	Triclinic	Monoclinic
Space Group	$P\ \bar{1}$	$P2_1/c$	$P2_1$	$P\ \bar{1}$	$P2_1/c$
a (Å)	5.728(5)	14.530(3)	6.0662(3)	7.252(5)	7.2124(15)
b (Å)	7.416(5)	5.7472(13)	14.1399(5)	11.594(5)	5.8634(13)
c (Å)	12.487(5)	12.345(3)	12.0037(5)	13.535(5)	12.443(3)
α (°)	105.745(5)	90	90	64.666(5)	90
β (°)	98.559(5)	107.326(1)	90.232(2)	75.500(5)	108.521(2)
γ (°)	90.003(5)	90	90	89.803(5)	90
Volume (Å^3)	504.4(6)	984.1(4)	1029.61(8)	988.8(9)	498.94(19)
Z	2	4	4	4	2
Z′	1	1	2	2	0.5
ρ (g/cm^3)	1.43	1.466	1.401	1.459	1.446
μ (mm^{-1})	0.110	0.113	0.108	0.112	0.111
***F* (000)**	224	448	448	448	224
$\theta_{min,max}$ (°)	1.7, 25.0	2.9, 25.0	1.7, 25.0	1.7, 25.0	3.0, 25.0
$h_{min,max}$; $k_{min,max}$; $l_{min,max}$	-6, 5; -8, 8; -14, 14;	-16, 17; -3, 6; -14, 14	-3, 7; -16, 16; -14, 13	-8, 8; -13, 13; -16, 15	-8, 8; -3, 3; -14, 14
No. of reflections.	7796	5454	5190	11528	2208
No. unique/ observed reflections.	1761/1513	1734/1639	2896/2703	3474/3181	606/579
No. of parameters	145	145	289	303	74
wR_2_obs, R_obs	0.117, 0.045	0.010, 0.033	0.222, 0.074	0.162, 0.058	0.075, 0.027
$\Delta\rho_{min,\ max}$ (eÅ^{-3})	-0.28, 0.43	-0.20, 0.26	-0.41, 0.54	-0.44, 0.79	-0.19, 0.10
GooF	1.126	1.039	1.084	1.092	1.082

Table 2.2: Crystallographic data for the compounds **1-13**. (contd)

DATA	**6**	**7**	**8**	**9A**
Formula	$C_{13}H_9F_2N$	$C_{13}H_9F_2N$	$C_{13}H_9F_2N$	$C_{13}H_9F_2N$
FW	217.21	217.21	217.21	217.21
CCDC No.	884988	884989	884990	884991
Solvent system	CH_3CN	CH_3OH	*In situ*	C_6H_{12}
Morphology	Block	Block	Block	Plate
Crystal System	Orthorhombic	Monoclinic	Monoclinic	Monoclinic
Space Group	$P2_12_12_1$	$P2_1/c$	$P2_1/c$	$P2_1/c$
a (Å)	6.4645(2)	7.2019(11)	15.393(9)	9.8109(9)
b (Å)	12.0553(4)	5.8995(10)	3.851(2)	3.7789(3)
c (Å)	13.1914(4)	12.292(2)	22.616(2)	27.044(3)
α (°)	90	90	90	90
β (°)	90	108.789(6)	132.377(7)	90.991(5)
γ (°)	90	90	90	90
Volume (Å^3)	1028.03(6)	494.44(14)	990.3(10)	1002.5(2)
Z	4	2	4	4
Z′	1	0.5	1	1
ρ (g/cm^3)	1.403	1.459	1.457	1.439
μ (mm^{-1})	0.108	0.112	0.112	0.111
***F* (000)**	448	224	448	448
$\theta_{min,max}$ (°)	2.3, 25.0	3.0, 25.0	2.4, 25.0	1.5, 25.0
$h_{min,max}$; $k_{min,max}$; $l_{min,max}$	-6, 7; -14, 14; -15, 15	-8, 8; -5, 7; -14, 13	-18, 18; -2, 2; -26, 26	-11, 11; -4, 4; -32, 31
No. of reflections.	19712	3719	4157	8802
No. unique/ observed reflections.	1815/1766	864/752	1266/1062	1781/1555
No. of parameters	145	79	145	145
wR_2_obs, R_obs	0.112, 0.037	0.147, 0.045	0.205, 0.076	0.093, 0.034
$\Delta\rho_{min,max}$ (eÅ^{-3})	-0.18, 0.41	-0.31, 0.36	-0.58, 0.36	-0.19, 0.39
GooF	1.132	1.172	1.109	1.102

Table 2.2: Crystallographic data for the compounds **1-13**.(contd)

DATA	**9B**	**10**	**11**	**12**	**13**
Formula	$C_{13}H_9F_2N$	$C_{13}H_{10}FN$	$C_{13}H_{10}FN$	$C_{13}H_{10}FN$	$C_{13}H_{10}FN$
FW	217.21	199.22	199.22	199.22	199.22
CCDC No.	884992	884980	884981	884982	884983
Solvent system	CH_3OH	C_2H_5OH	*In situ*	CH_2Cl_2+C_6H_{12}	CH_2Cl_2+C_6H_{12}
Morphology	Plate	Plate	Block	Thin rod	Block
Crystal System	Orthorhombic	Monoclinic	Monoclinic	Orthorhombic	Triclinic
Space Group	$P2_12_12_1$	$P2_1/n$	$P2_1/c$	$P2_12_12_1$	$P\bar{1}$
a (Å)	3.8396(6)	5.6613(1)	12.022(2)	6.3184(3)	5.5942(10)
b (Å)	11.871(2)	25.0212(5)	7.9133(16)	12.0035(6)	7.2247(14)
c (Å)	22.205(4)	7.1416(1)	12.242(4)	13.3787(7)	12.569(2)
α (^{0})	90	90	90	90	91.985(10)
β (^{0})	90	90.216(1)	119.589(2)	90	97.697(10)
γ (^{0})	90	90	90	90	90.286(10)
Volume (Å^3)	1012.2(3)	1011.62(3)	1012.8(4)	1014.68(9)	503.10(16)
Z	4	4	4	4	2
Z′	1	1	1	1	1
ρ (g/cm^3)	1.425	1.308	1.307	1.304	1.315
μ (mm^{-1})	0.110	0.090	0.090	0.089	0.090
***F* (000)**	448	416	416	416	208
$\theta_{min,max}$ (^{o})	1.9, 27.5	1.6, 23.5	3.2, 25.0	2.3, 25.0	2.8, 26.4
$h_{min,max}$; $k_{min,max}$; $l_{min,max}$	-4, 4; -10, 15; -23, 28	-6, 6; -27, 27; -8, 7	-14, 14; -6, 6; -14, 14	-7, 7; -13, 14; -15, 7	-6, 6; -9, 9; -15, 15
No. of reflections.	8465	6169	4446	2946	6030
No. unique/ observed reflections.	2299/2144	1494/1356	1395/1290	1724/ 1612	2034/1635
No. of parameters	145	136	185	136	136
wR$_2$_obs, R_obs	0.092, 0.034	0.080, 0.032	0.259, 0.103	0.094, 0.037	0.105, 0.041
$\Delta\rho_{min,max}$(eÅ^{-3})	-0.28, 0.23	-0.18, 0.30	-0.35, 0.76	-0.17, 0.33	-0.20, 0.45
GooF	1.125	1.048	1.168	1.061	1.046

2.5 Results

It is noteworthy that due to the presence of electron withdrawing fluorine atoms in the molecular framework, the acidity of the neighbouring hydrogens in the phenyl ring gets increased in addition to the imine hydrogen that is highly acidic. In the absence of strong hydrogen bond donors, the leading features in the crystal packing of all the compounds primarily consist of C–H···F and C–H···π intermolecular interactions.

It is important to mention here that in the structural analysis of the compounds reported in this thesis, Cg1, Cg2, Cg3 and Cg4 refer to the center of gravity of the rings formed by C1-C6, C7-C12, C14-C19 and C20-C25 respectively. The symbol '*' with an interaction indicates that those have contributions from both C–H···π and C–H···F interactions.

2.5.1. 4-fluoro-*N*-(4-fluorobenzylidene)aniline

Structure of compound **1** is solved in the triclinic centrosymmetric $P\bar{1}$ space group with Z = 2, Z′ = 1 (figure 2.1a). The molecules in the crystal lattice have been found to be positionally disordered around the central C=N bond, with the occupancy of each conformer being 0.5. There exist conformational differences between the two parts of the disordered molecule. The carbon atoms of the two phenyl rings are at the same positions while the C=N has been found to orient in different direction in the second conformation. The conformational difference between the two parts has been accounted by measuring the angles between the ring planes and the central H1A–C1A=N1A and H1B–C1B=N1B planes that are listed in the table 2.1d. Molecular sheets, parallel to the *ac* plane, were found to form through C–H···F hydrogen bonds, involving H6 with F2 (SE_{G09} = -1.1 kcal/mol) and H12 with F1 (SE_{G09} = -1.1 kcal/mol) (table 2.1a, figure 2.1b). These sheets are further interlinked across the center of inversion *via* weak C–H···π intermolecular interactions forming molecular layers in the solid state (table 2.1b, figure 2.1c).

Table 2.1a: Intermolecular interactions metrics and their stabilization energies in **1**

Code	C–H···F	*D* C···F /Å	*d* H···F /Å	θ ∠C–H···F/º	Symmetry Code	SE_{G09} kcal/mol	ρ (eÅ^{-3})	$\nabla^2\rho$ (eÅ^{-5})
1	C6–H6···F2	3.361(2)	2.67	131	x, y+1, z+1	-1.1	0.027	0.555
	C12–H12···F1	3.372(2)	2.69	130	x-1, y-1, z-1	-1.1	0.027	0.555

Table 2.1b: Geometrical parameters for C–H···π interactions in **1**

Code	C–H···π	C···π (Å)	H···π (Å)	∠C–H···π (º)	Symmetry Code
1	C3–H3···Cg2	3.506 (2)	2.86	126	1-x, 2-y, -z
	C6–H6···Cg2	3.526(3)	2.82	131	2-x, 1-y, -z
	C9–H9···Cg1	3.461(2)	2.77	130	1-x, 1-y, -z
	C12–H12···Cg1	3.544 (2)	2.85	130	2-x, 2-y, -z

Table 2.1d: Dihedral angles between different planes of the structure of **1**

Conformer 1	θ1A	11.8º
	θ2A	43.9º
Conformer 2	θ1B	35.3º
	θ2B	18.1º

θ1A	Angle between the plane of the benzaldehyde ring with the H1A–C1A=N1A plane
θ2A	Angle between the plane of the aniline ring with the H1A–C1A=N1A plane
θ1B	Angle between the plane of the benzaldehyde ring with the H1B–C1B=N1B plane
θ2B	Angle between the plane of the aniline ring with the H1B–C1B=N1B plane

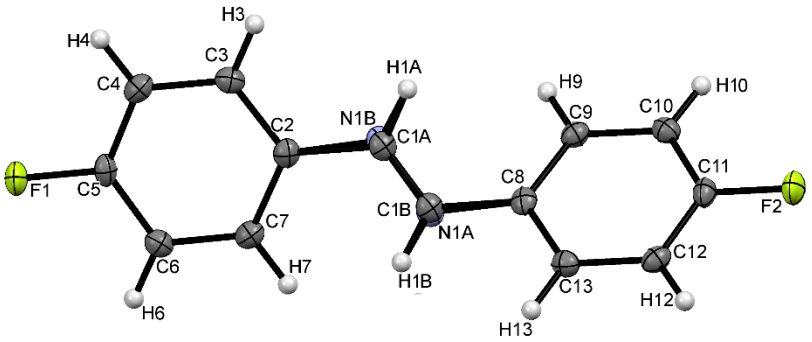

2.1a

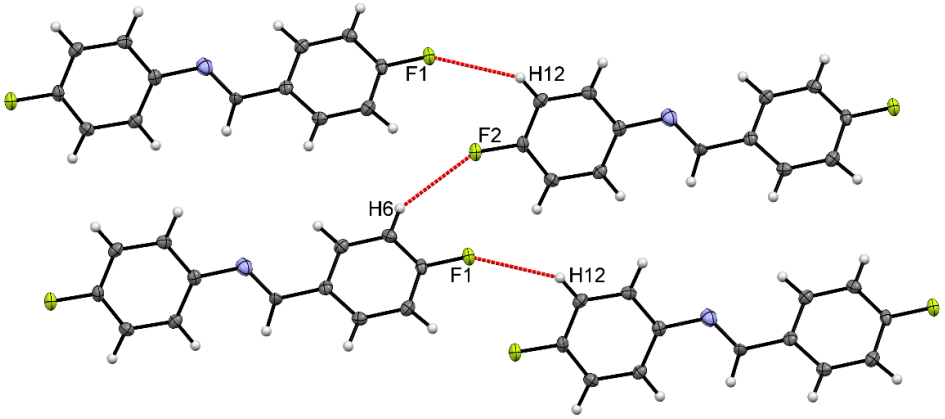

2.1b

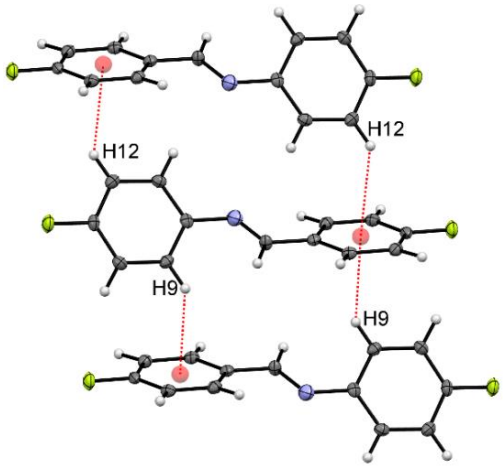

2.1c

Figure 2.1: (a) ORTEP of **1** drawn with 50% ellipsoidal probability, **(b)** formation of sheets viewed down the *ac* plane by C−H···F hydrogen bonds in **1**, **(c)** formation of a molecular layer *via* weak C−H···π interactions in **1.**

N.B. Disordered atoms were omitted for clarity.

2.5.2. 3-fluoro-*N*-(4-fluorobenzylidene)aniline

Compound **2** crystallized in the monoclinic centrosymmetric $P2_1/c$ space group (figure 2.2a). Molecules, which are symmetrically related through center of inversion, form molecular layers by the generation of head to head and tail to tail dimers, involving H11 and H6 with F2 and F1 respectively (table 2.2a, figure 2.2b). The molecular layers thus formed, get further interweaved through weak C–H···F hydrogen bonds (involving H13 with F2) along with C–H···π interactions (involving H4, H7, H9, and H12) (table 2.2a and 2.2b, figure 2.2b). The stabilization energies associated with the dimers interacting *via* C–H···F hydrogen bonds were found to lie in the range between -0.5 to -1.6 kcal/mol (table 2.2a), which illustrates weak but significant contribution towards stabilization of the crystal structure by these interactions.

Table 2.2a: Intermolecular interactions metrics and their stabilization energies in **2**

Code	C–H···F	*D* C···F /Å	*d* H···F /Å	θ ∠C–H···F/º	Symmetry Code	SE_{G09} kcal/mol	ρ (eÅ^{-3})	$\nabla^2\rho$ (eÅ^{-5})
2	C6–H6···F1	3.219(1)	2.52	128	1-x, -y, 1-z	-1.3	0.039	0.758
	C13–H13···F2	3.469(1)	2.55	161	x, -y-$^1/_2$, z-$^1/_2$	-1.6	0.036	0.707
	C11–H11···F2	3.326(2)	2.55	134	-x, 1-y, -z	-0.5	0.038	0.695

Table 2.2b: Geometrical parameters for C–H···π interactions in **2**

Code	C–H···π	C···π (Å)	H···π (Å)	∠C-H···π(°)	Symmetry Code
2	C4–H4···Cg1	3.460(1)	2.80	129	1-x, $^1/_2$+y, $^3/_2$-z
	C7–H7···Cg2	3.448(1)	2.81	125	x, $^1/_2$-y, $^1/_2$+z
	C9–H9···Cg1	3.469(1)	2.74	134	x, $^3/_2$-y, z-$^1/_2$
	C12–H12···Cg2	3.441(1)	2.73	133	-x, y-$^1/_2$, $^1/_2$-z

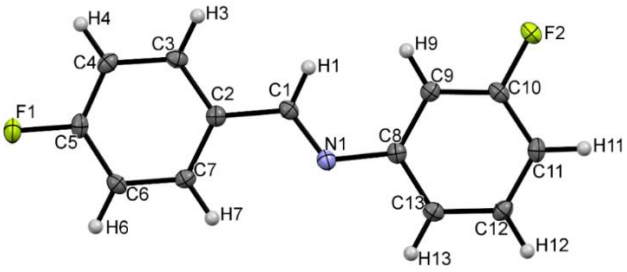

2.2a

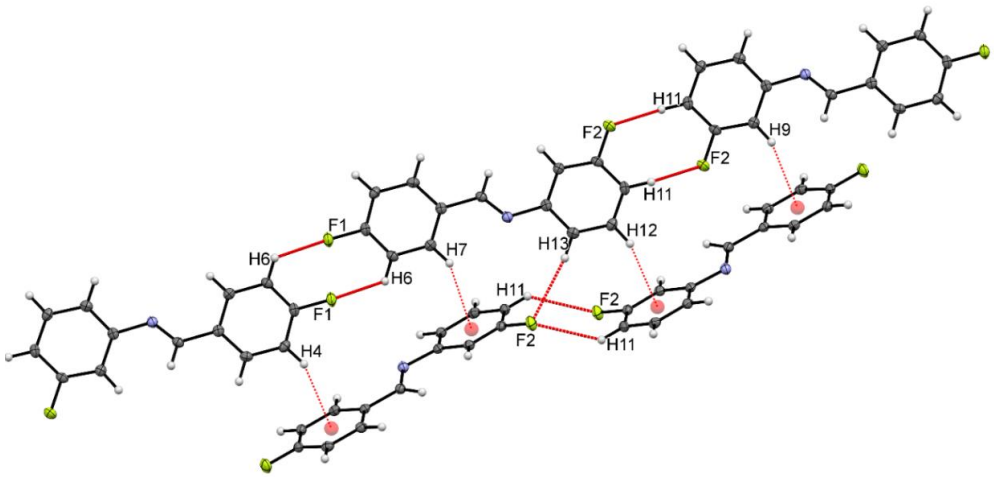

2.2b

Figure 2.2: (a) ORTEP of **2** drawn with 50% ellipsoidal probability, **(b)** formation of molecular layers and their bondage by C−H···F and C−H···π intermolecular interactions in **2**.

2.5.3. 2-fluoro-*N*-(4-fluorobenzylidene)aniline

Compound **3** has been found to crystallize in the monoclinic non-centrosymmetric $P2_1$ space group with Z′ = 2 (figure 2.3a). Two molecules (A and B) of the asymmetric unit are interconnected through weak C–H···π interaction (figure 2.3d). Both the molecules (A and B) of the asymmetric unit are involved in the formation of molecular chains through short, highly directional and significantly C–H···F hydrogen bond involving imine hydrogen H1 with F2 [2.32Å, 162°, -4.8 kcal/mol] and H14 with F4 [2.30 Å, 161°, -4.8 kcal/mol] respectively (table 2.3a, figure 2.3b and 2.3c). The molecular chains are further interwoven through weak C–H···π (involve H9, H12, H17 and H22) interactions and thus generating the alternate …ABAB… layers, along the crystallographic *b*-axis (table 2.3b, figure 2.3d).

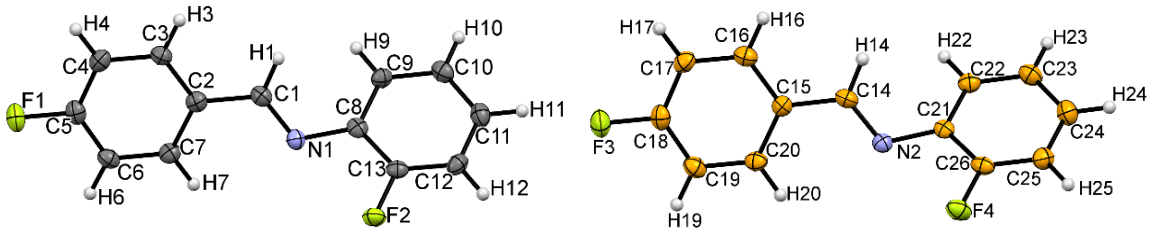

2.3a

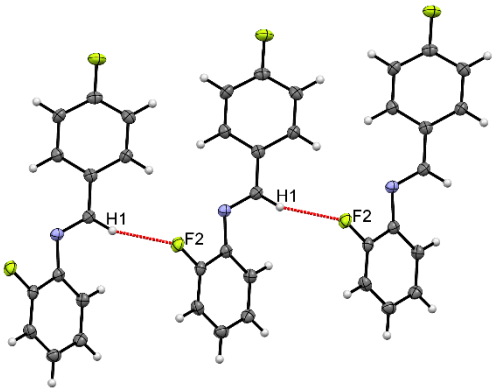

2.3b

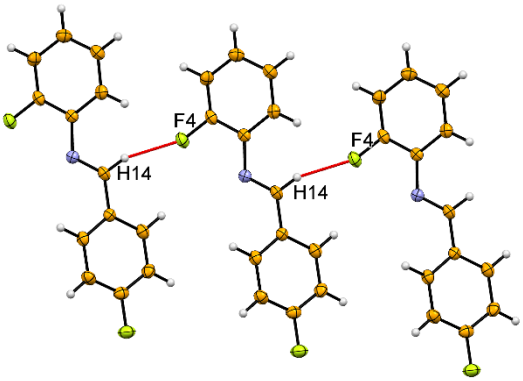

2.3c

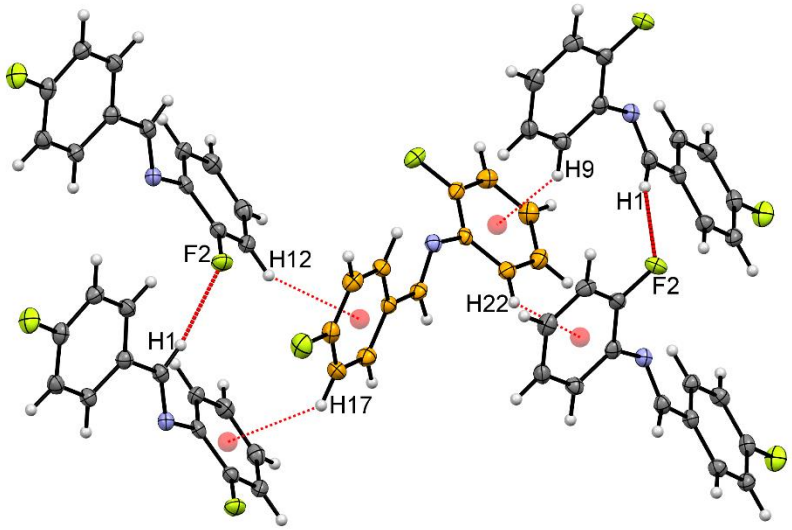

2.3d

Figure 2.3: (a) ORTEP of **3** drawn with 50% ellipsoidal probability, **(b)** formation of molecular chains of first molecule of the asymmetric unit, **(c)** formation of molecular chains (layer B) of second molecule of the asymmetric unit, **(d)** interconnection of the above formed two layers *via* C−H···π interactions, thus resulting in the formation of alternate .....ABAB..... layers in **3**.

Table 2.3a: Intermolecular interactions metrics and their stabilization energies in **3**.

Code	C–H···F	*D* C···F /Å	*d* H···F /Å	θ ∠C–H···F/º	Symmetry Code	SE_{G09} kcal/mol	*ρ* (eÅ^{-3})	$\nabla^2\rho$ (eÅ^{-5})
3	C1–H1···F2	3.214(7)	2.32	162	x+1, y, z	-4.8	0.068	1.110
	C10–H10···F2	3.357(8)	2.66	131	x, y, z-1	-0.7	0.034	0.603
	C14–H14···F4	3.242(7)	2.30	161	x-1, y, z	-4.8	0.068	1.135

Table 2.3b: Geometrical parameters for C–H···π interactions in **3**.

Code	C–H···π	C···π (Å)	H···π (Å)	∠C-H···π(°)	Symmetry Code
3	C17–H17···Cg2	3.448(6)	2.80	126	x, y, z
	C9–H9···Cg4	3.444(7)	2.66	140	-x, y+$^1/_2$, 1-z
	C22–H22···Cg2	3.414(6)	2.63	140	1-x, y-$^1/_2$, 1-z
	C12–H12···Cg3	3.642(7)	2.87	139	x+1, y, z

2.5.4. 4-fluoro-*N*-(3-fluorobenzylidene)aniline

The structure of compound **4** was solved in the triclinic centrosymmetric $P\ \bar{1}$ space group with two molecules (A and B) in the asymmetric unit (figure 2.4a). Both the molecules of the asymmetric unit were found to be disordered. The type of disorder and its refinement details have been described in detail in the section 2.3.4. The atoms of only the major conformer of both the molecules were considered for intermolecular interactions analysis (table 2.4a and 2.4b). The molecule **A** packs through the formation of layer motifs parallel to the *bc* plane with the utilization of weak C–H···F hydrogen bonds (involving H5A with F1A and H10A with F2A forming dimeric motifs) (table 2.4a, figure 2.4b). These layers join among themselves through another C–H···F hydrogen bond involving H5A with F2A to form sheets (table 2.4a, figure 2.4b). The second molecule **B** of the asymmetric unit pack in the similar manner (molecular dimer formation through C–H···F hydrogen bond involving H23A with F4A and H18A with F3A) to generate layers parallel to the *bc* plane, which further get interlinked *via* C–H···F hydrogen bond involving H18A with F4A, resulting in the formation of sheets (table 2.4a, figure 2.4c). These two sheets of the molecules **A** and **B** further interact in the lattice through weak C–H···π and C–H···F (involving H13A with F3A and H20A with F1A) intermolecular interactions (table 2.4a and 2.4b, figure 2.4d). The stabilization energies evaluated for all C–H···F hydrogen bonds present in the crystal structure of this compound range between 1.1–2.5 kcal/mol.

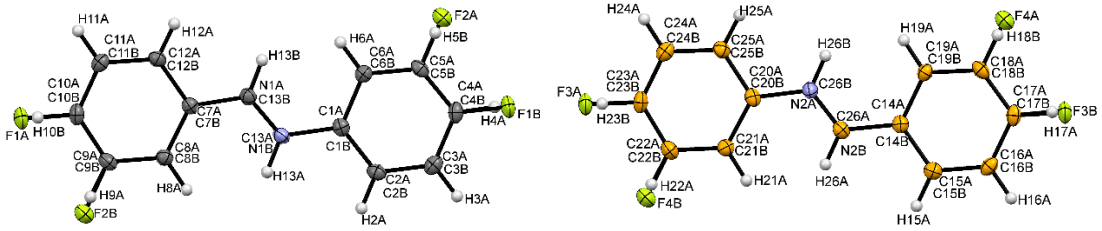

2.4a

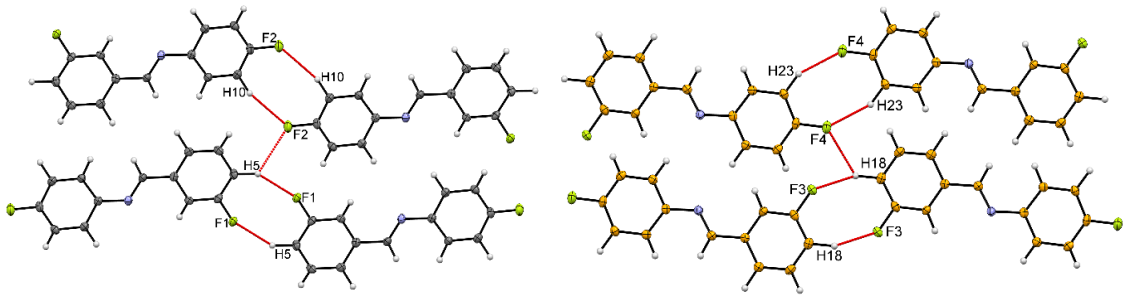

2.4c

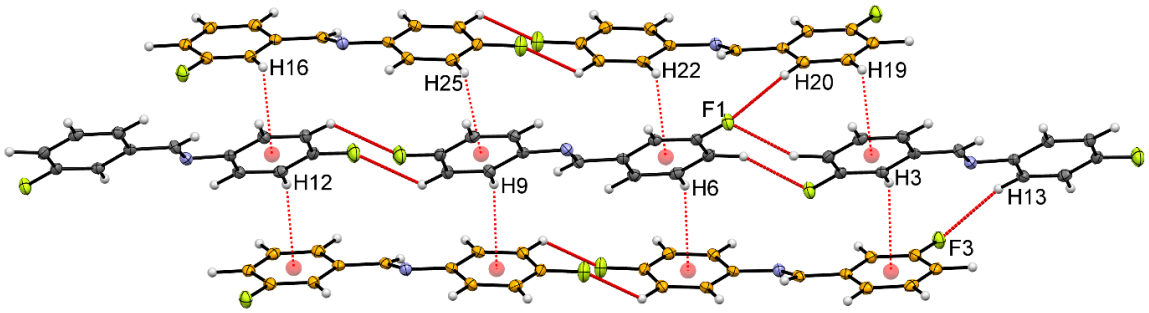

2.4d

Figure 2.4: (a) ORTEP of **4** drawn with 50% ellipsoidal probability, **(b)** formation of molecular sheets by molecules A through C−H···F hydrogen bonds, **(c)** C−H···F hydrogen bonds which interconnects molecule B and form molecular sheets, **(d)** packing of molecules displaying the formation of alternate layers of molecular sheets of A and B *via* C−H···F and C−H···π interactions in **4**.

N.B. The disordered hydrogen and carbon atoms having a lower occupancy have been omitted for clarity and also the suffix 'A' after the label of each atom has also been removed for simplicity.

Table 2.4a: Intermolecular interactions metrics and their stabilization energies in **4**

Code	C–H···F	*D* C···F /Å	*d* H···F /Å	θ ∠C–H···F/º	Symmetry Code	SE_{G09} kcal/mol	*ρ* (eÅ^{-3})	$\nabla^2\rho$ (eÅ^{-5})
4	C23A–H23A···F4	3.354(4)	2.56	140	-x, 1-y, -z-1	-1.4	0.035	0.690
	C5A–H5A···F2	3.318(3)	2.70	128	1-x, -y, 2-z	-1.1	0.026	0.543
	C18A–H18A···F3	3.274(4)	2.53	135	-x, -y, 1-z	-1.1	0.040	0.770
	C5A–H5A···F1	3.366(1)	2.56	136	x, y, z+1	-1.1	0.037	0.715
	C13A–H13A···F3*	3.494(3)	2.59	160	-x, -y, 1-z	-2.2	0.032	0.642
	C10A–H10A···F2	3.513(4)	2.50	155	x, y, z-1	-1.8	0.031	0.606

Table 2.4b: Geometrical parameters for C–H···π interactions in **4.**

Code	C–H···π	C···π (Å)	H···π (Å)	∠C-H···π(°)	Symmetry Code
4	C3A–H3A···Cg4	3.478(4)	2.80	129	x+1, y, z+1
	C15A-H15A···Cg1	3.460(4)	2.80	127	1-x, -y, 1-z
	C5A-H5A···Cg3	3.522(4)	2.84	130	-x, -y, 1-z
	C18A-H18A···Cg2	3.491(4)	2.85	126	x-1, y, z
	C9A-H9A···Cg4	3.463(4)	2.78	130	1-x, 1-y, -z
	C22A-H22A···Cg1	3.465(4)	2.75	132	x, y, z-1
	C12A-H12A···Cg3	3.436(4)	2.75	130	x, y, z
	C25A-H25A···Cg2	3.439(4)	2.72	133	-x, 1-y, -z

2.5.5. 3-fluoro-*N*-(3-fluorobenzylidene)aniline

The structure of the compound **5** is solved in the monoclinic centrosymmetric space group $P2_1/c$ with Z = 2 (Z′ = 0.5). The Z′ = 0.5 in the true molecule with no symmetry within the molecule, recommends the presence of static disorder around the imine bond (C=N), which creates the second half of the molecule around the inversion center (figure 2.5a). Linear chains involving dimeric C–H···F hydrogen bonds (SE_{G09} = -1.6 kcal/mol) (namely H5A with F1) have been in the crystal lattice of compound 5 (table 2.5a, figure 2.5b), which interlinks with the other chains in the lattice by another independent set of C–H···F hydrogen bonds, involving H4A with F1A (-2.6 kcal/mol) and C–H···π interactions, involving H5A and H2A of the aromatic ring (table 2.5a and 2.5b, figure 2.5b).

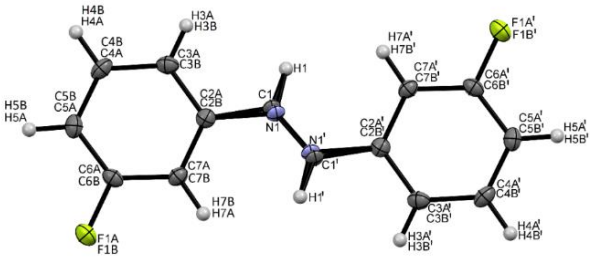

2.5a

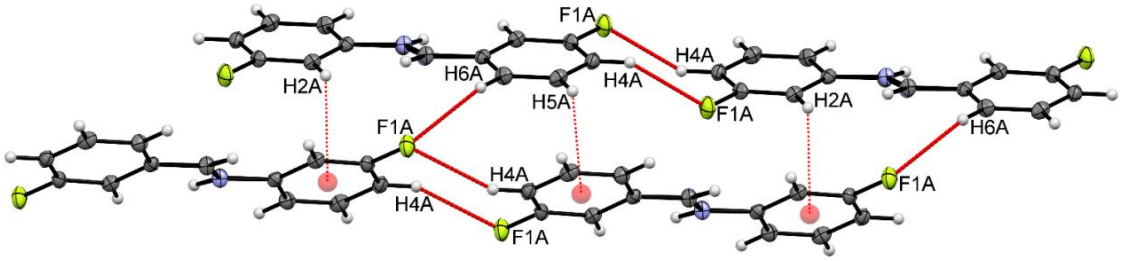

2.5b

Figure 2.5: (a) ORTEP of **5** drawn with 50% ellipsoidal probability, the atom labels with prime (′) indicates the part of the molecule, which is generated due to the presence of crystallography inversion symmetry at the C=N bond; **(b)** molecular layer formation and their linkage through C–H···F hydrogen bonds and C–H···π interactions respectively.

Table 2.5a: Intermolecular interactions metrics and their stabilization energies in **5**

Code	C–H···F	*D* C···F /Å	*d* H···F /Å	θ ∠C–H···F/º	Symmetry Code	SE_{G09} kcal/mol	ρ (eÅ^{-3})	$\nabla^2\rho$ (eÅ^{-5})
5	C4A–H4A···F1A	3.322(1)	2.52	135	2-x, -y, 1-z	-1.6	0.032	0.642
	C6A–H6A···F1A*	3.483(2)	2.53	152	x, -y-$^1/_2$, z-$^1/_2$	-2.6	0.031	0.606

Table 2.5b: Geometrical parameters for C–H···π interactions in **5.**

Code	C–H···π	C···π (Å)	H···π (Å)	∠C-H···π (°)	Symmetry Code
5	C5A–H5A···Cg1	3.512(2)	2.84	129	1-x, $^1/_2$+y, $^1/_2$-z
	C2A–H2A···Cg1	3.443(2)	2.75	130	-x, y-$^1/_2$, $^1/_2$-z

2.5.6. 2-fluoro-*N*-(3-fluorobenzylidene)aniline

Compound **6** crystallized in the orthorhombic non-centrosymmetric $P2_12_12_1$ space group with Z = 4 (figure 2.6a). A short and highly directional C–H···F hydrogen bond, involving the imine hydrogen H1 and F2 [2.47Å, 163º] leads to the formation of a

molecular ladder along the crystallographic *a* axis (table 2.6a, figure 2.6b). These molecular ladders get further interconnected through weak C–H···π (involving H5 and H10) intermolecular interactions (table 2.6b, figure 2.6c). Down the crystallographic *bc* plane, a herringbone pattern has been found in the crystal packing of this compound (figure 2.6b).

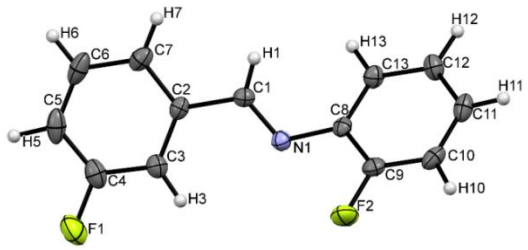

2.6a

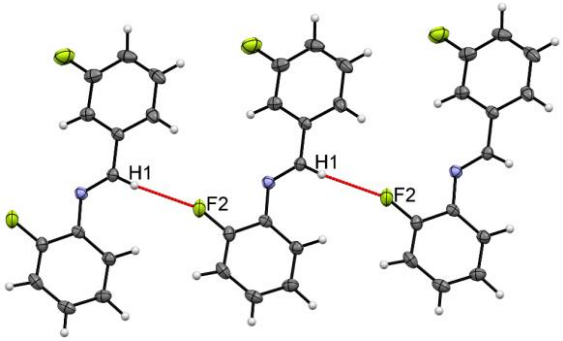

2.6b

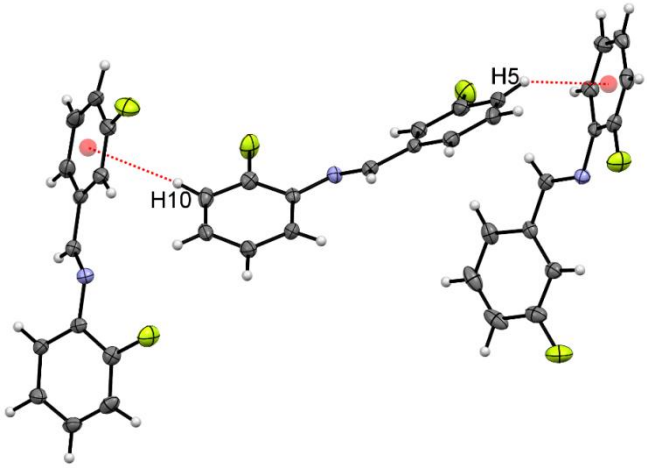

2.6c

Figure 2.6: (a) ORTEP of **6** drawn with 50% ellipsoidal probability, **(b)** formation of a molecular ladder along *b*-axis by C–H···F hydrogen bonds in **6**, which further by the utilization of C–H···π interactions show the formation of a herringbone motif**.**

Table 2.6a: Intermolecular interactions metrics and their stabilization energies in **6**

Code	C–H···F	*D* C···F /Å	*d* H···F /Å	θ ∠C–H···F/º	Symmetry Code	SE_{G09} kcal/mol	ρ (eÅ^{-3})	$\nabla^2\rho$ (eÅ^{-5})
6	C1–H1···F2	3.392(3)	2.47	163	x-1, y, z	-4.1	0.041	0.768

Table 2.6b: Geometrical parameters for C–H···π interactions in **6.**

Code	C–H···π	C···π (Å)	H···π (Å)	∠C-H···π (°)	Symmetry Code
6	C5–H5···Cg2	3.625(6)	2.78	149	1-x, $^1/_2$+y, $^1/_2$-z
	C10-H10···Cg1	3.736(1)	2.89	149	$^3/_2$-x, -y, $^1/_2$+z

2.5.7. 4-fluoro-*N*-(2-fluorobenzylidene)aniline

Compound **7** has been found to crystallize in the monoclinic centrosymmetric space group $P2_1/c$ with Z = 2 (Z′ = 0.5) (figure 2.7a). Just like in compound **5**, the presence of half of the molecules in the asymmetric unit, suggests the presence of crystallographic disorder in its crystal structure, the description about which has been given in detail in the section 2.3.4. In the crystal packing of the molecules, molecular sheet are generated *via* dimeric C–H···F hydrogen bonds, involving hydrogens H6A with F2 (-0.6 kcal/mol) and H1 with F1 (-2.6 kcal/mol) down the *bc* plane (table 2.7a, figure 2.7b). Also, the C–H···π interactions, involving H7A and H4A along with C–H···F hydrogen bonds, involving H6A and F1 (-0.1 kcal/mol) in between the sheet-like structures, provide further stability to the crystal lattice (table 2.7a and 2.7b, figure 2.7c).

Table 2.7a: Intermolecular interactions metrics and their stabilization energies in **7**

Code	C–H···F	*D* C···F /Å	*d* H···F /Å	θ ∠C–H···F/º	Symmetry Code	SE_{G09} kcal/mol	ρ (eÅ^{-3})	$\nabla^2\rho$ (eÅ^{-5})
7	C6A–H6A···F2	3.277(3)	2.54	136	2-x, -y, 1-z	-0.6	0.041	0.775
	C1–H1···F1	3.154(3)	2.32	146	1-x, 1-y, -z	-2.6	0.067	1.154
	C6A–H6A···F1*	3.241(4)	2.61	127	x, $^1/_2$-y, z+$^1/_2$	-0.1	0.035	0.596

Table 2.7b: Geometrical parameters for C–H···π interactions in **7**

Code	C-H···π	C···π (Å)	H···π (Å)	∠C-H···π (°)	Symmetry Code
7	C4A–H4A···Cg1	3.535(4)	2.86	131	$^1/_2$+x, 1-y, z-$^1/_2$
	C7A–H7A···Cg1	3.451(3)	2.78	130	x-$^1/_2$, -y, z-$^1/_2$

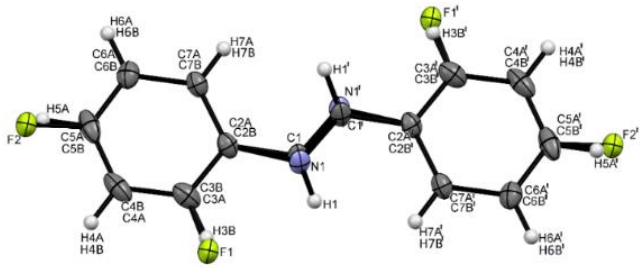

2.7a

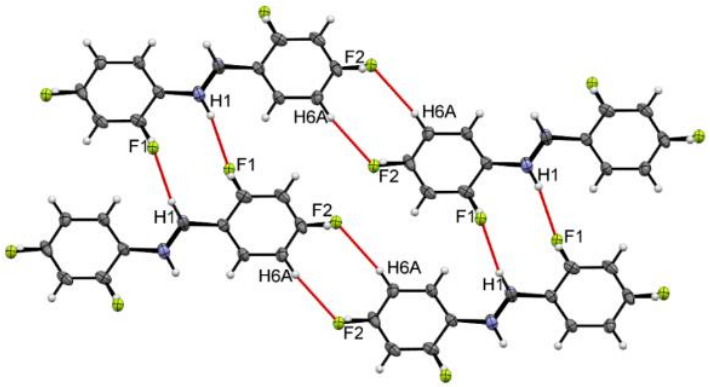

2.7b

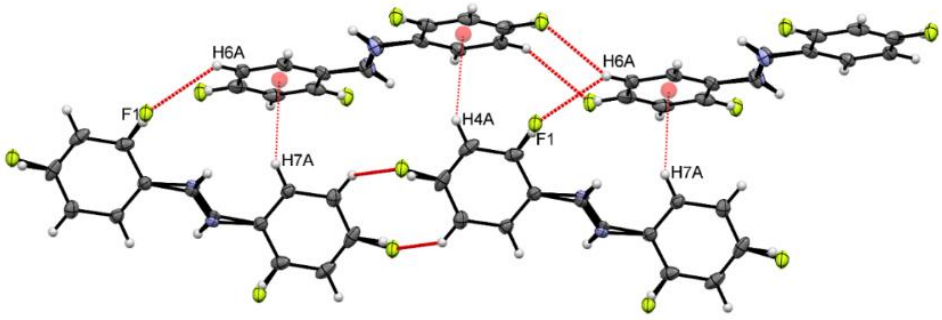

2.7c

Figure 2.7: (a) ORTEP of **7** drawn with 50% ellipsoidal probability, the atom labels with prime (′) indicates the part of the molecule, which is generated due to the presence of crystallography inversion symmetry at the C=N bond; **(b)** packing of 7 down the *bc* plane showing the formation of the molecular sheet *via* weak C–H···F hydrogen bond, **(c)** the weak C–H···π and C–H···F intermolecular interactions down the *ac* plane in **7**.

2.5.8. 3-fluoro-*N*-(2-fluorobenzylidene)aniline

Compound **8** crystallized in the monoclinic space group $P2_1/c$ with Z = 4 (figure 2.8a). The molecules in the crystal lattice leads to the formation of heterodimers by C–H···F hydrogen bonds, involving H9 and H1 with F1 (SE_{G09} = -4.8 kcal/mol) (table 2.8, figure 2.8b), which extend over the crystal lattice (figure 2.8c). C–H···F hydrogen bonds

in the crystal lattice of compound **8** have been found to be bifurcated through which molecules propagate along the crystallographic *b*-axis (again involving H9 and H1 with F1) and thus generating a chain of heterodimers along that axis.

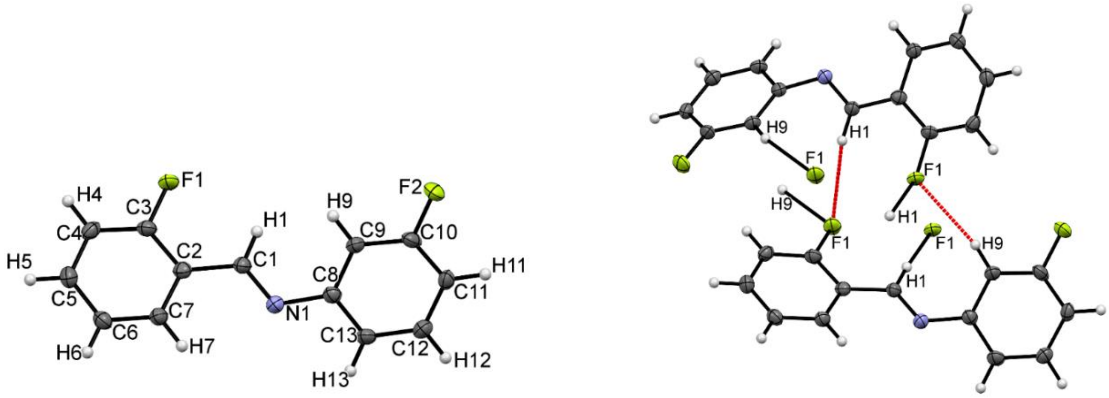

2.8a **2.8b**

Figure 2.8: (a) ORTEP of **8** drawn with 50% ellipsoidal probability, **(b)** formation of molecular heterodimeric motif by weak C–H···F hydrogen bonds in **8**.

Table 2.8: Intermolecular interactions metrics and their stabilization energies in **8**

Code	C–H···F	*D* C···F/Å	*d* H···F/ Å	θ ∠C–H···F/ °	Symmetry Code	SE_{G09} kcal/mol	*ρ* ($eÅ^{-3}$)	$\nabla^2\rho$ ($eÅ^{-5}$)
8	C1–H1···F1	3.470(7)	2.67	157	1-x, y-$^1/_2$, $^1/_2$-z	-4.8	0.038	0.734
	C9–H9···F1	3.546(6)	2.55	169	1-x, y-$^1/_2$, $^1/_2$-z		0.030	0.584

2.5.9 2-fluoro-*N*-(2-fluorobenzylidene)aniline

Compound **9** exist in two polymorphic forms, **9A**, and **9B**. But, the morphology (plate-like) of both the compounds have been found to be similar. Polymorph **9A** was crystallized from the non-polar solvent hexane while polymorph **9B** was crystallized from the polar solvent methanol (MeOH). In both the polymorphs, the conformational disorder exists around the C=N bond, which has been elaborately described in section 2.3.4.

2.5.9A 2-fluoro-*N*-(2-fluorobenzylidene)aniline (Polymorph A)

Polymorph **9A** was indexed to the monoclinic $P2_1/c$ space group with Z = 4 (figure 2.9Aa). Through weak C–H···F hydrogen bonds (involving H6 with F2, -3.1 kcal/mol) discrete molecular dimers have been found to form in the crystal lattice of **9A** and no other significant interactions were seen between these dimers (table 2.9A, figure 2.9Ab).

2.5.9B. 2-fluoro-*N*-(2-fluorobenzylidene)aniline (Polymorph B):

The second polymorph of **9** (**9B**) crystallized in the orthorhombic non-centrosymmetric $P2_12_12_1$ space group with Z = 4 (figure 2.9Ba). Bifurcated C–H···F hydrogen bonds involving H5 and H10 with F2 have been found to form in the crystal lattice of **9B** along the crystallographic *b*- and *a*- axis respectively (table 2.9B, figure 2.9Bb). It is noteworthy that no C–H···π interactions have been found in both the crystal forms of **9**.

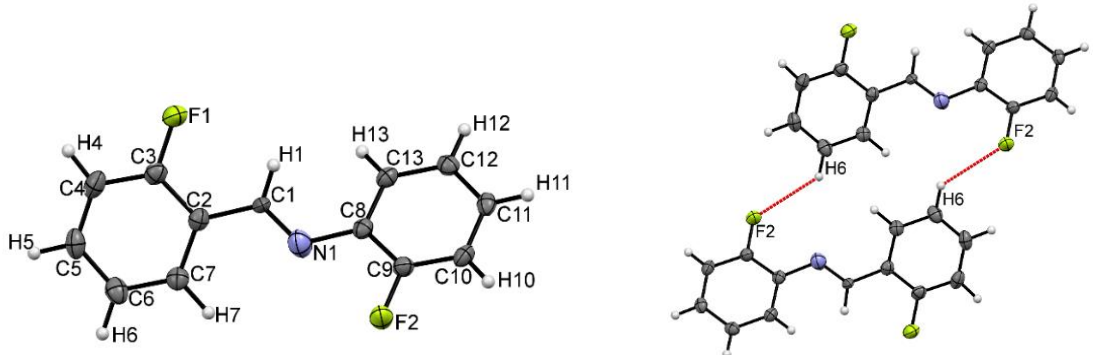

2.9Aa **2.9Ab**

Figure 2.9A: (a) ORTEP of **9A** drawn with 50% ellipsoidal probability (only the major conformer is shown), **(b)** molecular dimers formed *via* C–H···F hydrogen bonds in **9A**.

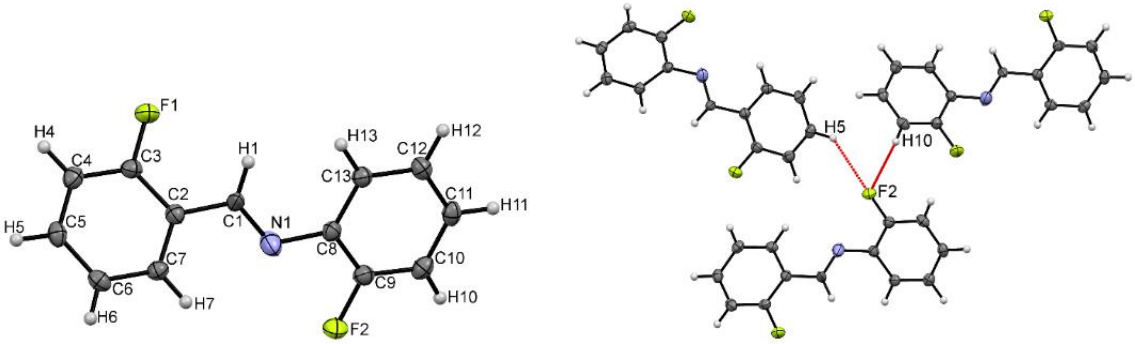

2.9Ba **2.9Bb**

Figure 2.9B: (a) ORTEP of **9B** (only the major conformer) drawn with 50% ellipsoidal probability, **(b)** molecular sheet *via* bifurcated C–H···F hydrogen bonds in **9B**.

Table 2.9A: Intermolecular interactions metrics and their stabilization energies in **9A**

Code	C–H···F	*D* C···F /Å	*d* H···F /Å	θ ∠C–H···F/°	Symmetry Code	SE_{G09} kcal/mol	*ρ* (eÅ^{-3})	$\nabla^2\rho$ (eÅ^{-5})
9A	C6–H6···F2	3.377(2)	2.68	131	-x, 1-y, 1-z	-3.1	0.026	0.560

Table 2.9B: Intermolecular interactions metrics and their stabilization energies in **9B**

Code	C–H···F	*D* C···F /Å	*d* H···F /Å	θ ∠C–H···F/º	Symmetry Code	SE_{G09} kcal/mol	ρ (eÅ^{-3})	$\nabla^2\rho$ (eÅ^{-5})
9B	C5–H5···F2	3.335(2)	2.62	132	1-x, y+$^1/_2$,$^1/_2$-z	-3.5	0.028	0.558
	C10–H10···F2	3.588(2)	2.64	176	x-$^1/_2$,$^1/_2$-y, -z	-1.9	0.027	0.555

2.5.10. *N*-benzylidene-4-fluoroaniline

This structure of **10** was solved in the monoclinic centrosymmetric $P2_1/n$ space group (figure 2.10a). Molecular sheet have been formed through bifurcated weak C–H···F hydrogen bonds, involving H4 and H6 with F1 (-1.4 kcal/mol and -1.6 kcal/mol respectively) by the utilization of 2_1 screw down the crystallographic *b*-axis (table 2.10a, figure 2.10c). Furthermore, weak C–H···π (involving H3 with Cg2, H10 and H112 with Cg1) interactions have been found in between the molecular sheets formed (table 2.10b, figure 2.10b).

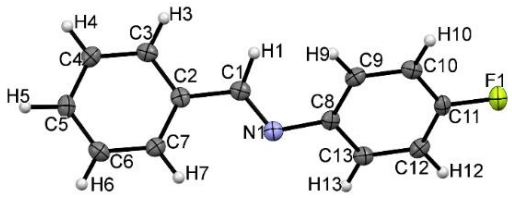

2.10a

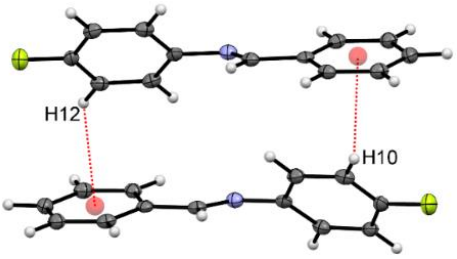

2.10b

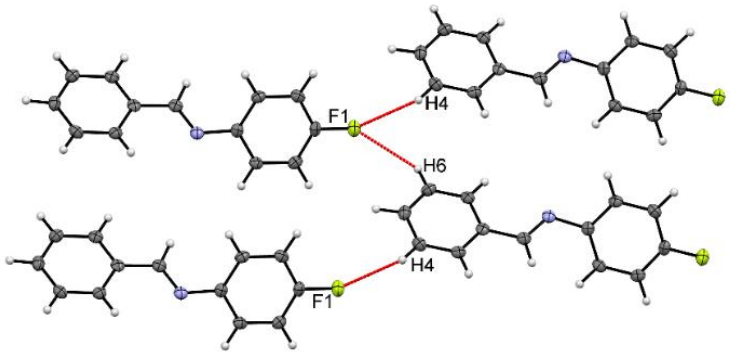

2.10c

Figure 2.10: (a) ORTEP of **10** drawn with 50% ellipsoidal probability, **(b)** View down the *ab* plane, depicting formation of molecular sheet *via* weak C–H···F hydrogen bonds in **10**, **(c)** C–H···π intermolecular interactions in the crystal lattice of **10**, viewing down the *ac* plane.

Table 2.10a: Intermolecular interactions metrics and their stabilization energies in **10**

Code	C–H···F	*D* C···F /Å	*d* H···F /Å	θ ∠C–H···F/º	Symmetry Code	SE_{G09} kcal/mol	*ρ* (eÅ^{-3})	$\nabla^2\rho$ (eÅ^{-5})
10	C4–H4···F1	3.255(2)	2.64	126	-x-$^1/_2$, y+$^1/_2$,$^1/_2$-z	-1.4	0.027	0.557
	C6–H6···F1	3.354(2)	2.66	130	$^3/_2$-x, y+$^1/_2$,$^1/_2$-z	-1.6	0.027	0.555

Table 2.10b: Geometrical parameters for C–H···π interactions in **10**

Code	C-H···π	C···π (Å)	H···π (Å)	∠C-H···π(°)	Symmetry Code
10	C3–H3···Cg2	3.407(2)	2.72	131	$^1/_2$+x, $^1/_2$-y, z-$^1/_2$
	C7–H7···Cg2	3.717(2)	2.98	128	x-$^1/_2$, $^1/_2$-y, z-$^1/_2$
	C10–H10···Cg1	3.552(2)	2.84	134	$^1/_2$+x, $^1/_2$-y, $^1/_2$+z
	C12–H12···Cg1	3.514(2)	2.84	130	x-$^1/_2$, $^1/_2$-y, z-$^1/_2$

2.5.11. *N*-benzylidene-3-fluoroaniline

Compound **11** was indexed to the monoclinic centrosymmetric $P2_1/c$ space group with Z = 4 (figure 2.11a). It is worth mentioning that this compound was crystallized using *in situ* crystallization technique and in this process cooling of the low-melting liquid results in trapping of both the major and minor conformer of this molecule. A 180° rotation of the entire molecule around the shorter axis results in the occurrence of the observed conformations, which is a very rare process because of the involvement of the steric interactions with the neighbouring molecules in the crystalline lattice.[129(a)]

During the packing analysis of **11**, the interactions involving only the major conformer have been considered for simplicity. In its crystal lattice, molecular chains involving weak C–H···F interactions (involving H9A with F1A, -3.3 kcal/mol) have been found to form with the utilization of *c*-glide (table 2.2a, figure 2.11b). These chains are further interconnected through dimeric C–H···π interactions involving H6A (table 2.2b, figure 2.11c).

Table 2.11a: Intermolecular interactions metrics and their stabilization energies in **11**

Code	C–H···F	*D* C···F /Å	*d* H···F /Å	θ ∠C–H···F/º	Symmetry Code	SE_{G09} kcal/mol	*ρ* (eÅ^{-3})	$\nabla^2\rho$ (eÅ^{-5})
11	C9A–H9A···F1A	3.412(11)	2.42	164	x, $^1/_2$-y, z+$^1/_2$	-3.2	0.064	1.102

Table 2.11b: Geometrical parameters for C–H···π interactions in **11.**

Code	C-H···π	C···π (Å)	H···π (Å)	∠C-H···π (°)	Symmetry Code
11	C6A-H6A···Cg2	3.605(9)	2.86	136	1-x, -y, -z

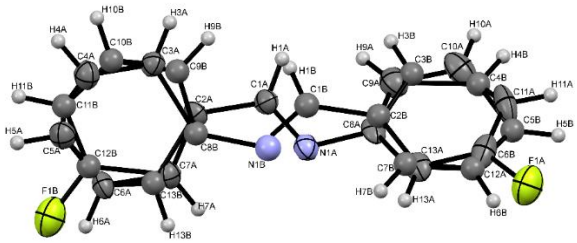

2.11a

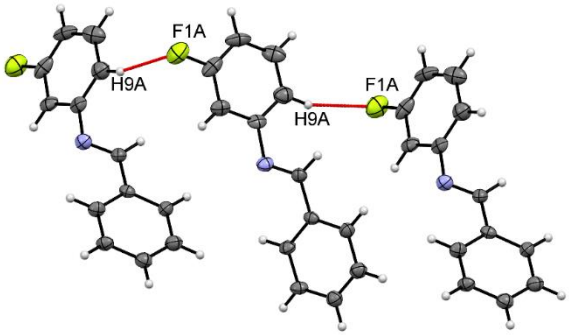

2.11b

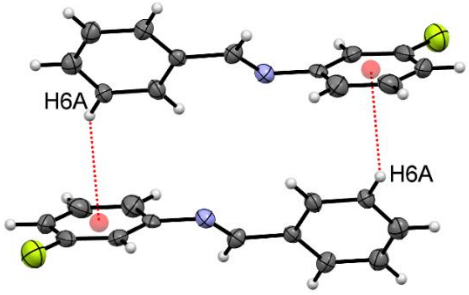

2.11c

Figure 2.11: (a) ORTEP of **11** drawn with 50% ellipsoidal probability, **(b)** formation of molecular chains through, **(c)** dimeric C–H···π intermolecular interactions in **11**, which interconnect the chains formed in figure 11(b).

2.5.12. *N*-benzylidene-2-fluoroaniline

Compound **12** crystallized in the orthorhombic non-centrosymmetric $P2_12_12_1$ space group with Z = 4 (figure 2.12a). A short and highly directional C–H···F hydrogen bond (2.32Å, 168°, -3.9 kcal/mol), involving the imine hydrogen H1 with F1 have been found to pack the molecules along the crystallographic *a*-axis (table 2.12a, figure 2.12b). These molecular chains unify along the crystallographic *b*-axis through weak C–H···π (involving H5 with Cg2) interactions (table 2.12b, figure 2.12b). The herringbone pattern has been found in the crystal packing of **12**, with the utilization of weak C–H···N (involving H11 with N1) and C–H···π (involving H12) intermolecular interactions (table 2.12a, and 2.12b, figure 2.12c).

Table 2.12a: Intermolecular interactions metrics and their stabilization energies in **12**

Code	C–H···F	*D* C···F /Å	*d* H···F /Å	θ ∠C–H···F/º	Symmetry Code	SE_{G09} kcal/mol	ρ (eÅ^{-3})	$\nabla^2\rho$ (eÅ^{-5})
12	C1–H1···F1	3.387(2)	2.38	171	x-1, y, z	-3.9	0.067	1.112
	C9–H9···N1	3.552(2)	2.69	147	x-$^1/_2$, $^3/_2$-y, 2-z	-0.4	0.031	0.606

Table 2.12b: Geometrical parameters for C–H···π interactions in **12**

Code	C-H···π	C···π (Å)	H···π (Å)	∠C-H···π(°)	Symmetry Code
12	C5–H5···Cg2	3.617(2)	2.78	148	2-x, y-$^1/_2$, $^1/_2$-z
	C12-H12···Cg1	3.717(1)	2.86	150	$^3/_2$-x, 1-y, $^1/_2$+z

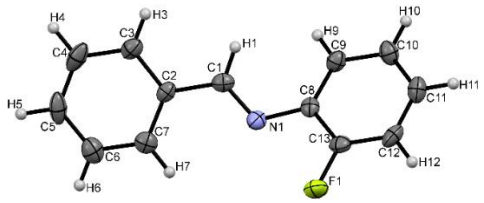

2.12a

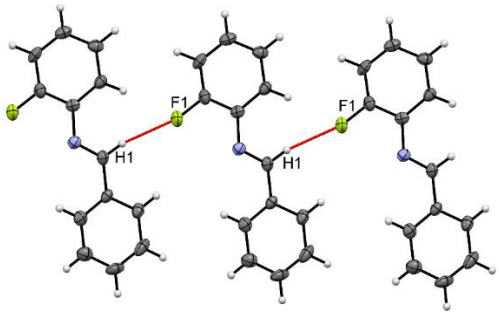

2.12b

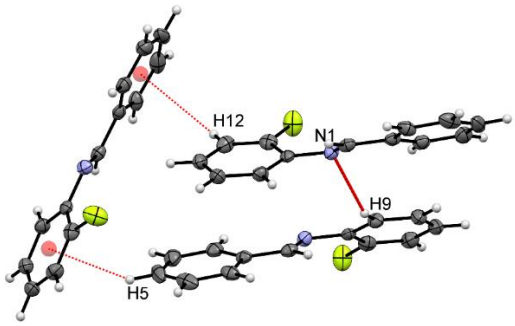

2.12c

Figure 2.12: (a) ORTEP of **12** drawn with 50% ellipsoidal probability, **(b)** packing view down the *ab* crystallographic plane *via* weak C–H···F and C–H···π intermolecular interactions in **12**, **(c)** weak C–H···N and C–H···π interactions leading to the formation of a herringbone sheet down the *bc* plane in **12**.

2.5.13. *N*-(4-fluorobenzylidene)aniline

Compound **13** was indexed to the triclinic centrosymmetric space group $P\ \bar{1}$ with $Z = 2$ (figure 2.13a). The molecules in the crystal leads to the formation of molecular sheets in the *ac* plane through bifurcated weak C–H···F hydrogen bonds, involving H12 and H10 with F1 (-1.3 kcal/mol and -1.3 kcal/mol respectively) (table 2.13a, figure 2.13b). Further, through C–H···π interactions, involving acidic H4 and H6 with electron- rich phenyl ring Cg2 and H9 and H13 with Cg1, these sheets get interlinked (table 2.13b, figure 2.13c and 2.13d).

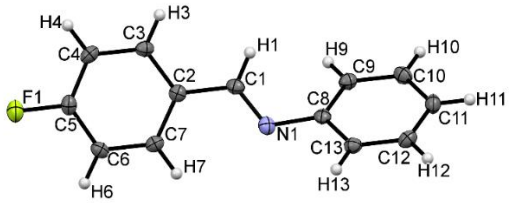

2.13a

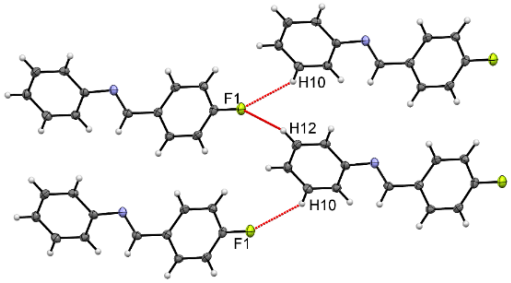

2.13b

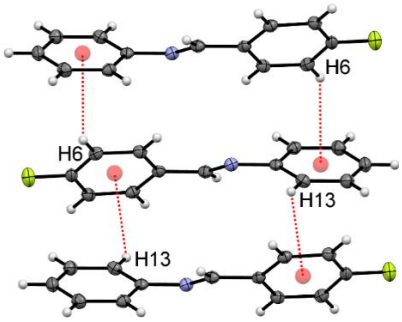

2.13c

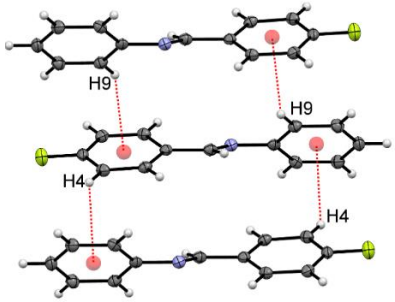

2.13d

Figure 2.13: (a) ORTEP of **13** drawn with 50% ellipsoidal probability, **(b)** molecular sheet down the *ac* plane *via* bifurcated weak C–H···F hydrogen bonds in **13**, **(c)** molecular sheets interacting through C–H···N hydrogen bonds across the inversion center, **(d)** packing of molecules in **13** *via* weak C–H···π intermolecular interactions.

Table 2.13a: Intermolecular interactions metrics and their stabilization energies in **13**

Code	C–H···F	*D* C···F /Å	*d* H···F /Å	θ ∠C–H···F/º	Symmetry Code	SE_{G09} kcal/mol	*ρ* (eÅ^{-3})	$\nabla^2\rho$ (eÅ^{-5})
13	C10–H10···F1	3.290(2)	2.65	124	x, y, 1+z	-1.3	0.034	0.659
	C12–H12···F1	3.272(2)	2.66	128	x-1, y, 1+z	-1.3	0.032	0.651

Table 2.13b: Geometrical parameters for C–H···π interactions in **13**

Code	C–H···π	C···π (Å)	H···π (Å)	∠C–H···π(°)	Symmetry Code
13	C4–H4···Cg2	3.506(2)	2.82	129	1-x, -y, -z
	C6–H6···Cg2	3.538(2)	2.83	132	2-x, 1-y, -z
	C9–H9···Cg1	3.478(2)	2.71	136	1-x, 1-y, -z
	C13–H13···Cg1	3.610(2)	2.92	128	2-x, -y, -z

2.5.14. *N*-(3-fluorobenzylidene)aniline

This compound was found exist in the liquid state at 25°C. Several attempts to grow single crystal using *in situ* crystallization technique were unsuccessful. The compounds always led to the formation of glassy material on cooling and did not show any sign of crystallization on several cooling and heating cycles using the Oxford cryosystem. This process was followed by recurring attempts to allow for sudden heating or cooling by switching off the CO_2 LASER. Hence, the structure of this compound could not be determined.

2.5.15. *N*-(2-fluorobenzylidene)aniline

This compound also exists in the liquid state at 25°C. Numerous tries to crystallize the compound by cooling it to 200 and then to 150 K, were failed. OHCD was also used to prompt crystallization by a sudden thermal shock to the liquid at 200K. But all our attempts to crystallize **15** were unsuccessful. Hence, the structure of this compound could also not be determined.

2.6 Discussion

In-depth structural investigation of these thirteen compounds in the series of fluorine substituted *N*-benzylideneanilines helps us to understand the role of weak intermolecular interactions in stabilizing the crystal packing in the absence of any strong hydrogen bonds. The crystal packing in these compounds are found to be mainly directed by the short, significantly directional (in some cases almost linear) C–H···F and C–H···π interactions (tables 2.1a/b to 2.13a/b). The stabilization energies associated with the weak C-H···F hydrogen bonds for different supramolecular motifs have also been calculated and the values are listed in the corresponding interaction tables. The stabilization energies have been found to be in the range from 1 to 5 kcal/mol. The hydrogen bond type character of C–H···F interactions has been indicated by recent charge density analyses[124] and also from

the crystallographic database studies.[73(a)] In the current study, the stabilization energies of the dimers interacting through C−H···F hydrogen bonds, with a H···F distance between 2.2 and 2.67 Å and the angle ∠C−H···F ranging between 130° and 168° are higher (3 kcal/mol or more). Probably these weak C −H···F hydrogen bonds monitors the preorganization of the molecules in the formation of molecular layers or chains and then, such layer of molecules are adhered with the adjacent layers by the involvement of weak C −H···π interactions and additional independent C −H···F hydrogen bonds.

It is worth comparing the similarities and differences, which occur in the crystal packing on substitution of the fluorine atom on the molecular framework containing the *N*-benzylideneaniline moiety. The parent compound, *N*-benzylideneaniline exist in the monoclinic $P2_1/c$ space group with Z = 4 [a = 12.1211(9) Å, b = 7.7182(5) Å, c = 11.8429(9) Å, β = 118.341(1)°].[125] In the crystal packing of *N*-benzylideneaniline,[129] molecules are arranged in such a way that their long axis becomes parallel to the crystallographic *a*-axis. The incorporation of the fluorine atom at the *ortho*- position in case of **12** has fully transformed the crystal structure (orthorhombic $P2_12_12_1$) in comparison to the unsubstituted one. While, the compound with the substitution of the fluorine atom at the *meta*- position in *N*-benzylideneaniline (compound **11**) has been found to be isostructural[126] with the parent compound. Furthermore, the substitution of a fluorine atom at the *para*-position on either of the phenyl ring (compounds **10** and **13**) has resulted in entirely different packing characteristics in comparison to its unsubstituted analogue. Though, the former (**10**) crystallized in the monoclinic $P2_1/n$ space group and the latter (**13**) in the triclinic $P\ \bar{1}$, yet the packing features of both these compounds **10** and **13** have been found to be similar. The relationship between the lattice parameters of these compounds is, $a = a'$; $b = 2c'$; $c = b'$ wherein *a*, *b*, *c* and a', b', c' are the lattice parameters of **10** and **13** respectively. It is also an interesting observation that compounds **1** (difluorinated) and **13** (monofluorinated) crystallize in the identical space group (triclinic $P\ \bar{1}$), and display isostructurality in the solid state (figure 2.1b and 2.13b). The isostructural behaviour has also been exhibited by the compounds **6** and **12**. Both these compounds display the formation of short, directional and highly stabilizing C–H···F hydrogen bonds in their crystal lattices (figure 2.6b and 2.12b). Compound **9**, in which fluorine atoms are substituted at the *ortho*- position of both the phenyl rings possess two polymorphic forms; the monoclinic form being centrosymmetric and the orthorhombic form being non-centrosymmetric. The positional disorder has been exhibited in both these forms (**9A** and

9B), but dissimilarity has been procreated in terms of the nature of weak C–H···F hydrogen bonds. It is presumed that the presence of both crystallographic and orientational disorder has given rise to the generation of polymorphs.

The Cambridge Structural Database[127] search[128] has been done for *N*-benzylideneaniline derivatives to link the packing features of the related compounds with the present series of compounds. Crystal structures containing any strong hydrogen bond donor (e.g. hydroxyl and amino groups) or acceptor (amino nitrogen and oxygen) groups have not been chosen for the comparison.

The crystal packing of compounds containing bromo[129(a)], chloro[129(b),(c)] and cyano[129(d)] groups at the *para*- position of both the phenyl rings (**BRZBRA, CBZCAN/01, AMEREQ**) possess different packing features than its fluorinated analogue (compound **1**). The **CBZCAN** (chlorine substitution at the *para* position on both side) possess Cl···Cl interactions with no C–H···Cl contacts in its crystal packing, while the latter have C–H···F hydrogen bonds. This ascertains the fact that fluorine, unlike other halogens, prefers C–H···F rather than F···F interactions.

Furthermore, substitutional analogues of compound **2** (*para* to the benzaldehyde ring and *meta* to the aniline ring) are **RONKEK**[129(e)] **(Cl, *p, m*); RONKIO**[129(e)] **(Br, *p, m*), RONKOU**[129(e)] **(Br, *p*; Cl, *m*;), RONKUA**[129(e)] **(Cl, *p*; Br, *m*)**. The chloro and bromo analogues of **2** have similar unit cell dimensions and thus could be isostructural (monoclinic, non-centrosymmetric $P2_1$), whereas **2** was indexed to the monoclinic centrosymmetric $P2_1/c$ space group. In the similar manner, structural analogues of **4**, where one substituent is present at the *meta* position of the benzaldehyde ring and other at the *para* position of the aniline ring, i.e. **RONLAH (Cl, *m*; Br, *p*;)**, **RONLEL**[129(e)] **(Br, *m, p*)**, also depict isostructurallity among themselves (centrosymmetric monoclinic, $P2_1/c$), while compound **4** has been found to crystallize in the triclinic $P\bar{1}$ with Z′ = 2.

The crystal structures of other halogen substituted *N*-benzylideneanilines [*meta* to both the benzaldehyde and aniline moieties] resulted in the following CSD REFCODES: **WEMHUR**[129(f)] **(Cl, *m, m*)** (crystallized in the monoclinic $P2_1/n$) were found to be different than that of the related halogenated analogue **WEMJAZ**[129(f)] **(Cl: *m*; Br: *m*)**, **WEMJED**[129(f)] **(Br, *m, m*)**, **WEMJIH**[129(f)] **(Br, *m*; Cl, *m*)**, which crystallized in the orthorhombic non-centrosymmetric $P2_12_12_1$ space group. Among these, the unit cell dimensions and packing features of only **WEMJAZ** and **WEMJED** shows isostructurality. The only reported analogue of compound **7** in the CSD is 4-Bromo-*N*-(2-

chlorobenzylidene)aniline (**EVONEJ**),[129(e)] the crystal packing of which was found to be entirely altered from its fluorinated analogue.

It is evident from the above discussion that the parent moiety have resulted into different structural motifs with the incorporation of the fluorine atoms at different positions on either one or on both the rings. It is noteworthy that positional and crystallographic disorder have a significant contribution in deciding the conformation and stability of the molecule in the solid state. In the crystal structures of these compounds, well-defined supramolecular motifs involving organic fluorine have been observed which steer the packing of molecules in the absence of strong hydrogen bond donors, but with the support of weak C–H···π interactions. The stabilizing role of C–F group in altering the crystal packing through the presence of weak, but cooperative C–H···F hydrogen bonds get further highlighted through these observations.

2.7 Conclusions

It has been shown through the thorough structural studies of the thirteen structures in this chapter, that 'organic fluorine' is capable of guiding the packing of molecules in the crystal lattice by the formation of various supramolecular synthons majorly involving C–H···F hydrogen bonds. The *N*-benzylideneaniline molecular skeleton allows to investigate the changes that get manifested when a fluorine atom is substituted on the phenyl ring and its position is varied over the phenyl ring. Variation in the position of the substituent is equivalent to the change in the electronic feature of the molecule. This variation has resulted in the positional disorder in the crystal structures in addition to the conformational changes in the parent moiety. It is obvious from in-depth structural analysis of these molecules along with their related compounds in the CSD that there is a delicate interplay of steric and electronic factors that direct the final molecular conformation and subsequent crystal packing in these compounds. This understanding may also have implications in the serendipitous phenomenon of polymorphism in the solid state. Several supramolecular synthons, (namely dimers and chains), based on C–H···F hydrogen bonds have been identified in these structures. The stabilization energies of the dimer, interacting through C–H···F hydrogen bonds are in the range of 1-5 kcal/mol. It is also noteworthy that C–H···F hydrogen bonds with H···F distance between 2.2 to 2.65 Å and the angle ∠C–H···F ranging between 130 and 165^{o} provide higher stabilization energies (3 kcal/mol or more) to the concerned dimers. It has been presumed through the current study that probably weak

C–H···F hydrogen bonds control the pre-organization of the molecules in the formation of molecular layers, which are held together by the involvement of weak C–H···π interactions, and additional independent C–H···F hydrogen bonds.

Chapter 3

Structural Investigation on Replacement of Fluorine by Chlorine/Bromine in Dihalogenated *N*-benzylideneanilines

Chapter 3

3.1 Introduction

The structural landscape of mono and di-fluorinated *N*-benzylideneanilines have been investigated in the previous chapter. Our observation in the previous chapter indicated that organic fluorine plays a significant role in directing the crystal packing through various intermolecular interactions in the absence of strong hydrogen bonds. The energetics and topological features of these interactions indicate that the C–H···F hydrogen bonds are weak in nature, but shows directionality to a great extent. Among the structural studies in the previous chapter 2, we came across different supramolecular synthons offered by C–F group and we have also shown that the change in the position of the fluorine atom resulted in an entirely different packing features of the molecules in the cases of mono and di-fluorinated *N*-benzylideneanilines. Through the stabilization energy calculations of the concerned dimers, we have pointed out that the C–H···F hydrogen bonds showed significant directionality ($\angle$C–H···F >160^{o}). In this chapter, we intend to extend our analysis to another series of halogen (F, Cl, and Br) substituted *N*-benzylideneanilines (Scheme 3.1), which provide us the opportunity to study the role of very weak hydrogen bonds (C–H···X, X = F, Cl and Br) and other weaker interactions (such as C–X···X and C–X···π, X = F, Cl and Br) offered by various C–X (X = F, Cl and Br) groups present at different positions on the aromatic rings. Herein, the structural comparison has been done between the di-fluorinated *N*-benzylideneanilines with the structures of molecules made by replacing one of the fluorine atoms of the previous system by either Cl or Br. In this chapter, we intend to present the various types of supramolecular motifs offered by fluorine,

chlorine and bromine in identical chemical environment and aim to determine the strengths and the directionality of these intermolecular forces in the crystal lattices.

Scheme 3.1

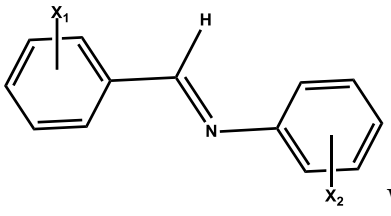

Where X_1, X_2 = -F, -Cl, -Br ; $X_1 \neq X_2$

3.2 Synthesis and Characterization

All the starting materials, namely *ortho*-, *meta*- and *para*- halogenated benzaldehydes and anilines were purchased from Sigma-Aldrich and were used without further purification. Equimolar amounts of corresponding benzaldehyde and aniline were dissolved in dichloromethane (DCM) at 298 K. To this mixture, anhydrous Na_2SO_4 was added to remove the water molecules produced during the condensation reaction. The solution was stirred for ~10 minutes and then the solvent was evaporated under reduced pressure to get the condensed product. Pure crystals were obtained by recrystallization from different organic solvents like methanol, ethanol, hexane, ethyl acetate, chloroform, and DCM. All the synthesized compounds were characterized by ^{1}H NMR (400MHz, Bruker Biospin Avance-III NMR spectrometer) (ESI, figures S3.1:1 to S3.1:36) and FTIR (Bruker Tensor 72, equipped with diamond cell ATR) (ESI, figures S3.2:1 to S3.2:36) spectroscopy.

Scheme 3.2 describes the scheme for the synthesized compounds and the method of nomenclature used in this manuscript. The structures of first nine compounds belonging to this scheme have already been analyzed in the first chapter. Out of 36 (**16** to **51**, Table 3.I) newly synthesized compounds, 27 compounds were found to be solids at room temperature (25 ^{o}C), while the remaining nine compounds (**20**, **27**, **29**, **30**, **38**, **44**, **45**, **47**, and **48**) were found to be liquids. Compound **16**, **18**, **36** and **22** were found to exhibit polymorphism. In the further discussion we will use '**A**' as an abbreviation for the phenyl ring originating from benzaldehyde group and '**B**' for the phenyl ring originating from aniline moiety.

Scheme 3.2:

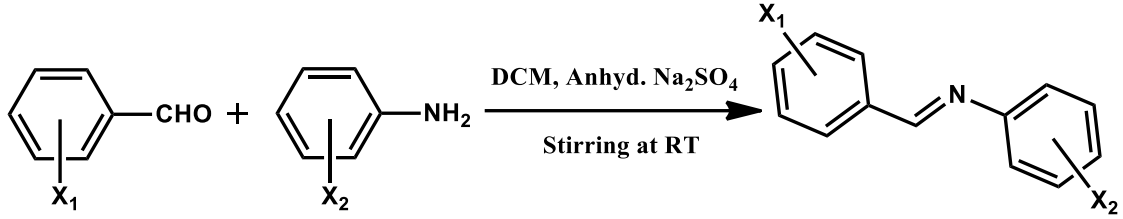

Where X_1, X_2 = -F, -Cl, -Br ; $X_1 \neq X_2$

Table 3.1: Compound Identification Table

Code	X_1	X_2
1	p-F	p-F
2	p-F	m-F
3	p-F	o-F

Code	X_1	X_2
4	m-F	p-F
5	m-F	m-F
6	m-F	o-F

Code	X_1	X_2
7	o-F	p-F
8	o-F	m-F
9	o-F	o-F

Code	X_1	X_2
16	p-Br	p-F
17	p-Br	m-F
18	p-Br	o-F

Code	X_1	X_2
19	m-Br	p-F
20*	m-Br	m-F
21	m-Br	o-F

Code	X_1	X_2
22	o-Br	p-F
23*	o-Br	m-F
24	o-Br	o-F

Code	X_1	X_2
25	p-F	p-Br
26	p-F	m-Br
27*	p-F	o-Br

Code	X_1	X_2
28	m-F	p-Br
29*	m-F	m-Br
30*	m-F	o-Br

Code	X_1	X_2
31	o-F	p-Br
32	o-F	m-Br
33	o-F	o-Br

Code	X_1	X_2
34	p-Cl	p-F
35	p-Cl	m-F
36	p-Cl	o-F

Code	X_1	X_2
37	m-Cl	p-F
38*	m-Cl	m-F
39	m-Cl	o-F

Code	X_1	X_2
40	o-Cl	p-F
41	o-Cl	m-F
42	o-Cl	o-F

Code	X_1	X_2
43	p-F	p-Cl
44*	p-F	m-Cl
45*	p-F	o-Cl

Code	X_1	X_2
46	m-F	p-Cl
47*	m-F	m-Cl
48*	m-F	o-Cl

Code	X_1	X_2
49	o-F	p-Cl
50	o-F	m-Cl
51	o-F	o-Cl

* indicates the compounds which are found to be liquids at 25 ºC. Out of these liquid compounds, structures of only **23** and **44** could be determined.

3.3 Crystallography:

3.3.1 Powder X-ray Diffraction

As described in the previous chapter, PXRD patterns were recorded on a Rigaku Ultima IV diffractometer following the same experimental conditions. The observed PXRD patterns have been compared (using WINPLOTR[110]) with the simulated PXRD patterns generated from the crystal coordinates using Mercury[111] (ESI, figures S3.3:1 to S3.3:28). All the PXRD patterns are reported in the ESI.

3.2 Crystal Growth, Single Crystal Data Collection, Structure Solution and Refinement

Single crystals of desired size and quality were grown by slow evaporation by dissolving compound in different solvents or solvent mixtures such as methanol, ethanol, toluene, DCM/hexane, chloroform/hexane, ethyl acetate/hexane, methanol/hexane and acetone/hexane. Table 3.1 describes the method of nomenclature used in this study for all the obtained isomeric molecules.

The details of the single crystal X-ray data collection and data reduction for all the compounds are the same as given in the second chapter. The crystallographic tables for all the compounds are included in the discussion of the respective groups.

3.3.3 Crystal Growth and Data Collection for Liquids

Out of 36 synthesized compounds, compounds **20**, **23**, **27**, **29**, **30**, **38**, **44**, **45**, **47** and **48** were found to be liquids at room temperature (25 ^{o}C). Out of these, the structure of compound **23** (Melting point 22 ^{o}C) could be determined when the room temperature was around 20 ^{o}C. The structure of compound **44** was determined by *in situ* crystallization technique. The compound was mounted on the diffractometer as described in the previous chapter. But, the strategy applied for its crystallization was different, which is explained below.

To solidify the liquid, the capillary was first cooled at 200K/hr to 180K. At the same rate, then it was heated from 180 to 220K. Still images were taken from time to time to see if there is any formation of crystals. It has been seen that at 210 K, compound got converted into a polycrystalline material. After that, the compound was heated at 200 K/hr from 220 K to 260 K. But, it remained polycrystalline. Then at 260 K, a few cycles of zone melting scans using the CO_2 LASER of the OHCD were repeated for 6 hours to grow single crystal in the capillary. After the formation of a single crystal, one ϕ scan (scan width 0.3°, 1200

frames) data were collected keeping ω and κ fixed at 0° and the detector was fixed at 30° with a distance of 6.0 cm.

For the rest of the liquid compounds, the single crystal structure could not be determined as all those compounds were not crystallizing even by repeated heating or cooling cycles. Rather, they were forming only glassy material. DSC's of all those compounds have not shown any features too except in compound **29**, where a sharp peak has been seen in DSC, but still could not be crystallized *in situ*.

3.3.4. Crystallographic Modelling of Disorder

The compounds **33** and **51** were found to exhibit positional disorder due to in-plane flipping of the molecule around the C=N bond. But compounds **23** and **41** were found to have positional disorder due to the rotation of the aniline ring around the C8–N1 bond. All these positional disorders were treated following the same procedure described in the earlier chapter. The occupancy ratio for the two parts in **23**, **41**, **33**, and **51** were found to be 0.617(4):0.383(4), 0.525(2):0.475(2), 0.909(1):0.091(1), and 0.544(2):0.456(2) respectively.

3.4 Theoretical Calculations

The gas phase stabilization energies of the dimers involving C–H···F hydrogen bonds have been calculated using Gaussian09 as described in the chapter 2. Furthermore, the topological properties of the electron density, are also studied for C–H···F hydrogen bonds as has been explained in detail in chapter 2. The electron density (ρ), and the Laplacian of the electron density ($\nabla^2\rho$) at the (3, -1) bond critical points (BCPs) are listed in the tables containing the geometrical parameters of the intermolecular interactions.

3.5 Results

Among the compounds studied herein, four compounds (**16**, **18**, **36** and **28**) exhibited polymorphism. We aim to present the structural comparison of the new compounds with those discussed in the second chapter. For better understanding, we had sub-divided all the compounds into various groups such that the halogen substitution in one ring is kept constant and the same is varied in the other ring.

Class 1. When F is at the *para* position of the A ring

1a. The *para* position of B ring is substituted by F, Cl and Br. (**1**, **43**, **25**)

1b. The *meta* position of B ring is substituted by F, Cl and Br (**2**, **44**, **26**)

1c. The *ortho* position of B ring is substituted by F, Cl and Br (**3**, **45**, **27**)

Class 2. When F is at the *meta* position of the A ring

2a. The *para* position of B ring is substituted by F, Cl and Br. (**4**, **46**, **28**)

2b. The *meta* position of B ring is substituted by F, Cl and Br (**5**, **47**, **29**)

2c. The *ortho* position of B ring is substituted by F, Cl and Br (**6**, **48**, **30**)

Class 3. When F is at the *ortho* position of the A ring

3a. The *para* position of B ring is substituted by F, Cl and Br. (**7**, **49**, **31**)

3b. The *meta* position of B ring is substituted by F, Cl and Br (**8**, **50**, **32**)

3c. The *ortho* position of B ring is substituted by F, Cl and Br (**9**, **51**, **33**)

Class 4. When F is at the *para* position of the B ring

4a. The *para* position of A ring is substituted by F, Cl and Br. (**1**, **34**, **16**)

4b. The *meta* position of A ring is substituted by F, Cl and Br (**4**, **37**, **19**)

4c. The *ortho* position of A ring is substituted by F, Cl and Br (**7**, **40**, **22**)

Class 5. When F is at the *meta* position of the B ring

5a. The *para* position of A ring is substituted by F, Cl and Br. (**2**, **35**, **17**)

5b. The *meta* position of A ring is substituted by F, Cl and Br (**5**, **38**, **20**)

5c. The *ortho* position of A ring is substituted by F, Cl and Br (**8**, **41**, **23**)

Class 6. When F is at the *ortho* position of the B ring

6a. The *para* position of A ring is substituted by F, Cl and Br. (**3**, **36**, **18**)

6b. The *meta* position of A ring is substituted by F, Cl and Br (**6**, **39**, **21**)

6c. The *ortho* position of A ring is substituted by F, Cl and Br (**9**, **42**, **24**)

Structural comparison of the compounds belonging to class 1a and 4a

The compound **1** (with F at the *para* position of both the rings) have been found to crystallize in the centrosymmetric triclinic $P\bar{1}$ space group with Z = 2. The packing of the molecules of **1** in its crystal structure reveals the formation of molecular sheets through C−H···F hydrogen bonds involving both the F atoms (F1 and F2) (table 3.1b, figure 3.1a).

The replacement of the F atom in the B ring by Cl and Br, (i.e. in **43** and **25** respectively), results in the formation of entirely different supramolecular motifs in the crystal lattice. In **43**, a hexameric network has been found to form through type I C–Cl···Cl–C interactions along with weak C–H···F and C–H···Cl hydrogen bonds as shown in figure 3.1b. In the case of **25**, a monoclinic structure with $Z' = 3$ was encountered and C–H···N hydrogen bonds and type I interhalogen C–F···Br–C interactions (figure 3.1c) were majorly observed in its crystal lattice.

Among the compounds of group **4a** (**1**, **34**, **16**), only the compound **16** exists in two polymorphic forms (namely **16F1** and **16F2**). Structures of both **16F1** and **34** are solved in the monoclinic centrosymmetric $P2_1/c$ space group with Z = 4. Both the compounds have been found to be isostructural because of the similarity in the unit cell dimensions as well as in their packing features. In both the structures, zigzag molecular chains were formed through C–H···F hydrogen bonds involving H12 with F1 (table 3.1b, figure 3.1d, and 3.1e). These chains are similar to those formed in the structure of **1** (table 3.1b, figure 3.1a). These pair of antiparallel chains are further interconnecting through C–H···Cl hydrogen bonds in case of **34** and by type I C–Br···Br–C interactions in case of **16F1** (table 3.1b, figure 3.1d, and 3.1e). The type I homo halogen interactions found in **16F1** are in contrast to the remark made by Nayak *et al.*,[91(b)] in the cases of fluorinated benzenanilides. Through his study, he has revealed the preference for type II geometry for homo/hetero halogen short contacts involving heavier halogens (Br and Cl), which has not been found by us in the compound studied. Moreover, it is also noteworthy that the structure of **16F2** involves entirely different kind of molecular network *via* C–H···F hydrogen bond involving the imine proton and C–H···Br hydrogen bond (table 3.1b, figure 3.1f), thus crystallized in the orthorhombic $Pna2_1$ space group with Z = 8 and $Z' = 2$. A number of different weak C–H···π interactions have also been found in the structures of the above-described compounds as well (ESI, table S3.1a, figures S3.1a-S3.1h).

Table 3.1a: Crystallographic data for the compounds belonging to class **1a** and **4a**.

Identification code	**43**	**25**	**34**	**16F1**	**16F2**
Formula	$C_{13}H_9ClFN$	$C_{13}H_9BrFN$	$C_{13}H_9ClFN$	$C_{13}H_9BrFN$	$C_{13}H_9BrFN$
Formula weight	233.66	278.12	233.66	278.12	278.12
CCDC No.	904772	904759	904765	904752	904753
Solvent system	CH_3COCH_3	CH_3OH	$CH_3COOC_2H_5$	CH_2Cl_2+C_6H_{12}	C_2H_5OH
Morphology	Block	Plate	Block	Rect. Block	Plate
Crystal system	Triclinic	Monoclinic	Monoclinic	Monoclinic	Orthorhombic
Space group	$P\ \bar{1}$	$P2_1/c$	$P2_1/c$	$P2_1/c$	$Pna2_1$
a/Å	9.240(2)	15.2489(5)	23.596(2)	23.950(5)	11.646(4)
b/Å	9.283(2)	15.6548(5)	6.3391(4)	6.3629(15)	26.988(8)
c/Å	13.168(3)	17.0477(7)	7.0801(4)	7.2093(15)	7.113(2)
α/°	81.794(5)	90.00	90.00	90.00	90.00
β/°	80.917(5)	123.158(1)	95.323(4)	94.890(7)	90.00
γ/°	77.366(5)	90.00	90.00	90.00	90.00
Volume/Å^3	1081.5(4)	3406.9(2)	1054.5(1)	1094.7(4)	2235.6(11)
Z	4	12	4	4	8
Z′	2	3	1	1	1
ρ_{calc}(g/cm^3)	1.435	1.627	1.472	1.688	1.653
μ/mm^{-1}	0.334	3.602	0.343	3.737	3.659
***F*(000)**	480	1656.0	480	552	1104
$\theta_{min,max}$ (°)	1.6, 25.0	1.9, 25.0	2.6, 25.0	2.6, 25.0	2.3, 25.0
$h_{min,max}$; $k_{min,max}$; $l_{min,max}$	-10, 10; -11, 10; -15, 15	-16, 18; -18, 18; 20, 14	-28, 24; -7, 7; -8, 8	-28, 27; -3, 7; -8, 8	-13, 13; -32, 32; -3, 8
No. of reflections	7091	24812	4831	8569	12225
No. of Observed Reflections	3820	6024	1863	1945	3060
No. of unique reflections	3053	5149	1670	1681	2760
R(int)	0.0206	0.0285	0.0197	0.0309	0.0362
Data/restraints/ parameters	3820/0/361	6024/0/541	1863/0/181	1945/0/145	3060/1/284
GooF	1.042	1.040	1.126	1.031	1.038
R_obs	0.045	0.040	0.036	0.026	0.024
wR_2(obs)	0.106	0.101	0.082	0.065	0.048
$\Delta\rho_{min,max}$ (eÅ^{-3})	-0.34, 0.06	-1.13, 2.41	-0.39, 0.27	-0.38, 0.77	-0.25, 0.23

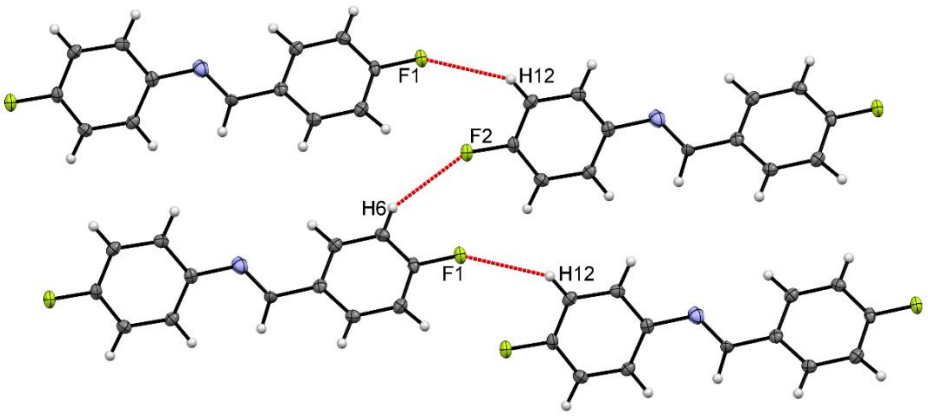

3.1a

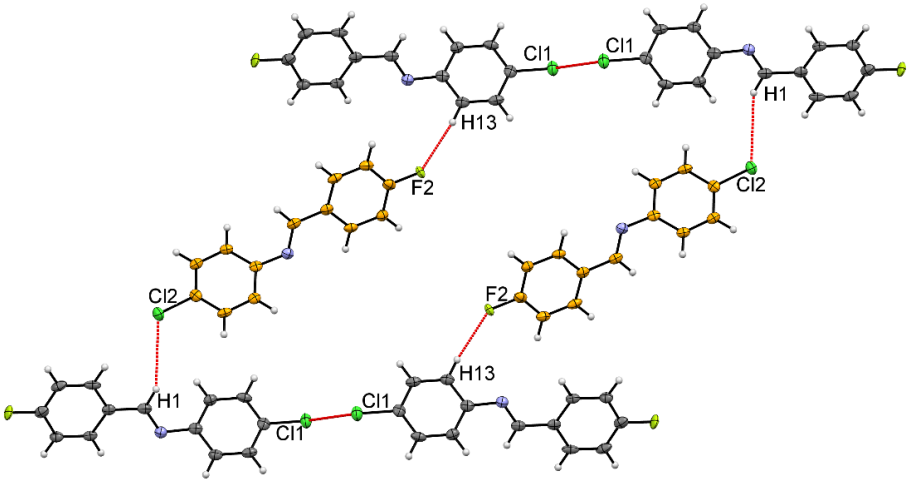

3.1b

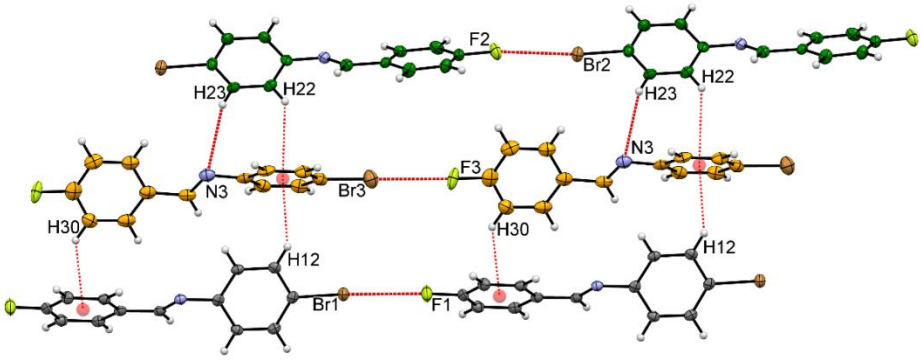

3.1c

Figure 3.1: (a) Sheet formation in **1** *via* weak C–H···F hydrogen bonds, **(b)** formation of hexameric unit in **43** by C–H···F, C–H···Cl hydrogen bonds and type I C–Cl···Cl interactions, **(c)** Molecular chains formed through C–H···π and type I C–F···Br interactions, by three molecules of the asymmetric unit of **25**.

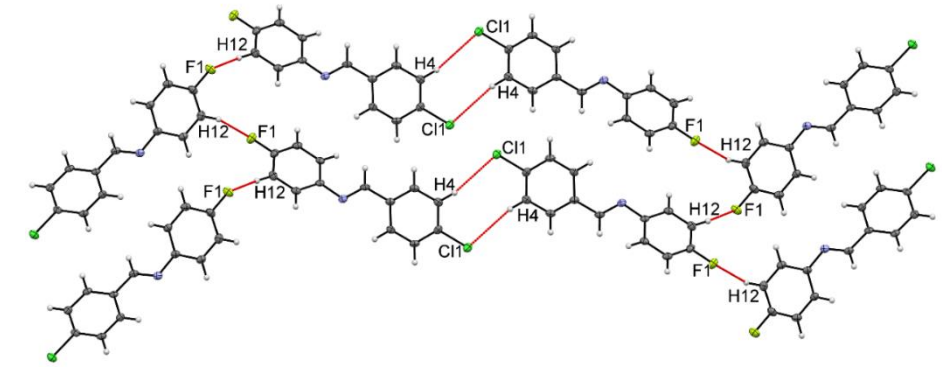

3.1d

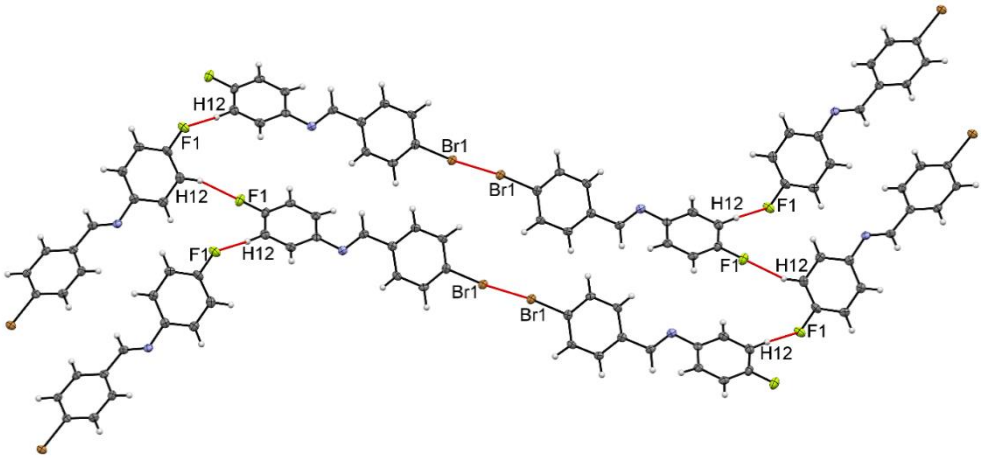

3.1e

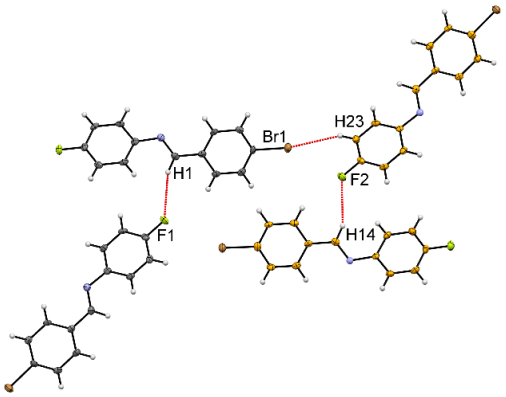

3.1f

Figure 3.1: (d) formation of zigzag chains through weak C–H···F hydrogen bonds and their interconnection *via* weak C–H···Cl hydrogen bonds in **34**, **(e)** zigzag chains formation through weak C–H···F hydrogen bonds, which further interacts by type I C–Br···Br interaction in **16F1**, **(f)** molecular network, which is found to form by weak C–H···F and C–H···Br hydrogen bonds in **16F2**.

Table 3.1b: Details of intermolecular interactions, computed stabiliztion energies and topological parameters of compounds **1**, **43**, **25**, **34**, **16F2** and **16F1**.

Code	C–D···A (D = H, Cl, Br; A = F, Cl, Br, N)	*d* D···A /Å	θ ∠C–D···A/º	Symmetry Code	SE_{G09} kcal/mol	ρ (eÅ^{-3})	$\nabla^2\rho$ (eÅ^{-5})
1	C6–H6···F2	2.67	131	x, y+1, z+1	-1.1	0.027	0.555
	C12–H12···F1	2.69	130	x-1, y-1, z-1	-1.1	0.027	0.555
43	C13–H13···F2	2.44	150	x, y, z	-2.5	0.047	0.893
	C26–H26···F1	2.51	143	1-x, y+1, 1+z	-2.2	0.041	0.772
	C11–Cl1···Cl1	3.45	124	1-x, 1-y, -z	-0.7	0.054	0.724
25	C11–Br1···F1	3.15	161	x-1, y, z-1	-0.3	0.041	0.748
	C11–Br2···F2	3.07	166	x-1, y, z-1	-0.3	0.047	0.797
	C11–Br3···F3	3.07	170	1+x, y, 1+z	-0.4	0.047	0.869
	C32–H32···N1	2.75	150	x-1, $^1/_2$-y, z-$^1/_2$	-4.6	0.041	0.555
	C17–H17···N1	2.75	157	1-x, y+$^1/_2$,$^1/_2$-z	-4.7	0.034	0.531
	C23–H23···N3	2.69	145	1-x, 1-y, 1-z	-4.5	0.041	0.603
34	C12–H12···F1	2.56	153	1-x, y-$^1/_2$,$^1/_2$-z	-1.0	0.035	0.694
	C4–H4···Cl1	2.99	166	-x, -y, -z	-1.5	0.034	0.700
16F1	C12–H12···F1	2.57	153	1-x, y+$^1/_2$,$^1/_2$-z	-1.0	0.034	0.676
	C5–Br1···Br1	3.63	143	-x, 1-y, -z	-0.5	0.047	0.531
16F2	C1–H1···F1	2.68	153	x+$^1/_2$, $^1/_2$-y, z	-1.5	0.027	0.531
	C14–H14···F2	2.68	155	x-$^1/_2$, $^3/_2$-y, z	-1.5	0.027	0.555
	C23–H23···Br1	2.91	147	x+$^1/_2$, $^3/_2$-y, z	-0.1	0.034	0.531

The gas phase stabilization energies for the molecular dimers formed by weak C–H···F hydrogen bonds lies between 1.0 and 2.5 kcal/mol in the cases of compounds **1**, **43**, **34**, **16F1** and **16F2**, while for C–H···N hydrogen bonds it lies in the range of 4-5 kcal/mol. Existence of BCPs in all the cases of C–H···F hydrogen bonds and C–X_1···X_2 interactions have been found AIM calculations, through the values of electron densities (ρ) and Laplacian ($\nabla^2\rho$) found at the BCPs of C–X_1···X_2 interactions are very low. These values are in the similar range with those reported by Munshi and Guru Row for weak C–H···O hydrogen bonds through the experimental charge density analysis.[130] In this group, it has been found that the replacement of F in the A ring by the heavier halogens have entirely altered the crystal packing, while the similar replacement in the B ring has kept some features of their difluorinated analogues (i.e. formation of molecular chains involving H12 with F1) intact as described above.

Table 3.2a: Crystallographic data for the compounds belonging to class **1b** and **5a**.

Identification code	**44**	**26**	**35**	**17**
Formula	$C_{13}H_9ClFN$	$C_{13}H_9BrFN$	$C_{13}H_9ClFN$	$C_{13}H_9BrFN$
Formula weight	233.66	278.12	233.66	278.12
CCDC No.	904773	904760	967464	904754
Solvent system	CH_3OH	C_2H_5OH	$CH_3COOC_2H_5$	CH_2Cl_2+C_6H_{12}
Morphology	Block	Plate	Needle	Plate
Crystal system	Monoclinic	Monoclinic	Monoclinic	Monoclinic
Space group	$P2_1/c$	$P2_1/c$	$P2_1/c$	$P2_1/c$
a/Å	12.626(2)	12.8032(8)	11.504(2)	11.664(2)
b/Å	7.004(1)	7.0146(4)	4.725(1)	4.7226(9)
c/Å	12.228(2)	12.2477(8)	24.275(4)	21.437(4)
α/°	90.00	90.00	90.00	90.00
β/°	92.568(1)	92.867(2)	127.34(1)	113.688(8)
γ/°	90.00	90.00	90.00	90.00
Volume/Å^3	1080.3(3)	1098.6(1)	1049.1(3)	1079.5(3)
Z	4	4	4	4
Z′	1	1	1	1
ρ_{calc} (g/cm^3)	1.437	1.682	1.479	1.711
μ/mm^{-1}	0.335	3.723	0.345	3.789
***F*(000)**	480	552	480	552
$\theta_{min,max}$ (°)	3.2, 25.0	3.2, 25.0	1.9, 25.0	1.9, 25.0
$h_{min,max}$; $k_{min,max}$; $l_{min,max}$	-15, 15; -6, 6; -14, 14	-15, 15; 0, 8; 0, 14;	-13, 13; -5, 3; -28, 27	-8, 13; -3, 5; -25, 24
No. of reflections	4852	6185	3888	5336
No. of Observed Reflections	1540	1946	1825	1882
No. of unique reflections	1475	1719	1335	1439
R(int)	0.0193	0.0283	0.0362	0.0468
Data/restraints/ parameters	1540/0/181	1946/0/181	1825/0/145	1882/0/145
GooF	1.056	1.046	1.027	1.067
R_obs	0.026	0.023	0.045	0.041
wR_2(obs)	0.070	0.065	0.106	0.073
$\Delta\rho_{min,max}$ (eÅ^{-3})	-0.19, 0.04	-0.34, 0.47	-0.29, 0.78	-0.66, 0.64

Structural comparison of the compounds belonging to class 1b and 5a

Compound **2** was found to crystallize in the monoclinic centrosymmetric $P2_1/c$ space group. Head to head and tail to tail dimers across the inversion centers are formed through C–H···F hydrogen bonds, thereby generating molecular layers (table 3.2b, figure 3.2a). These layers further interact with the adjacent layers by weak C–H···F hydrogen bonds and C–H···π interactions.

All the compounds belonging to the subclass **1b** and **5a** crystallize in $P2_1/c$ space group with $Z' = 1$. Further, the compounds **44** and **26** of class **1b** are isostructural, but with different packing characteristics in comparison to **2**. In the structures of **44** and **26**, weak C–H···F hydrogen bonds are involved in the molecular chain formation, which are further interlinked through type II C–F···X (X = Cl or Br) (in **44** and **26** respectively) heterohalogen interactions, thus generating a sheet-like structure in the *ac* plane (table 3.2b, figure 3.2b, and 3.2c).

In the similar manner, the compounds **35** and **17** are also isostructural and have no similarity in the packing features with compound **2**. In the crystal structures of both **35** and **17**, molecular dimers involving H9 and H1 with F1 are formed by the molecules, which are symmetrically related through the center of inversion (table 3.2b, figure 3.2d and 3.2e). The fluorine atom involved in these dimers forms bifurcated C–H···F hydrogen bonds. These dimers further translate along the *c* glide through C–H···X (X = Cl or Br) hydrogen bonds in the compounds **35** and **17** respectively (table 3.2b, figure 3.2d, and 3.2e).

All the three structures belonging to the sub-group **1b** have numerous weak C–H···π interactions present in their respective lattices (ESI, table S3.2, figure S3.2a-S3.2c), while weak C–H···π interactions have been replaced by weak C–H···X (X = Cl or Br) hydrogen bonds in the cases of **35** and **17** (table 3.2b, figure 3.2d and 3.2e).

The stabilization energies of the dimers (SE_{G09}) formed by C–H···F hydrogen bonds in the cases of **44** and **26** are about -1.2 kcal/mol, which is lesser than the energies of the dimers formed in the case of compound **2** (-1.3 and -1.6 kcal/mol), in which two C–H···F hydrogen bonds are involved in the molecular dimer formation. The stabilization energies of the dimers (SE_{G09}) formed by the C–H···F hydrogen bonds in the cases of **35** and **17** are about -3.5 kcal/mol, which is much more than those observed earlier because four C–H···F hydrogen bonds have been found between the two interacting molecules.

Table 3.2b: Details of intermolecular interactions, computed stabiliztion energies and topological parameters of compounds **2**, **44**, **26**, **35** and **17**

Code	C–D···A (D= H, Br; A = F, Cl, Br)	*d* (D···A/Å)	θ (∠C–D···A/°)	Symmetry Code	SE_{G09} kcal/mol	ρ (eÅ^{-3})	$\nabla^2\rho$ (eÅ^{-5})
2	C6–H6···F1	2.52	128	1-x, -y, 1-z	-1.3	0.039	0.758
	C11–H11···F2	2.55	134	-x, 1-y, -z	-1.6	0.038	0.695
	C13–H13···F2	2.55	161	x, -y-$^1/_2$, z-$^1/_2$	-0.5	0.036	0.707
44	C11–H11···F1	2.52	164	x-1, $^3/_2$-y, z-$^1/_2$	-1.2	0.036	0.710
	C10–Cl1···F1	3.13	160, 113	x-1, y, z	-0.4	0.041	0.797
26	C11–H11···F1	2.63	166	x-1, $^1/_2$-y, z-$^1/_2$	-1.2	0.027	0.548
	C10–Br1···F1	3.14	162,114	1+x, y, z	-0.6	0.047	0.821
35	C1–H1···F1	2.56	153	1-x, 1-y, 1-z	-3.3	0.036	0.678
	C9–H9···F1	2.76	156	1-x, 1-y, 1-z		0.023	0.471
	C11–H11···Cl1	2.89	168	1+x, $^1/_2$-y, $^1/_2$+z	-1.0	0.041	0.579
17	C1–H1···F1	2.58	155	1-x, 1-y, 1-z	-3.9	0.034	0.659
	C9–H9···F1	2.66	162	1-x, 1-y, 1-z		0.030	0.589
	C11–H11···Br1	2.97	170	x, $^1/_2$-y, z-$^1/_2$	-2.4	0.041	0.555

The AIM calculations for these structures specified the existence of BCPs in all the cases of C–H···X (X = F, Cl or Br) hydrogen bonds and C–X1···X2 interactions with very small values of electron densities (ρ) and Laplacians ($\nabla^2\rho$) as seen earlier, indicating the weak closed shell nature of these interactions. In the case of group **1b**, the replacement of F in the A ring by the heavier halogens have brought different packing features by the introduction of interhalogen contacts (figures 3.2a, 3.2b and 3.2c), while the introduction of weak C–H···X (X = Cl or Br) hydrogen bonds has been found to create different packing features in the structures of group 5a (figures 3.2a, 3.2d and 3.2e). It is also noteworthy that the interchange of Cl with Br or vice-versa has not changed the crystal packing and the stabilization energies involving C–H···F hydrogen bonds (table 3.2b, figures 3.2b vs. 3.2c and 3.2d vs. 3.2e).

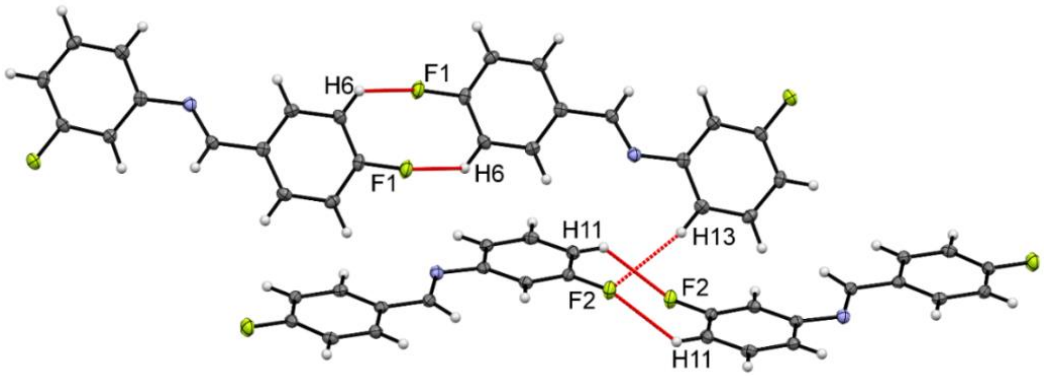

3.2a

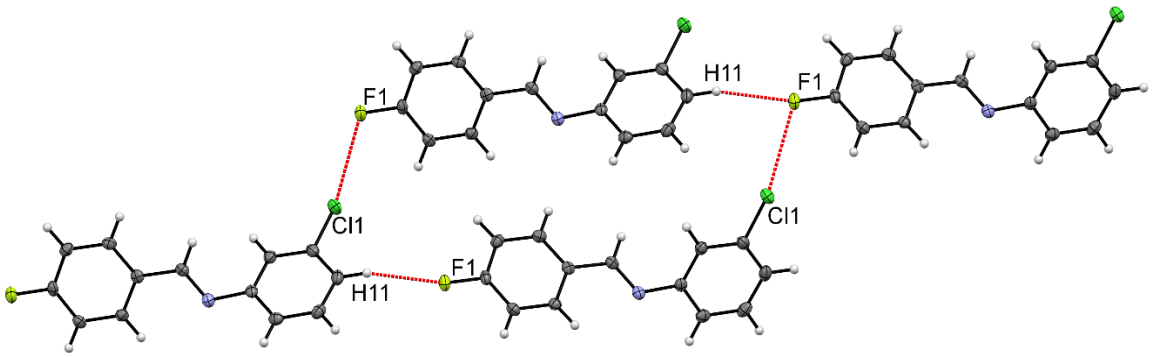

3.2b

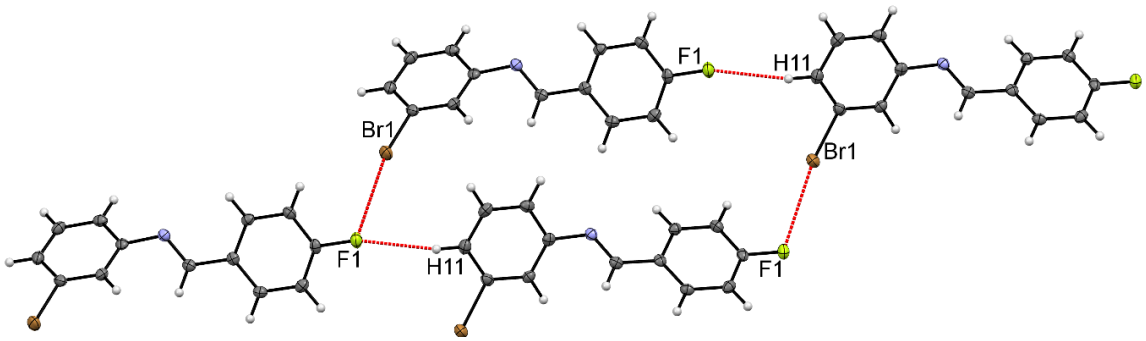

3.2c

Figure 3.2: (a) Propagating dimers in **2**, which are further interconnecting through C–H···F hydrogen bonds, **(b)** formation of molecular sheets by the combination of C–H···F hydrogen bond and type II C–F···Cl inteactions in **44**, **(c)** molecular sheets formed by the utilization of C–H···F hydrogen bond and type II C–F···Br inteactions in **26**;

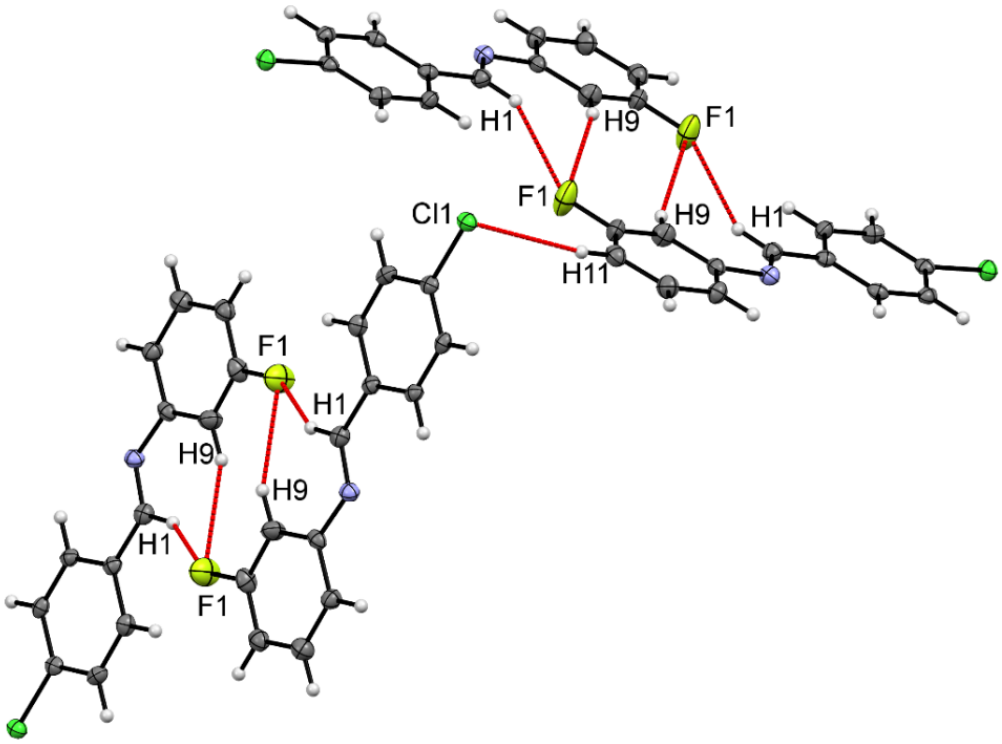

3.2d

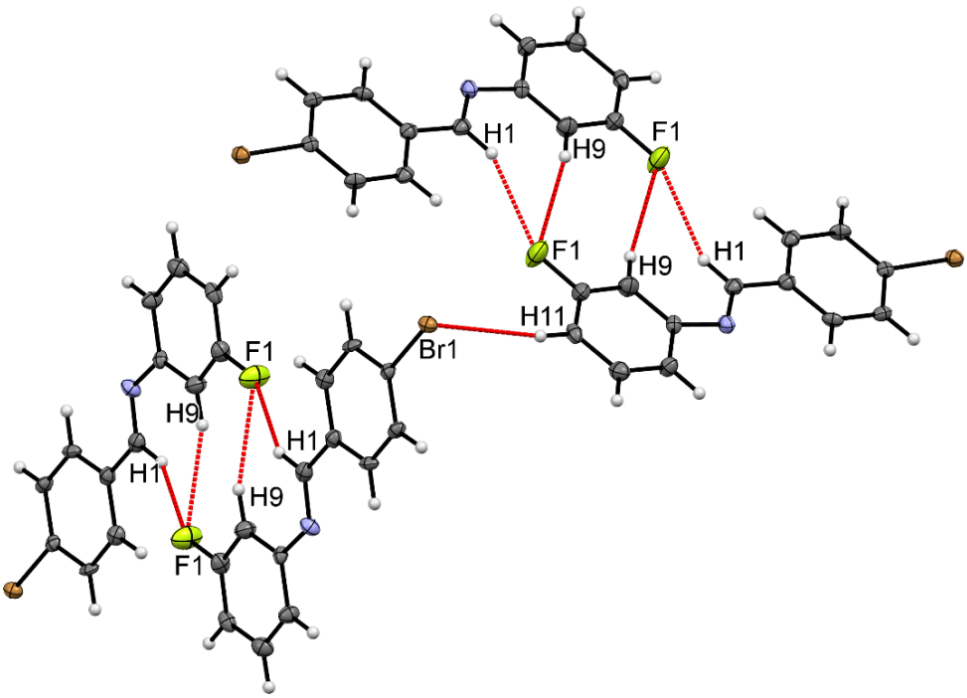

3.2e

Figure 3.2: (d) propagating dimers formed by C–H···F and C–H···Cl hydrogen bonds in **35 (e)** formation of dimers and their propagation in the lattice through C–H···F and C–H···Br hydrogen bonds respectively in **17**.

Table 3.3a: Crystallographic data for the compounds belonging to class **1c** and **6a**.

Identification code	**36F1**	**36F2**	**18F1**	**18F2**
Formula	$C_{13}H_9ClFN$	$C_{13}H_9ClFN$	$C_{13}H_9BrFN$	$C_{13}H_9BrFN$
Formula weight	233.66	233.66	278.12	278.12
CCDC No.	904766	967465	967460	967467
Solvent system	CH_3COCH_3	CH_3OH	CH_3COCH_3 + CH_3OH	CH_2Cl_2+C_6H_{12}
Morphology	Plate	Needle	Block	Plate
Crystal system	Orthorhombic	Orthorhombic	Orthorhombic	Monoclinic
Space group	$P2_12_12_1$	$Pna2_1$	$P2_12_12_1$	$P2_1$
a/Å	6.182(2)	26.077(3)	6.1982(5)	13.424(2)
b/Å	7.123(2)	5.8390(7)	7.1066(7)	6.0702(6)
c/Å	25.074(8)	14.513(2)	25.399(2)	15.467(2)
α/°	90.00	90.00	90.00	90.00
β/°	90.00	90.00	90.00	115.534(6)
γ/°	90.00	90.00	90.00	90.00
Volume/Å^3	1104.1(6)	2209.78(4)	1118.77(2)	1137.2(2)
Z	4	8	4	4
Z′	1	2	1	2
ρ_{calc}(g/cm^3)	1.406	1.40	1.65	1.627
μ/mm^{-1}	0.328	0.327	3.656	3.597
***F*(000)**	480	960	552	552
$\theta_{min,max}$ (°)	3.0, 25.0	2.1, 26.4	1.6, 25.0	1.5, 25.7
$h_{min,max}$; $k_{min,max}$; $l_{min,max}$	-7, 7; -7, 8; -12, 29	-32, 28; -7, 7; -18, 18	-7, 7; -8, 8; -30, 29	-16, 13; -7, 6; -18, 18
No. of reflections	3797	8743	5888	7418
No. of Observed Reflections	1927	2870	1754	3850
No. of unique reflections	1776	3643	1987	3422
R(int)	0.0193	0.045	0.042	0.0368
Data/restraints/parameters	1927/0/181	3643/0/289	1927/0/145	3850/1/289
GooF	1.046	1.041	0.957	1.074
R_obs	0.027	0.042	0.027	0.047
wR_2(obs)	0.060	0.087	0.049	0.010
$\Delta\rho_{min,max}$ (eÅ^{-3})	-0.14, 0.16	-0.30, 0.23	-0.44, 0.46	-0.66, 0.61

Structural comparison of the compounds belonging to class 1c and 6a

Compound **3** has been found to crystallize in the monoclinic noncentrosymmetric $P2_1$ space group with $Z' = 2$ and the molecules within the asymmetric unit are interlinked *via* weak C−H···π interactions (ESI, table S3.3). Molecular chains through short, highly directional, and significantly stabilizing C−H···F hydrogen bonds involving the imine hydrogen H1 with F1 and H14 with F4 has been formed by both the molecules of the asymmetric unit respectively (table 3.3b, figure 3.3a).

The other two compounds of the group **1c** (**45** and **27**), exist in the liquid state at room temperature (25 °C). Sharp solidification or melting feature have not been seen in the DSC data on **45** and **27**. Single crystals suitable for the structural analysis of these compounds using *in situ* crystallization technique could not be grown in spite of the several attempts. In the compounds **45** and **27**, the replacement of F at the *ortho*- position of the B ring by Cl and Br respectively eliminate the feasibility of the formation of C−H···F hydrogen bonds involving imine hydrogen, which was present in the case of **3**, thus lowered the melting point of **45** and **27**. A similar trend was perceived earlier by Vasylyeva and Merz in the fluorinated benzonitriles.[131]

Among the compounds of group **6a** (**3**, **36**, **18**), compounds **36** and **18** exist in two polymorphic forms (**36F1**, **36F2**, **18F1**, and **18F2**). Out of those, structures of **36F1** and **18F1** are solved in the orthorhombic non-centrosymmetric $P2_12_12_1$ space group with $Z = 4$ with similar unit cell dimensions. In the crystal lattices of both the compounds **36F1** and **18F1**, chains have been found to form through C–H···F hydrogen bonds (involving H1 with F1) along the *b*-axis and C–H···π interactions interconnect these chains along the *c*-axis (table 3.3b, figure 3.3b to 3.3e). Thus, these compounds can be considered as isostructural

Compounds **3** and **18F2** crystallize in the same space group $P2_1$, but with different unit cell dimensions, while the structure **36F2** was solved in the orthorhombic $Pna2_1$ space group. In the structures of all these three (**3**, **36F2**, and **18F2**), two molecules in the asymmetric unit have been found. The common feature that has been found in all the structures (**3**, **36F1**, **36F2**, **18F1**, and **18F2**), even in both the molecules of the asymmetric unit (**3**, **36F2** and **18F2**), is the formation of C–H···F hydrogen bonds involving F atom (present in the *ortho*- position) of the B ring with the imine hydrogen H1 (table 3.3b, figure 3.3a, 3.3b, 3.3c, 3d, 3.3f, and 3.3h). The chains formed through this interaction interact

with other chains, either formed by the set of same molecules (**36F1**, **18F1**, and **18F2**) or by the set of other molecules of the asymmetric unit (**3** and **36F2**) through C–H···π interactions (figure 3.3d, 3.3e, and 3.3g). Unlike other compounds of group **6a**, in the structure of **18F2**, the molecules constituting the asymmetric unit are interacting through C–H···F hydrogen bond (table 3.3b, figure 3.3h).

It is noteworthy that C–H···F hydrogen bonds involving the acidic imine hydrogen H1, have slightly higher values of electron density at their BCPs (0.054-0.068 eÅ^{-3}). Also, the values of the stabilization energies of the dimers interacting through this C–H···F hydrogen bond have been found to be higher (~ 2 kcal/mol) than those observed in the earlier cases involving aromatic protons (table 3.3b).

Table 3.3b: Details of intermolecular interactions, computed stabiliztion energies and topological parameters of compounds **3**, **36F1**, **36F2**, **18F1** and **18F2**.

Code	C–H···F	*d* (H···F/Å)	θ (∠C–H···F/°)	Symmetry Code	SE_{G09} (kcal/mol)	ρ (eÅ^{-3})	$\nabla^2\rho$ (eÅ^{-5})
3	C1–H1···F2	2.32	162	x+1, y, z	-4.8	0.068	1.110
	C14–H14···F4	2.30	161	x-1, y, z	-4.8	0.068	1.135
	C10–H10···F1	2.66	131	x, y, z+1	-0.7	0.034	0.603
36F1	C1–H1···F1	2.40	160	1-x, y-$^1/_2$, $^1/_2$-z	-4.8	0.056	0.987
18F1	C1–H1···F1	2.44	156	x+1, y, z	-5.0	0.054	0.958
18F2	C1–H1···F1	2.35	168	x, y-1, z	-5.1	0.060	1.045
	C14–H14···F2	2.41	159	x, y+1, z	-5.1	0.054	0.958
	C23–H23···F1	2.43	142	x, y-1, z	-1.3	0.049	0.927
36F2	C1–H1···F1	2.37	173	x, y-1, z	-5.0	0.054	0.990
	C14–H14···F2	2.38	168	x, y+1, z	-5.1	0.054	0.990

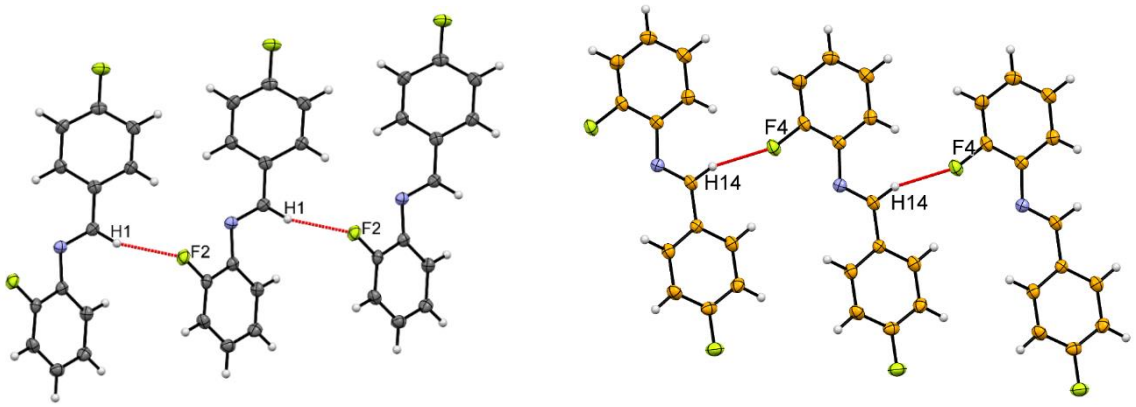

3.3a

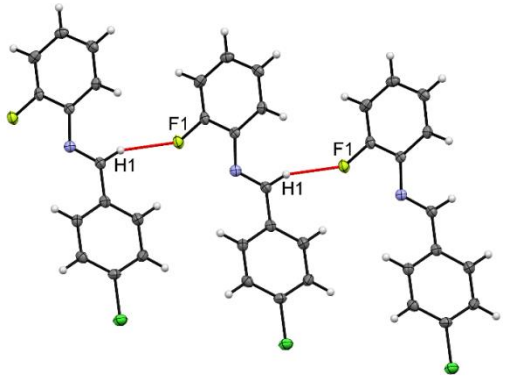

3.3b

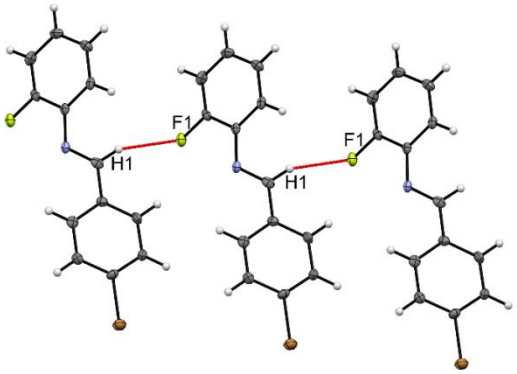

3.3c

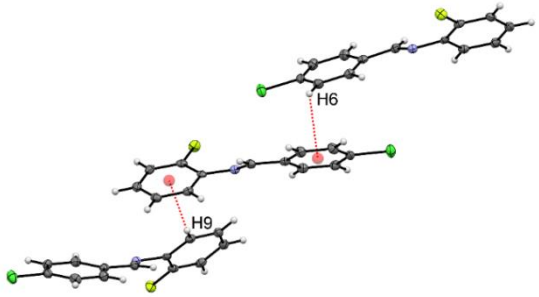

3.3d

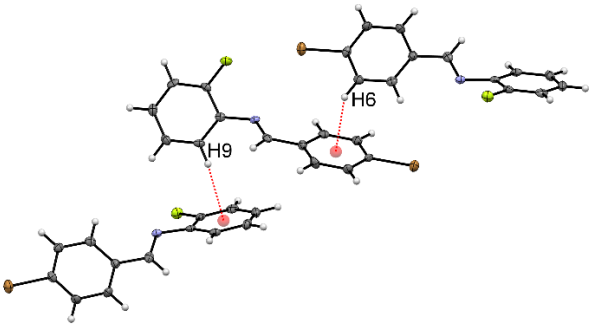

3.3e

Figure 3.3: Formation of molecular chains through the involvement of imine hydrogen with *ortho*- fluorine of A ring in both the molecules of the asymmetric unit of **3** in **3.3a**; similar type of chain formation in **36F1** and **18F1**, which have been shown in figure **3.3b** and **3.3c**.C–H···π interactions in the structures of **36F1** and **18F1** through which chains formed in figure 3.3b and 3.3c are interlinked are shown in figure **3.3d** and **3.3e** respectively;

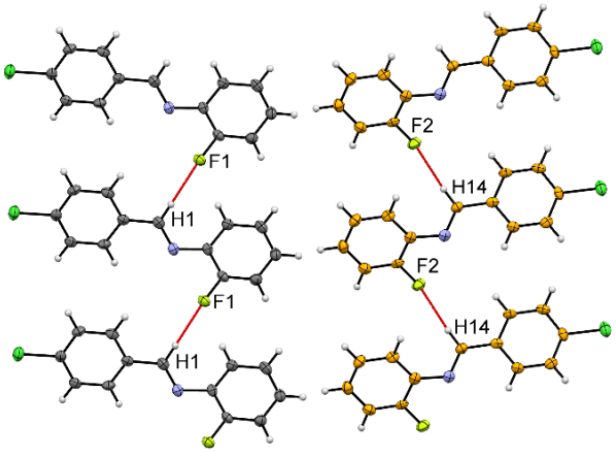

3.3f

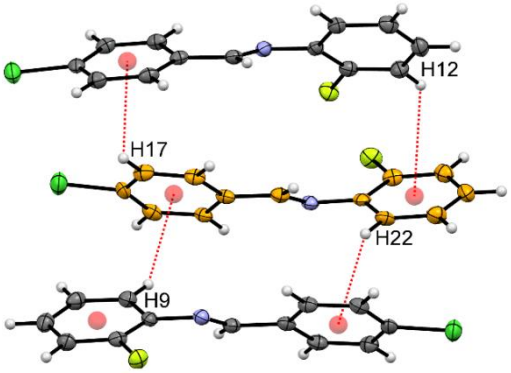

3.3g

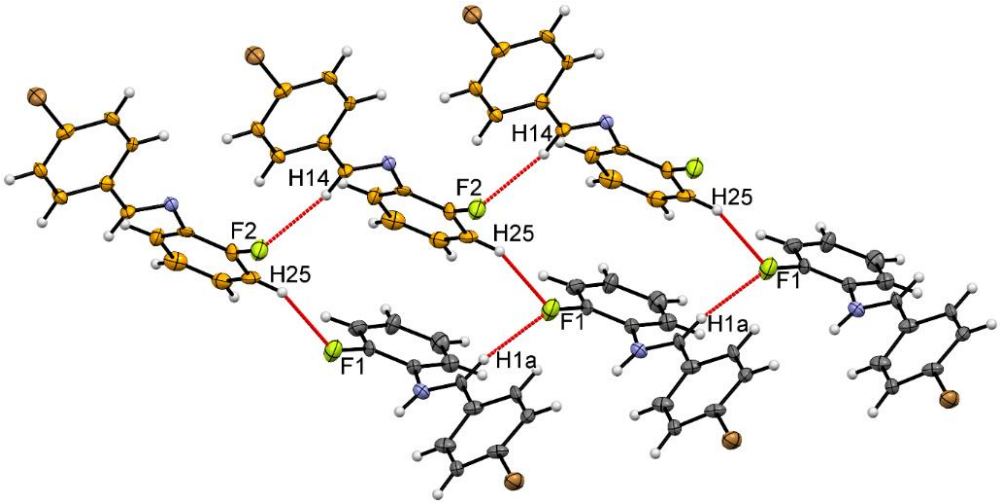

3.3h

Figure 3.3: Formation of molecular chains in **36F2** through C–H···F hydrogen bonds and their interconnection *via* C–H···π interactions in figure **3.3f** and **3.3g** respectively; **(h)** formation of ladder type structure through C–H···F hydrogen bonds in **18F2**.

Table 3.4a: Crystallographic data for the compounds belonging to class **2a** and **4b**.

Identification code	**46**	**28F1**	**28F2**	**37**	**19**
Formula	$C_{13}H_9ClFN$	$C_{13}H_9BrFN$	$C_{13}H_9BrFN$	$C_{13}H_9ClFN$	$C_{13}H_9BrFN$
Formula weight	233.66	278.12	278.12	233.66	278.12
CCDC No.	904774	904761	967463	904767	904755
Solvent system	CH_3COCH_3	CH_3COCH_3 + CH_3OH	CH_2Cl_2+C_6H_{12}	$CH_3COOC_2H_5$	CH_3OH
Morphology	Block	Rect. Prism	Block	Plate	Plate
Crystal system	Monoclinic	Orthorhombic	Monoclinic	Monoclinic	Monoclinic
Space group	$P2_1$	$P2_12_12_1$	$P2_1$	$P2_1/c$	$P2_1/c$
a/Å	8.371(1)	3.9096(7)	8.4843(3)	24.330(6)	24.639(3)
b/Å	5.8235(6)	10.202(2)	5.8153(2)	6.156(2)	6.1809(6)
c/Å	11.239(1)	27.608(6)	11.3383(5)	7.129(2)	7.2279(7)
α/°	90.00	90.00	90	90.00	90.00
β/°	95.359(4)	90.00	94.559(2)	96.144(3)	96.537(5)
γ/°	90.00	90.00	90	90.00	90.00
Volume/Å^3	545.5(1)	1101.11(3)	557.65(4)	1054.5(1)	1093.6(2)
Z	2	4	2	4	4
Z′	0.5	1	1	1	1
ρ_{calc}(g/cm^3)	1.423	1.678	1.656	1.462	1.689
μ/mm^{-1}	0.332	3.715	3.668	0.341	3.741
***F*(000)**	240	552	552	480	552
$\theta_{min,max}$ (°)	2.4, 25.0	2.1, 25.0	3.1, 32.7	2.5, 25.0	2.5, 24.7
$h_{min,max}$; $k_{min,max}$; $l_{min,max}$	-9, 9; -6, 6; -13, 13	-4, 4; 0, 12; -15, 32	-10, 10; -7, 5; -11, 14	-21, 28; -7, 2; -8, 6	-28, 28; -7, 5; -8, 7
No. of reflections	3114	4619	2988	4982	6660
No. of Observed Reflections	1610	1913	1817	1863	1851
No. of unique reflections	1578	1769	1757	1743	1686
R(int)	0.0141	0.0196	0.0159	0.014	0.0318
Data/restraints/parameters	1610/0/181	1913/0/177	1817/1/145	1863/0/181	1851/0/145
GooF	1.086	1.062	1.028	1.065	1.044
R_obs	0.021	0.024	0.019	0.029	0.026
wR$_2$(obs)	0.054	0.052	0.046	0.079	0.070
$\Delta\rho_{min,max}$ (eÅ^{-3})	-0.18, 0.11	-0.25, 0.41	-0.28, 0.26	-0.26, 0.32	-0.37, 0.72

Structural comparison of the compounds belonging to class 2a and 4b

The structure of compound **4** was solved in the space group $P\bar{1}$ with Z = 4 and Z′ = 2. This compound forms molecular layer motifs through dimeric C–H···F hydrogen bonds, which further interweave with other layers by weak C−H···F hydrogen bonds (table 3.4b, figure 3.4a) and C−H···π interactions (ESI, table S3.4).

Completely altered crystal packings has been observed in the structures of **46** and **28** belonging to the subclass **2a**, which are formed by the replacement of F on the B ring by Cl or Br. While, **46** exist in only one form, two different polymorphs are found for the compound **28**, namely **28F1** and **28F2**. The compounds **46** and **28F1** crystallize in the monoclinic non-centrosymmetric $P2_1$ space group with Z = 2 and are considered to be isostructural because of their similarity in the unit cell dimensions as well as in the packing characteristics. Zigzag chains in the crystal structures of **46** and **28F1** are formed through weak C–H···F hydrogen bonds involving H5 with F1 (table 3.4b, figure 3.4b and 3.4c). A chain of heterodimers *via* combination of weak C–H···F hydrogen bond (involving H9 with F1) and C–H···π interactions (table 3.4b, figure 3.4d and 3.4e) has also been seen in the crystal packing of both **46** and **28F1**. The compound **28F2** crystallized in the orthorhombic non-centrosymmetric $P2_12_12_1$ space group and display different arrangement of molecules in their crystal lattice. This arrangement involves the formation of C–H···N hydrogen bonds and weak type II C–F···Br interactions (table 3.4b, figure 3.4f) in the building of complete molecular framework.

In the similar manner, ample variation in the packing features has been observed on the replacement of F on the A ring by Cl or Br (**37** and **19**). Structures of both the compounds **37** and **19** belonging to the sub-class **4b**, are solved in the monoclinic centrosymmetric $P2_1/c$ space group with Z = 4. Molecular ribbon like formation involving C–H···F hydrogen bonds has been observed in the *ab* plane (table 3.4b, figure 3.4g and 3.4h). This kind of molecular ribbon formation was also seen in the structures of **34** and **16F1** (table 3.1b, figure 3.1d and 3.1e). These molecular ribbons further unify through type I C–X···X (X = Cl or Br) interactions (table 3.4b, figure 3.4g and 3.4h). In between the sheets formed through C–H···F hydrogen bonds, weak C–H···π interactions in the *ac* plane and C–X···X (X = Cl or Br) interactions have also been observed.

The topological properties at the BCPs, have been calculated between the interacting pair of molecules. The values of ρ and Laplacian ($\nabla^2\rho$) at the BCP have been found to be similar to the values found in the cases of weak interactions observed and are reported in the table 3.4b. In this case also, the structural features found in the case of **4** do not match with the other structures of its group members, in which one of the fluorine was replaced by Cl or Br.

Table 3.4b: Details of intermolecular interactions, computed stabiliztion energies and topological parameters of compounds **4**, **46**, **28**, **37** and **19**.

Code	C–D···A (D = H, Br, Cl, A = F, Cl, Br, N)	*d* (D···A/Å)	θ (∠C– D···A/º)	Symmetry Code	SE_{G09} kcal/mol	ρ (eÅ^{-3})	$\nabla^2\rho$ (eÅ^{-5})
4	C13A–H13A···F3A	2.59	160	-x, -y, 1-z	-0.3	0.032	0.642
	C16A–H16A···F1A	2.62	157	x, y, z-1	-0.6	0.031	0.606
	C18A–H18A···F3A	2.53	135	-x, -y, 1-z	-1.1	0.040	0.770
	C23A–H23A···F4A	2.56	140	-x, 1-y, -z-1	-1.4	0.035	0.690
	C5A–H5A···F1A	2.56	136	1-x, -y, 2-z	-1.1	0.037	0.715
	C5A–H5A···F2A	2.70	128	x, y, z+1	-1.1	0.026	0.543
46	C5–H5···F1	2.62	136	-x, y+$^1/_2$, 1-z	-0.7	0.034	0.659
	C9–H9···F1	2.70	156	1-x, y+$^1/_2$, 1-z	-1.3	0.023	0.480
28F1	C5–H5···F1	2.65	138	-1-x, y-$^1/_2$, 1-z	-0.7	0.031	0.616
	C9–H9···F1	2.65	156	2-x, y-$^1/_2$, 1-z	-1.4	0.026	0.536
28F2	C4–H4···N1	2.70	172	1-x, y+$^1/_2$, $^3/_2$-z	-2.8	0.041	0.579
	C11–Br1···F1	3.15	166, 119	$^1/_2$-x, 1-y, z-$^1/_2$	-0.8	0.047	0.797
37	C10–H10···F1	2.62	126	1-x, y+$^1/_2$, $^3/_2$-z	-0.9	0.031	0.623
	C6–Cl1···Cl1	3.56	139	2-x, -y, 1-z	-0.1	0.034	0.507
19	C10–H10···F1	*2.63*	126	2-x, y-$^1/_2$, $^3/_2$-z	-0.8	0.031	0.618
	C6–Br1···Br1	3.60	139	1-x, 2-y, 2-z	-0.3	0.047	0.555

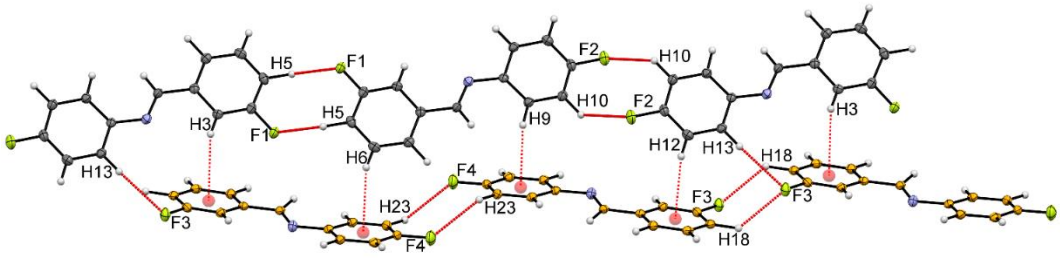

3.4a

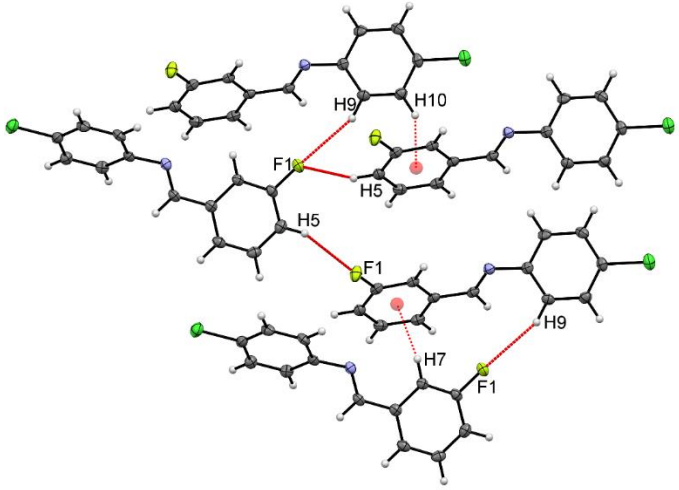

3.4b

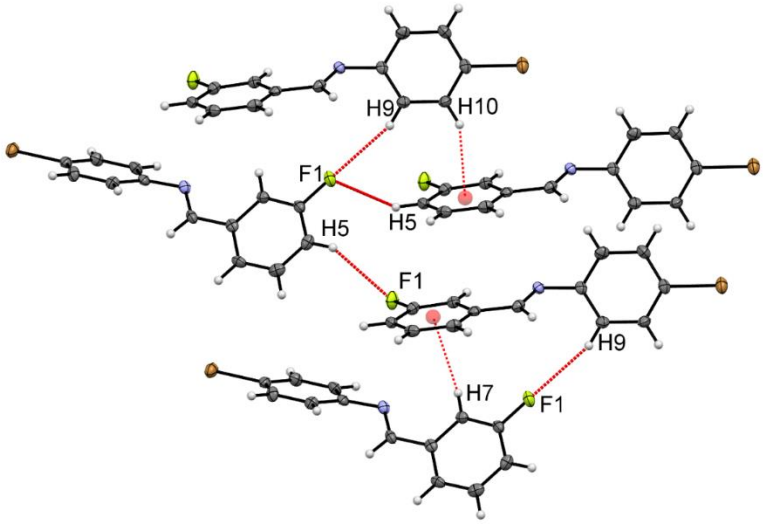

3.4c

Figure 3.4: (a) Formation of dimers and their interconnection through C–H···F hydrogen bonds and C–H···π interactions in **4**; formation of molecular network in **46** and **28** formed through C–H···F hydrogen bonds and C–H···π interactions in figure **3.4b** and **3.4c** respectively.

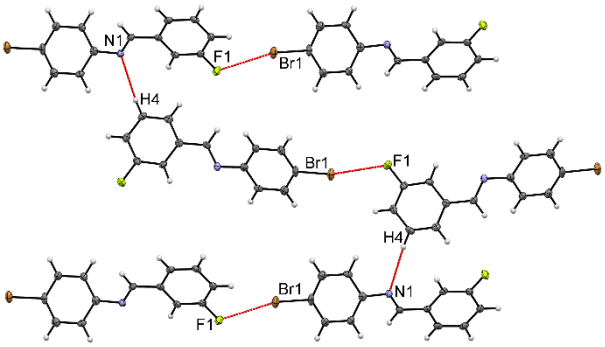

3.4d

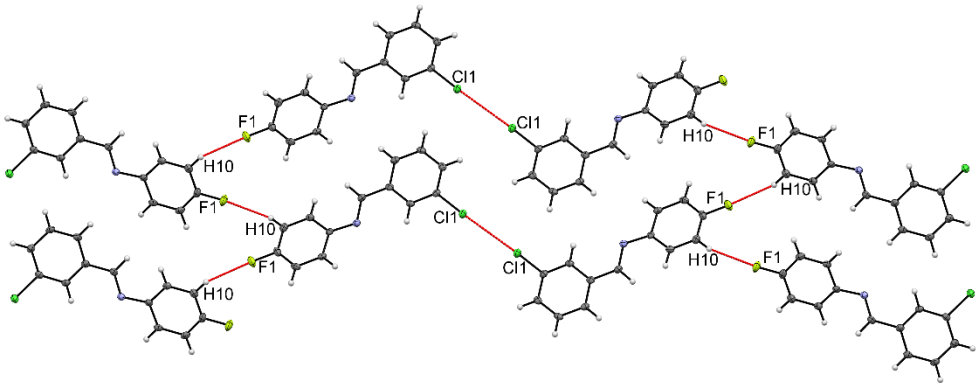

3.4e

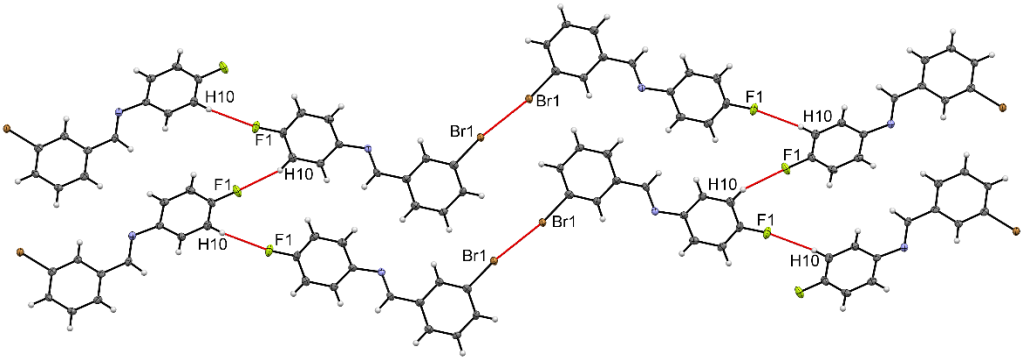

3.4f

Figure 3.4: (d) formation of molecular chains through weak C–H···N hydrogen bonds and C–F···Br interactions in **28F1**, **(e)** molecular sheet formation through weak C–H···F hydrogen bonds and C–Cl···Cl interactions in **37**, **(f)** C–H···F hydrogen bonds and C–Br···Br interactions, forming molecular sheets in **19**.

Table 3.5a: Crystallographic data for the compounds belonging to class **2c** and **6b**.

Identification code	**39**	**21**
Formula	$C_{13}H_9ClFN$	$C_{13}H_9BrFN$
Formula weight	233.66	278.12
CCDC No.	904768	967461
Solvent system	C_2H_5OH	CH_3COCH_3
Morphology	Block	Block
Crystal system	Orthorhombic	Orthorhombic
Space group	$P2_12_12_1$	$P2_12_12_1$
a/Å	6.1450(1)	6.1317(4)
b/Å	12.8880(3)	13.1483(8)
c/Å	13.6233(3)	13.8815(9)
α/°	90.00	90
β/°	90.00	90
γ/°	90.00	90
Volume/Å^3	1078.92(4)	1119.2(2)
Z	4	4
Z′	1	1
ρ_{calc} (g/cm^3)	1.438	1.651
μ/mm^{-1}	0.335	3.655
***F*(000)**	480	552
$\theta_{min,\ max}$ (°)	2.2, 25.0	2.1, 28.3
$h_{min,max}$; $k_{min,max}$; $l_{min,max}$	-7, 7; -15, 11; -16, 13	-8, 5; -16, 17; -17, 18
No. of reflections	7193	6479
No. of Observed Reflections	1897	2768
No. of unique reflections	1871	2547
R(int)	0.0161	0.0307
Data/restraints/parameters	1897/0/181	2768/0/145
GooF	1.046	0.992
R_obs	0.020	0.027
wR$_2$(obs)	0.052	0.055
$\Delta\rho_{min,max}$ (eÅ^{-3})	-0.14, 0.16	-0.60, 0.41

Structural comparison of the compounds belonging to class 2b and 5b

All the compounds belonging to the sub-class **2b** (**5**, **47**, **29**) and **5b** (**5**, **38**, **20**) exist as liquids at 25 ^{o}C. Among these, the crystal structure of **5** was determined using *in situ* crystallization technique, while crystals of the others could not be grown in the same way. The DSC data of the compounds **20** and **47** have not shown any indication of solidification in the cooling and heating cycles (25 ^{o}C to -100 ^{o}C and heated back to 25 ^{o}C) (ESI, table S3.9, figure S3.4:5, and S3.4:32). Though some features were seen for the compounds **29** and **38** in their DSC traces (ESI, table S3.9, figure S3.4: 14, and S3.4:23), yet the compounds could not be crystallized *in situ*.

Structural comparison of the compounds belonging to class 2c and 6b

Among the compounds belonging to the subclass **2c** (**6**, **30**, **48**), only **6** exists in the solid state at 25 ^{o}C, while others are found to be in the liquid state at the same temperature. Compound **6** form molecular chains by utilizing C–H···F hydrogen bonds involving imine hydrogen (H1) and C–H···π interactions. When the F atom on the B ring (which participates in the formation of C–H···F hydrogen bonds in **6**) was replaced by Cl or Br, then perhaps due to the absence of that particular C–H···F hydrogen bond, the compounds **30** and **48** exist as liquids as has been seen in the group **1c**. Crystal structures of **48** and **30** could not be determined *in situ* as none of them could be crystallized when cooled from room temperature to -170 ^{o}C in a quartz capillary on the diffractometer using Oxford cryosystem.

All the compounds belonging to the subclass **6b** (**6**, **21**, **39**), crystallize in the same space group $P2_12_12_1$ with similar unit cell dimensions and having almost similar packing features. Molecular chains have been found to form through C–H···F hydrogen bonds involving imine hydrogen i.e. H1 in the compound **6** (table 3.5b, figure 3.5a), while in the compounds **39** and **21**, the F atom has been found to be bifurcated and form hydrogen bonds by involving both imine and aromatic hydrogen (H1 and H3 respectively), (table 3.5b, figure 3.5c and 3.5d). Further, these chains are interwoven through quasi type I/type II inter-halogen C–F···X (X = Cl or Br) interactions[61] along the *b*-axis (table 3.5b, figure 3.5c and 3.5d). But in the case of **6**, propagation of the molecular chains occurs through C–H···π interactions (table 2.6b, figure 2.6c) and a similar C–F···F quasi type I/type II inter-halogen interaction has not been seen.

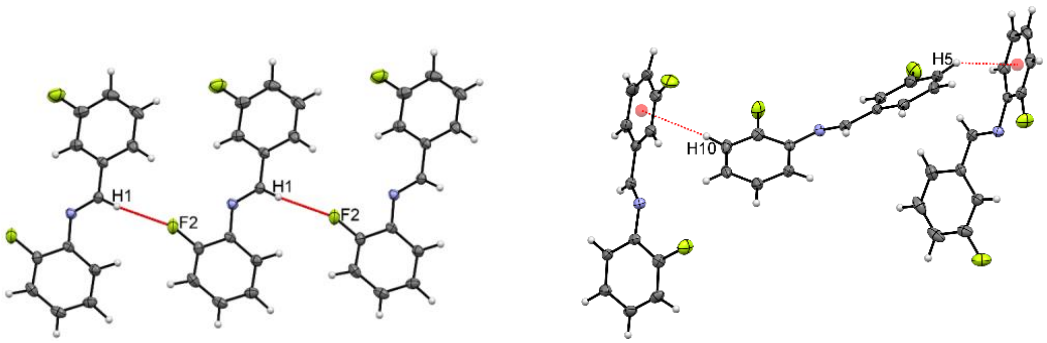

3.5a **3.5b**

Figure 3.5: (a) Formation of molecular chains in **6** *via* weak C–H···F hydrogen bonds; **(b)** interconnection of the molecular chains formed in **6** through C–H···π interactions.

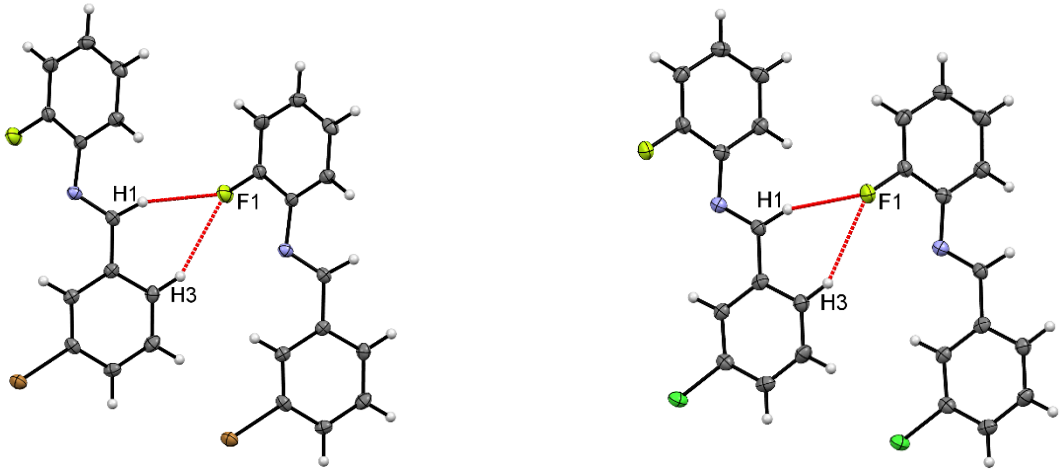

3.5c **3.5d**

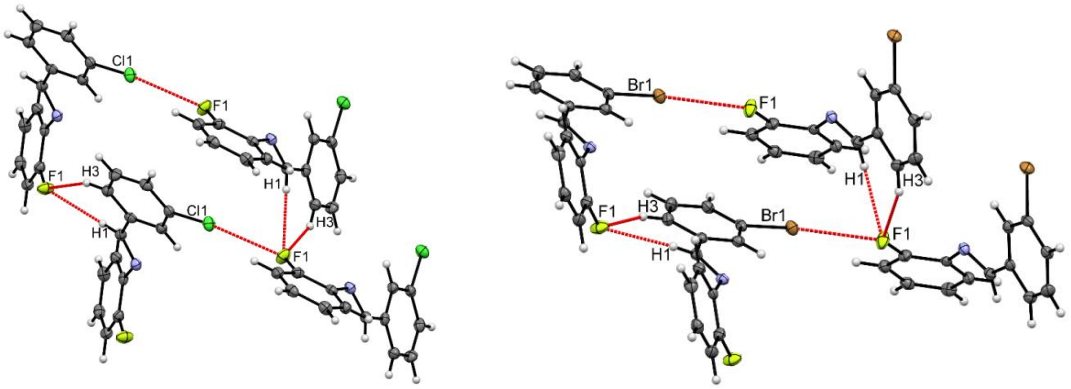

3.5e **3.5f**

Figure 3.5: (c) and **(d)** Formation of molecular chains *via* weak C–H···F hydrogen bonds in **21** and **39** respectively; **(e)** and **(f)** Interconnecting molecular layers through quasi type I/type II C–F···Cl and C–F···Br interactions in **21** and **39** respectively.

The C–H···F hydrogen bonds involving H1 have higher electron densities at their BCPs (~ 0.048 eÅ^{-3}) as was also seen in the cases of compound **3**, **36F1**, **36F2**, **18F1** and **18F2**. Also, the values of the stabilization energies of the dimers formed by this C–H···F hydrogen bond lie in the range between -4.1 and -5.3 kcal/mol. The C–H···F hydrogen bonds formed involving H3 in the case of the compounds **39** and **21**, have lower values of electron densities at their BCPs (0.027 and 0.029 eÅ^{-3}), thus their contribution towards the stabilization energy must be lesser in comparison to the stabilization energy provided by the C–H···F hydrogen bond involving H1 with F1.

Table 3.5b: Details of intermolecular interactions, computed stabiliztion energies and topological parameters of compounds **6**, **39** and **21**

Code	C–D···F (D = H, Cl, Br)	*d* (D···F/Å)	θ (∠C–D···F/º)	Symmetry Code	SE_{G09} (kcal/mol)	*ρ* (eÅ^{-3})	$\nabla^2\rho$ (eÅ^{-5})
6	C1–H1···F1	2.47	163	x-1, y, z	-4.1	0.041	0.768
39	C1–H1···F1	2.46	153	x+1, y, z	-4.9	0.048	0.864
	C3–H3···F1	2.66	149	x+1, y, z		0.027	0.558
	C6–Cl1···F1	3.02	133,161	1-x, $^1/_2$+y, $^1/_2$-z	-0.1	0.054	0.966
21	C1–H1···F1	2.49	152	x-1, y, z	-5.3	0.045	0.823
	C3–H3···F1	2.64	150	x-1, y, z		0.029	0.594
	C6–Br1···F1	3.05	135,161	-x, y-$^1/_2$, $^1/_2$-z	-0.4	0.054	0.966

Structural comparison of the compounds belonging to class 3a and 4c

The structure of compound **7** was solved in the monoclinic space group $P2_1/c$ with Z = 2 (Z′ = 0.5). The molecule shows positional disorder due to its in-plane flipping around the C=N bond with 0.5 occupancy. Because of this flipping, the molecule becomes symmetrical in its crystal structure and thus only half of the molecule is present in the asymmetric unit. The molecules of compound **7** pack in the crystal lattice by the formation of molecular sheets *via* dimeric C–H···F hydrogen bonds (table 3.6b, figure 3.6a), which further get intertwined through both C–H···F hydrogen bonds and C–H···π interactions (table 2.7a, figure 2.7(c)), thereby making different types of supramolecular motifs as reported in chapter 2.

Table 3.6a: Crystallographic data for the compounds belonging to class **3a** and **4c**.

Identification code	**49**	**31**	**40**	**22**
Formula	$C_{13}H_9ClFN$	$C_{13}H_9BrFN$	$C_{13}H_9ClFN$	$C_{13}H_9BrFN$
Formula weight	233.66	278.12	233.66	278.12
CCDC No.	904775	904762	904769	967462
Solvent system	C_2H_5OH	CH_3COCH_3	CH_2Cl_2+C_6H_{12}	$CH_3COOC_2H_5$
Morphology	Rectangular block	Block	Irregular	Needle
Crystal system	Monoclinic	Monoclinic	Monoclinic	Monoclinic
Space group	$P2_1/c$	$P2_1/c$	$P2_1/c$	$P2_1/c$
a/Å	13.129(1)	13.4031(9)	3.8515(8)	3.8890(4)
b/Å	11.0236(8)	11.0048(9)	25.069(6)	24.937(3)
c/Å	7.6940(6)	7.7272(7)	10.864(2)	11.0177(10)
α/°	90.00	90.00	90.00	90.00
β/°	106.445(5)	106.161(4)	93.302(3)	93.160(5)
γ/°	90.00	90.00	90.00	90.00
Volume/Å^3	1068.0(1)	1094.7(2)	1047.2(4)	1066.9(2)
Z	4	4	4	4
Z′	1	1	1	1
ρ_{calc} (g/cm^3)	1.453	1.688	1.482	1.732
μ/mm^{-1}	0.339	3.737	0.345	3.834
***F*(000)**	480	552.0	480	552
$\theta_{min,\ max}$ (°)	2.5, 26.4	2.4, 25.0	1.6, 25.1	2.0, 25.0
$h_{min,max}$; $k_{min,max}$; $l_{min,max}$	-12, 16; -13, 13; -9, 7	-15, 15; -13, 10; -9, 8;	-4, 4; -29, 29; -12, 11	-4, 2; -29, 28; -13, 12
No. of reflections	9936	5574	5691	5135
No. of Observed Reflections	2186	1779	1874	1875
No. of unique reflections	1844	1925	1705	1616
R(int)	0.0439	0.0181	0.0184	0.0262
Data/restraints/parameters	2186/0/181	1925/0/181	1874/0/181	1875/1/145
GooF	1.077	1.038	1.12	1.036
R_obs	0.037	0.021	0.030	0.025
wR_2(obs)	0.090	0.053	0.078	0.060
$\Delta\rho_{min,max}$ (eÅ^{-3})	-0.31, 0.28	-0.38, 0.38	-0.30, 0.25	-0.44, 1.02

The compounds belonging to the group **3a** (**7**, **49**, and **31**) and **4c** (**7**, **40**, **22**) have been found to crystallize in the same space group as **7**. But, unlike **7**, none of the compounds of the group **3a** and **4c** was disordered. Weak C–H···Cl and C–H···Br hydrogen bonds form molecular chains along *a*-axis involving the same H atom (H6) (table 3.6b, figure 3.6b, and 3.6c) in **49** and **31** respectively. The chains thus formed are then fastened by weak C–H···π interactions in the crystal lattice of both the compounds (ESI, table S3.6, figure S3.6a, and S3.6b). Therefore, the compounds **49** and **31** are isostructural.

Similarly, in the lattices of isostructural compounds **40** and **22** of group **4c**, C–H···X (X = Cl or Br) hydrogen bonds configure molecular zigzag chains along the *c*-axis by the involvement of same H atom (H12) (table 3.6b, figure 3.6d and 3.6e).

It is noteworthy that unlike **7**, C–H···F hydrogen bonds have not been found in the structures **49**, **31**, **40** and **22**. Rather, C–H···X (X = Cl or Br) hydrogen bonds instead of interhalogen interactions play a significant contribution in the packing of molecules in the crystal lattice.

The stabilization energies of the dimer formed through C–H···F hydrogen bonds (involving H1 with F1) in **7** has been found to be much more than those formed through weak C–H···X (X = Cl or Br) hydrogen bonds in the compounds **49**, **31**, **40** and **22**. The values of the electron density and Laplacian found at the BCPs of C–H···X (X = F, Cl or Br) hydrogen bonds, have almost similar values except for the C–H···F hydrogen bond involving H1 with F1, which is much more stabilizing as discussed above.

Table 3.6b: Details of intermolecular interactions, computed stabiliztion energies and topological parameters of compounds **7**, **49**, **31**, **40** and **22**.

Code	C–H···X (X = F, Cl, Br)	*d* H···X/Å	θ ∠C–H···X/°	Symmetry Code	SE_{G09} (kcal/mol)	ρ (eÅ^{-3})	$\nabla^2\rho$ (eÅ^{-5})
7	C6A–H6A···F1	2.61	127	2-x, -y, 1-z	-0.1	0.035	0.596
	C6A–H6A···F2	2.54	136	x, $^1/_2$-y, z+$^1/_2$	-0.6	0.041	0.775
	C1–H1···F1	2.32	146	1-x, 1-y, -z	-2.6	0.067	1.154
49	C6–H6···Cl1	2.99	130	x+1, $^3/_2$-y, z+$^1/_2$	-0.7	0.034	0.507
31	C6–H6···Br1	3.07	134	x-1, $^1/_2$-y, z-$^1/_2$	-0.9	0.041	0.483
40	C12–H12···Cl1	2.99	136	x, $^1/_2$-y, z+$^1/_2$	-0.7	0.034	0.483
22	C12–H12···Br1	3.08	133	x, $^1/_2$-y, z+$^1/_2$	-0.4	0.034	0.435

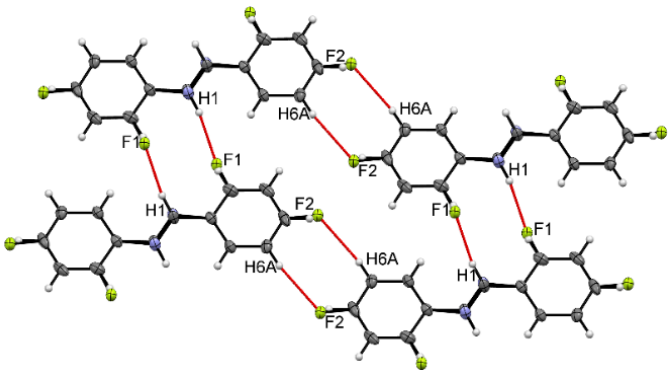

3.6a

Figure 3.6: (a) C–H···F hydrogen bonds present in the crystal structure of **7**.

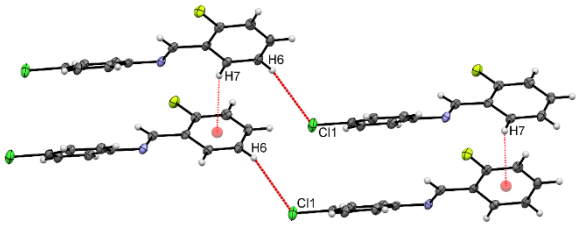

3.6b

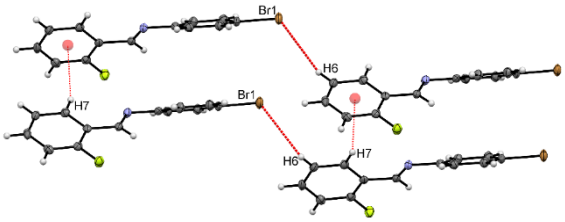

3.6c

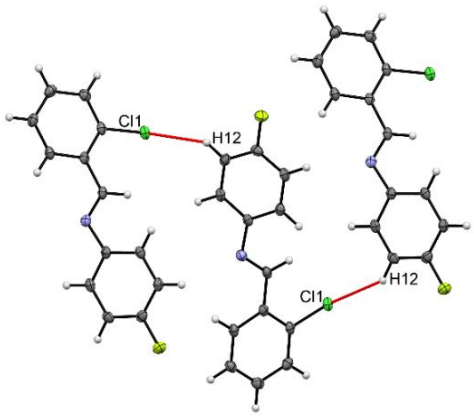

3.6d

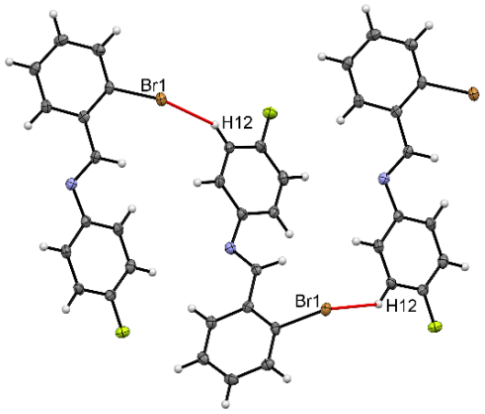

3.6e

Figure 3.6: (b) formation of chains *via* weak C–H···Cl hydrogen bonds, which further interconnect through weak C–H···π interactions in **49**; **(c)** chains formation and their interconnection *via* weak C–H···Br hydrogen bonds and weak C–H···π interactions respectively in **31**; **(d)** formation of zigzag chains along *c*-axis through C–H···Cl hydrogen bonds in **40**, **(e)** molecular chain formation through C–H···Br hydrogen bonds in **22**.

Table 3.7a: Crystallographic data for the compounds belonging to class **3b** and **5c**.

Identification code	**50**	**32**	**41**	**23**
Formula	$C_{13}H_9ClFN$	$C_{13}H_9BrFN$	$C_{13}H_9ClFN$	$C_{13}H_9BrFN$
Formula weight	233.66	278.12	233.66	278.12
Temperature	100.0 K	100.0 K	100.0 K	100.0 K
CCDC No.	904776	904763	904770	904757
Solvent system	C_2H_5OH	CH_3COCH_3	C_6H_{12}	CH_3OH
Morphology	Block	Plate	Irregular	Irregular
Crystal system	Monoclinic	Monoclinic	Orthorhombic	Orthorhombic
Space group	$P2_1/c$	$P2_1/c$	$P2_12_12_1$	$P2_12_12_1$
a/Å	15.377(5)	15.490(1)	3.8567(2)	3.9037(9)
b/Å	3.925 (1)	3.9477(2)	12.0890(8)	12.190(3)
c/Å	22.648(8)	24.348 (2)	22.859(2)	22.760(5)
α/°	90	90.00	90.00	90
β/°	129.569(9)	133.511(3)	90.00	90
γ/°	90	90.00	90.00	90
Volume/Å^3	1053.8(6)	1079.8 (1)	1065.8(1)	1083.03(4)
Z	4	4	4	4
Z′	1	1	1	1
ρ_{calc} (g/cm^3)	1.473	1.711	1.456	1.71
μ/mm^{-1}	0.343	3.788	0.339	3.777
***F*(000)**	480	552	480	552
$\theta_{min,max}$ (°)	1.7, 26.4	1.8, 25.0	1.8, 25.0	2.9, 25.0
$h_{min,max}$; $k_{min,max}$; $l_{min,max}$	-19, 19; -4, 4; -27, 28	-17, 18; -4, 4; -28, 28;	-7, 7; -7, 8; -12, 29	-3, 4; -14, 14; -24, 27
No. of reflections	6284	7459	7013	4097
No. of Observed Reflections	2139	1798	1859	1926
No. of unique reflections	1861	1915	1748	1892
R(int)	0.0254	0.0203	0.0256	0.0130
Data/restraints/parameters	2139/0/181	1915/0/181	1859/0/175	1926/0/175
GooF	1.054	1.059	1.085	1.046
R_obs	0.029	0.019	0.027	0.024
wR_2(obs)	0.071	0.048	0.064	0.063
$\Delta\rho_{min,max}$ (eÅ^{-3})	-0.23, 0.28	-0.26, 0.31	-0.24, 0.04	-0.27, 0.21

Structural comparison of the compounds belonging to class 3b and 5c

Compounds belonging to the group **3b** (**8**, **50**, **32**) crystallize in the monoclinic centrosymmetric $P2_1/c$ space group with Z = 4. These compounds exhibit similar structural features. In the compound **8**, F atom at the *para*- position of the B ring does not participate in any interaction. Therefore, the replacement of that particular F by Cl or Br, does not alter the crystal packing. Compounds of this group form heterodimers by the use of weak C–H···F hydrogen bonds, involving H9 and H1 with F1 (table 3.7b, figure 3.7a, 3.7b, and 3.7c) in their respective crystal lattices.

However, the replacement of F present at the *ortho*- position of the A ring by Cl or Br (**41** and **23**), completely alters the crystal packing. All the three compounds of group **5c** exist as liquids at 30 ^{o}C. Compound **8** was crystallized by *in situ* crystallization technique, while the crystals of the compounds **23** and **41** were grown in a refrigerator maintained at -20 ^{o}C and those were mounted quickly in a cold room at about 20 ^{o}C and were transferred to the diffractometer with the Oxford cryosystem maintained at 0 ^{o}C. Compounds **41** and **23** crystallize in the orthorhombic non-centrosymmetric $P2_12_12_1$ space group with Z = 4 and are isostructural. Both the structures **41** and **23**, are disordered due to the rotation of the aryl ring around the N–C(Ar) bond. Therefore, fluorine atom on the B ring has been found to be present at both the *meta*- position of the B ring (F1A and F1B) with the occupancy of 0.5 at each position. The major part in the structure of both the compounds form linear chains through C–H···F hydrogen bonds (involving H5 with F1A) (table 3.7b, figure 3.7d, and 3.7e) in their crystal lattices. Whereas, in the minor part of the structures, the atom F1B is trifurcated and is involved in the formation of hydrogen bond with H1 and H9B. Additionally, type I inter-halogen C–F···X (X = Cl or Br) interactions have also been observed in the crystal lattices of **41** and **23** respectively (table 3.7b, figure 3.7f, and 3.7g).

The stabilization energies provided by the heterodimers formed in the cases of **8**, **50** and **32** lie in the range between -4.8 and -5.3 kcal/mol. The stabilization energies of the dimers formed in the cases of **41** and **23** are much less than those found for **8**, **50** and **32**. The values of the electron densities and Laplacians found at the BCPs, which exist between C–H···F hydrogen bonds, lies within the same range.

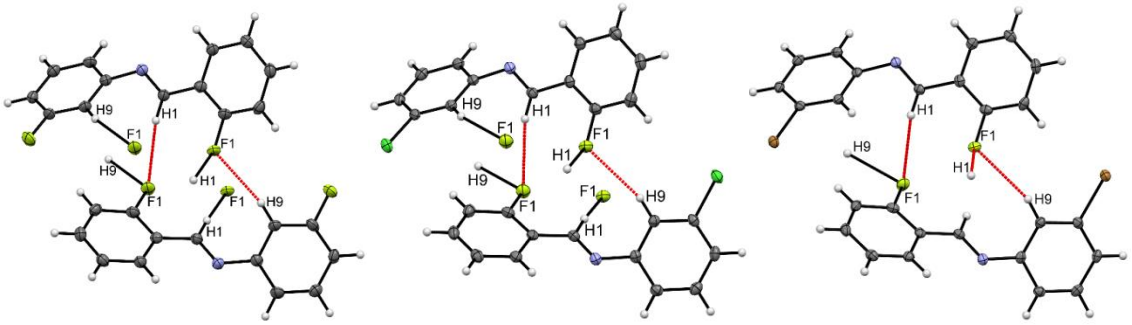

3.7a **3.7b** **3.7c**

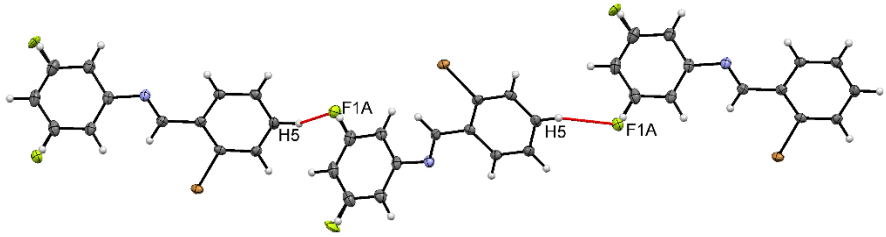

3.7d

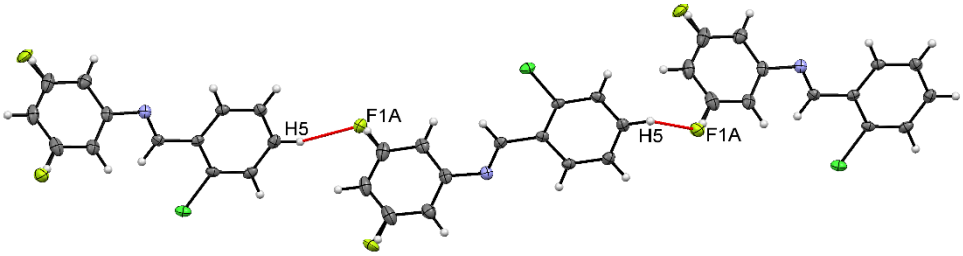

3.7e

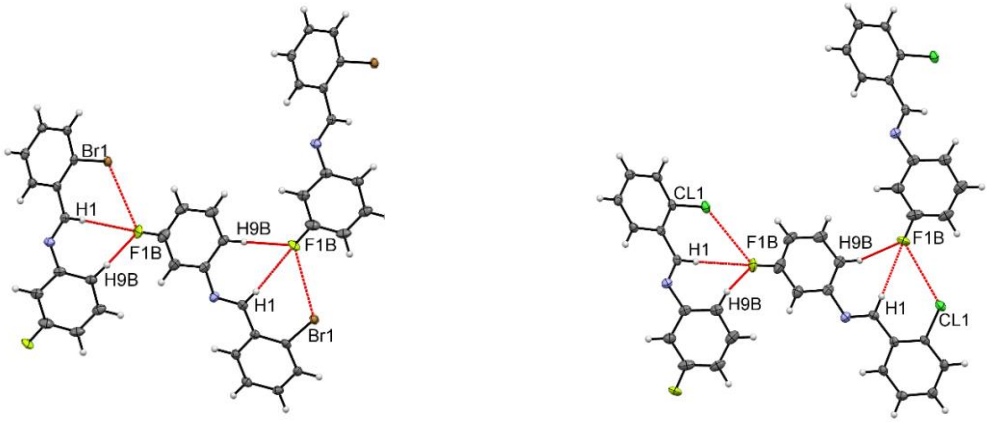

3.7f **3.7g**

Figure 3.7: (a) Formation of heterodimers in **8** *via* weak C–H···F hydrogen bonds, **(b)** weak C–H···F hydrogen bonds, which results in the formation of heterodimers in **50**, **(c)** formation of heterodimers in **32** *via* weak C–H···F hydrogen bonds, **(d)** and **(e)** C–H···F hydrogen bonds by the major part of the crystal structure leading to the formation of linears chains in **23** and **41** respectively, **(f)** and **(g)** network formation through C–H···F hydrogen bonds by the minor part of the crystal structure of **23** and **41** respectively.

Table 3.7b: Details of intermolecular interactions, computed stabiliztion energies and topological parameters of compounds **8**, **50**, **32**, **41** and **23**.

Code	C–D···A (D = H, Cl, Br; A = F)	d (D···A/Å)	θ (∠C–D···A/°)	Symmetry Code	SE_{G09} (kcal/mol)	ρ ($eÅ^{-3}$)	$\nabla^2\rho$ ($eÅ^{-5}$)
8	C9–H9···F1	2.55	169	1-x, y-$^1/_2$, $^1/_2$-z	-4.8	0.038	0.734
	C1–H1···F1	2.67	157	1-x, y-$^1/_2$, $^1/_2$-z		0.030	0.584
50	C9–H9···F1	2.61	164	2-x, y-$^1/_2$, $^3/_2$-z	-4.83	0.032	0.628
	C1–H1···F1	2.69	155	2-x, y+$^1/_2$, $^3/_2$-z		0.027	0.546
32	C9–H9···F1	2.66	163	2-x, y+$^1/_2$, $^3/_2$-z	-5.3	0.029	0.570
	C1–H1···F1	2.70	154	2-x, y-$^1/_2$, $^3/_2$-z		0.026	0.531
41	C1–H1···F1B	2.61	167	1-x, y+$^1/_2$, $^3/_2$-z	-1.2	0.028	0.575
	C9B–H9B···F1B	2.56	125	1-x, y+$^1/_2$, $^3/_2$-z		0.043	0.797
	C3–Cl1···F1B	3.30	120, 125	1-x, y+$^1/_2$, $^3/_2$-z		0.039	0.756
	C5–H5···F1A	2.57	124	$^1/_2$-x, 1-y, z-$^1/_2$	-1.2	0.043	0.797
23	C1–H1···F1B	2.66	163	1-x, y-$^1/_2$, $^3/_2$-z	-0.8	0.025	0.521
	C9B–H9B···F1B	2.55	126	1-x, y-$^1/_2$, $^3/_2$-z		0.043	0.801
	C3–Br1···F1B	3.31	116, 123	1-x, y-$^1/_2$, $^3/_2$-z		0.047	0.676
	C5–H5···F1A	2.62	124	$^3/_2$-x, 1-y, z-$^1/_2$	-1.4	0.029	0.716

Structural comparison of the compounds belonging to class 3c and 6c

Among the compounds belonging to the group **3c** (**9**, **51**, **33**), compound **9** exists as two polymorphs (**9F1** and **9F2**). The compounds **9F1** and **51** were crystallized in $P2_1/c$ space group, while the structures **9F2** and **33** were solved in $P2_12_12_1$ and *Pbcn* space groups respectively. All the compounds of this group have been found to be positionally disordered around C=N bond. Structures **9F1** and **9F2** were refined with 0.5 occupancy of both the parts, while in the structures **33** and **51**, the occupancy ratio of the two parts were found to be 0.91 : 0.09 and 0.55 : 0.45 respectively. Bifurcated C–H···F hydrogen bonds have been found in the lattice of compound **9F2** (table 3.8b, figure 3.8b), while rest of the compounds belonging to the group **3c** form dimers in their respective crystal structure through C6–H6···X (X = F1 or Cl1 or Br1) hydrogen bonds (table 3.8b, figure 3.8a, 3.8c and 3.8d). Then, these dimers proliferate in the lattice through C–H···Cl hydrogen bonds in the case of compound **51** (table 3.8b, figure 3.8c) and through C–H···π interactions in the structure of **33** (ESI, table S3.8, figure 3.8d), while in **9F1**, no other interaction between the molecular dimer has been seen.

Table 3.8a: Crystallographic data for the compounds belonging to class **3c** and **6c**.

Identification code	**51**	**33**	**42**	**24**
Formula	$C_{13}H_9ClFN$	$C_{13}H_9BrFN$	$C_{13}H_9ClFN$	$C_{13}H_9BrFN$
Formula weight	233.66	278.12	233.66	278.12
CCDC No.	967466	904764	904771	904758
Solvent system	CH_3OH	CH_3COCH_3	C_2H_5OH	CH_3OH
Morphology	Plate	Block	Block	Plate
Crystal system	Monoclinic	Orthorhombic	Orthorhombic	Monoclinic
Space group	$P2_1/c$	*Pbcn*	*Pbca*	$P2_1/c$
a/Å	10.030(4)	12.9933(6)	12.4117(3)	12.112(2)
b/Å	3.8427(15)	11.4999(5)	9.8248(2)	3.9009(7)
c/Å	28.062(11)	14.9358(7)	17.9456(4)	23.337(5)
α/°	90	90.00	90.00	90.00
β/°	90.806(8)	90.00	90.00	104.714(4)
γ/°	90	90.00	90.00	90.00
Volume/Å^3	1081.4(7)	2231.7(2)	2188.33(8)	1066.5(4)
Z	4	8	8	4
Z′	1	1	1	1
ρ_{calc} (g/cm^3)	1.435	1.656	1.418	1.732
μ/mm^{-1}	0.334	3.666	0.331	3.835
***F*(000)**	480	1104	960	552
$\theta_{min,max}$ (º)	2.0, 25.0	2.7, 27.8	2.3, 26.4	2.2, 25.3
$h_{min,max}$; $k_{min,max}$; $l_{min,max}$	-5, 11; -4, 4; -32, 33	-7, 15; -13, 13; -17, 16;	-15, 7; -11, 12; -20, 22	-14, 12; -4, 2; -27, 25
No. of reflections	6584	12745	11432	6185
No. of Observed Reflections	1909	1712	2235	1873
No. of unique reflections	1640	1973	1979	1658
R(int)	0.0221	0.0274	0.018	0.0283
Data/restraints/parameters	1909/0/157	1973/13/157	2235/0/181	1873/0/177
GooF	1.043	1.058	1.039	1.051
R_obs	0.036	0.024	0.028	0.025
wR_2(obs)	0.084	0.051	0.074	0.060
$\Delta\rho_{min,max}$ (eÅ^{-3})	-0.34, 0.24	-0.32, 0.26	-0.27, 0.26	-0.40, 0.51

No similarity has been discerned in the crystal packing of the compounds belonging to the sub-class **6c** (**9**, **42**, **24**). The structure of **42** was solved in the orthorhombic centrosymmetric *Pbca* space group with Z = 8. The molecules of **42** form two types of heterodimers using weak C–H···F and C–H···N hydrogen bonds parallel to the *b*-axis (table 3.8b, figure 3.8e) and by involving C–H···F and C–H···Cl hydrogen bonds parallel to the *a*-axis (table 3.8b, figure 3.8f). Compound **24** has been found to crystallize in the monoclinic centrosymmetric $P2_1/c$ space group with Z = 4. The molecules related by the center of inversion interact through dimeric C–H···F hydrogen bonds, which are further interconnected among themselves by another C–H···F hydrogen bonds (table 3.8b, figure 3.8g). In this case, the F atom has been found to be trifurcated and the Br atom in the A ring does not involve in any intermolecular interaction.

It has been found that the stabilization energies provided by C6–H6···X (X = Cl1 or Br1) hydrogen bonds are similar as are found in the compounds **51** and **33**, but lesser than that provided by C6–H6···F1 hydrogen bond in the case of **9F1**. The values of the electron density and the Laplacian at the BCPs found between C–H···X (X = F, Cl or Br) hydrogen bonds lie in the range of 0.026–0.037 eÅ^{-3}, while values for the same involving the imine proton in C–H···N hydrogen bond is 0.054 eÅ^{-3}.

Table 3.8b: Details of intermolecular interactions, computed stabiliztion energies and topological parameters of compounds **9F1**, **9F2**, **51**, **33**, **42** and **24**

Code	C–H···X (X = N, F, Cl, Br)	*d* (H···X/Å)	θ (∠C–H···X/°)	Symmetry Code	SE_{G09} kcal/mol	ρ (eÅ^{-3})	$\nabla^2\rho$ (eÅ^{-5})
9A	C6–H6···F2	2.68	131	-x, 1-y, 1-z	-6.1	0.026	0.560
9B	C5–H5···F2	2.62	132	1-x, y+$^1/_2$, $^1/_2$-z	-3.5	0.028	0.558
	C12–H12···F2	2.64	176	x-$^1/_2$, $^1/_2$-y, -z	-1.9	0.027	0.555
51	C4A–H4A···Cl1A	2.87	142	x+1,y+1, z	-1.4	0.041	0.628
	C6A–H6A···Cl1A	2.87	133	1-x, 2-y, 1-z	-4.3	0.041	0.628
33	C6A–H6A···Br1A	3.04	126	-x, -y, 1-z	-4.4	0.041	0.555
42	C11–H11···F1	2.60	131	1-x, y+$^1/_2$, $^1/_2$-z	-0.8	0.037	0.715
	C12–H12···N1	2.57	140	1-x, y+$^1/_2$, $^1/_2$-z	-2.9	0.054	0.772
	C9–H9···F1	2.60	142	x-$^1/_2$, y, $^1/_2$-z	-1.0	0.035	0.676
	C5–H5···F1	2.53	139	x-$^1/_2$, $^1/_2$-y, 1-z	-1.1	0.036	0.719
	C6–H6···Cl1	2.98	120	x+$^1/_2$, $^1/_2$-y, 1-z	-1.5	0.041	0.555
24	C5–H5···F1	2.65	124	2-x, y-$^1/_2$,$^3/_2$-z	-4.4	0.029	0.608
	C6–H6···F1	2.69	122	2-x, y-$^1/_2$, $^3/_2$-z		0.029	0.601
	C12–H12···F1	2.67	144	2-x, 3-y, 1-z	-1.7	0.023	0.447

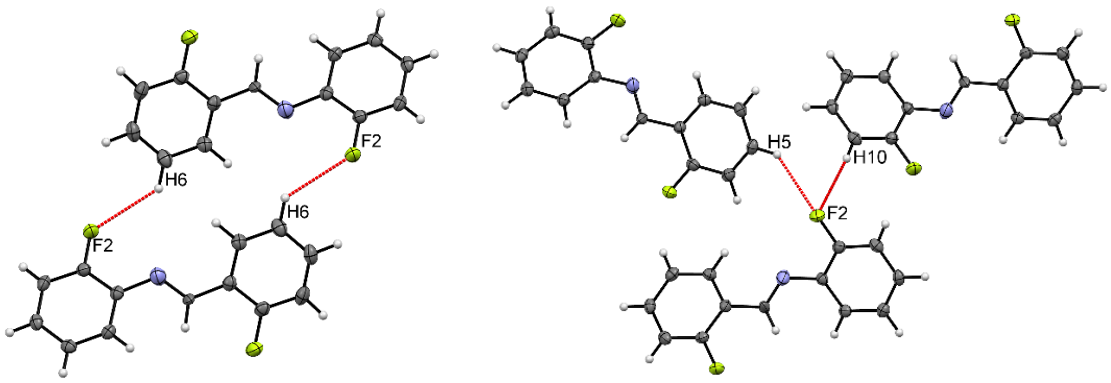

3.8a **3.8b**

Figure 3.8: (**a**) Formation of molecular sheet of dimers formed *via* weak C−H···F hydrogen bonds in **9F1**, **(b)** the packing of **9F2** in its crystal structure, *via* bifurcated C−H···F hydrogen bonds.

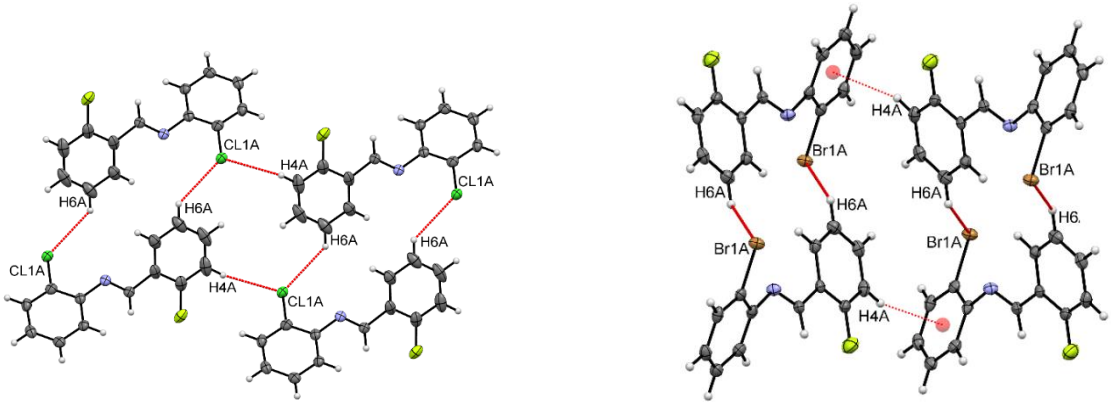

3.8c **3.8d**

Figure 3.8: **(c)** formation of dimers and their propagation through weak C–H···Cl hydrogen bonds in **51**; **(d)** molecular dimer formation and its propagation in the crystal lattice of **33** through weak C–H···Br and C–H···π interactions respectively.

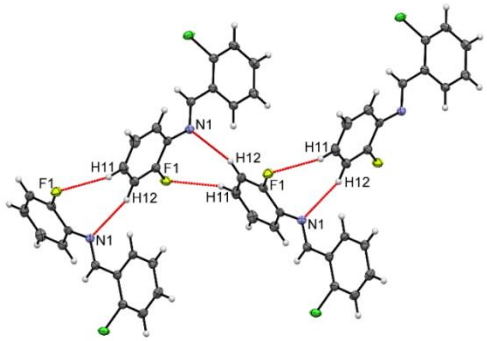

3. 8e

Figure 3.8: **(e)** Propagating dimers along the *b*-axis in the structure of **42**.

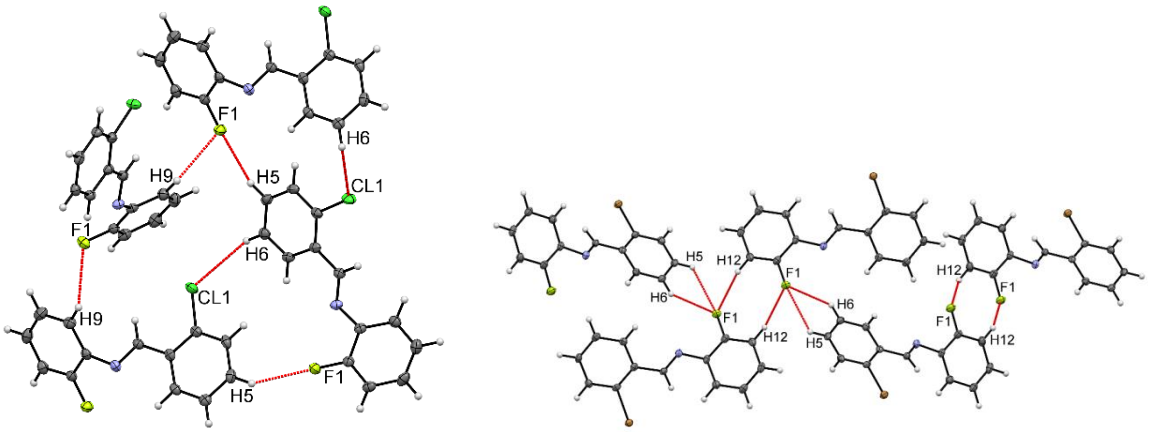

3.8f **3.8g**

Figure 3.8: **(f)** formation of heterodimers and its extension in the crystal structure of **42** through combination of C–H···F and C–H···Cl hydrogen bonds; **(g)** trifurcated C–H···F hydrogen bonds, which interconnect the molecules in the crystal structure of **24**.

3.6 Discussion

It is evident from the above structural discussion that these molecules mainly pack involving C–H···F hydrogen bonds with the cooperative effects of other weaker interactions such as C–X···X and C–H···π. The topological parameters [ρ, $\nabla^2\rho$, $V(\mathbf{r}_{CP})$, $G(\mathbf{r}_{CP})$ and $E(\mathbf{r}_{CP})$] at the (3, -1) bond critical point of all C–H···F hydrogen bonds have been plotted against R_{ij} (length of the bond path as found using AIM2000) using SigmaPlot[132] and the plotted points are fitted with a suitable exponential function (figure 3.9). These plots with the equations and the corresponding values of R^2 are reported in the following figures [figure 3.9a and 3.9b, (ESI, table S3.8)]. These plots show similar trends as were observed by Munshi and Guru Row in their analysis of C–H···O hydrogen bonds using both experimental and theoretical charge density analysis.[130] Therefore, it may be concluded that C–H···F interactions can also be classified as weak hydrogen bonds similar to C–H···O hydrogen bonds. In the following paragraphs, the various features and trends that we have found in the structures reported herein, will be highlighted.

1. The above structural description clearly indicates that the *chloro*- and *bromo*- analogues display similar packing features and in many cases they are found to be isostructural in general, while the corresponding fluorinated derivatives have exhibited different packing characteristics, thereby producing different crystal structures altogether. Only a few *chloro*- and *bromo*- analogues (**43** and **25**, **42** and **24**) did not show similarity in their crystal packing as was observed in all the other cases.

2. We observed that some of the packing features of the *difluoro* compounds (1-9) remain intact even in the crystal packing of their corresponding *chloro*- and *bromo*- analogues in the eight compounds studied here.

3. The first example of this feature has been observed in the cases, where the fluorine atom is present at the *para*- position on the B ring, and either Cl or Br is present at the *para*- or *meta*- position on the A ring (class **4a** and **4b**). In these cases, the formation of same type of zigzag chains through C–H···F hydrogen bonds involving the *para*-F on the B ring (**1**, **34**, **16**, **37** and **19**) (figures 3.1a, 3.1d, 3.1e, 3.4e and 3.4f) have been observed. Additionally, in the cases of **3**, **18**, **36**, **6**, **21** and **39**, where F is present on the *ortho*- position of the B ring and F/Cl/Br is present at the *para*- or *meta*- position on the A ring, the structures of those compounds have been majorly influenced by the intermolecular C–H···F hydrogen bond (with stabilization energy in the range of 4-5 kcal/mol) involving the imine hydrogen and *o*-F of the B ring. It is noteworthy that in the above structures, the halogen atom present on the A ring generally did not participate in any of the intermolecular interactions (figures 3.3a to 3.3h).

4. The robustness of the synthons found in **3**, **6** and **8** was experienced, when the non-interacting fluorine was replaced by Cl or Br in the cases of compounds belonging to the class **3b** (**8**, **32** and **50**) (figures 3.7a, 3.7b and 3.7c), the class **6a** (**3**, **36** and **18**) (figures 3.3a, 3.3b, 3.3c, 3.3f and 3.3h) and the class **6b** (**6**, **21** and **39**) (figures 3.5a, 3.5c and 3.5d).

5. On the other hand, when the interacting fluorine is replaced by Cl or Br, then the possibility of the robust synthon found in **3** and **6** was removed, due to which the resulting compounds (**27**, **30**, **45**, and **48**) were found to be liquids at ambient conditions.

6. Further, it is noteworthy that the dimers involving imine H in the formation of C–H···F hydrogen bonds have higher stabilization energies (4-5 kcal/mol), than those involving aromatic hydrogens (<4 kcal/mol). This feature is further reinforced by the higher values of [ρ (0.041–0.068 eÅ^{-3}) and $\nabla^2\rho$ (0.77–1.14 eÅ^{-5})] at the BCPs found for the C–H···F hydrogen bonds involving imine H in comparison to those involving aromatic hydrogens [ρ (0.023–0.043 and $\nabla^2\rho$ (0.47–0.80 eÅ^{-5})].

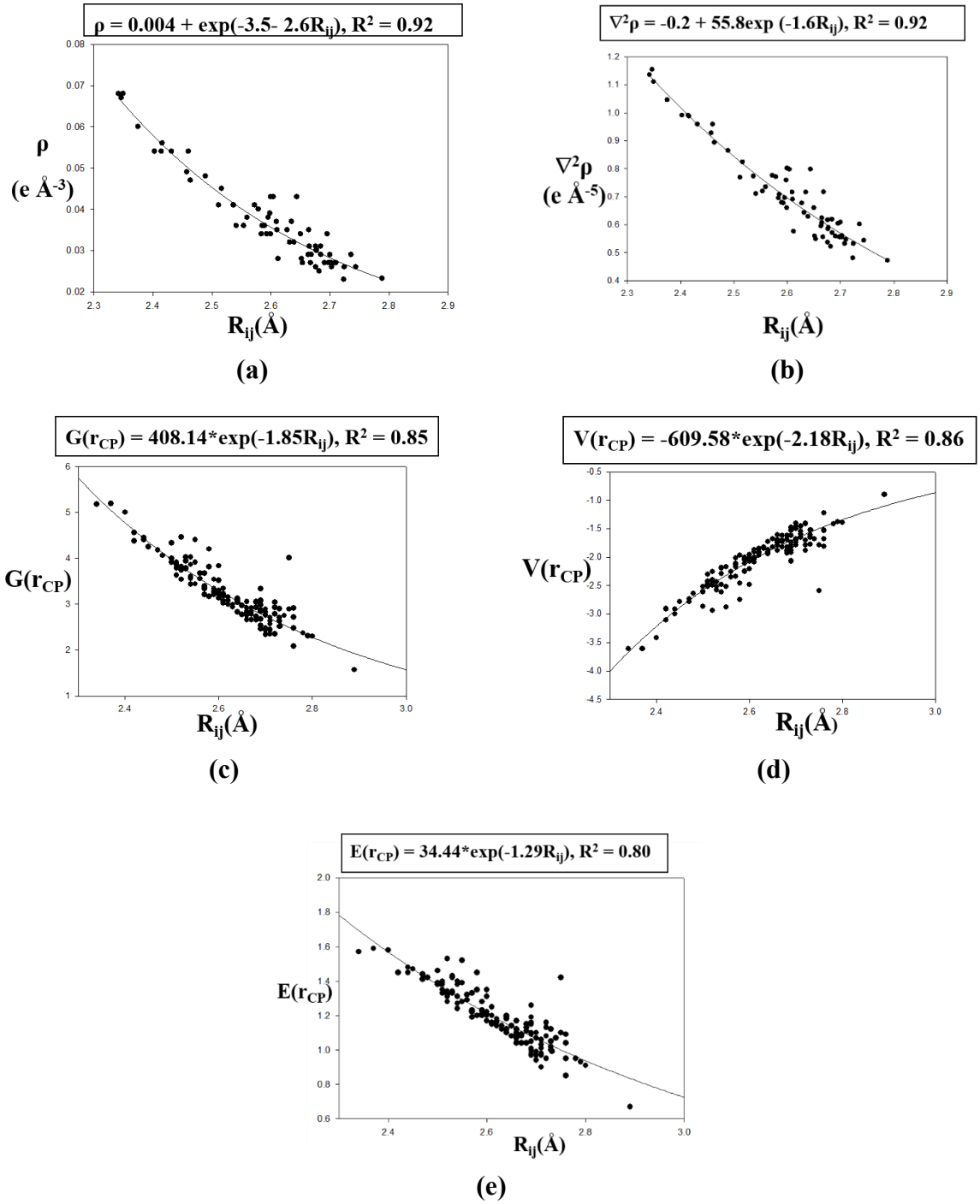

Figure 3.9: 2D plot between **(a)** ρ vs R_{ij}, **(b)** $\nabla^2\rho$ vs R_{ij}, **(c)** $G(\mathbf{r}_{CP})$ vs R_{ij}, **(d)** $V(\mathbf{r}_{CP})$ vs R_{ij}, and **(e)** $E(\mathbf{r}_{CP})$ vs R_{ij}.

3.7 Conclusions

This study underlines the importance of "organic fluorine" in displaying unique features in the crystal packing of the fluorinated molecules in comparison to its heavier halogen analogues, present in a series of isomeric *N*-benzylideneanilines. In this systematic analysis, the robustness of the supramolecular synthons involving C–H···F hydrogen bonds

in the absence of –COOH, –OH, –NH–, –NH_2, *etc*. groups has been emphasized. Thus, the distinctiveness of "organic fluorine" among the halogens have been notified through this systematic study of the structures. The stabilization energies supported by the topological properties affirm the strength and directional nature of C–H···F hydrogen bonds. The stabilization energies provided by dimers formed by C–H···F hydrogen bonds involving imine hydrogen have been found to be similar to those provided by other weak hydrogen bonds such as C–H···N and C–H···O. Halogen···halogen interactions over C–H···X (X = Cl or Br) hydrogen bonds are preferred for the heavier halogens, which is in accordance with earlier observations by other research groups. Through AIM calculations on the extracted dimers from the crystal structure, BCPs have always been found between the atoms interacting through C–H···F hydrogen bonds with the positive value of Laplacian. This illustrates the closed shell nature of the interactions between the atoms involved, irrespective of their stabilization energies and the nature of concerned hydrogen involved. Hence, in the current chapter, we gain better understanding of the fluorine mediated intermolecular interactions in the presence of its heavier analogues (Cl or Br).

Chapter 4

Study of Robustness of the Synthons Involving C–H···F Hydrogen Bond(s): Insights from the Structural and Computational Analyses of Tetrafluorinated *N*-benzylideneanilines

Chapter 4

4.1 Introduction

The role of C–H···F hydrogen bonds in determining the packing motifs in the system of *N*-benzylideneanilines have been established in the previous chapters. The robustness of synthons involving C–H···F hydrogen bonds have also been substantiated by the replacement of non-interacting F with Cl or Br. This chapter deals with the influence of addition of more F atoms to the robustness of the synthons discussed in chapter 3. In addition to that, we also intend to correlate the formation of synthons with that of the position of the substituents. A few robust synthons involving C–H···F hydrogen bonds have been identified in these molecules. To quantify the contributions of the interactions involved in those synthons, *ab-initio* calculations have also been done. Additionally, topological properties of these C–H···F interactions have been studied through AIM (atoms in molecules) analysis.

4.2.1 Synthesis and Characterization

All the compounds were synthesized by the same procedure as was given in the chapter 1. Scheme **6.1** describes all the synthesized molecules. There are six different *difluoro* substituted benzaldehydes and anilines namely 2,3; 2,4; 2,5; 2,6; 3,4; 3,5. A total of 36 (6×6) compounds were synthesized by using various combinations of difluorobenzaldehydes and difluoroanilines as can be inferred from the scheme **6.2**. Out of 36 synthesized compounds, 35 compounds were found to be solid at room temperature (25

^{o}C), and only one compound was found to exist as liquid (containing 2,6-difluoroaniline and 2,6-difluorobenzaldehyde).

All the synthesized compounds were characterized by ^{1}H NMR (400 MHz, Bruker Biospin Avance-III NMR spectrometer) (ESI, figures S4.1:1 to S4.1:36) and FTIR spectroscopy (Bruker Tensor 72, equipped with diamond cell ATR) (ESI, figures S4.2:1 to S4.2:36). Melting points (table S4.1) were determined from the DSC data (Perkin Elmer DSC 8000) (ESI, figures S4.4:1 to S4.4:36). The ORTEP of all the compounds have been drawn at 50% probability for the non-H atoms using Mercury 3.3 and are shown with the atom labels (ESI, figures S4.5:1 to S4.5:36).

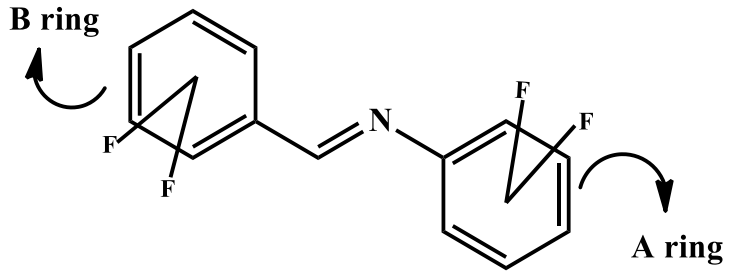

Scheme 4.1: Tetrafluoro substituted *N*-benzylideneanilines

Scheme 4.2: Possible combination of different *difluoro* substituted benzaldehydes and anilines, which were condensed together to give the required product.

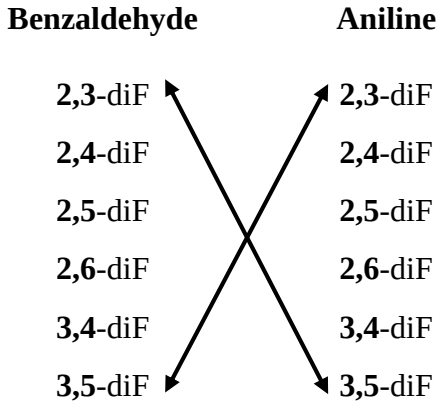

Table 4.1a: Compound Identification Table

Code	Position of F atoms on B ring	Position of F atoms on A ring
52	3,4	2,3
53	3,4	2,4
54	3,4	2,5
55	3,4	2,6
56	3,4	3,4
57	3,4	3,5
58	3,5	2,3
59	3,5	2,4
60	3,5	2,5
61	3,5	2,6
62	3,5	3,4
63	3,5	3,5
64	2,3	2,3
65	2,3	2,4
66	2,3	2,5
67	2,3	2,6
68	2,3	3,4
69	2,3	3,5

Code	Position of F atoms on B ring	Position of F atoms on A ring
70	2,4	2,3
71	2,4	2,4
72	2,4	2,5
73	2,4	2,6
74	2,4	3,4
75	2,4	3,5
76	2,5	2,3
77	2,5	2,4
78	2,5	2,5
79	2,5	2,6
80	2,5	3,4
81	2,5	3,5
82	2,6	2,3
83	2,6	2,4
84	2,6	2,5
85(L)	2,6	2,6
86	2,6	3,4
87	2,6	3,5

4.3 Crystallography

4.3.1 Powder X-ray diffraction studies

Powder X-ray Diffraction (PXRD) data were recorded on a Rigaku Ultimia IV diffractometer following the same strategy as has been discussed in the earlier chapters for all the solid compounds.

The PXRD patterns have been simulated from the crystal coordinates using Mercury 3.3 and have been compared with the observed PXRD patterns (using WINPLOTR) (ESI, figures S4.3:1 to S4.3:35) as was done earlier.

4.3.2 Crystal Growth, Single Crystal Data Collection, Structure Solution and Refinement

Single crystals of all the purified solids were grown from different solvents and solvent mixtures (table 4.1b) at the low temperature using slow solvent evaporation. Single crystal X-ray diffraction data collection, structure solution, and refinements were done for

all the compounds by following the same procedure as discussed in the chapter 2. Table 4.1b lists the crystal and refineent data for all the compounds. All the geometric calculations and the generation of publication material were done following the same procedure as done for the earlier chapters.

4.4 Theoretical Calculations

4.4.1 Stabilization Energy Calculations

Our studied compounds don't possess any strong hydrogen bonding sites. Therefore, the interactions present in our system are of the type of C–H···π, π···π, C–H···F, C–F···F–C, C–F···π. Out of these our main interest is to study the robustness of the synthons formed by the utilization of C–H···F hydrogen bonds. Therefore, the stabilization energies of the molecular dimers formed through C–H···F hydrogen bonds have been calculated at MP2 level of theory at 6-31+G(d) basis set using Gaussian09 (G09) as described in detail in the previous chapter. The stabilization energies ($SE_{G09} = E_{dimer} - 2\times E_{monomer}$) of these dimers were corrected for the basis set superposition error (BSSE) by using counterpoise method. Gauss view was used to visualize the molecules during Gaussian calculations.

4.4.2 AIM Calculations

To study the topological properties of the C–H···F hydrogen bonds, Atoms in Molecules (AIM) calculations were done on the dimers obtained from the crystal structures using AIM2000. In all the studied dimers, a (3, -1) bond critical point (BCP) has been observed between the interacting H and F atoms. The topological properties of all C–H···F hydrogen bonds have been calculated at the BCPs. The electron density (ρ), Laplacian ($\nabla^2\rho$), local potential ($V(\mathbf{r}_{CP})$), kinetic ($G(\mathbf{r}_{CP})$) and total energy densities ($E(\mathbf{r}_{CP})$), which were found at BCPs, have been plotted against bond path (R_{ij}) using sigma plot.

Table 4.1b: Crystallographic Data for the compounds **52**–**87**

Identification code	**52**	**53**	**54**	**55**	**57**
Formula	$C_{13}H_7F_4N$	$C_{13}H_7F_4N$	$C_{13}H_7F_4N$	$C_{13}H_7F_4N$	$C_{13}H_7F_4N$
FW	253.2	253.2	253.2	253.2	253.2
CCDC No.	1008431	1008432	1008433	1008434	1008435
Solvent system	CH_3OH	CH_3COCH_3	CH_3OH	CH_2Cl_2+C_6H_{12}	$CH_3COOC_2H_5$
Morphology	Plate	Block	Needle	Block	Rod
Crystal System	Monoclinic	Orthorhombic	Monoclinic	Monoclinic	Monoclinic
Space Group	*Pn*	*Pna*2$_1$	*C*2/*c*	*P*2$_1$/*c*	*P*2$_1$/*c*
a (Å)	4.5622(6)	13.5270(9)	12.799(2)	5.9148(3)	25.7588(17)
b (Å)	9.9940(12)	3.7794(3)	6.5794(8)	7.4926(4)	3.7207(3)
c (Å)	11.5383(12)	21.0491(13)	25.265(4)	23.9195(13)	22.6104(16)
α (^{0})	90.00	90.00	90.00	90.00	90.00
β (^{0})	90.826(6)	90.00	95.749(8)	93.722(2)	90.424(4)
γ (^{0})	90.00	90.00	90.00	90.00	90.00
Volume (Å^3)	526.03(11)	1076.11(13)	2116.9(5)	1057.81(10)	2166.9(3)
Z	2	4	8	4	8
Z′	1	1	1	1	2
ρ (g/cm^3)	1.599	1.563	1.589	1.590	1.56
μ (mm^{-1})	0.144	0.141	0.143	0.143	0.141
***F* (000)**	256.0	512.0	1024.0	512.0	1024.8
$\theta_{min,max}$ (^{o})	2.7, 25.0	1.9, 25.0	1.9, 25.0	2.8, 25.0	2.4, 25.0
h_{min}, h_{max}; k_{min}, k_{max}; .l_{min}, l_{max}	-5, 5; -11, 11; -13, 13	-16, 12; -3, 4; -25, 23	-15, 15; -7, 7; -30, 28	-3, 7; -8, 8; -28, 28	-30, 28; -3, 4; -26, 21
No. of reflections.	2281	3901	5170	7170	14247
No. of unique reflections.	1365	1750	1868	1863	3831
No of observed reflections	1335	1630	1598	1687	3345
No. of parameters	163	163	163	163	326
wR$_2$_obs, R_obs	0.072, 0.027	0.097, 0.038	0.085, 0.032	0.073, 0.026	0.204, 0.037
$\Delta\rho_{min,max}$ (eÅ^{-3})	-0.17, 0.16	-0.25, 0.33	-0.20, 0.20	-0.22, 0.18	-0.51, 0.44
GooF	1.078	1.080	1.053	1.052	1.135

Table 4.1b: Crystallographic Data for the compounds **52**–**87** (Continued)

Identification code	**58**	**59**	**60**	**61**	**63**
Formula	$C_{13}H_7F_4N$	$C_{13}H_7F_4N$	$C_{13}H_7F_4N$	$C_{13}H_7F_4N$	$C_{13}H_7F_4N$
FW	253.2	253.2	253.2	253.2	253.2
CCDC No.	1008436	1008437	1008438	1008439	1008440
Solvent system	C_2H_5OH	CH_2Cl_2	CH_3CN	CH_2Cl_2+C_6H_{12}	$CH_3COOC_2H_5$+ C_6H_{12}
Morphology	Block	Block	Needle	Irregular	Plate
Crystal System	Monoclinic	Monoclinic	Monoclinic	Orthorhombic	Orthorhombic
Space Group	*Pc*	*C*2/*c*	$P2_1/c$	$P2_12_12_1$	$Pca2_1$
a (Å)	12.496(5)	25.983(2)	7.2368(5)	5.4757(11)	27.6959(14)
b (Å)	3.7100(14)	7.3160(6)	6.6503(5)	7.7423(15)	3.68490(10)
c (Å)	22.745(9)	24.834(2)	22.2218(14)	24.406(5)	21.5993(10)
α (^{0})	90.00	90.00	90.00	90.00	90.00
β (^{0})	93.123(5)	113.707(5)	97.167(3)	90.00	90.00
γ (^{0})	90.00	90.00	90.00	90.00	90.00
Volume (Å^3)	1052.9(7)	4322.3(6)	1061.11(13)	1034.7(3)	2204.35(16)
Z	4	16	4	4	8
Z′	2	2	1	1	1
ρ (g/cm^3)	1.597	1.556	1.585	1.625	1.53
μ (mm^{-1})	0.144	0.140	0.143	0.147	0.138
***F* (000)**	512.0	2048.0	512.0	512.0	1024.0
$\theta_{min,\ max}$ (^{o})	2.4, 27.1	2.9, 27.3	2.8, 25.0	2.7, 25.0	1.5, 25.1
h_{min}, h_{max}; k_{min}, k_{max}; l_{min}, l_{max}	-16, 14; -2, 4; -26, 29	-30, 33; -9, 9; -32, 32	-8, 8; -6, 7; -26, 26	-5, 6; -9, 6; -29, 29	-27, 33; -4, 4; -25, 26
No. of reflections.	5417	24110	7190	5704	13533
No. of unique reflections.	0.0446	0.0402	0.0150	0.0188	0.0347
No of observed reflections	3878	4848	1870	1812	4145
No. of parameters	325	325	163	163	325
wR_2_obs, R_obs	0.123, 0.054	0.097, 0.044	0.073, 0.027	0.078, 0.027	0.095, 0.042
$\Delta\rho_{min,max}$ (eÅ^{-3})	-0.17, 0.16	-0.25, 0.33	-0.20, 0.20	-0.22, 0.18	-0.51, 0.44
GooF	1.078	1.080	1.053	1.052	1.135

Table 4.1b: Crystallographic Data for the compounds **52**–**87** (Continued)

Identification code	**64**	**65**	**66**	**68**	**69**
Formula	$C_{13}H_7F_4N$	$C_{13}H_7F_4N$	$C_{13}H_7F_4N$	$C_{13}H_7F_4N$	$C_{13}H_7F_4N$
FW	253.2	253.2	253.2	253.2	253.2
CCDC No.	1008441	1008442	1008443	1008444	1008445
Solvent system	CH_3CN	CH_2Cl_2+C_6H_{12}	$CH_3COOC_2H_5$	CH_3OH	$CH_3COOC_2H_5$
Morphology	Needle	Block	Plate	Block	Plate
Crystal System	Triclinic	Monoclinic	Triclinic	Monoclinic	Monoclinic
Space Group	$P\ \bar{1}$	$P2_1$	$P\ \bar{1}$	$P2_1$	$P2_1/c$
a (Å)	6.8244(6)	11.0553(15)	6.8223(8)	9.756(3)	16.497(2)
b (Å)	7.6412(7)	3.6976(4)	7.5505(8)	4.674(2)	3.7422(4)
c (Å)	10.8203(10)	13.0135(14)	11.2975(14)	11.257(4)	17.009(2)
α (^{0})	79.604(6)	90.00	80.541(7)	90.00	90.00
β (^{0})	83.948(6)	98.716(4)	86.409(7)	99.132(17)	94.425(8)
γ (^{0})	69.737(6)	90.00	66.173(7)	90.00	90.00
Volume (Å^3)	520.07(8)	525.82(3)	525.11(19)	506.81(14)	1046.96(7)
Z	2	2	2	2	4
Z′	1	1	1	1	1
ρ (g/cm^3)	1.62	1.60	1.60	1.66	1.61
μ (mm^{-1})	0.146	0.144	0.145	0.150	0.145
***F* (000)**	256.0	256.0	256.0	256.0	512.0
$\theta_{min,\ max}$ (^{o})	2.9, 25.0	1.9, 25.0	3.0, 25.0	2.6, 25.0	1.8, 25.0
h_{min}, h_{max}; k_{min}, k_{max}; l_{min}, l_{max}	-7, 8; -9, 9; -12, 12	-13, 9; -4, 3; -15, 14	-8, 7; -8, 8; -13, 12	-11, 10; -4, 5; -13, 13	-19, 19; -4, 4; -20, 19
No. of reflections.	3815	2304	4918	3341	5300
No. of unique reflections.	1821	1766	1840	1386	1854
No of observed reflections	1597	1394	1467	1276	1501
No. of parameters	163	163	163	163	163
wR$_2$_obs, R_obs	0.115, 0.039	0.184, 0.045	0.083, 0.034	0.091, 0.041	0.085, 0.033
$\Delta\rho_{min,max}$(eÅ^{-3})	-0.30, 0.37	-0.32, 0.96	-0.24, 0.23	-0.17, 0.47	-0.21, 0.17
GooF	1.118	1.058	1.048	1.076	1.021

Table 4.1b: Crystallographic Data for the compounds **52**–**87** (Continued)

Identification code	**70**	**71**	**73**	**74**	**75**
Formula	$C_{13}H_7F_4N$	$C_{13}H_7F_4N$	$C_{13}H_7F_4N$	$C_{13}H_7F_4N$	$C_{13}H_7F_4N$
FW	253.2	253.2	253.2	253.2	253.2
CCDC No.	1008446	1008447	1008448	1008449	1008450
Solvent system	CH_3OH	CH_2Cl_2+ $CH_3COOC_2H_5$	CH_3CN	C_2H_5OH	C_2H_5OH
Morphology	Block	Rod	Needle	Block	Irregular
Crystal System	Triclinic	Monoclinic	Orthorhombic	Triclinic	Orthorhombic
Space Group	$P\ \bar{1}$	$P2_1$	$P2_12_12_1$	$P\ \bar{1}$	$P2_12_12_1$
a (Å)	6.7242(6)	3.8029(4)	3.7270(7)	3.7169(6)	3.6872(3)
b (Å)	8.3077(7)	11.4621(14)	11.656(2)	11.5058(19)	12.9017(8)
c (Å)	10.3309(9)	12.2186(15)	25.035(5)	12.530(2)	22.262(2)
α (^{0})	74.956(4)	90.00	90.00	97.022(11)	90.00
β (^{0})	73.491(4)	94.778(6)	90.00	93.644(11)	90.00
γ (^{0})	74.437(4)	90.00	90.00	91.313(12)	90.00
Volume (Å^3)	522.43(8)	530.75(11)	1087.6(4)	530.52(15)	1059.02(1)
Z	2	2	4	2	4
Z′	1	1	1	1	1
ρ (g/cm^3)	1.61	1.59	1.55	1.58	1.59
μ (mm^{-1})	0.145	0.143	0.140	0.143	0.143
***F* (000)**	256.0	256.0	512.0	256.0	512.0
$\theta_{min,\ max}$ (^{o})	2.1, 25.0	2.4, 27.1	1.6, 25.0	1.6, 25.0	2.4, 25.0
h_{min}, h_{max}; k_{min}, k_{max}; l_{min}, l_{max}	-7, 7; -9, 9; -11, 12	-4, 4; -12, 14; -15, 15	-3, 4; -13, 11; -19, 29	-4, 4; -12, 13; -14, 14	-4, 3; -15, 13; -6, 26
No. of reflections.	5125	4729	4534	2973	3637
No. of unique reflections.	1835	1976	1771	1861	1796
No of observed reflections	1556	1936	1340	1371	1539
No. of parameters	163	191	163	171	163
wR_2_obs, R_obs	0.089, 0.032	0.066, 0.024	0.125, 0.051	0.110, 0.046	0.075, 0.037
$\Delta\rho_{min,max}$(eÅ^{-3})	-0.23, 0.22	-0.18, 0.21	-0.22, 0.40	-0.29, 0.25	-0.18, 0.17
GooF	1.047	1.068	0.999	1.043	1.023

Table 4.1b: Crystallographic Data for the compounds **52**–**87** (Continued)

Identification code	**76**	**77**	**78**	**80**	**81**
Formula	$C_{13}H_7F_4N$	$C_{13}H_7F_4N$	$C_{13}H_7F_4N$	$C_{13}H_7F_4N$	$C_{13}H_7F_4N$
FW	253.2	253.2	253.2	253.2	253.2
CCDC No.	1008462	1008463	1008464	1008465	1008466
Solvent system	CH_3CN+ $CH_3COOC_2H_5$	$CH_3COOC_2H_5$	CH_2Cl_2	CH_3OH	C_6H_{12}+ $CH_3COOC_2H_5$
Morphology	Needle	Plate	Needle	Block	Thin Plate
Crystal System	Monoclinic	Triclinic	Monoclinic	Monoclinic	Orthorhombic
Space Group	$P2_1/c$	$P\ \bar{1}$	$P2_1/c$	$P2_1/c$	$P2_12_12_1$
a (Å)	6.8363(4)	7.3598(10)	6.6472(4)	13.7505(4)	3.7226(6)
b (Å)	13.8701(8)	12.5972(14)	15.8920(9)	3.7574(1)	13.105(2)
c (Å)	11.6974(6)	12.6690(16)	10.0448(5)	26.3533(7)	21.768(4)
α (°)	90.00	70.079(7)	90.00	90.00	90.00
β (°)	105.915(3)	75.851(8)	92.712(3)	130.149(2)	90.00
γ (°)	90.00	78.418(7)	90.00	90.00	90.00
Volume (Å^3)	1066.6(1)	1061.9(2)	1059.92(2)	1040.7(2)	1062.0(3)
Z	4	4	4	4	4
Z′	1	2	1	1	1
ρ (g/cm^3)	1.58	1.58	1.59	1.62	1.58
μ (mm^{-1})	0.142	0.143	0.143	0.146	0.143
***F* (000)**	512.0	512.0	512.0	512.0	512.0
$\theta_{min,\ max}$ (°)	2.9, 28.7	1.7, 25.0	2.4, 25.0	1.7, 25.0	1.8, 25.0
h_{min}, h_{max}; k_{min}, k_{max}; l_{min}, l_{max}	-9, 4; -13, 18; -15, 15	-8, 5; -14, 13; -15, 11	-5, 7; -18, 16; -11, 11	-16, 16; -4, 4; -31, 30	-2, 4; -15, 15; -25, 25
No. of reflections.	8250	9688	5694	7150	5829
No. of unique reflections.	2757	3727	1864	1827	1852
No of observed reflections	2196	2465	1610	1533	1542
No. of parameters	163	325	163	163	163
wR_2_obs, R_obs	0.091, 0.037	0.094, 0.042	0.080, 0.032	0.087, 0.033	0.066, 0.037
$\Delta\rho_{min,max}$(eÅ^{-3})	-0.29, 0.31	-0.23, 0.42	-0.19, 0.20	-0.22, 0.31	-0.18, 0.16
GooF	1.064	1.010	1.051	1.045	1.062

Table 4.1b: Crystallographic Data for the compounds **52**–**87** (Continued)

Identification code	**82**	**83**	**84**	**86**	**87**
Formula	$C_{13}H_7F_4N$	$C_{13}H_7F_4N$	$C_{13}H_7F_4N$	$C_{13}H_7F_4N$	$C_{13}H_7F_4N$
FW	253.2	253.2	253.2	253.2	253.2
CCDC No.	1008467	1008468	1008471	1008469	1008470
Solvent system	CH_3OH	$CH_3COOC_2H_5$	C_2H_5OH	CH_3COCH_3	CH_2Cl_2+ $CH_3COOC_2H_5$
Morphology	Block	Needle	Irregular	Needle	Thin Plate
Crystal System	Monoclinic	Monoclinic	Monoclinic	Triclinic	Monoclinic
Space Group	*Cc*	$P2_1/c$	$P2_1/c$	$P\bar{1}$	$P2_1/c$
a (Å)	7.004(3)	10.0995(3)	7.092(2)	6.790(1)	7.345(2)
b (Å)	30.750(13)	9.0827(3)	30.276(10)	6.803(1)	21.755(6)
c (Å)	10.041(4)	18.1054(4)	10.124(3)	12.062(2)	14.366(4)
α (^{0})	90.00	90.00	90.00	84.04(1)	90.00
β (^{0})	99.000(5)	141.529(1)	99.046(4)	85.23(1)	109.888(3)
γ (^{0})	90.00	90.00	90.00	72.40(1)	90.00
Volume (Å^3)	2135.9(15)	1033.23(5)	2146.6(12)	527.4(2)	2158.6(3)
Z	8	4	8	2	8
Z′	1	1	2	1	2
ρ (g/cm^3)	1.57	1.63	1.57	1.59	1.56
μ (mm^{-1})	0.142	0.147	0.141	0.144	0.141
***F* (000)**	1024.0	512.0	1024.0	256.0	1024.0
$\theta_{min,\ max}$ (^{o})	2.4, 25.0	2.3, 25.0	2.2, 27.1	1.7, 25.0	2.4, 25.0
h_{min}, h_{max}; k_{min}, k_{max}; l_{min}, l_{max}	-3, 8; -36, 36; -11, 11	-8, 12; -8, 10; -21, 15	-9, 3; -37, 38; -12, 12	-8, 7; -8, 4; -14, 14	-8, 8; -11, 25; -16, 16
No. of reflections.	5980	5467	13669	5009	12186
No. of unique reflections.	2697	1822	4719	1848	3800
No of observed reflections	2393	1532	3430	1361	2846
No. of parameters	325	163	325	163	325
wR$_2$_obs, R_obs	0.067, 0.032	0.086, 0.033	0.010, 0.044	0.223, 0.081	0.078, 0.037
$\Delta\rho_{min,max}$(eÅ^{-3})	-0.21, 0.15	-0.31, 0.23	-0.27, 0.24	-0.38, 0.86	-0.23, 0.19
GooF	1.023	1.057	1.019	1.106	1.041

4.5 Results and Discussion

Out of 35 solid compounds with tetrafluoro substituents, crystals of 30 compounds could be grown and the structures of these 30 compounds were determined. Out of 36 possible compounds, only one of the compound (**85**) was found to be liquid, which could not be crystallized using *in situ* crystallization technique in spite of the several attempts made. The detailed structural descriptions of these compounds are given in the ESI. We intend to carry forward the results of our previous chapter, where we had described some synthons, which have been found to remain unaltered upon replacement of non-interacting F with Cl or Br. In the following sections, we would discuss the robustness of those synthons on the addition of more number of fluorine atoms in the system studied.

Synthon I (A, B and C): The following synthons **I(A), I(B) and I(C)** involving the imine hydrogen have been found to occur frequently in the studied compounds (figure 4.1). In chapter 3, it was pointed out that structures of compounds **3**, **18**, **36**, **6**, **21** and **39**, (F at the *ortho*- position on the A ring; F/Cl/Br at *para*- or *meta*- position on the B ring) is majorly directed by the short, directional and sufficiently stabilizing intermolecular C–H···F hydrogen bonds (with stabilization energy in the range of 4-5 kcal/mol) involving imine hydrogen and the *o*-F of the A ring. The same has been observed here as well. When the position of the fluorine atom on the B ring is either 3,4 or 3,5 and one of the fluorine present at A ring is at the *ortho* position then this type of synthons have always been observed. In these particular synthons, the adjacent H present at the A or B ring may also involve in C–H···F hydrogen bond formation depending upon the orientation of the acceptor molecule with respect to the donor molecule. It is noteworthy that, the C–H···F hydrogen bonds involving imine H has always been observed to be short (mostly between 2.3-2.5 Å) and directional and the neighbouring hydrogen bonds are formed in a cooperative manner.

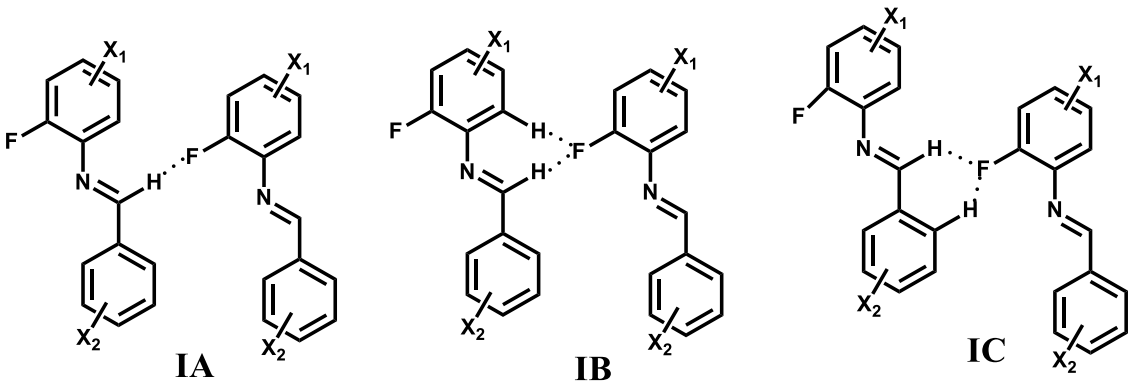

Figure 4.1: A schematic representation of the synthons **I(A)**, **I(B)** and **I(C)**

Occurrence of synthon I(A)/I(C) in dihalogen substituted *N*-benzylideneanilines

When a fluorine atom is present at the *ortho* position of A ring and 2nd F/Cl/Br are present at the *para* or *meta* position of B ring (**3**, **18**, **36**, **6**, **21** and **39**), the following dimers consist of short and directional C–H···F hydrogen bonds (with stabilization energy in the range of 4-5 kcal/mol) are observed in their crystal lattices (figure 4.2, table 4.1).

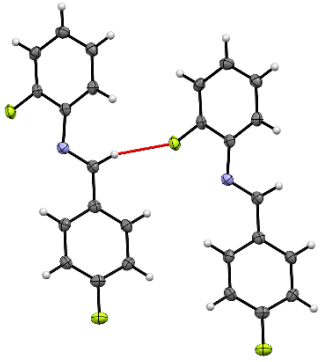

3: **4F(B)-2F(A)**

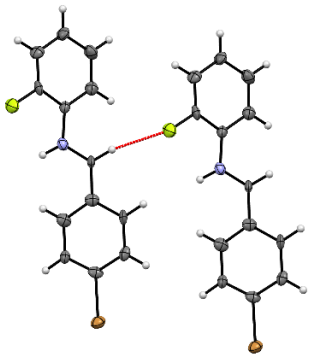

18: **4Br(B)-2F(A)**

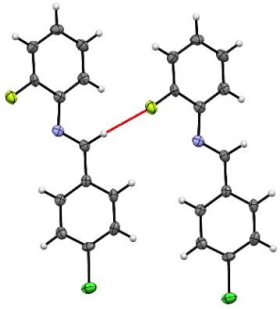

36: **4Cl(B)-2F(A)**

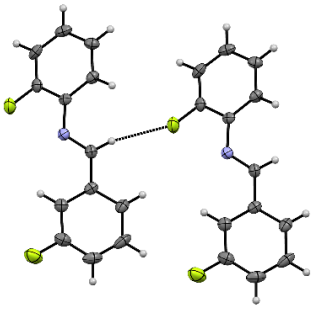

6: 3F(B)-2F(A)

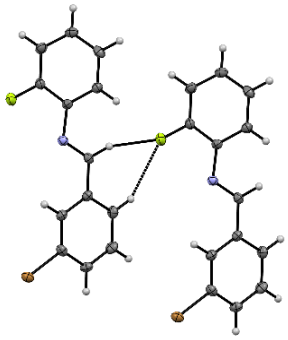

21: 3Br(B)-2F(A)

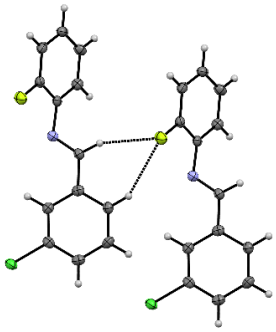

39: 3Cl(B)-2F(A)

Figure 4.2: Formation of synthon I(A) and I(C) in the cases of compound **3**, **18, 36, 6**, **21** and **39**.

Occurrence of synthon I(A)/I(B) in tetrafluoro substituted *N*-benzylideneanilines

In the compounds **52**, **53**, **54** and **55**, where position of one of the F on the A ring is *ortho* (the possible substitutions will be 2,3; 2,4; 2,5; 2,6), and the position of the fluorine atoms on the B ring is either 3,4 or 3,5; synthon I(A) has been observed (figure 4.3, table 4.1) except in the compound **53**: **3,4-diF(B)–2,4-diF(A).**

Table 4.1: Details of the geometrical parameters for all C–H···F hydrogen bonds, the values of electron densities and Laplacians at their BCPs.

Code	C–H···F	*d* (H···F/Å)	θ (∠C–H···F/º)	Symmetry Code	SE_{G09} kcal/mol	*ρ* ($eÅ^{-3}$)	$\nabla^2\rho$ ($eÅ^{-5}$)
3	C1–H1···F2	2.32	162	x+1, y, z	-4.8	0.068	1.110
	C14–H14···F4	2.30	161	x-1, y, z	-4.8	0.068	1.135
18F1	C1–H1···F1	2.44	156	x+1, y, z	-5.0	0.054	0.958
18F2	C1–H1···F1	2.35	168	x, y-1, z	-5.1	0.060	1.045
	C14–H14···F2	2.41	159	x, y+1, z	-5.1	0.054	0.958
36F1	C1–H1···F1	2.31	160	1-x, y-$^1/_2$, $^1/_2$-z	-4.8	0.056	0.987
36F2	C1–H1···F1	2.37	173	x, y-1, z	-5.0	0.054	0.990
	C14–H14···F2	2.38	168	x, y+1, z	-5.1	0.054	0.990
6	C1–H1···F1	2.47	163	x-1, y, z	-4.1	0.041	0.768
21	C1–H1···F1	2.46	153	x+1, y, z	-5.3	0.045	0.823
	C3–H3···F1	2.66	149	x+1, y, z		0.029	0.594
39	C1–H1···F1	2.49	152	x-1, y, z	-4.9	0.048	0.864
	C3–H3···F1	2.64	150	x-1, y, z		0.027	0.558
52	C1–H1···F4	2.47	136	x+$^1/_2$, -y-2, z+$^1/_2$	-3.4	0.052	0.892
54	C1–H1···F4	2.52	162	x, y-1, z	-4.7	0.042	0.721
55	C1–H1···F4	2.34	166	x+1, y, z	-3.9	0.064	1.043
58	C1–H1···F8	2.63	145	x, -y+2, z+$^1/_2$	-4.0	0.032	0.586
59	C1–H1···F8	2.40	173	$^1/_2$-x, $^1/_2$-y, -z	-3.5	0.049	0.897
60	C1–H1···F4	2.40	173	$^1/_2$-x, $^1/_2$-y, -z	-4.4	0.044	0.710
61	C1–H1···F4	2.53	166	x-1, y, z	-5.0	0.047	0.699
71	C1–H1···F4	2.66	173	-x+1, y-$^1/_2$, -z	-4.1	0.029	0.528
	C9–H9···F4	2.54	122	1-x, y-$^1/_2$, -z		0.043	0.801
77	C14–H14···F5	2.45	167	-x, 1-y, 2-z	-2.8	0.042	0.754
	C22–H22···F5	2.58	134	-x, 1-y, 2-z		0.044	0.732
83	C1–H1···F4	2.47	162	x-1, $^1/_2$-y, z-$^1/_2$	-2.1	0.051	0.862
	C9–H9···F4	2.53	148	x-1, $^1/_2$-y, z-$^1/_2$		0.042	0.831

Synthon I(B) has been identified in compounds 71, 77 and 83, where the positions of F atoms on the A ring is 2,4 and on the B ring are 2,4; 2,5 and 2,6 (figure 4.4, table 4.1).

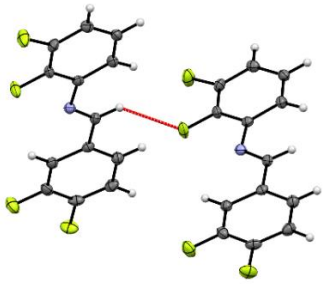

52: **3,4-diF(B)–2,3-diF(A)**

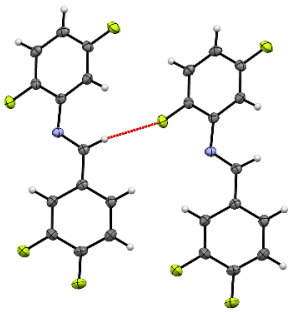

54: **3,4-diF(B)–2,5-diF(A)**

55: **3,4-diF(B)–2,6-diF(A)**

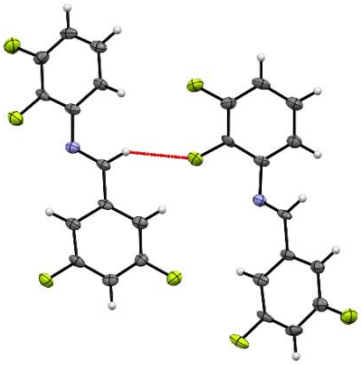

58: **3,5-diF(B)–2,3-diF(A)**

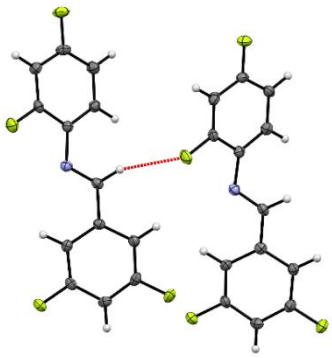

59: **3,5-diF(B)–2,4-diF(A)**

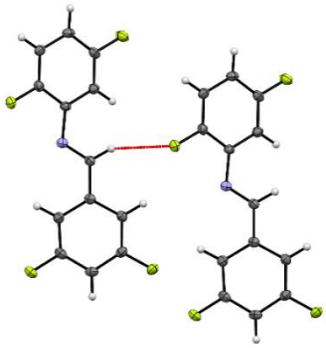

60: **3,5-diF(B)–2,5-diF(A)**

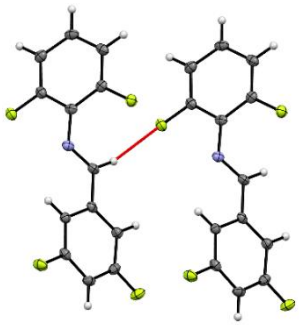

61: **3,5-diF(B)–2,6-diF(A)**

Figure 4.3: Formation of synthon I(A) in the compounds **52**, **54**, **55**, **58**, **59**, **60** and **61.**

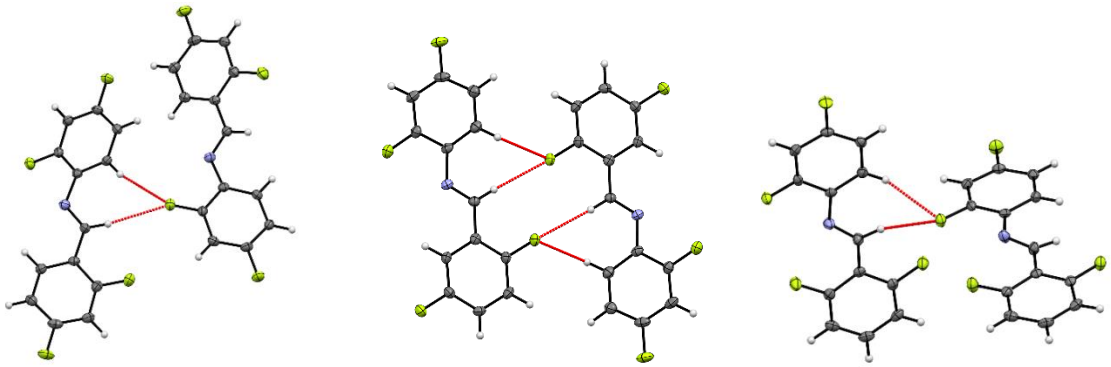

71: **2,4-diF(B)–2,4-diF(A)** **77**: **2,5-diF(B)–2,4-diF(A)** **83**: **2,6-diF(B)–2,4-diF(A)**

Figure 4.4: Formation of synthon I(B) in the compounds **71**, **77**, and **83.**

Thus, from the above discussion, the following points can be summarized:

1. When one of the fluorine atom of the A ring is present at the *ortho* position (the possible substitutions will be 2,3; 2,4; 2,5; 2,6), the formation of synthons mentioned in figure 4.1 becomes highly likely. But, it also depends on the position of F atoms on the B ring.

2. It was noticed earlier that when the position of F/Cl/Br on the B ring is either *para*- or *meta* in case of dihalogen substituted system (**3**, **18**, **36**, **6**, **21** and **39**) and 3,4 or 3,5 in case of tetrafluoro substituted system (**52**, **54**, **55**, **58**, **59**, **60** and **61**) ; then the synthons I(A) or I(C) have been found in their crystal structures.

3. Moreover, if the positions of F on the B ring is at 2,3; 2,4; 2,5 and 2,6; then, the possibility of the formation of synthons I(A), I(B) or I(C) is removed. The only exception to this is observed in the compounds **71**, **77** and **83**, where the synthon I(B) has been found to form in their crystal packing, even when the position of F atom on the B ring is 2,4; 2,5 or 2,6 (**71**, **77** and **83**).

4. Furthermore, the stabilization energies (SE_{G09}) of the dimers, interacting through these synthons have been found to be generally > 3.5 kcal/mol along with the higher values of electron densities at their BCPs (0.03–0.07 $eÅ^{-3}$).

Result of CSD Analysis

Based on the interaction table 1, it is seen that distances and angles of C–H···F hydrogen bonds in the above-studied dimers lie in the range of 2.4 to 2.7 Å and 130° to 170° respectively. Therefore, searches were done for the synthons I(A), I(B) and I(C) in the CSD[127] (CSD Version 5.35, May-2014 update) with the following set of search criterions:

(**a**) H···F distance range: 2.4 to 2.7 Å, (**b**) ∠C–H···F range: 130^o to 170^o, (**c**) 3D coordinated determined, (**d**) R factor (≤ 0.1), (**e**) Not disordered, (**f**) No errors, (**g**) Not Polymeric, (**h**) No ions, (**i**) No powder structures, (**j**) Only Organics

The number of hits found for the synthon I(A), I(B) and I(C) are 23, 1 and 2 respectively. Out of these, three compounds having synthon I(A) in their crystal packing and one compound for each of synthons I(B) and I(C) were selected for the calculation of stabilization energies using G09 and at MP2 level of theory with 6-31+G(d) basis set as was done for our molecules. From the table 4.2, it is apparent that the stabilization energies for the molecules having synthon I(A) significantly match with the stabilization energies and the geometric parameters observed in the molecules studied by us. The only representative of synthon I(B) available from the database has two occurrences of the synthon I(B) and two C–H···N hydrogen bonds in the formation of a dimer in its crystal structure. Consequently, the stabilization energy of the dimer of this molecule (CSD REFCODE RICMOG) is much higher than the others. On the other hand, one out of two hits for the synthon I(C) shows much lower stabilization due to poor directionality (∠C–H···F < 140°).

Table 4.2: Details of the geometrical parameters for the C–H···F hydrogen bonds and their interaction energies.

Synthon	Refcode	*d* (H···F/Å)	θ (∠C–H···F/^{o})	SE_{G09} kcal/mol
IA	YAJHIC	2.54	148	-3.7
	BANGOM02	2.52	164	-3.2
	AYUSAP	2.63	156	-3.7
IB	RICMOG	2.52	170	-11.6
		2.66	140	
IC	MIGPAU04	2.40	129	-1.7
		2.61	130	
	QACTUL	2.61	147	-3.5
		2.64	145	

Synthon II: This synthon consist of dimers, where H and F of one ring interact with the F and H of the other (figure 4.5). This synthon can be categorized into two types:

- *Head to head or tail to tail dimers*: In this particular case, both the interacting atoms belong to the same ring.
- *Head to tail dimers*: In this case, the atoms of *B ring* participate in the interaction with the atoms of *A ring*.

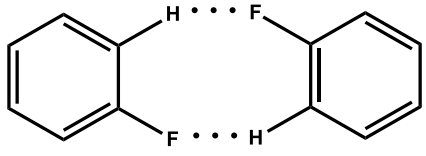

Figure 4.5: A schematic representation of the synthon II

When the positions of the substituents at both the rings are either 2,3-2,3 (**64**) or 2,4-2,4 (**71**); **head to tail dimers** have been found. This type of dimers have also been observed in the compounds **61** (3,5-2,6) and **86** (2,6-3,4) (figure 4.6, table 4.3) with the involvement of *o*-F of A ring and *m*-F of B ring in **61** and vice-versa (*o*-F of B ring and *m*-F of A ring) in **86**. It is worth mentioning that the dimers found in **64** and **71** are different from those observed in **61** and **86** with respect to the spatial arrangements of the interacting molecules.

Head to head and tail to tail dimers have also been found in many other structures of the studied system (figure 4.7, table 4.3). The formation of this kind of supramolecular motifs were also seen in the series of difluoro substituted *N*-benzylideneaniline in the compounds with one fluorine at the *meta*- position of A ring and other at the *para*- or *meta*- position of B ring (figure 4.7, table 4.3). These head to head, tail to tail, and head to tail dimers leads to the formation of molecular chains or ribbons in the crystal lattices. Although, the abundance of synthon II was found to be more in our compounds, but the stabilization energies of the dimers formed by synthon II were found to be lower (generally < 2.5 kcal/mol) than those observed for the dimers formed by the synthons I(A), I(B) and I(C). Both, the electron density and Laplacian at the BCPs for these dimers were found to be lesser than the values obtained for the dimers formed by the synthons I(A), I(B) and I(C). This shows that the C–H···F interactions responsible for the synthon II are marginally weaker than the same in the synthons I(A), I(B) and I(C).

Head to tail dimers:

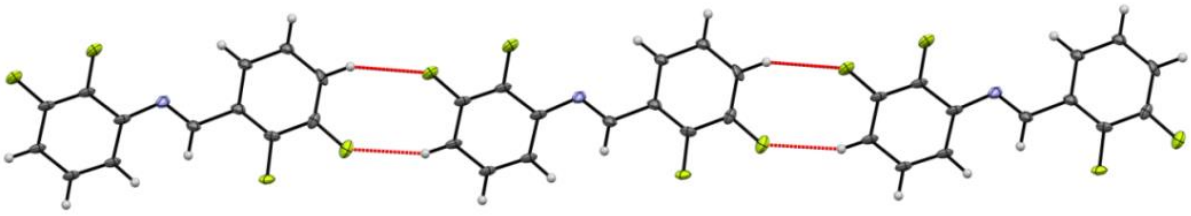

64: **2,3-diF(B)-2,3-diF(A)**

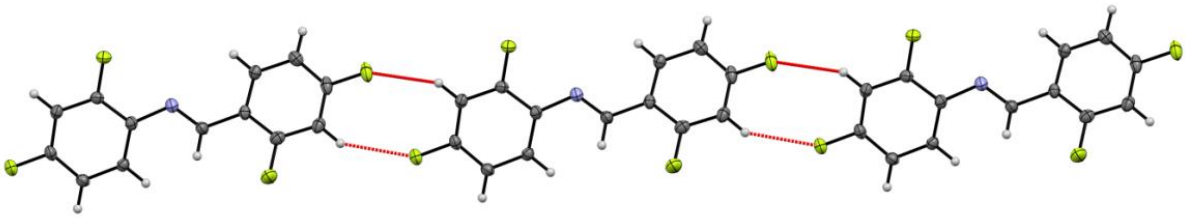

71: **2,4-diF(B)-2,4-diF(A)**

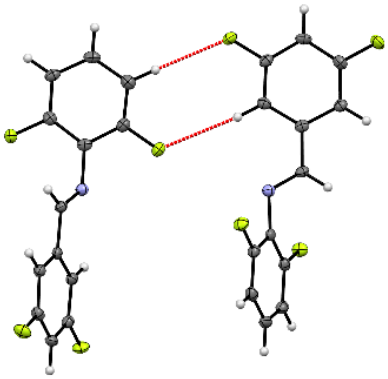

61: **3,5-diF(B)-2,6-diF(A)**

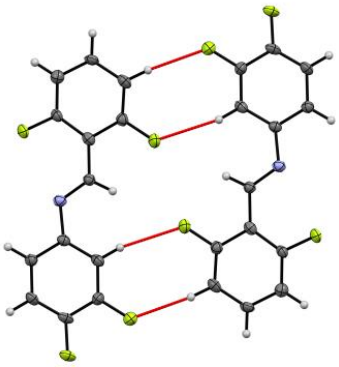

86: **2,6-diF(B)-3,4-diF(A)**

Figure 4.6: formation of synthon II (head to tail dimers) in the compounds **64**, **71**, **61** and **86**.

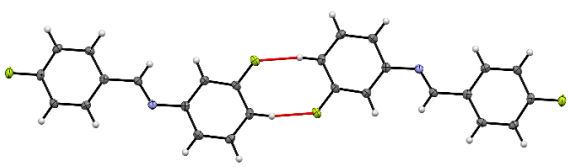

2: 4-F(B)-3-F(A)

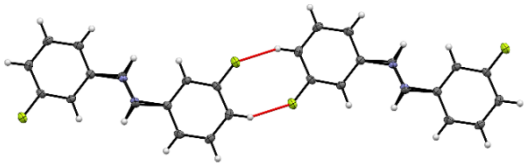

5: 3-F(B)-3-F(A)

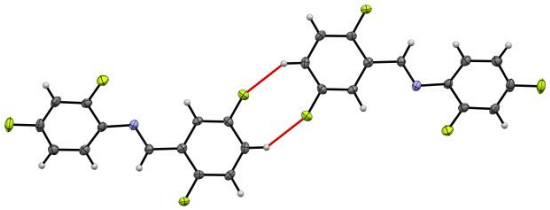

77: 2,5-diF(B)-2,4-diF(A)

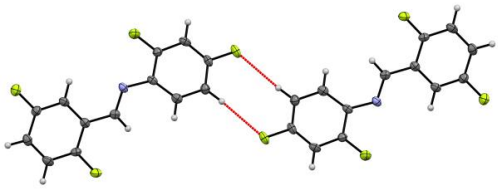

77: 2,5-diF(B)-2,4-diF(A)

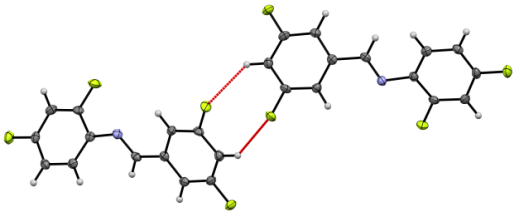

59: 3,5-diF(B)-2,4-diF(A)

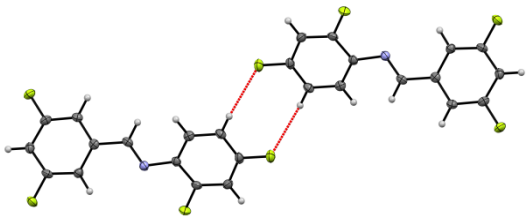

59: 3,5-diF(B)-2,4-diF(A)

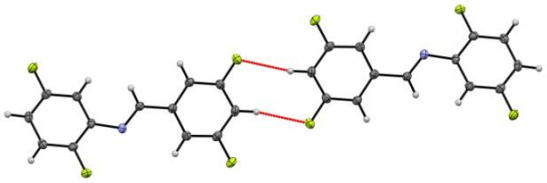

60: 3,5-diF(B)-2,5-diF(A)

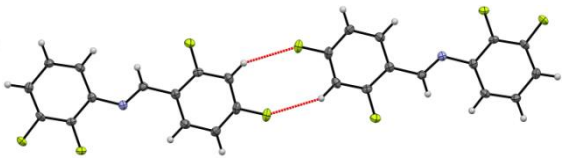

70: 2,4-diF(B)-2,3-diF(A)

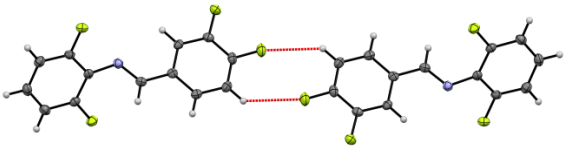

55: 3,4-diF(B)-2,6-diF(A)

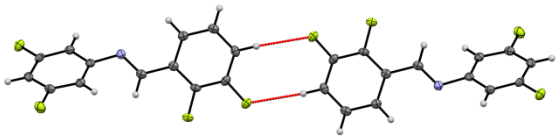

69: 2,3-diF(B)-3,5-diF(A)

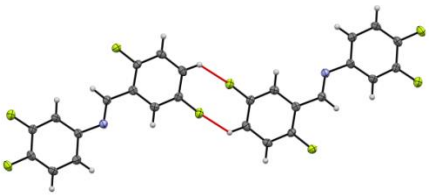

80: 2,5-diF(B)-3,4-diF(A)

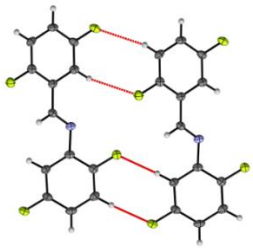

78: 2,5-diF(B)-2,5-diF(A)

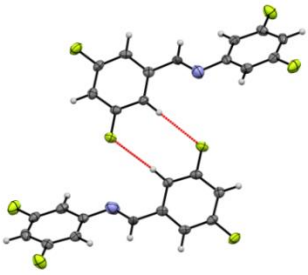

63: 3,5-diF(B)-3,5-diF(A)

Figure 4.7: Formation of synthon III (head to head and tail to tail dimers) in the compounds **2**, **5**, **77**, **59**, **60**, **70**, **55**, **69, 80, 78,** and **63.**

Table 4.3: Details of the geometrical parameters for all the C–H···F hydrogen bonds, the values of electron densities and Laplacians at their BCPs.

Code	C–H···F	*d* (H···F/Å)	θ (∠C–H···F/º)	Symmetry Code	SE_{G09} kcal/mol	ρ (eÅ^{-3})	$\nabla^2\rho$ (eÅ^{-5})
64	C18–H18···F8	2.69	149	x+1, y-1, z+1	-2.1	0.022	0.512
	C24–H24···F6	2.49	158	x-1, y+1, z-1		0.038	0.793
71	C4–H4···F3	2.47	146	x-1, y, z+1	-1.7	0.041	0.824
	C12–H12···F2	2.67	131	x+1, y, z-1		0.037	0.562
61	C3–H3···F3	2.47	169	-x, y+$^1/_2$, $^1/_2$-z	-2.5	0.042	0.881
	C10–H10···F1	2.65	168	-x, y-1/2, $^1/_2$-z		0.027	0.568
86	C4–H4···F3	2.66	134	1-x, -y, 1-z	-4.7	0.028	0.608
	C9–H9···F1	2.70	134	1-x, -y, 1-z		0.026	0.560
55	C4–H4···F1	2.66	138	3-x, -y, 1-z	-2.0	0.032	0.552
59	C10–H10···F3	2.53	147	-x, 1-y, -z	-2.0	0.044	0.771
	C5–H5···F2	2.56	138	1-x, y, $^1/_2$-z	-1.6	0.032	0.692
60	C5–H5···F1	2.56	138	1-x, y, $^1/_2$-z	-1.3	0.042	0.748
	C11–H11···F3	2.66	162	$^1/_2$-x, y+$^1/_2$,$^1/_2$-z	-2.0	0.032	0.542
70	C4–H4···F2	2.52	151	1-x, -1-y, 1-z	-1.9	0.041	0.729
	C11–H11···F3	2.63	160	-x, -y, 2-z	-2.3	0.034	0.587
69	C5–H5···F2	2.69	161	1-x, 1-y, -z	-1.9	0.042	0.658
2	C11–H11···F2	2.55	134	-x, 1-y, -z	-1.6	0.039	0.697
5	C5–H5···F1	2.53	135	2-x, -y, 1-z	-1.5	0.036	0.683
77	C10–H10···F3	2.59	162	1-x, 2-y, 1-z	-2.1	0.045	0.671
	C18–H18···F6	2.53	133	-x, 2-y, 1-z	-2.1	0.042	0.772
80	C5–H5···F2	2.63	125	1-x, 2-y, -z	-1.9	0.029	0.648
66	C12–H12···F3	2.45	153	x-1, y, z	-3.8	0.042	0.841
	C9–H9···F4	2.44	154	x+1, y, z		0.041	0.862
78	C12–H12···F3	2.59	155	x+1, y, z	-4.2	0.033	0.657
	C9–H9···F4	2.57	154	x-1, y, z		0.042	0.703
	C7–H7···F1	2.63	147	x+1, y, z		0.034	0.602
	C4–H4···F2	2.64	147	x-1, y, z		0.033	0.604
63	C20–H20···F2	2.50	175	x-$^1/_2$, -y, z	-2.0	0.035	0.683
	C7–H7···F6	2.57	168	x+$^1/_2$, -y, z		0.043	0.784

Result of CSD Analysis

A CSD (CSD Version 5.35, May-2014 update) search was performed on the synthon II with the same distance and angle ranges and set of criterions that were used for the synthons I(A), I(B) and I(C). Even in CSD, the abundance of this synthon has been found to be more than those mentioned earlier. Among the 277 hits from this search, 14 simple molecules were chosen for the calculation of stabilization energies as was done before and these value are found to lie in the range of -1.5 to -2.8 kcal/mol.

Table 4.4: Details of the geometrical parameters for the C–H···F hydrogen bonds and their stabilization energies.

Refcode	*d* (H···F/Å)	θ (∠C–H···F/º)	SE_{G09} kcal/mol
ABAKIZ	2.69	141	-1.5
ATOZOY	2.68	135	-1.7
BESZUW	2.53	143	-1.5
CICTOY	2.65	152	-2.4
DIBCOH	2.67	160	-2.5
DUTREQ	2.67	148	-2.8
ENUKAA	2.61	143	-1.6
QOSBAC	2.56	147	-1.8
RAGFAI	2.62	146	-2.4
ROFPUY	2.63	154	-1.7
SESTOB	2.62	138	-1.4
ULELUT	2.63	145	-1.8
UREKIM	2.45	156	-1.6
YICFEX01	2.58	152	-1.2

Synthon III: When both the fluorine atoms are present on the adjacent carbon atoms of the aromatic ring, then there is a tendency for the formation of synthon III (figure 4.8).

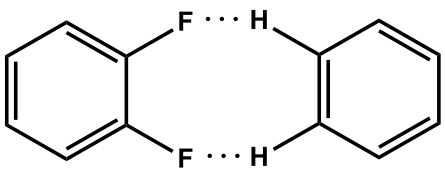

Figure 4.8: A schematic representation of the synthon III

In the system under study, the possibility of the formation of this kind of synthon is only with 2,3 and 3,4-difluoro substituted compounds. Among the 20 possible such molecules, only 6 of them were found to contain this synthon. When the F atoms were present at 2,3 position on the A ring, then the compounds **64**, **70**, **76** and **82** with F substitutions at 2,3; 2,4; 2,5; and 2,6 respectively, display the formation of synthon III (figure 4.9, table 4.5) in their crystal packing.

Table 4.5: Details of the geometrical parameters for all the C–H···F hydrogen bonds, the values of electron densities and Laplacians at their BCPs

Code	C–H···F	*d* (H···F/Å)	θ (∠C–H···F/º)	Symmetry Code	SE_{G09} kcal/mol	ρ (eÅ^{-3})	$\nabla^2\rho$ (eÅ^{-5})
64	C10–H10···F2	2.48	134	x-1, y, z	-4.2	0.042	0.816
	C9–H9···F1	2.58	172			0.034	0.650
70	C10–H10···F3	2.49	127	x+1, y, z	-3.2	0.044	0.841
	C9–H9···F4	2.61	166			0.033	0.623
76	C4–H4···F2	2.63	155	x+1, y, z	-4.3	0.028	0.592
	C10–H10···F3	2.48	136			0.044	0.811
	C9–H9···F4	2.57	172			0.034	0.672
	C7–H7···F1	2.62	155	x-1, y, z		0.026	0.589
82	C10–H10···F3	2.67	159	x+1, y, z	-2.6	0.027	0.567
	C9–H9···F4	2.63	149			0.029	0.518
55	C11–H11···F2	2.60	127	x, $^1/_2$-y, z-$^1/_2$	-1.9	0.032	0.664
	C10–H10···F1	2.59	168			0.034	0.643
86	C6–H6···F4	2.69	159	x, y, z-1	-1.9	0.030	0.521
	C5–H5···F3	2.63	120			0.031	0.662

In addition to these, synthon III has also been observed in the structures of **55** and **86**, where the positions of the substituents on one of the ring are 3,4 and on the other ring are 2,6 (figure 4.10, table 4.5). Rest of the molecules having two adjacent fluorine atoms either preferred synthon I(A, B and C) or synthon II or were found to be non-centrosymmetric and were found to pack by other weak hydrogen bonds (ESI, structural descriptions of the compounds **52** to **54**, **56** to **58**, **62**, **65** to **69**, **74**, **76**, **80**, **82**, **86**).

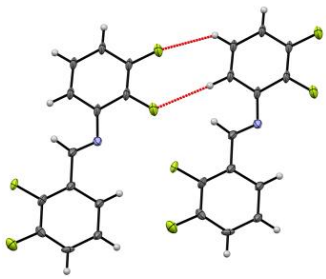

64: **2,3-diF(B)-2,3-diF(A)**

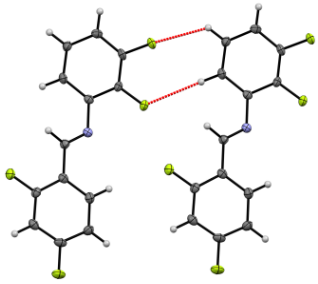

70: **2,4-diF(B)-2,3-diF(A)**

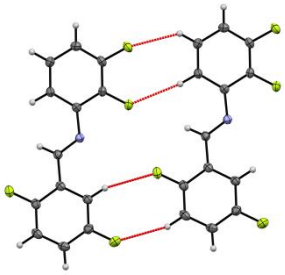

76: **2,5-diF(B)-2,3-diF(A)**

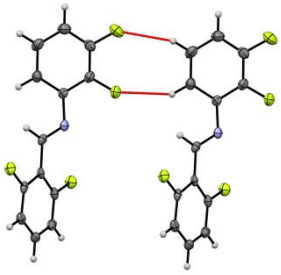

82: **2,6-diF(B)-2,3-diF(A)**

Figure 4.9: formation of synthon III in the compounds **64**, **70**, **76** and **82**.

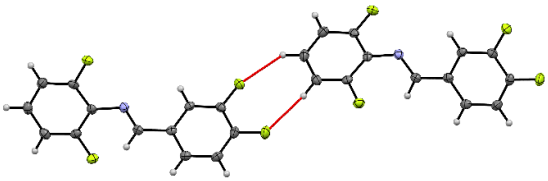

55: **3,4-diF(B)-2,6-diF(A)**

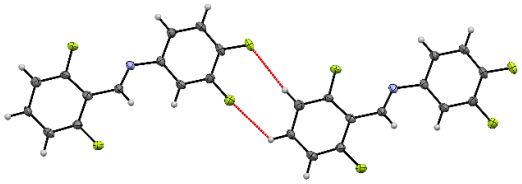

86: **2,6-diF(B)-3,4-diF(A)**

Figure 4.10: Formation of synthon III in the compounds **55** and **86**.

From the table 4.5, it is observed that the stabilization energies for the dimers having synthon III have been found to lie in the range from -1.9 to -4.3 kcal/mol. Two C–H···F hydrogen bonds in this synthon are dissimilar in nature. Therefore, two H···F distances and two ∠C–H···F angles are found to be different in each compound. It has observed that the C–H···F interactions with shorter H···F distances are associated with smaller ∠C–H···F angles. This synthon in the structures of **64**, **70** and **76** have been seen to be more stabilizing (**SE**$_{G09}$ > 3 kcal/mol), while the same for the other three are found to be less stabilizing (**SE**$_{G09}$ < 3 kcal/mol).

Result of CSD Analysis

A similar CSD search was done on this synthon also, which has resulted in the 49 structures, containing this synthon in their crystal lattices. Out of those, stabilization

energies have been calculated for seven of them (table 4.6). The stabilization energies of these dimers vary from -1.0 to -3.6 kcal/mol.

Table 4.6: Details of the geometrical parameters for the C–H···F hydrogen bonds and their stabilization energies.

Refcode	*d* (H···F/Å)	θ (∠C–H···F/º)	SE_{G09} kcal/mol
ASIJER	2.63	142	-1.0
	2.66	151	
HORVOA	2.60	157	-1.0
	2.66	148	
MIKGOD	2.59	144	-1.5
	2.62	157	
AKUNOK	2.67	164	-1.1
	2.52	138	
PUGDEB	2.60	142	-1.6
	2.58	144	
HORVUG	2.53	156	-1.0
	2.59	139	
UCOVEN	2.42	169	-3.6
	2.64	138	

Synthon IV: The 4th robust synthon observed in chapter 1 and 2, is a dimer (figure 4.11) formed when one fluorine atom was present at the *ortho* position of the B ring and the other halogen (F or Cl or Br) was present at the *meta* position of A ring. As described in the chapter 3, this synthon remained unaltered upon replacement of non-interacting F with Cl or Br (figure 4.12). We have further found that this synthon does not change even on the addition of fluorine atoms at the *meta*- or *para*- position of both the phenyl rings (figure 4.13 and 4.14).

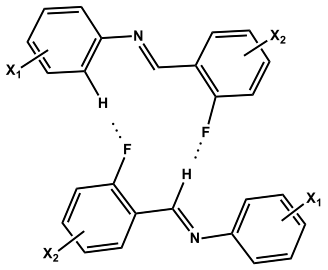

Figure 4.11: A schematic representation of the synthon IV

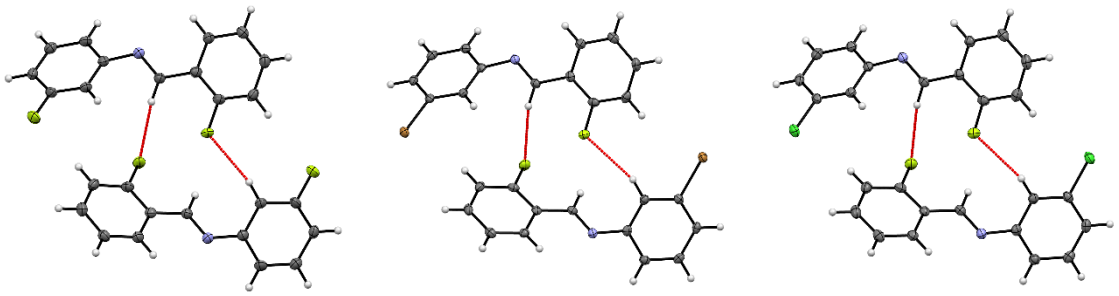

8: **2F(B)-3F(A)** **23**: **2F(B)-3Br(A)** **50**: **2F(B)-3Cl(A)**

Figure 4.12: formation of synthon IV in the compounds **8**, **23**, and **32.**

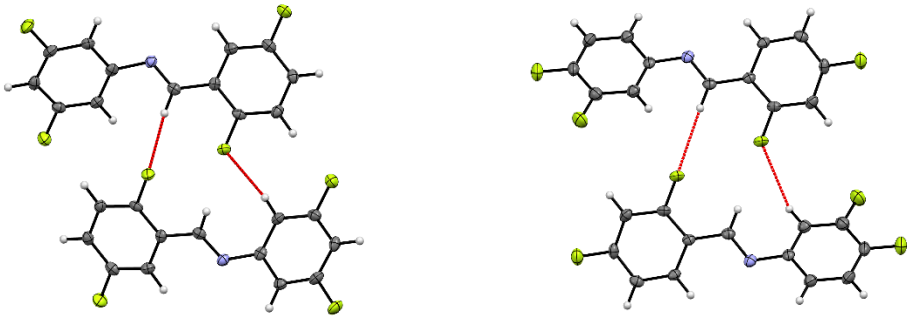

81: **2,5-diF(B)-3,5-diF(A)** **74**: **2,4-diF(B)-3,4-diF(A)**

Figure 4.13: Formation of synthon IV in the compounds **81** and **74** (Addition of fluorine at the *m* or *p*- position of both the rings)

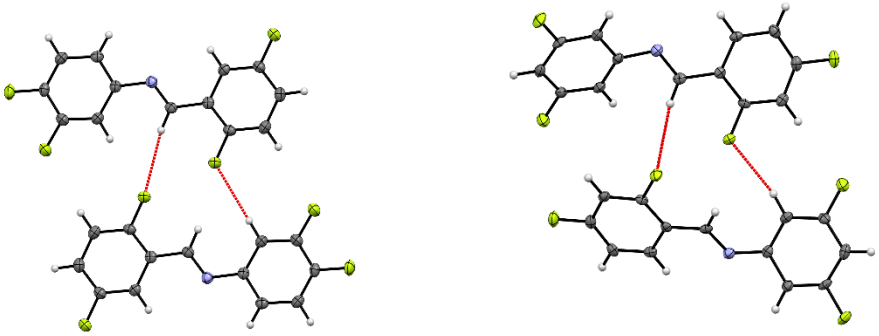

80: **2,5-diF(B)-3,4-diF(A)** **75**: **2,4-diF(B)-3,5-diF(A)**

Figure 4.14: Formation of synthon IV in the compounds **80** and **75** (Addition of fluorine at the *m*-position of one phenyl ring and at the *p*-position of second phenyl ring and vice-versa)

This synthon is highly specific for this kind of model system. Therefore, CSD search was not done for this synthon. But, it is to be noted that the dimers formed by this synthon are highly stabilizing in nature. The stabilization energies offered by these dimers are ≥ 4 kcal/mol and the value of electron densities and Laplacian at the BCPs are supportive for moderately strong C–H···F hydrogen bonds (table 4.7).

Table 4.7: Details of the geometrical parameters for all the C–H···F hydrogen bonds, the values of electron densities and Laplacians at their BCPs

Code	C–H···F	*d* (H···F/Å)	θ (∠C–H···F/º)	Symmetry Code	SE_{G09} kcal/mol	ρ (eÅ^{-3})	$\nabla^2\rho$ (eÅ^{-5})
8	C9–H9···F11	2.55	169	1-x, y-$^1/_2$, $^1/_2$-z	-4.8	0.038	0.734
	C1–H1···F1	2.67	157			0.030	0.584
32	C9–H9···F1	2.61	164	2-x, y-$^1/_2$, $^3/_2$-z	-5.3	0.029	0.570
	C1–H1···F1	2.69	155			0.026	0.531
50	C9–H9···F1	2.66	163	2-x, y+$^1/_2$, $^3/_2$-z	-4.8	0.032	0.628
	C1–H1···F1	2.70	154			0.027	0.546
74	C9–H9···F1	2.76	134	1-x, -y, 1-z	-3.9	0.019	0.470
	C1–H1···F1	2.66	172			0.031	0.628
75	C9–H9···F1	2.51	169	x-$^1/_2$, $^3/_2$-y, -z	-3.9	0.042	0.78
	C1–H1···F1	2.71	162			0.021	0.477
80	C9–H9···F1	2.59	161	-x, 1-y, -z	-4.9	0.032	0.632
	C1–H1···F1	2.66	164			0.024	0.512
81	C9–H9···F1	2.48	172	x+$^1/_2$, -y-$^1/_2$, -z-2	-4.7	0.044	0.821
	C1–H1···F1	2.51	148			0.034	0.602

Results of Stabilization Energies Calculations

A 3D graph (figure 4.15) between the distances, angles and stabilization energies of the dimers, which had only one C–H···F hydrogen bond between the two interacting molecules, (table S32 in ESI) has been plotted. A minima in the energy surface has been found at a distance between 2.60-2.65 Å with the angle close to 170˚ (figure 4.15). The table containing all the values of distances, angles, interaction energies and topological properties of the interacting dimers has been given in ESI (table S4.31).

Results of AIM Calculations

The topological parameters [ρ, $\nabla^2\rho$, $V(\mathbf{r}_{CP})$, $G(\mathbf{r}_{CP})$ and $E(\mathbf{r}_{CP})$] at the (3, -1) bond critical point of C–H···F hydrogen bonds have been found to vary exponentially with the bond path. A similar trend was also observed for the dihalogen substituted *N*-benzylideneanilines as shown in figure 3.9 of chapter 3, thus representing the weak hydrogen bond type character of C–H···F interactions. These plots along with the fitted equations and the corresponding values of R^2 have been given in figure 4.16, and the values of these parameters are given in table S4.32 (ESI).

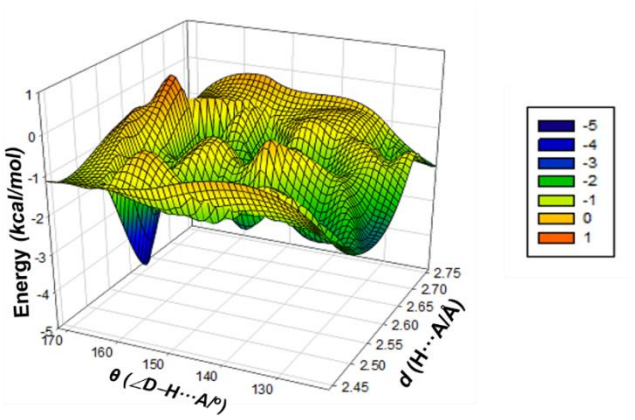

Figure 4.15: 3D plot between the distances, angles and energy for C–H···F hydrogen bonds, which have been found to form in the crystal lattice of the studied compounds.

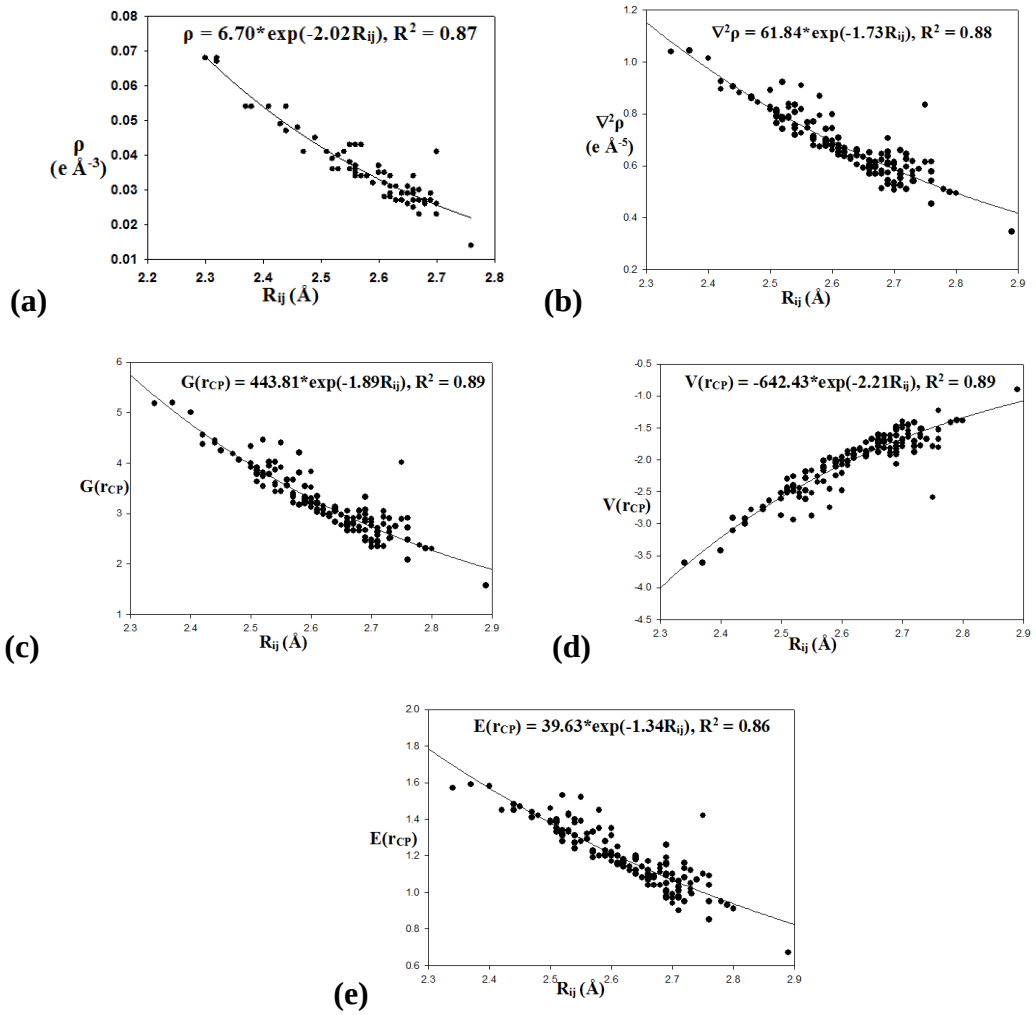

Figure 4.16: 2D plot between **(a)** ρ vs R_{ij}, **(b)** $\nabla^2\rho$ vs R_{ij}, **(c)** $G(\mathbf{r}_{CP})$ vs R_{ij}, **(d)** $V(\mathbf{r}_{CP})$ vs R_{ij}, and **(e)** $E(\mathbf{r}_{CP})$ vs R_{ij}.

Results of Thermal Analyses

It has been observed from the melting points (obtained from the DSC analyses) of halogen (*mono*-F, *di*-F, F-Cl, F-Br and *tetra*-F) substituted *N*-benzylideneanilines that *meta*- substituted compounds have lower melting points than their rest of the analogues. The compounds, where F is substituted on the *meta*- position of the aniline or the benzaldehyde ring and the substituent on the other ring (F, Cl or Br) is present at either *meta*- or *ortho*- position, have melting points lower than 30.0 ^{o}C except in the compound **6**. The reason for the higher melting point of compound **6** could be the presence of a highly short, directional, robust and stable synthon I(A). Furthermore, in tetrafluoro compounds, the melting points were found to be comparatively higher than the rest of the compounds of this series. This could be attributed to the higher molecular weight of the concerned compounds and presence of more interactions in their crystal lattices.

4.6 Conclusions

In this chapter, the capability of "organic fluorine" for the formation of recurring supramolecular synthons *via* weak C–H···F hydrogen bonds has been shown. Such type of repetitive supramolecular motifs have been observed in the system of difluoro, fluoro-bromo, fluoro-chloro and tetrafluoro substituted *N*-benzylideneanilines. An attempt has been made to find a correlation between a particular supramolecular synthon with the positions of the substituents. The recurring nature of the synthons has been affirmed by replacing one of the F of the molecular framework by its heavier analogue (Cl or Br) or by the addition of more F atoms to the same scaffold. The stabilization energies of most of these dimers lie in the range from 2 to 6 kcal/mol. The nature of C–H···F interactions has been shown to be of weak hydrogen type from the plots between their topological properties *versus* bond path. Moreover, from the 3D plot, containing the stabilization energies, distances and angles of C–H···F hydrogen bonds, it has been revealed that the stabilization energy is maximum for more directional C–H···F hydrogen bonds with angle (∠C–H···F) close to 170°. These observations provide indications for the stable, directional and to some extent predictive C–H···F hydrogen bonds and also highlights the recurring nature of supramolecular synthons based on C–H···F hydrogen bonds in the molecular systems, which don't possess the possibility of the formation of strong hydrogen bonds.

Chapter 5

Evaluation of Weak Interactions Involving Organic Fluorine *via* Experimental and Theoretical Charge Density analyses

Chapter 5

5.1 Introduction

The impact of organic fluorine in the crystal packing of halogen substituted *N*-benzylideneaniline has been established in the previous chapters. Interactions involving F (C–H···F, C–F···F–C and C–F···π) were identified and analysed on the basis of geometrical features (distance and angle). In our studied systems, mostly C–H···F hydrogen bonds were found to play the structure directing role in the crystal packing. To study these hydrogen bonds, a distance and angle cut-off criterion ($d \leq 2.70$ Å and $\angle C–H\cdots F \geq 120^{o}$) was applied based on the literature values. Then, gas phase calculations (Gaussian09, MP2 level, 6-31+G* basis set with counterpoise correction) were performed on those dimers, which were found to interact through F to have an estimate about the stabilization provided by these interaction in a particular dimer. After that, AIM analyses were done to establish the nature of these interactions. But, it is to be noted that all these calculations were done on the systems, which were modelled based on the spherical atom approximation. In this approximation, electrons density of an atom is assumed to be spherical, which is a very good approximation for the heavier atoms. This is because in the heavier atoms the total electron density of an atom is dominated by core electrons. However, the electron densities of the lighter atoms (C, N, O, F) need not to be spherical. The effect of bonding is the most pronounced on the lightest atom, H, which has no inner shell and is the element of concern to study hydrogen bonding.

Therefore, to get a real picture of these interactions, one needs to do the charge density analysis of the system under investigation, which is based on the aspherical modelling of the electron density. It takes into account the bonding and lone pair electron

densities of the atoms within the molecule and thus provides an ultimate tool for the understanding of these interactions beyond mere geometry. Several reviews have elucidated the chemical application of the charge density studies.[133] There also exist evidence for metal-metal bonding on the basis of charge density studies.[134] Detail investigation of several weak interactions (C–H···X; X = F, Cl, Br, O, π) have also been done by the charge density analysis to establish the nature of these interactions like hydrogen bond type, van der Waals' interaction, *etc*.[135] After multipolar modelling of the molecule, properties of the molecules (like net charge, dipole or quadrupole moments, interaction energies, *etc*.) can be evaluated to quite an accurate extent. On the basis of these accurate analyses, the nature of interactions can be identified.

In this chapter, initially the basics of charge density studies will be discussed followed by its implication to study fluorine mediated interactions in the system under investigation. Furthermore, quantification of interactions has been done by determining the amount of the charge transfer, which has taken place during the interaction.

5.2 Charge Density from X-ray Diffraction

X-rays have wavelengths ranging from 0.01 to 10 nm, which is of similar order as that of atomic distances. Therefore, X-rays have been used to probe the arrangement of atoms in the molecules that are arranged in a periodic array in the crystal lattice. The electrons in the atoms are responsible for the diffraction of X-rays. Therefore, it may become possible to use X-ray diffraction technique to discern the arrangement of electrons inside an atom. In 1915, Debye stated "the experimental study of the scattering of atoms, in particular for light atoms, should get more attention, since along this way it should be possible to determine the arrangement of the electrons in the atoms".[136] But, significant progress in this area has been made very recently.[133-135] This is primarily due to the unavailability of very accurate and high-resolution data in the past and also due to the success of spherical atom approximation in solving millions of structures in a short period of time. The spherical atom approximation assumes that the electron density of an atom in a molecule is spherically averaged. The major drawback of this model is the assumption that the position of the nuclei is at the maxima of electron density and its unaccountability of the deformation of the electron density of an atom in a molecule. The spherical atom approximation is appropriate to some extent for the heavy atoms, where the core scattering is quite effective, while, for the lighter atoms, valence electrons are more deformed and,

therefore, it becomes inappropriate for high-resolution studies. Moreover, the atoms are considered to be neutral in a molecule, whereas there are evidence that atoms in molecule carry partial charges.[137] All these limitations in the model, suggest some need for improvements, which are described in the following sections.

5.2.1 The Kappa Formalism

The first extension to the spherical atom approximation was the separation of the scattering contributions of the valence and core shells. Moreover, the expansion and contraction of the atomic valence shells and the charge-transfer between atoms have been allowed. This was first proposed by Coppens *et al.*,[138] and is called radial refinement or *kappa formalism*. In this formalism, atomic density is expressed as

$$\rho_{at}(\mathbf{r}) = \rho_{core}(\mathbf{r}) + P_v\kappa^3\rho_{valence}(\kappa\mathbf{r}) \qquad \textbf{(1)}$$

where, ρ_{at} (**r**) = Total electron density of an atom; ρ_{core} (**r**) = Core electron density of an atom; *Pv* = Valence population of an atom; κ = Radial Parameter, which allows for the contraction and expansion of the valence shell.

The radial coordinate **r** is scaled by the parameter κ; $\kappa > 1$ implies that same electron density can be obtained at lower value **r**, which means that valence shell is contracted and for the expanded valence shell, same electron density can only be obtained at higher value of **r**, thus κ will be less than 1.

Thus, with this model, the partial charges on the atoms in a molecule and the molecular dipole moment can be accounted for. Some improvements were made further to account for the non-spherical density functions, which is accounted in the multipole modelling.[137]

5.2.2 Multipole Modelling

Deformation of the electron density in a chemical bond can be accounted for by the multipole modelling. Several algorithms were proposed,[139] but the algorithm suggested by Hansen and Coppens[140] has been accepted widely. In this formalism, atomic density (ρ_{at}) is divided into three components, out of which one accounts for the core electron density (ρ_{core}), the second for the spherical expansion and contraction of the valence shell ($\rho_{valence}$) and third for the aspherical deformation of the valence electron density. The aspherical deformation is described through mathematical functions, in terms of real spherical

harmonics ($Y_{lm\pm}$) together with the radial expansion and contraction terms (R_l), which is modified by the scaling parameters κ and κ'.

$$\rho_{at}(\boldsymbol{r}) = \rho_{core}(\boldsymbol{r}) + P_v\kappa^3\rho_{valence}(\kappa\boldsymbol{r}) + \sum_{l=0}^{l\max}\kappa'^3 R_l(\kappa'\boldsymbol{r})\sum_{m=0}^{l} P_{lm\pm} Y_{lm\pm}(\theta,\phi) \quad \textbf{(2)}$$

This equation is taken from reference number 137, pp 67.

The atomic functions are described in terms of polar coordinates (***r***, θ and ϕ) defined on local axis centred on each atom. *Multipoles* are the density functions, which are the products of **r**- dependant *radial function* and θ- & ϕ- dependant *angular functions*.

5.2.3 Fundamentals of Electron Density Determination

The total electron density ($\rho(\boldsymbol{r})$) is calculated by Fourier transformation of the structure factors ($F(\boldsymbol{H})$):

$$\rho(\boldsymbol{r}) = \int F(\boldsymbol{H})\exp(-2\pi i\boldsymbol{H}.\boldsymbol{r})d\boldsymbol{H} \quad \textbf{(3)}$$

This equation is taken from reference number 137, pp 90.

The inadequacy of the model is evaluated based on the difference of calculated and residual density

$$\Delta\rho(\boldsymbol{r}) = \rho_{obs}(\boldsymbol{r}) - \rho_{cal}(\boldsymbol{r}) \quad \textbf{(4)}$$

This equation is taken from reference number 137, pp 92.

Moreover, in the multipole refinement electron density in the bonding regions and at the lone pair of electrons of an atom can also be accounted for. Whereas, in the independent atomic model (IAM), it is assumed that molecular electronic density (ED) is the superposition of isolated atomic electron densities ρ^o, which are assumed to be spherical. Thus, in IAM, a molecule is approximated as a *pro molecule* and its ED is the superposition of the spherical atomic densities of isolated atoms 'i' centred at R_i.

$$\rho_{pro}(\boldsymbol{r}) = \sum_{\text{atoms}}^{\text{all}} \rho(\mathbf{R}_i) \quad \textbf{(5)}$$

This equation is taken from reference number 137, pp 95.

Thus, the valence electron density or the deformation density[141] ($\Delta\rho_{defrm}$) of the atoms in molecules can be expressed through the difference of total electron density of the molecule ($\rho(\boldsymbol{r})$) (estimated through multipolar modelling) and the electron density of the pro molecule (estimated through IAM) ($\rho_{pro}(\boldsymbol{r})$).

$$\Delta\rho_{defrm}(\boldsymbol{r}) = \rho(\boldsymbol{r}) - \rho_{pro}(\boldsymbol{r}) \quad \textbf{(6)}$$

This equation is taken from reference number 137, pp 95.

If the observed structure factors are used in the calculation of electron density (ρ_{obs}), then the deformation density is the dynamic deformation density because observed structure factors include thermal effects. But, the difference in the electron density obtained through the multipole model with that of the spherical atom model does not account for the thermal vibrations, therefore deformation density obtained through this, is the static deformation density and is comparable to, the theoretical deformation density maps.

5.3 Data Collection Strategy and Processing

An appropriate strategy should be applied to the collection of charge density quality data. The strategy should be such that, the reflections up to maximum possible 2θ could be collected with the average multiplicity of at least 7-8. Furthermore, extreme care should also be taken for the reduction of the data and its further refinements.[141] The detailed methodology followed for such data collection and reduction are described in detail in the reviews by the Spackman,[142] Kortisanszky and Coppens,[143] and also in a Ph. D thesis by Munshi.[135(h)]

For merging, scaling, averaging and for the absorption correction, the program SORTAV[144] is exceptionally beneficial and has been used for both the compounds studied in this chapter. The empirical absorption correction in this program is based on done by fitting real spherical harmonic functions to the empirical transmission surface as sampled by the multiple equivalent measurements.[145]

5.4 Multipole Refinement using XD Package

The multipole refinement was done using Hansen-Coppens formalism,[140] by using the module XDLSM, which is a least square program incorporated in the XD package (Revision: 5.42, September 18, 2007).[146] The first step is to import the structural information from the final spherical atom refinement along with the structure factors to XD, and this is done by an XDINI module of XD. XDINI is an interface between the XD and other packages like WinGx, Olex2, *etc*.

Using XDLSM module of XD2006, the aspherical multipolar refinements based on *F* were performed. To begin with, the structural model was derived from the spherical atom approximation and the scattering factors for all atoms were derived from the Clementi and Roetti's[147] data bank of wave functions. The function, $\sum w(|F_0| - K|F_c|)^2$, was minimized in the multipolar refinement for all the reflections with $I/\sigma(I) > 3$. Initially, the scale factor, atomic positions (*xyz* coordinates), and atomic displacement parameters (ADP) were

refined step by step. After the refinement of the scale factor against the full resolution of the data set, xyz coordinates, and ADPs of the non-hydrogen atoms were refined with the reflections, observed at high angle with sin $\theta/\lambda > 0.7$ Å^{-1}. All further refinements were performed against the full range of data. The positions of all the hydrogen atoms were fixed to the average bond distance values obtained from the neutron diffraction distances available in the literature.[148] C–H distances, involving methyl (C–CH_3), primary (C2–CH_2), secondary (C3–CH) and aromatic carbons (C_{ar}–H), were fixed to the value 1.059, 1.092, 1.099 and 1.083 Å respectively. For non-hydrogen atoms, the multipole parameters (monopole, dipole, Octupole, Quadrupole and hexadecapole) were refined in a stepwise manner to achieve convergence. Twenty different sets of κ were refined for atoms belonging to the different chemical environment while, for all the hydrogen atoms, the default value of k was set to 1.2. It is to be noted that only the bond directed dipole (d_z) component was refined for the hydrogen atoms in the multipolar modelling. Afterward, the crystal geometry obtained at this stage, was used to determine the anisotropic thermal parameters of the hydrogen atom using SHADE server.[149] The values attained were incorporated in the input file, and further refinements were performed in the similar manner as discussed above. But, this time while performing the multipole refinement, the bond directed quadrupole components for H atoms were also refined. The values of κ', which were obtained from theoretical modelling, were incorporated in the input file to get the final model. This is known as kappa prime restricted multipole model (KRMM).[150] Throughout all the refinements, the constraint on the electroneutrality of the molecule has always been maintained.

5.5 Tests for the Success of the Model

Unlike spherical atom refinement, where the *R*-factor and Goodness of fit (*GooF*) are used to judge the quality of the model, the reliability of the multipole model is tested by generating residual density plots, deformation density plots and through Hirshfeld's rigid bond test,[151] which are described below in detail.

Residual electron density: The residual electron densities, which could not be modelled in the multipolar refinement, are calculated using XDFFT module of XD. The difference between observed electron density (F_{obs}) and the calculated multipole modelled electron density (F_{mult}) gives the residual electron density (equation 4). For a well fitted multipole model, this graph should be featureless.

Deformation Density Maps: Deformation densities reveal the bonding features within a molecule by eliminating the nuclear core contribution from the total electron density. It was obtained by subtracting the difference of spherical atom density (*fmod2*) from the multipole modelled electron density (*fmod1*) (equation 6). The reliability of the model is tested through the comparison of experimentally obtained static deformation density with that obtained from the theoretical structure factors generated using CRYSTAL14.[152]

Hirshfeld's Rigid Bond Test: The physical significance of thermal parameters can be obtained by testing them against rigid body model, which emphasize upon the rigidity of a chemical bond present in a molecule with respect to the lattice vibrations. For a rigid bond, the difference in the mean square displacement amplitudes (DMSDA) should satisfy the following conditions,

$$\text{Ideally,} \quad \Delta_{A,B} = Z^2_{A,B} - Z^2_{B,A} = 0 \qquad \textbf{(6a)}$$

$$\text{Practically,} \ \Delta_{A,B} = Z^2_{A,B} - Z^2_{B,A} < 10^{-3}\ \text{Å}^2 \qquad \textbf{(6b)}$$

Where, $Z_{A,B}$ – amplitude of the vibration of atom A in the direction of atom B and $Z_{B,A}$ - amplitude of the vibration of atom B in the direction of atom A.

5.6 Theoretical Structure Factors Calculations using CRYSTAL14

Periodic quantum mechanical calculations for the calculation of electronic wave function were done using the CRYSTAL14 (an *ab initio* program) with experimentally observed crystal coordinates, unit cell and space group information as input. These calculations were carried out using Density Functional Theory (DFT),[153] which accounts for the electron correlation unlike Hartree-Fock (HF) method.[154] The function chosen for the wave function calculation is B3LYP.[155] The corresponding Gaussian basis set 6-31G** is used to account for both the polarization and the diffuse functions.[156]

The input file for running CRYSTAL14 was created by supplying the information of space group, unit cell parameters, number of atoms, coordinates of the atoms and basis set (same for all) for each atom. The coefficient of the exponents for the basis set are taken from the website, "*https://bse.pnl.gov/bse/portal*". Other than these, shrinking factor (IS) is also one of the mandatory information in the input file. The value of IS determines the number of k points at which the Fock/KS matrix is diagonalized. CRYSTAL works on irreducible Brillouin zone (IBZ), where full information is generated by applying rotation

operators. The shrinking factor decides the total number of k points belonging to a lattice (called the Pack-Monkhorst net), with basis vectors:

$\mathbf{b_1}/is_1$, $\mathbf{b_2}/is_2$, $\mathbf{b_3}/is_3$, and $is_1=is_2=is_3=IS$, unless otherwise stated.

Where, $\mathbf{b_1}$, $\mathbf{b_2}$, $\mathbf{b_3}$ are the reciprocal lattice vectors, and is_1, is_2, is_3 are integers called the "shrinking factors".

Some other parameters than the above mentioned are also supplied in the SCF input file to control the convergence. Some of these parameters are **TOLDEE** (tolerance on the change in total energy), **MAXCYCLE** (maximum number of cycles), **FMIXING** (percent of Fock/KS matrices mixing), *etc*.

The parameter **TOLDEE** checks on the SCF energy convergence threshold and is defined by the variable ITOL. If the energy change between the two consecutive optimization steps is $< 10^{-ITOL}$, then it is assumed that the convergence of total energy is achieved. The default value of this parameter is 6.

Furthermore, the default value of the maximum number of SCF cycles is 50. But, this may also be modified by entering the **MAXCYCLE** keywords and giving it the required value (90 was used in the studied systems).

FMIXING is a parameter, which determines the percentage of Fock (Kohn-Sham) matrix mixing between the subsequent SCF cycles. The value of this parameter is defined by the variable IPMIX. The default value of this variable is 30% in CRYSTAL14, which was used for compounds studied by us. Percentage of Fock/KS matrices mixing at cycle *i* is defined as:

$$F_i' = (1 - p)F_i' + pF_i' - 1 \quad \textbf{(7)}$$

Where, *p* (input value of IPMIX) is the % of mixing. Too high value of *p* (>50%) causes the greater number of SCF cycles and can force the stabilization of the total energy value, without a real self-consistency. IPMIX = 0 should be set to switch this option off.

Upon convergence of energy ($\sim 1 \times 10^{-6}$), the periodic wave function was obtained. A list of unique reflections (*hkl* file) at the same resolution as observed in the experiment (1.16 $Å^{-1}$) were generated using a Fortran code, named "genhkl", which is based on the literature.[157] The input file for this program contains the cell info, segment info,[157] systematic absences and the maximum value of $\sin\theta/\lambda$. The wave function and the list of

unique reflections (*hkl*) thus obtained are used to generate theoretical structure factors by using the option 'XFAC' in the input file of "*runprop*" module of the CRYSTAL14. The input for CRYSTAL14 also contained information on the total number of reflections and the cell types (primitive or conventional).

The static structure factors obtained above are devoid of thermal effects. The multipolar refinements against the theoretical structure factors were carried out using XD2006 to obtain a static model of electronic charge distribution. Multipolar refinements of theoretical structure factor were performed to the same multipole levels as described for experimental charge density modelling. Additionally, κ' for non-hydrogen atoms were also refined during the multipolar refinements of the theoretical model while the same during the refinement of an experimental model was fixed to 1.00000 for all the atoms.

5.7 Evaluation of Topological Properties using XDPROP Module of XD

The module XDPROP implemented in the package XD is used for the calculation of one-electron properties and the topological analysis of the electron densities derived from experimental and theoretical multipole models. The module '*CPSEARCH'* of XD was used to search the bond critical points (BCPs) between the bonding and non-bonding atoms. The topological properties of those BCPs can be evaluated to study the types of interaction present between the two interacting atoms. These studies are based on Bader's Quantum Theory of Atom in Molecules (QTAIM), in which boundaries of atomic basins and integration of density functions within the basins can be defined.

The information obtained from QTAIM is based on the distribution of electron density (ED) within a molecule, which has been calculated experimentally through high-resolution X-ray data and theoretical structure factors using CRYSTAL14. QTAIM takes information from ED and reformulates the chemical concepts. The gradient of electron density is the basis of partitioning of a molecule into mutually exclusive regions in space, which are so-called "atoms". Gradient paths originate at one point and terminate at the other point without crossing each other. But, these gradient paths can meet each other at a point, where $\nabla\rho = 0$. Such a point is called critical point (CP), and positions of nuclei in a molecule always coincide with this type of CP. It can also be implied from the above statement that gradient paths are attracted to one type of critical point. Thus, an atom is an attractor of a number of such gradient paths, which originate at infinity and terminate at the nucleus after traversing a section of space, called atomic basin.[158]

In a molecule, there exist some gradient paths, which originates at infinity and instead of terminating at the nucleus, they terminate at a point between the two atoms. There could be many such gradient paths, which together result in a two-dimensional surface called interatomic surface (IAS). The point at which, these gradient paths terminate is called the Bond Critical Point (BCP). It is also a point where the value of ρ is maximum within IAS. Thus, we can define BCP as a point, the value of electron density at which is maximum in two dimensions, but not in the direction perpendicular to the IAS.[158] There exist another gradient paths in two opposite directions, which originate at the BCP and terminate at each of the two nuclei in either direction. This set of two gradient paths is called an atomic interaction line (AIL), which is a line of maximum electron density with respect to its neighbouring lines. Thus, AIL is perpendicular to IAS at the BCP and ρ is minimum at the BCP along AIL and maximum with respect to any lateral displacement in the plane tangential to IAS. Moreover, AIL becomes a bond path (BP) between two atoms if the whole molecule is in its minimum energy conformation. The collection of bond paths in a molecule, which is at its equilibrium geometry, is called the *molecular graph* (MG).[158]

There exist four types of critical points, which are classified using the Hessian matrix of electron density. Hessian matrix is a 3×3 matrix of second derivatives of ρ.[158] It has three mutually orthogonal eigenvectors along the principal axis of curvature, and it becomes a diagonal matrix when expressed with respect to the system of axes constituted by the principal axis of curvature. Then, each eigenvector becomes an axis and the corresponding eigenvalue (λ_1, λ_2, and λ_3 with $\lambda_1 \leq \lambda_2 \leq \lambda_3$) determines the profile of electron density along that axis. The number of nonzero eigenvalues is called the rank of a matrix and is denoted by 'r'. The number -1 is assigned to negative eigenvalues and +1 to the positive value. The sum of these values defines the signature of a CP and is denoted by 's'. Thus, a CP is labelled by mentioning both its rank and signature. It is noteworthy that the CPs in a stable molecule are all of rank 3, which gives rise to four possible type of CPs:

Table 5.1: Summary of four types of CPs[158, pp 74]

Name	Acronym	λ_1	λ_2	λ_3	(r,s)
(Non) nuclear attractor	(N)NA	–	–	–	(3, -3)
Bond critical point	BCP	–	–	+	(3, -1)
Ring critical point	RCP	–	+	+	(3, +1)
Cage critical point	CCP	+	+	+	(3, +3)

Thus, at **(3, –3)** CP, all curvatures are negative, and ρ is a local maximum, which defines the position of an atom within a molecule. At **(3, –1)** CP, two curvatures are negative and one is positive, which implies that ρ is a local maximum along two of the axes and a local minimum along the third orthogonal axis; this is found between every pair of nuclei linked by a chemical bond. At **(3, +1)** CP, two positive and one negative curvature is there; thus ρ is a local minimum along two of the axes and a local maximum along the third orthogonal axis; this is found at the center of a ring of bonded atoms. At **(3, +3)** CP, where all three curvatures are positive, and ρ is a local minimum, is called a cage critical point.

The eigenvalues of Hessian can also be used for the characterization of the type of bond. As discussed earlier, λ_1 and λ_2 describe the curvature of the electron density in an eigen plane. By convention, $\lambda_1 \leq \lambda_2 \leq 0$, but $|\lambda_2| \geq |\lambda_1|$, therefore $\lambda_1/\lambda_2 > 1$. Thus, in absolute terms, curvature in the direction of one eigenvector is always larger than in the other. The ratio between the two (i.e. λ_1/λ_2) will thus determine the disparity between the two orthogonal curvatures and will determine how elliptical the shape of the contour diagram is. This leads to the so-called ellipticity ε and is defined as

$$\varepsilon = (\lambda_1/\lambda_2) - 1 \qquad \textbf{(8)}$$

$\boldsymbol{\lambda_1 \neq \lambda_2}$, $\boldsymbol{\varepsilon \neq 0} \Rightarrow$ Bond has an elliptical cross section, as is the case in a π bond.

$\boldsymbol{\lambda_1 = \lambda_2}$, $\boldsymbol{\varepsilon = 0} \Rightarrow$ Bond is cylindrical, which occurs in linear molecules and is the characteristic of a typical of σ-bond.

$\boldsymbol{\lambda_2 = 0}$, $\boldsymbol{\varepsilon = \infty} \Rightarrow \rho$ in one direction does not change.

The strength of a bond or its bond order is well-defined by the amount of the charge density present at the BCP. An essential function of $\rho(\mathbf{r})$ is its second derivative, i.e. Laplacian $\nabla^2\rho(\mathbf{r})$, which is a scalar quantity and is defined as the sum of the eigenvalues $(\lambda_1 + \lambda_2 + \lambda_3)$ of the Hessian. The physical significance of the Laplacian is that it represents areas of local charge concentration and depletion. If at the BCP, $\nabla^2\rho < 0$, the density is locally concentrated, which results in a shared interaction. While, $\nabla^2\rho > 0$ implies that the electron density is depleted, which indicates a closed-shell type of interaction. Thus, electron densities, Laplacian, bond paths, curvatures, and bond ellipticities together represent the topology of the charge density distribution in a given molecule.

5.8 Koch and Popelier's Criteria[158]

Though, the existence and the nature of a bond can be specified through the topological analysis of electron density, yet full characterization of the bond (such as bond order, ionicity, conjugation, and hydrogen bonding) become only possible through the evaluation of properties at the BCP. Based on Bader's quantum theory of AIM, Koch and Popelier have proposed eight criteria to establish hydrogen bonding.[159] By utilizing these criteria, hydrogen bonds can be studied independently from IR, NMR, neutron diffraction techniques, *etc*. These criteria distinguish a hydrogen bond from a van der Waals interaction. Though the fulfilment of all the eight criteria is necessary to consider an interaction as a hydrogen bond, but the fourth condition is considered as necessary and sufficient to adequately describe a hydrogen bond. The eight criteria are the following:

Criterion 1: The existence of a BCP between a donor atom and an acceptor atom linked *via* a BP *topologically* (presence of BCP, BP, IAS) proves the existence of a hydrogen bond.

Criterion 2: There should be the existence of the *charge density* (ρ_b = 0.02–0.95 e Å^{-3}) evaluated at the BCP, and it should correlate with the overall hydrogen bond energy. The charge density parameters at the BCP are related to the local electronic kinetic energy density $G(\mathbf{r}_{CP})$ and the local potential energy density $V(\mathbf{r}_{CP})$ and thus to the local total energy density $E(\mathbf{r}_{CP})$ of the electrons by the following equations[122(a),160]

$$G(\mathbf{r}_{CP}) = (3/10)\,(3\pi^2)^{2/3}\rho^{5/3}(\mathbf{r}_{CP}) + (1/6)\,\nabla^2\rho(\mathbf{r}_{CP}) \qquad \textbf{(9)}$$

$$V(\mathbf{r}_{CP}) = (1/4)\nabla^2\rho(\mathbf{r}_{CP}) - 2G(\mathbf{r}_{CP}) \text{ and} \qquad \textbf{(10)}$$

$$E(\mathbf{r}_{CP}) = V(\mathbf{r}_{CP}) + G(\mathbf{r}_{CP}) \qquad \textbf{(11)}$$

Criterion 3: The values of Laplacian, $\nabla^2\rho_b(\mathbf{r})$, should be positive. Further, these values should lie within a sensible range (0.48-3.62 eÅ^{-5}).

Criterion 4: The positive interpenetration of the donor and the acceptor atom is the necessary and sufficient condition for the hydrogen bond formation. This penetration can be quantified by the following equations:

$$\Delta r_H = (r_H^o - r_H) > \Delta r_A = (r_A^o - r_A) \text{ and } \Delta r_H + \Delta r_A > 0 \qquad \textbf{(12)}$$

In the above equations, r_H^o and r_A^o are the non-bonding radii of the donor (D) and the acceptor, (A) atoms respectively and are taken to be equivalent to the gas phase van der Waals' radii.[79,161] Whereas, r_H and r_A, are the bonding radius of the hydrogen and the acceptor and are taken equal to the distances from their respective nucleus to its BCP.

Violation of any one of the above criteria proves the interaction to be of van der Waals type in nature. The rest of the four criteria can be evaluated by performing the integration over the atomic basins of the participating H atoms. These are purely based on the properties associated with the H atoms.

Criterion 5: The H atom loses electrons, and therefore its electronic population should decrease, which results in an increase in the net charge on the H atom.

Criterion 6: The atomic energy of the H atom is destabilized upon formation of a hydrogen bond. The difference in the total atomic energy of H in the hydrogen-bonded complex and the monomer should thus be positive. This condition strongly correlates with the 5th criterion.

Criterion 7: This criterion demands that there should be a decrease in the dipolar polarization (magnitude of the first moment, M) of the H atom upon the formation of a hydrogen bond, which essentially is the result of the loss of nonbonding density of the H atom in the free molecule.

Criterion 8: This final criterion states that the volume of H atom should decrease upon hydrogen bond formation.

5.9 Selection of Compounds for the Charge Density Analysis

Fluorine substituted isoquinoline derivatives [figure **5.1**, 1-(4-fluorophenyl)-6-methoxy-2-phenyl-1,2,3,4-tetrahydroisoquinoline (**IQ1**), 2-(2,3-difluorophenyl)-1-(2,5-difluorophenyl)-6-methoxy-1,2,3,4-tetrahydroisoquinoline (**IQ2**)] have been selected for the charge density studies on weak interactions involving organic fluorine for the following reasons:

1. These compounds are known to grow as a good quality single-crystals,[90] which could be suitable for high-resolution data collection.
2. These compounds do not have any strong hydrogen bond. These were mostly found to pack through C–H···F hydrogen bonds and C–F···F–C interactions.

3. Also, both these compounds had type I C–F···F–C interaction across the inversion center with ∠C–F···F = 170° in **IQ1** and 97° in **IQ2**.

It is to be noted that the experimental charge density study on **IQ1** is already reported by Chopra *et al*.,[162] However, no C–H···F interaction was reported in their study. Thus, for deeper understanding in the context of C–F···F–C and C–H···F interactions and in terms of the polarization of the electron density on F atom, we reconsidered this compound to carry out both experimental and theoretical charge density studies. In our study, C–H···F, C–H···O and C–F···F–C interactions have been shown in 3D deformation density maps, which helped visualizing the orientation of the charge depleted and charge concentrated regions.

5.10 Experimental

5.10.1 Synthesis

All the starting materials were purchased from Sigma-Aldrich and were used as received. One equivalent (eqv.) of 3-methoxyphenylacetic acid was coupled with 1.1 eqv. Of corresponding anilines to synthesize the resulting amide using EDC (1.2 eqv.) as a coupling reagent.[163] After purification by column chromatography, these amides are further reduced to secondary amines using $NaBH_4$ and I_2.[164] This secondary amine is further coupled with the 1.1 eqv. of corresponding benzaldehyde by refluxing both the compounds in the mixture of acetic acid and trifluoroacetic acetic acid in case of **IQ1**.[165] While, the second compound was synthesized by Mr. Hare Ram Yadav (lab-mate) by the standard procedure reported in the literature.[166] (Scheme 5.1)

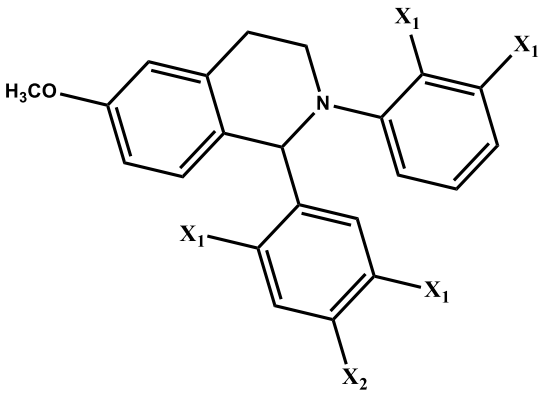

1-(4-fluorophenyl)-6-methoxy-2-phenyl-1,2,3,4-tetrahydroisoquinoline (**IQ1**), X_1 = H, X_2 = F

2-(2,3-difluorophenyl)-1-(2,5-difluorophenyl)-6-methoxy-1,2,3,4-tetrahydroisoquinoline (**IQ2**), X_1 = F, X_2 = H

Figure 5.1: 2D chemical structure of the synthesized molecules.

Reaction Scheme 5.1:

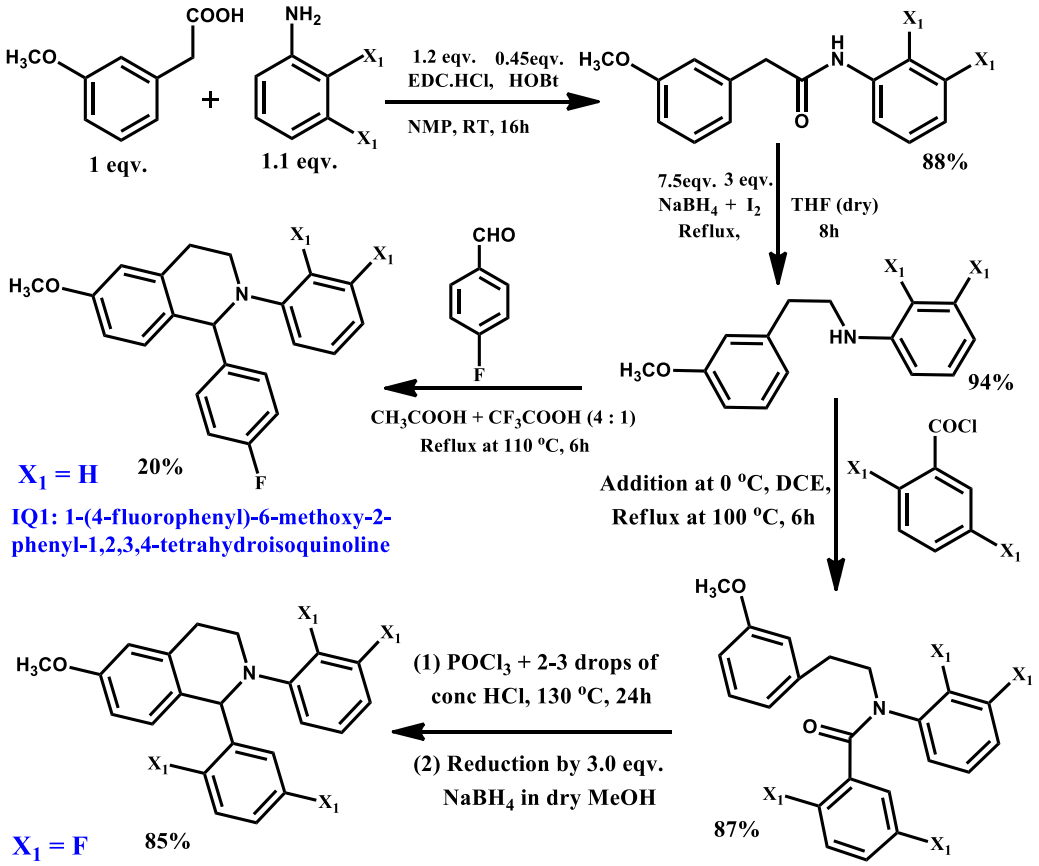

IQ1: 1-(4-fluorophenyl)-6-methoxy-2-phenyl-1,2,3,4-tetrahydroisoquinoline

IQ2: 2-(2,3-difluorophenyl)-1-(2,5-difluorophenyl)-6-methoxy-1,2,3,4-tetrahydroisoquinoline

5.10.2 Single Crystal Data Collection and Refinements

High-resolution single crystal X-ray diffraction data for the compounds **IQ1** and **IQ2** were collected using Bruker AXS KAPPA APEX-II CCD diffractometer equipped with sealed tube source (Monochromatic Mo – Kα radiation) and Agilent SuperNova (Dual source) X-ray diffractometer equipped with a micro focus source (Monochromatic Mo – Kα radiation) at 90 and 100 K respectively. Both the diffractometer are equipped with Oxford cryosystem 700Plus. For **IQ1**, high-resolution data were collected using 16 different sets of runs with different position of the detector (2θ) to cover up to 120.0° in 2θ with overall redundancy > 8. For 2θ positions, -30° to +30°, 10 seconds (s) exposure time was used, while for 2θ positions, -60° > 2θ > -30° and 60° < 2θ < 30°, 30 s exposure was given and for 2θ > ±90°, crystal was exposed to X-rays for 60 s to collect one frame. This data collection was done on a sealed tube source, and it took total six days to collect data. While, for **IQ2**, where the data have been collected on a micro focus source in 31 runs at different 2θ values with different exposure times (1 s for 2θ < 30°, 5 s for 60° < 2θ < 30° and 15 s for 2θ > 60°), the total time taken was 48 hours. Unit cell refinement for the data

sets for **IQ1** were done using Bruker APEX-II suit data reduction and integration were performed by SAINT V7.685A12 (Bruker AXS, 2009), while the same for **IQ2** were done by CrysAlisPro software.[167] Sorting, scaling, merging and empirical correction for absorption were done using SORTAV programme, in the WinGx suite.

5.10.2.1 Spherical Atom Refinement

The crystal structures were solved by using Olex2 using SHELXS-2013. These were further refined (based on F^2) in the spherical atom approximation by using SHELXL2013.

5.10.2.2 Experimental and Theoretical Multipole Refinement

Multipole refinements for both the compounds were performed as described in the section **5.4**. It is worth mentioning that the experimental multipole model was rebuilt by fixing the κ' values of non-hydrogen atoms to the values obtained from the theoretical multipole modelling.

Single point periodic quantum mechanical calculations were carried out using CRYSTAL14 at the B3LYP/6-31G** level of theory for the geometry obtained from the experimental charge density refinement as input. It is to be noted that the during the calculation of wave function, shrinking factors (IS1− IS3) along with the reciprocal lattice vectors were set to 8 (170 k-points in the irreducible Brillouin zone). The bielectronic Coulomb and exchange series values for the truncation parameter were set as ITOL1 − ITOL4 = 8 and ITOL5 = 17 for compound **IQ1** and no truncation parameters were set for compound **IQ2**. The level shifter was set to 0.7 hartree per cycle for better convergence for compound **IQ1** and no level shifter was set for compound **IQ2**. Upon convergence of energy ($\sim 10^{-6}$ Hartree), the periodic wave functions were obtained. The static theoretical structure factors were derived at the same resolutions ($\sin\theta/\lambda$ = 1.16 $Å^{-1}$) as observed in the experimental data sets as described above in section **5.6**. The atomic positions were held fixed to the values obtained from the experimental charge density values during the multipolar refinements. The detailed description for the calculation of theoretical structure factor using CRYSTAL14 has been given in section **5.6**. Multipolar refinements of the theoretical data were performed up to the same levels and in the similar stepwise manner as were done for the experimental charge density modelling to compare the results obtained from both the refinements.

The multipole refinement parameters obtained from the experimental and theoretical modelling for both the compounds **IQ1** and **IQ2** are given in table 5.2. While, the list of net atomic charges, κ and κ' parameters from both the theoretical and experimental models are given in table 5.2a and 5.2b for **IQ1** and **IQ2** respectively.

Table 5.2: Crystal data for the compounds **IQ1** and **IQ2**

DATA	**IQ1**	**IQ1_Literature**[162]	**IQ2**
Formula	$C_{22}H_{20}FNO$	$C_{22}H_{20}FNO$	$C_{22}H_{17}F_4NO$
FW	333.39	333.39	387.36
Temperature (K)	90	113	100
Solvent system	Acetone	--	Acetone
Morphology	Block	--	Block
Crystal System	Monoclinic	--	Monoclinic
Space Group	*C*2/*c*	*C*2/*c*	$P2_1/c$
a (Å)	16.389 (3)	16.414(9)	9.6431 (1)
b (Å)	9.2829(5)	9.300(6)	13.2597 (1)
c (Å)	23.390(5)	23.435(14)	13.9039 (1)
α (^{0})	90	90	90
β (^{0})	107.571 (6)	107.694(8)	100.0862 (9)
γ (^{0})	90	90	90
Volume (Å^3)	3391.5(9)	3408.2(9)	1750.34(3)
Z	8	8	4
Z′	1	1	1
ρ (g/cm^3)	1.306	1.300	1.470
μ (mm^{-1})	0.011	0.087	0.03
F (000)	1408	1407.8	800
$T_{min, max}$	0.945, 1.059	--	0.974, 0.997
$\theta_{min, max}$	1.8^o, 55.5^o	--	2.1^o, 56.0^o
$(Sin\theta/\lambda)_{max}$	1.16	1.10	1.16
Total no. of reflections	138662	--	141833
No. of unique reflections	22108	19037	22882
$[R(F^2)]_{Exp, Theory}$	0.0278, 0.0070	0.0494	0.0299, 0.0067
$[R_w(F^2)]_{Exp, Theory}$	0.0311, 0.0040	0.0612	0.0543, 0.0035
$S_{Exp, Theory}$	1.374, 2.731	2.932	1.707, 3.140
$(N_{obs}/N_{par})_{Exp, Theory}$	14.0, 27.4	21.6	15.8, 24.4
$\Delta\rho_{min,max}$ (eÅ^{-3}) (Exp)	-0.208, 0.210	-0.170, 0.191	-0.225, 0.239
$\Delta\rho_{min,max}$ (eÅ^{-3}) (Theory)	-0.169, 0.180	--	-0.198, 0.189

Table 5.2a: Atomic Charges, κ and κ′ for **IQ1** after theoretical and experimental refinements:

IQ1	Net Charge		κ		κ′
	Exp	***Theory***	**Exp**	***Theory***	***Theory***
F(1)	-0.523(18)	-0.177(4)	0.983(2)	1.000	1.200(10)
O(1)	-0.273(25)	-0.138(7)	0.983(2)	1.000	1.162(7)
N(1)	-0.068(34)	+0.094(10	0.999(3)	1.006	1.121(10)
C(1)	-0.097(41)	-0.131(14	1.010(3)	0.993	0.829(4)
C(2)	-0.049(62)	-0.080(19	1.011(5)	0.996(1)	0.870(8)
C(3)	+0.000(61)	-0.099(18	1.022(4)	0.994(1)	0.900(6)
C(4)	-0.053(86)	-0.144(20	1.003(6)	0.994(1)	0.881(7)
C(5)	+0.182(65)	-0.067(17	1.022(4)	0.994(1)	0.900(6)
C(6)	+0.055(44)	-0.101(13	1.010(3)	0.993	0.829(4)
C(7)	+0.082(51)	-0.036(23	1.043(4)	1.003(2)	0.877(9)
C(8)	-0.205(46)	-0.081(18	1.025(3)	0.997(1)	0.894(6)
C(9)	-0.205(48)	-0.083(18	1.029(3)	1.001(1)	0.869(5)
C(10)	-0.105(57)	-0.045(20	1.024(4)	0.995(2)	0.910(7)
C(11)	-0.048(50)	-0.090(17	1.029(3)	1.001(1)	0.869(5)
C(12)	-0.168(45)	-0.093(18	1.025(3)	0.997(1)	0.894(6)
C(13)	-0.111(51)	-0.182(18	1.010(4)	0.988(1)	0.889(7)
C(14)	-0.103(58)	-0.268(16	1.003(5)	0.987(1)	0.918(7)
C(15)	-0.177(66)	-0.139(18	0.991(5)	0.989(1)	0.877(7)
C(16)	+0.031(63)	-0.003(26	1.000(5)	0.997(2)	0.869(9)
C(17)	-0.232(61)	-0.083(25	0.994(4)	0.995(2)	0.799(8)
C(18)	-0.098(58)	-0.026(22	1.007(4)	0.996(2)	0.892(8)
C(19)	-0.253(52)	-0.126(18	1.007(3)	0.997(1)	0.874(6)
C(20)	-0.258(55)	-0.076(21	0.999(4)	0.998(2)	0.872(7)
C(21)	+0.118(50)	-0.109(19	1.007(3)	0.997(1)	0.874(6)
C(22)	-0.289(70)	-0.187(14	0.991(5)	0.997(1)	0.908(5)
H(2)	+0.085(19)	+0.115(6)	1.200	1.200(10)	1.200
H(3)	+0.130(22)	+0.097(5)	1.200	1.200(10)	1.200
H(4)	+0.041(24)	+0.115(5)	1.200	1.200(10)	1.200
H(5)	-0.045(22)	+0.109(5)	1.200	1.200(10)	1.200
H(6)	-0.006(25)	+0.109(5)	1.200	1.200(10)	1.200
H(8)	+0.184(15)	+0.123(5)	1.200	1.200(10)	1.200
H(9)	+0.261(16)	+0.136(5)	1.200	1.200(10)	1.200
H(11)	+0.134(18)	+0.149(5)	1.200	1.200(10)	1.200
H(12)	+0.278(15)	+0.131(5)	1.200	1.200(10)	1.200
H(13)	+0.197(16)	+0.147(6)	1.200	1.200(10)	1.200
H(14A)	+0.183(16)	+0.126(5)	1.200	1.200(10)	1.200
H(14B)	+0.083(21)	+0.118(5)	1.200	1.200(10)	1.200
H(15A)	+0.173(15)	+0.128(4)	1.200	1.200(10)	1.200
H(15B)	+0.17340	+0.12800	1.200	1.200(10)	1.200
H(18)	+0.179(17)	+0.122(6)	1.200	1.200(10)	1.200
H(19)	+0.234(15)	+0.121(5)	1.200	1.200(10)	1.200
H(21)	+0.103(19)	+0.133(5)	1.200	1.200(10)	1.200
H(22A)	+0.152(15)	+0.123(4)	1.200	1.200(10)	1.200
H(22B)	+0.15260	+0.12360	1.200	1.200(10)	1.200
H(22C)	+0.15260	+0.12360	1.200	1.200(10)	1.200

Table 5.2b: Atomic Charges, κ and κ′ for **IQ2** after theoretical and experimental refinements:

IQ2	Net Charge		κ		κ′
	Exp	***Theory***	**Exp**	***Theory***	***Theory***
F(1)	-0.490(33)	*-0.244(5)*	0.977(2)	*0.992*	*1.014(1)*
F(2)	-0.588(35)	*-0.242(5)*	0.965(3)	*0.991*	*0.998(1)*
F(3)	-0.354(34)	*-0.249(5)*	0.979(3)	*0.991*	*1.004(1)*
F(4)	-0.661(37)	*-0.250(5)*	0.954(3)	*0.991*	*1.004(1)*
O(1)	-0.385(48)	*-0.229(7)*	0.975(3)	*0.991*	*1.010(1)*
N(1)	+0.245(60)	*-0.056(10)*	1.009(5)	*0.996*	*1.002(1)*
C(1)	+0.059(92)	*-0.126(19)*	1.020(7)	*1.003(1)*	*1.010(1)*
C(2)	+0.330(86)	*+0.143(19)*	1.037(7)	*1.016(1)*	*1.026(1)*
C(3)	-0.234(101	*+0.011(18)*	0.990(7)	*1.009(1)*	*1.119(2)*
C(4)	-0.104(116	*+0.082(20)*	1.003(8)	*1.009(1)*	*0.877(8)*
C(5)	-0.070(114	*+0.050(20)*	0.995(8)	*1.006(1)*	*0.894(8)*
C(6)	+0.342(101	*+0.089(20)*	1.036(8)	*1.008(1)*	*0.886(8)*
C(7)	+0.156(102	*-0.077(20)*	1.021(8)	*1.003(1)*	*0.845(8)*
C(8)	+0.201(101	*+0.047(19)*	1.007(8)	*1.007(1)*	*0.904(7)*
C(9)	+0.124(128	*+0.093(20)*	1.008(9)	*1.010(1)*	*0.885(8)*
C(10)	-0.394(136	*+0.094(20)*	0.984(8)	*1.009(1)*	*0.866(7)*
C(11)	-0.047(111	*+0.016(18)*	0.998(8)	*1.005(1)*	*0.892(7)*
C(12)	-0.329(110	*+0.123(20)*	0.996(7)	*1.011(1)*	*0.886(8)*
C(13)	-0.009(93)	*+0.109(17)*	1.000(7)	*1.008(1)*	*0.883(7)*
C(14)	-0.220(101	*+0.127(17)*	0.992(7)	*1.010(1)*	*0.893(6)*
C(15)	-0.481(114	*+0.236(19)*	0.981(7)	*1.014(1)*	*0.901(8)*
C(16)	+0.168(106	*-0.101(21)*	1.012(8)	*0.998(1)*	*0.863(8)*
C(17)	+0.130(99)	*-0.020(21)*	1.022(8)	*1.004(1)*	*0.874(9)*
C(18)	+0.230(103	*+0.037(20)*	1.030(8)	*1.004(1)*	*0.895(8)*
C(19)	+0.172(113	*+0.096(20)*	1.015(8)	*1.010(1)*	*0.894(8)*
C(20)	-0.008(102	*-0.076(18)*	1.008(8)	*1.002(1)*	*0.858(6)*
C(21)	-0.173(112	*+0.141(20)*	0.999(8)	*1.010(1)*	*0.882(9)*
C(22)	-0.585(124	*+0.387(19)*	0.976(8)	*1.026(1)*	*0.913(6)*
H(4)	+0.265(28)	*-0.000(7)*	1.200	*1.119(2)*	*1.083(3)*
H(5)	+0.128(30)	*-0.007(7)*	1.200	*1.119(2)*	*1.083(3)*
H(6)	+0.229(26)	*-0.007(7)*	1.200	*1.119(2)*	*1.083(3)*
H(9)	+0.118(34)	*-0.003(7)*	1.200	*1.119(2)*	*1.083(3)*
H(10)	+0.174(35)	*+0.004(7)*	1.200	*1.119(2)*	*1.083(3)*
H(12)	+0.206(27)	*-0.003(7)*	1.200	*1.119(2)*	*1.083(3)*
H(13)	+0.221(25)	*-0.002(7)*	1.200	*1.119(2)*	*1.083(3)*
H(14A)	+0.100(31)	*-0.002(7)*	1.200	*1.119(2)*	*1.083(3)*
H(14B)	+0.220(28)	*-0.016(7)*	1.200	*1.119(2)*	*1.083(3)*
H(15A)	+0.191(24)	*-0.023(6)*	1.200	*1.119(2)*	*1.083(3)*
H(15B)	+0.19120	*-0.02360*	1.200	*1.119(2)*	*1.083(3)*
H(18)	+0.134(30)	*-0.013(7)*	1.200	*1.119(2)*	*1.083(3)*
H(19)	+0.093(32)	*-0.014(7)*	1.200	*1.119(2)*	*1.083(3)*
H(21)	+0.126(31)	*-0.019(7)*	1.200	*1.119(2)*	*1.083(3)*
H(22A)	+0.191(27)	*-0.025(5)*	1.200	*1.119(2)*	*1.083(3)*
H(22B)	+0.19170	*-0.02560*	1.200	*1.119(2)*	*1.083(3)*
H(22C)	+0.19170	*-0.02560*	1.200	*1.119(2)*	*1.083(3)*

5.11 Results and Discussion

The following sections describe the structural analyses of both the compounds under investigation along with their topological features, which have been derived from their experimental and theoretical charge density studies. These analyses are based on the distribution of charge density inside the molecule.

5.11.1 Structures of IQ1 and IQ2

The colourless block shape crystals for both the compounds were grown by slow solvent evaporation of its solution in acetone at ~ -20 ^{o}C. The compound **IQ1** (figure 5.2a) and **IQ2** (figure 5.3a) crystallize in the monoclinic centrosymmetric *C*2/*c* and $P2_1/c$ space group with Z = 8 and 4 respectively. The compound packs in the crystal lattice by the utilization of weak C–H···O and C–H···F hydrogen bonds and type I C–F···F–C (figures 5.2b-5.2d and 5.3b-5.3g, table 5.3) interactions.

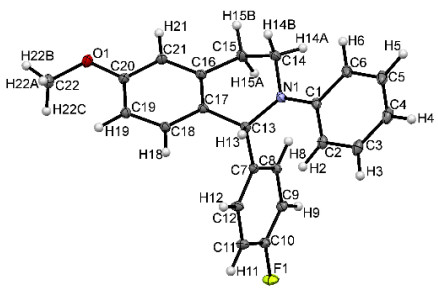

5.2a

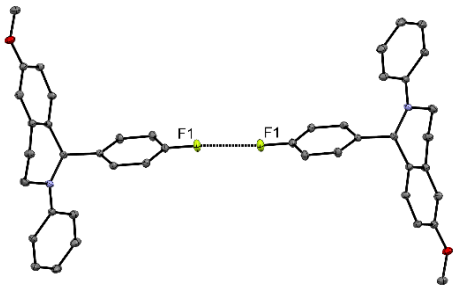

5.2b

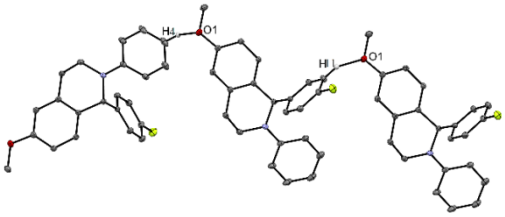

5.2c

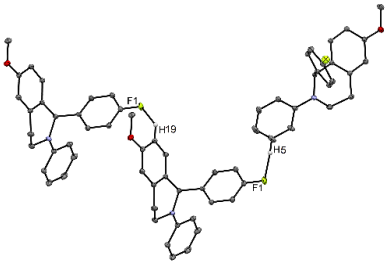

5.2d

Figure 5.2: **(a)** ORTEP of compound **IQ1** with atom labelling. **(b)** Intermolecular C–F···F–C interactions across the inversion center in the structure of **IQ1**. **(c)** C–H···O hydrogen bonds in the crystal lattice of **IQ1**. **(d)** Molecular chain formation in the structure of **IQ1** through C–H···F hydrogen bonds.

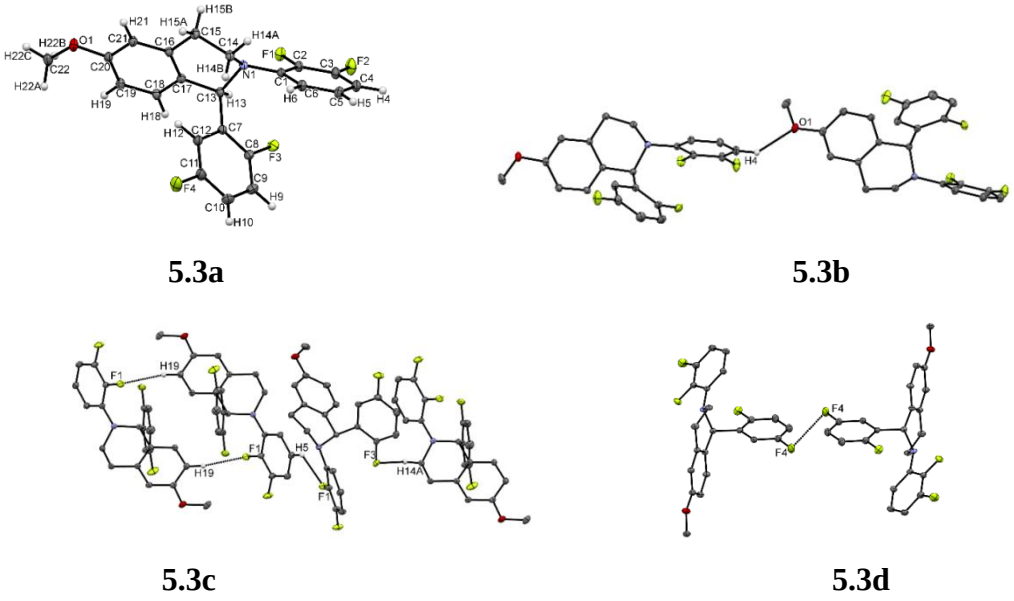

Figure 5.3: (a) ORTEP of compound **IQ2** with atom labelling. **(b)** C–H···O hydrogen bonds in the crystal lattice of **IQ2**. **(c)** Molecular dimer and chain formation through C–H···F hydrogen bonds in the structure of **IQ2**. **(d)** Intermolecular C–F···F–C interactions across the inversion center in the structure of **IQ2**.

Table 5.3: Geometrical parameters of the interactions present in the structures of **IQ1** and **IQ2**.

Code	C–D···F (D = H, F)	*d* D···F /Å	θ ∠C–D···F/°	Symmetry Code
IQ1	C11–H11···O1	2.55	124	x, y-1, z
	C4–H4···O1	2.69	141	x, y-1, z
	C5–H5···F1	2.63	158	x, -y, z+$^1/_2$
	C6–H6···F1	2.86	132	$^1/_2$-x, y+$^1/_2$, $^1/_2$-z
	C19–H19···F1	2.70	121	x-$^1/_2$, y+$^1/_2$, z
	C10–F1···F1–C10	2.65	171	$^1/_2$-x, -$^1/_2$-y, -z
IQ2	C4–H4···O1	2.59	130	x-1, $^1/_2$-y, z+$^1/_2$
	C5–H5···F1	2.52	133	x, $^1/_2$-y, z+$^1/_2$
	C19–H19···F1	2.52	168	-x, 1-y, 1-z
	C14–H14A···F3	2.47	135	-x, y-$^1/_2$, -z+1+$^1/_2$
	C15–H15A···F2	2.69	125	x+1, y, z
	C11–F4···F4–C11	2.87	97	1-x, 1-y, 2-z

Table 5.4a. The parameters characterizing the intramolecular bond critical points for **IQ1**. The values of the same, obtained from the periodic calculation, are given in *italics*.

Bonds	ρ_b	$\nabla^2\rho_b$	d_1 (A−CP)	d_2 (CP−B)	λ_1	λ_2	λ_3	ε
F1–C10	2.02(2)	-17.66(8)	0.824	0.534	-16.75	-16.61	15.69	0.01
	1.77	*-11.47*	*0.840*	*0.518*	*-12.60*	*-12.09*	*13.21*	*0.04*
O1–C20	2.15(2)	-21.73(7)	0.838	0.528	-17.39	-16.16	11.82	0.08
	2.02	*-16.67*	*0.817*	*0.548*	*-15.78*	*-14.18*	*13.29*	*0.11*
O1–C22	1.95(2)	-18.19(6)	0.833	0.587	-16.22	-15.00	13.04	0.08
	1.76	*-12.03*	*0.838*	*0.584*	*-13.00*	*-12.83*	*13.80*	*0.01*
N1–C1	2.17(1)	-18.82(5)	0.815	0.578	-17.39	-15.40	13.96	0.13
	2.06	*-15.90*	*0.783*	*0.609*	*-16.08*	*-13.56*	*13.74*	*0.19*
N1–C13	1.92(2)	-11.75(5)	0.801	0.667	-14.32	-13.93	16.50	0.03
	1.76	*-10.60*	*0.813*	0.655	*-13.06*	*-11.84*	*14.30*	*0.10*
N1–C14	1.86(2)	-13.18(6)	0.827	0.630	-14.11	-13.59	14.51	0.04
	1.80	*-11.60*	*0.811*	*0.646*	*-13.49*	*-12.28*	*14.18*	*0.10*
C1–C2	2.20(1)	-20.33(4)	0.735	0.677	-16.60	-14.40	10.67	0.15
	2.05	*-14.44*	*0.723*	*0.690*	*-14.59*	*-12.54*	*9.68*	*0.16*
C1–C6	2.13(1)	-18.38(3)	0.717	0.695	-15.57	-13.43	10.62	0.16
	2.04	*-17.13*	*0.726*	*0.686*	*-14.43*	*-12.25*	*9.54*	*0.18*
C2–C3	2.23(1)	-20.52(4)	0.707	0.686	-16.91	-14.72	11.11	0.15
	2.11	*-17.99*	*0.693*	*0.699*	*-15.34*	*-12.72*	*10.06*	*0.21*
C3–C4	2.20(1)	-19.24(4)	0.701	0.696	-16.12	-14.34	11.22	0.12
	2.10	*-18.08*	*0.698*	*0.699*	*-15.34*	*-12.81*	*10.06*	*0.20*
C4–C5	2.27(2)	-21.82(5)	0.653	0.741	-17.32	-14.85	10.35	0.17
	2.11	*-18.38*	*0.700*	*0.694*	*-15.40*	*-12.94*	*9.96*	*0.19*
C5–C6	2.23(2)	-20.86(4)	0.695	0.699	-17.39	-14.21	10.74	0.22
	2.09	*-17.66*	*0.707*	*0.686*	*-15.02*	*-12.39*	*9.76*	*0.21*
C7–C8	2.20(1)	-17.66(4)	0.682	0.715	-17.39	-14.21	10.74	0.22
	2.08	*-16.95*	*0.701*	*0.697*	*-15.05*	*-12.43*	*10.53*	*0.21*
C7–C12	2.14(1)	-16.46(4)	0.703	0.696	-15.91	-13.48	12.93	0.18
	2.09	*-17.20*	*0.702*	*0.697*	*-15.09*	*-12.63*	*10.52*	*0.20*
C7–C13	1.69(1)	-12.13(3)	0.773	0.759	-12.30	-11.37	11.54	0.08
	1.67	*-11.29*	*0.758*	*0.773*	*-11.16*	*-10.74*	*10.62*	*0.04*
C8–C9	2.19(1)	-18.10(3)	0.692	0.706	-16.60	-14.02	12.52	0.18
	2.06	*-16.60*	*0.696*	*0.703*	*-14.64*	*-12.46*	*10.50*	*0.17*
C9–C10	2.34(1)	-21.77(4)	0.670	0.716	-18.57	-15.32	12.12	0.21
	2.18	*-20.22*	*0.653*	*0.733*	*-16.41*	*-13.52*	*9.71*	*0.21*
C10–C11	2.26(1)	-19.97(4)	0.754	0.631	-17.35	-14.35	11.73	0.21
	2.18	*-20.14*	*0.727*	*0.659*	*-16.29*	*-13.58*	*9.74*	*0.20*
C11–C12	2.18(1)	-18.44(4)	0.731	0.664	-16.31	-14.14	12.00	0.15
	2.08	*-16.77*	*0.702*	*0.694*	*-14.66*	*-12.59*	*10.47*	*0.16*
C13–C17	1.71(1)	-11.92(3)	0.760	0.761	-11.44	-11.28	10.80	0.01
	1.69	*-11.93*	*0.785*	*0.736*	*-11.29*	*-10.89*	*10.26*	*0.04*
C14–C15	1.74(1)	-13.50(3)	0.762	0.758	-12.52	-11.43	10.45	0.10
	1.71	*-12.65*	*0.786*	*0.735*	*-11.55*	*-11.20*	*10.10*	*0.03*
C15–C16	1.83(1)	-15.27(3)	0.744	0.754	-12.79	-12.59	10.10	0.02
	1.76	*-12.84*	*0.747*	*0.751*	*-11.80*	*-11.33*	*10.29*	*0.04*

C16–C17	2.27(1)	-22.00(3)	0.691	0.709	-16.51	-14.91	9.42	0.11
	2.08	*-17.25*	*0.711*	*0.689*	*-14.73*	*-12.31*	*9.79*	*0.20*
C16–C21	2.18(1)	-19.25(3)	0.708	0.686	-16.07	-13.48	10.29	0.19
	2.08	*-16.51*	*0.695*	*0.699*	*-14.58*	*-12.21*	*10.28*	*0.19*
C17–C18	2.29(1)	-21.57(3)	0.668	0.728	-16.86	-14.55	9.84	0.16
	2.09	*-17.37*	*0.699*	*0.697*	*-14.72*	*-12.48*	*9.83*	*0.18*
C18–C19	2.20(1)	-19.43(4)	0.669	0.726	-16.41	-13.80	10.78	0.19
	2.08	*-17.18*	*0.693*	*0.702*	*-14.87*	*-12.56*	*10.26*	*0.18*
C19–C20	2.23(1)	-20.47(3)	0.679	0.718	-16.40	-14.51	10.45	0.13
	2.10	*-17.76*	*0.679*	*0.719*	*-15.20*	*-12.60*	*10.04*	*0.21*
C20–C21	2.21(1)	-20.10(4)	0.769	0.631	-16.06	-13.73	9.70	0.17
	2.10	*-18.35*	*0.723*	*0.677*	*-15.48*	*-12.76*	*9.89*	*0.21*

Table 5.4b. The parameters characterizing the intramolecular bond critical points for **IQ2**. The values of the same, obtained from the periodic calculation, are given in *italics*.

Bonds (A–B)	ρ_b	$\nabla^2\rho_b$	d_1 (A−CP)	d_2 (CP−B)	λ_1	λ_2	λ_3	ε
F1–C2	2.05(3)	-18.75(14)	0.824	0.522	-17.97	-17.02	16.25	0.06
	1.86	*-13.18*	*0.829*	*0.518*	*-14.21*	*-13.54*	*14.57*	*0.05*
F2–C3	2.04(2)	-20.52(14)	0.853	0.496	-15.95	-15.41	10.84	0.04
	1.83	*-11.85*	*0.838*	*0.509*	*-12.91*	*-12.82*	*13.89*	*0.01*
F3–C8	2.00(2)	-22.83(14)	0.848	0.508	-18.01	-17.09	12.27	0.05
	1.81	*-13.88*	*0.843*	*0.513*	*-13.52*	*-13.21*	*12.85*	*0.02*
F4–C11	2.04(3)	-18.04(15)	0.830	0.524	-15.83	-15.04	12.84	0.05
	1.80	*-12.66*	*0.841*	*0.514*	*-13.02*	*-12.87*	*13.22*	*0.01*
O1–C20	2.19(2)	-21.59(11)	0.834	0.526	-17.12	-17.06	12.60	0.00
	2.01	*-18.14*	*0.832*	*0.531*	*-15.67*	*-14.00*	*11.52*	*0.12*
O1–C22	1.94(3)	-23.76(12)	0.881	0.542	-16.16	-15.34	7.75	0.05
	1.73	*-11.28*	*0.843*	*0.583*	*-12.54*	*-12.28*	*13.54*	*0.02*
N1–C1	2.17(2)	-19.48(8)	0.774	0.640	-18.62	-16.51	15.66	0.13
	1.98	*-14.32*	*0.791*	*0.625*	*-14.86*	*-13.53*	*14.07*	*0.10*
N1–C13	1.81(2)	-14.04(7)	0.816	0.665	-14.32	-13.68	13.96	0.05
	1.74	*-10.90*	*0.824*	*0.656*	*-12.71*	*-12.09*	*13.90*	*0.05*
N1–C14	1.93(2)	-16.67(8)	0.810	0.655	-15.44	-14.91	13.68	0.04
	1.76	*-11.02*	*0.824*	*0.644*	*-12.89*	*-11.85*	*13.71*	*0.09*
C1–C2	2.22(2)	-22.15(5)	0.660	0.738	-18.28	-14.62	10.75	0.25
	2.15	*-19.21*	*0.686*	*0.710*	*-16.55*	*-13.05*	*10.38*	*0.27*
C1–C6	2.11(2)	-18.80(6)	0.736	0.664	-16.02	-13.76	10.98	0.16
	2.09	*-17.61*	*0.709*	*0.691*	*-15.00*	*-12.53*	*9.92*	*0.20*
C2–C3	2.39(2)	-25.46(8)	0.639	0.747	-20.28	-15.57	10.38	0.30
	2.23	*-20.61*	*0.690*	*0.695*	*-17.75*	*-13.58*	*10.72*	*0.31*
C3–C4	2.32(2)	-24.64(6)	0.735	0.649	-18.67	-15.07	9.10	0.24
	2.16	*-19.52*	*0.732*	*0.652*	*-15.66*	*-13.07*	*9.21*	*0.20*
C4–C5	2.23(2)	-21.39(6)	0.689	0.705	-17.06	-14.23	9.90	0.20
	2.08	*-16.92*	*0.685*	*0.707*	*-14.58*	*-12.18*	*9.84*	*0.20*

C5–C6	2.23(2)	-21.93(6)	0.740	0.653	-17.83	-14.75	10.65	0.21
	2.11	*-17.47*	*0.695*	*0.697*	*-15.11*	*-12.63*	*10.27*	*0.20*
C7–C8	2.28(2)	-22.82(5)	0.678	0.716	-18.14	-15.01	10.33	0.21
	2.11	*-17.61*	*0.665*	*0.727*	*-15.01*	*-12.23*	*9.62*	*0.23*
C7–C12	2.21(2)	-18.77(5)	0.663	0.736	-16.23	-13.35	10.81	0.22
	2.04	*-16.01*	*0.704*	*0.694*	*-13.89*	*-11.95*	*9.83*	*0.16*
C7–C13	1.73(1)	-14.31(4)	0.754	0.776	-12.36	-12.26	10.30	0.01
	1.63	*-10.62*	*0.769*	*0.762*	*-10.45*	*-10.29*	*10.11*	*0.02*
C8–C9	2.30(2)	-24.65(6)	0.687	0.701	-18.78	-15.48	9.61	0.21
	2.18	*-19.69*	*0.724*	*0.661*	*-16.27*	*-13.21*	*9.79*	*0.23*
C9–C10	2.26(2)	-21.93(6)	0.695	0.697	-17.31	-14.18	9.57	0.22
	2.10	*-17.51*	*0.701*	*0.687*	*-14.80*	*-12.59*	*9.88*	*0.17*
C10–C11	2.38(2)	-24.63(7)	0.708	0.676	-18.61	-15.26	9.24	0.22
	2.18	*-19.86*	*0.669*	*0.717*	*-16.18*	*-13.43*	*9.76*	*0.20*
C11–C12	2.33(2)	-23.98(6)	0.744	0.640	-18.18	-14.99	9.19	0.21
	2.17	*-19.25*	*0.720*	*0.663*	*-16.17*	*-13.24*	*10.15*	*0.22*
C13–C17	1.79(1)	-14.93(4)	0.776	0.738	-13.56	-12.15	10.78	0.12
	1.71	*-12.71*	*0.772*	*0.743*	*-11.90*	*-11.18*	*10.38*	*0.06*
C14–C15	1.81(2)	-15.64(4)	0.751	0.771	-12.97	-12.40	9.73	0.05
	1.72	*-13.20*	*0.767*	*0.755*	*-11.68*	*-11.33*	*9.81*	*0.03*
C15–C16	1.78(1)	-13.20(5)	0.805	0.701	-12.19	-11.55	10.54	0.06
	1.72	*-12.46*	*0.748*	*0.760*	*-11.45*	*-11.14*	*10.12*	*0.03*
C16–C17	2.17(2)	-19.42(5)	0.714	0.686	-15.97	-14.33	10.88	0.11
	2.07	*-16.88*	*0.709*	*0.690*	*-14.68*	*-12.37*	*10.17*	*0.19*
C16–C21	2.23(2)	-21.88(5)	0.700	0.695	-17.17	-14.63	9.92	0.17
	2.09	*-17.60*	*0.706*	*0.689*	*-14.68*	*-12.37*	*10.17*	*0.19*
C17–C18	2.13(2)	-17.93(5)	0.713	0.682	-16.08	-13.29	11.44	0.21
	2.09	*-17.58*	*0.685*	*0.709*	*-14.89*	*-12.63*	*9.93*	*0.18*
C18–C19	2.22(2)	-20.37(6)	0.709	0.684	-16.96	-14.67	11.25	0.16
	2.09	*-17.49*	*0.704*	*0.688*	*-14.77*	*-12.48*	*9.76*	*0.18*
C19–C20	2.27(2)	-22.02(6)	0.672	0.727	-17.16	-15.15	10.30	0.13
	2.11	*-18.40*	*0.671*	*0.726*	*-15.30*	*-12.60*	*9.50*	*0.21*
C20–C21	2.26(2)	-22.18(5)	0.674	0.721	-17.25	-14.67	9.74	0.18
	2.13	*-19.25*	*0.738*	*0.656*	*-15.53*	*-12.97*	*9.25*	*0.20*

5.11.2 Analysis of the Results of Multipolar Refinements of IQ1 and IQ2

Though, the multipolar model for **IQ1** has already been reported by Chopra *et al*.,[162] yet, a better modelling could be done in the present case (table 5.2). This is evident from the residual density plots, max. DMSDA value for Hirshfeld's rigid bond test [13×10^{-4} Å^2 for the bond N(1)–C(1)], number of unique reflections, R-factor as can be seen from table 5.2. The final choice of the multipole model was made after a careful evaluation of several

factors like residual densities, R-factor, deformation density maps, *etc*., which are described in detail in the following section.

1. In Hirshfeld's rigid bond test, the values for the maximum difference in mean square displacement amplitude (DMSDA) were found to be 7×10^{-4} Å^2 for the bond N(1)–C(1) for **IQ1** and 6×10^{-4} Å^2 for the bonds F(2)–C(3) and F(4)–C(11) for **IQ2**, which indicate that the atomic thermal vibrations have been properly accounted for during the multipole modelling.

2. The maximum and minimum values of residual electron densities over the asymmetric unit are given in table 5.2 for the compound **IQ1** and **IQ2** respectively. This indicates that the electron density of the molecule has been suitably modelled.

3. Static deformation density maps, which are free from thermal vibrations of the molecule, are used to determine the success of the model. These maps envisage the difference between the multipolar and static atom models. The appearance of the electron density in the bonding regions and lone-pair deformation densities elucidates the sensibility of a model. The static deformation density maps obtained after the multipole analysis of both the experimental and the theoretical structure factors are in good agreement, as can be seen from figure 5.5a and 5.5b. The lone pair of electrons of oxygen and fluorine can be clearly visualized from these maps.

4. The topological parameters of the intramolecular covalent bonds for the non-H atoms, obtained after the experimental and theoretical multipolar modelling of the system studied, are given in table 5.4a and 5.4b. The agreement between these values validates the success of the model and also indicates that the topological and charge density properties retrieved from both the methodologies (experimental and theoretical) are comparable.

5. In both the compounds, for all the covalent bonds associated with the electronegative atoms (O, N or F), the BCPs lie close to less electronegative atom i.e. carbon (table 5.4a and 5.4b). The maximum difference in the location of the BCPs between experiment and theory is 0.04 Å for the C15−C16 bond in IQ1 and C20−C21 bond in **IQ2**.

6. The bond order of a covalent bond can be estimated from the values of ε, both from experiment and theory. It has been observed that the single bonds are associated

with the lower values of ε while the value of ε for the double bonds has been found to be higher (table 5.4a and 5.4b).

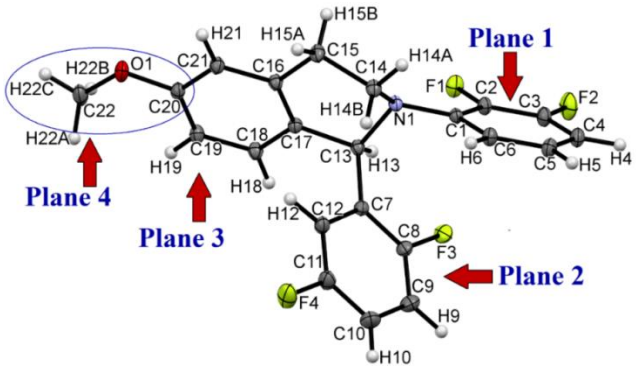

Figure 5.4: Number Scheme used in the compound **IQ2** and labelling of the different planes of the molecule. The same has been used for **IQ1** also.

5.11.2.1 Residual Electron Density Plots: The residual density maps from both theoretical as well as experimental multipole model are shown in different planes of the molecule. The positive (solid red lines) and negative (broken blue lines) contours start at 0.05 eÅ^{-3} with intervals of 0.05 eÅ^{-3}. Maps obtained from the theoretical refinement are shown on left--hand side while from the experimental refinements are shown on the right-hand side.

Table 5.5a: Values of Residual electron densities in different planes of the **IQ1**

IQ2	*Peak (Theory)*	*Hole (Theory)*	Peak (Exp)	Hole (Exp)
Plane 1	*0.088*	*0.131*	0.193	0.139
Plane 2	*0.196*	*0.188*	0.206	0.164
Plane 3	*0.141*	*0.150*	0.197	0.199
Plane 4	*0.248*	*0.188*	0.185	0.150

Table 5.5b: Values of Residual electron densities in different planes of the **IQ2**

IQ1	*Peak (Theory)*	*Hole (Theory)*	Peak (Exp)	Hole (Exp)
Plane 1	*0.150*	*0.167*	0.229	0.167
Plane 2	*0.131*	*0.162*	0.195	0.180
Plane 3	*0.086*	*0.130*	0.181	0.138
Plane 4	*0.140*	*0.147*	0.184	0.143

IQ1

Plane 1

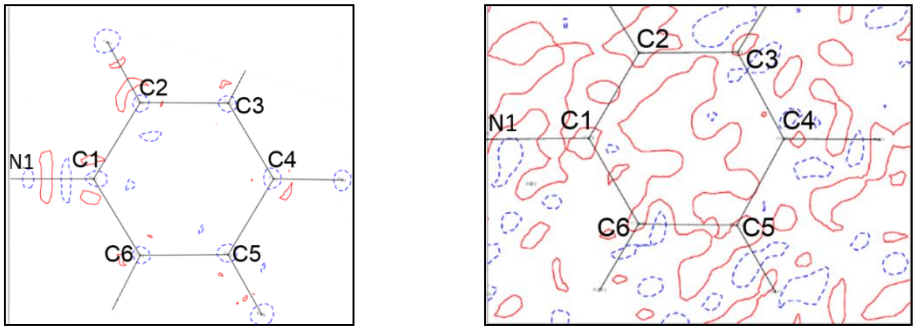

Plane 2

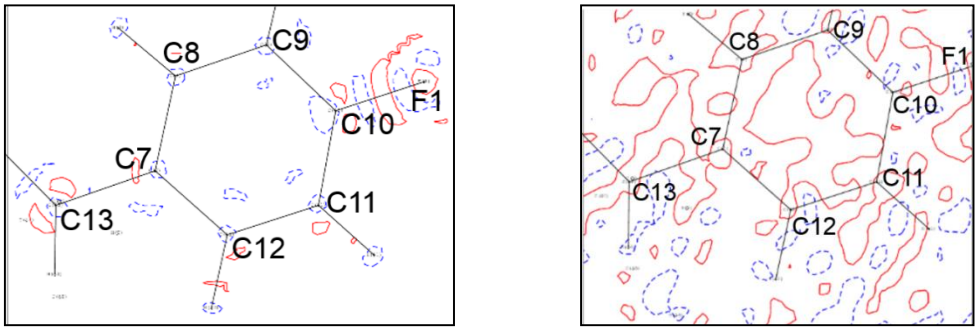

Plane 3

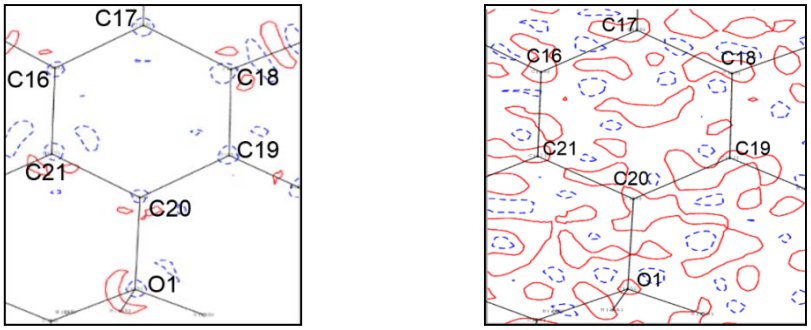

Plane 4

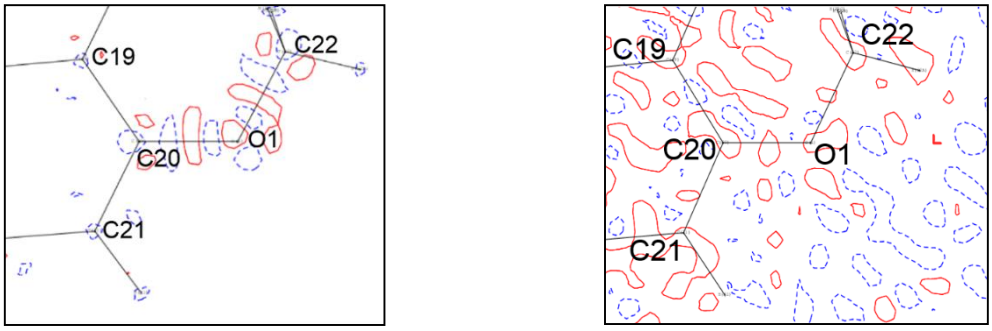

Figure 5.4a: Residual electron density maps in different planes of the compound **IQ1** (Theoretical – Left, Experimental – Right).

IQ2

Plane 1

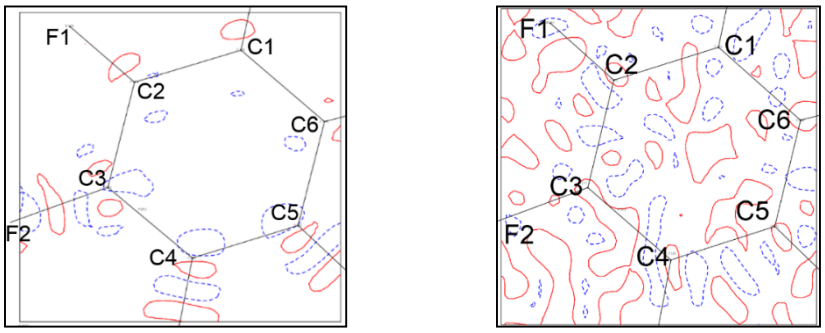

Plane 2

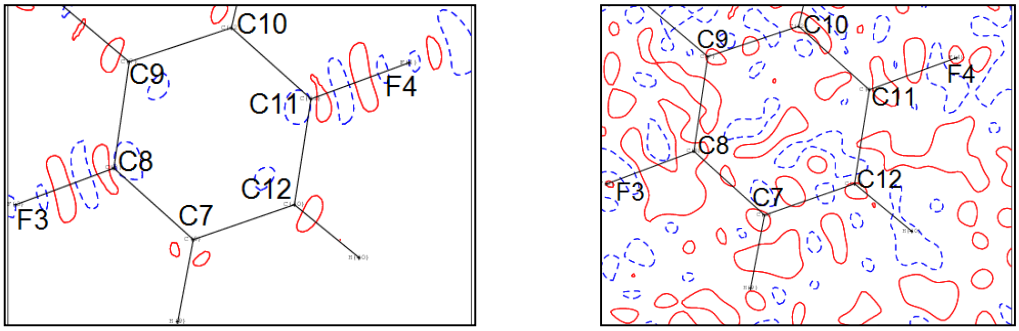

Plane 3

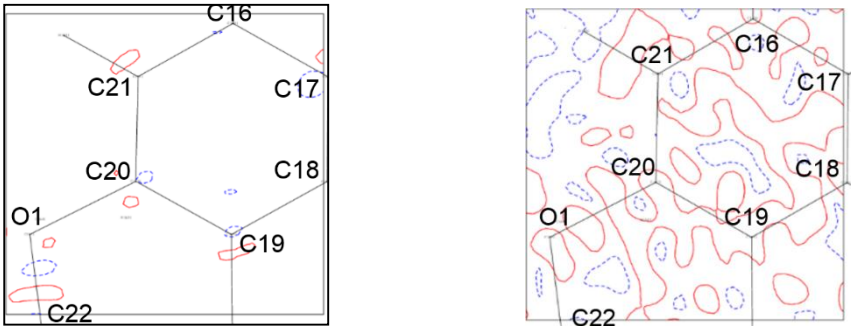

Plane 4

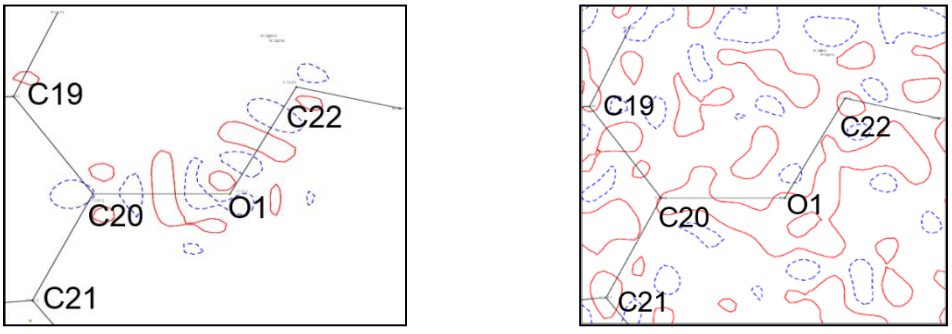

Figure 5.4b: Residual electron density maps in different planes of the compound **IQ2** (Theoretical – Left; Experimental – Right).

5.11.2.2 Static Deformation Density Plots: The static deformation electron density plots from both theoretical as well as experimental multipole model are shown in different planes of the molecule. For all static deformation density maps the positive (solid red lines) and negative (broken blue lines) contours start at 0.05 eÅ^{-3} with intervals of 0.05 eÅ^{-3}.

IQ1

Plane 1

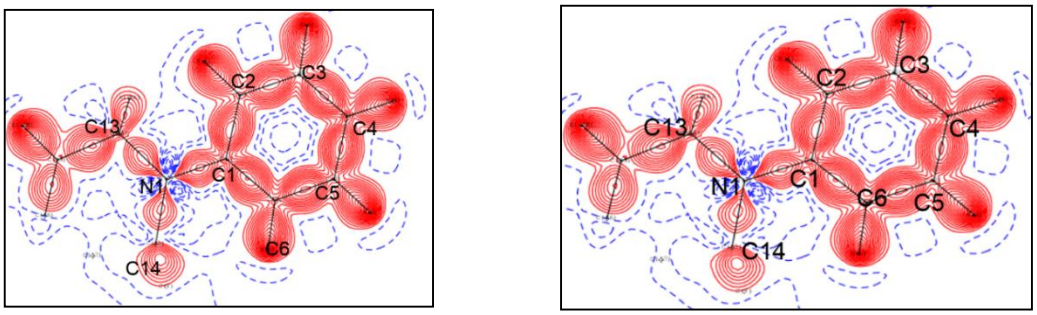

Plane 2

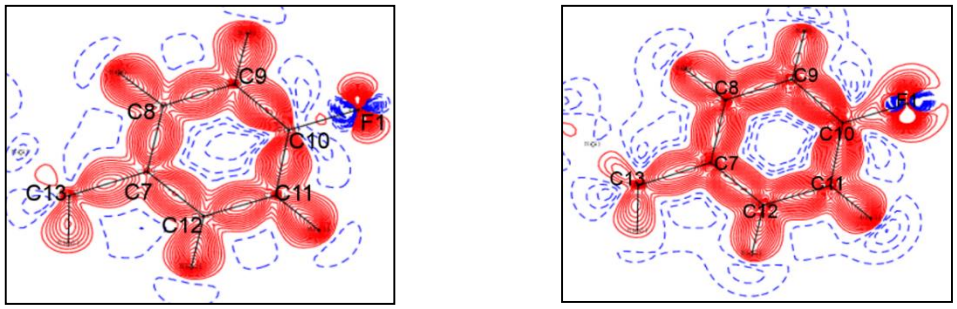

Plane 3

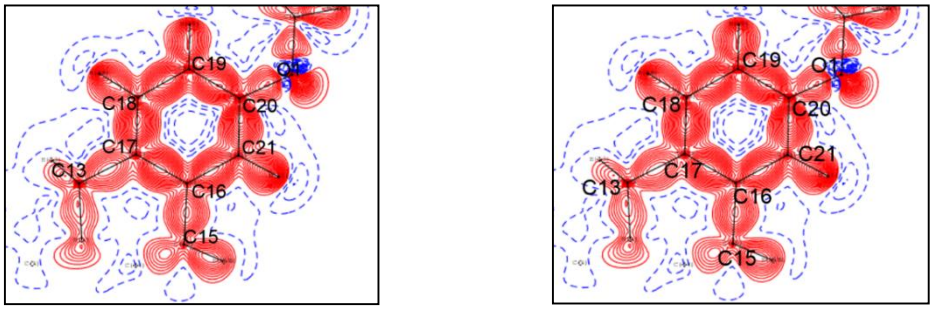

Plane 4

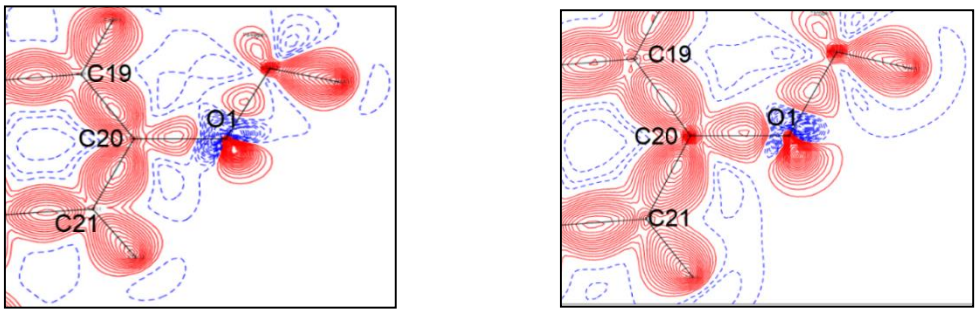

Figure 5.5a: Static deformation density plots in different planes of the compound **IQ1** (Theoretical – Left; Experimental – Right).

IQ2

Plane 1

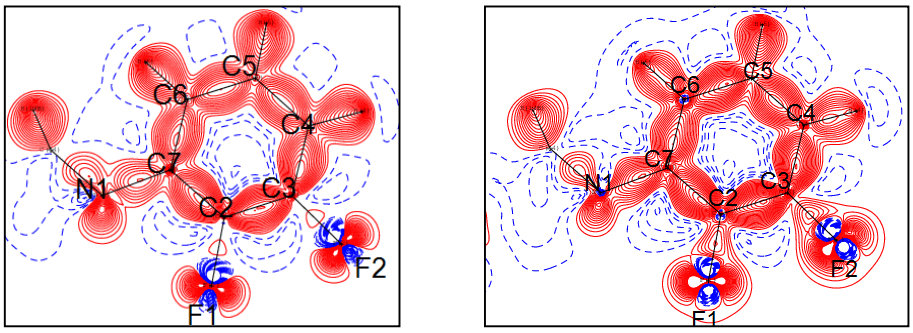

Plane 2

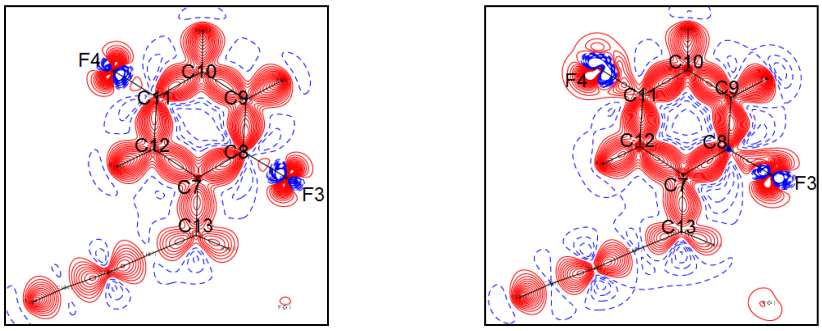

Plane 3

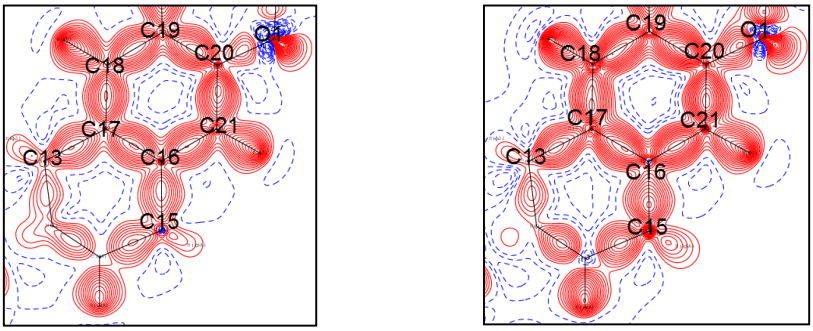

Plane 4

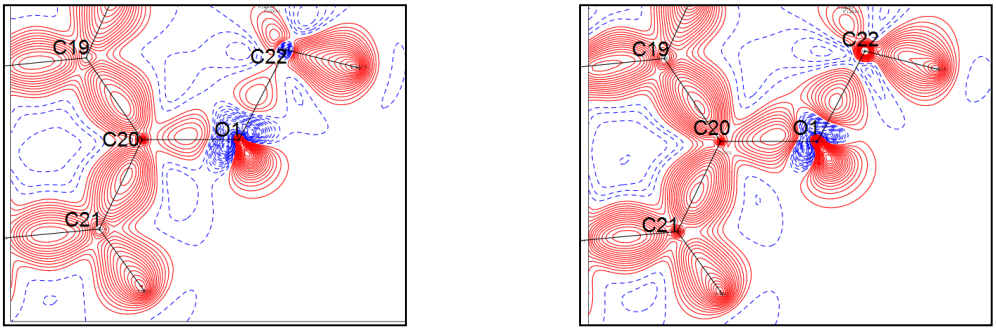

Figure 5.5b: Static deformation density plots in different planes of the compound **IQ2** (Theoretical – Left; Experimental – Right).

5.11.2.3 Laplacian Plots: In the valence shell of a free atom, charge concentration is uniform throughout the sphere. But, it becomes non-uniform upon formation of a molecule. This non-uniformity in the charge concentration leads to the local maxima and minima in the valence shell. This kind of shell structure can be revealed by Laplacian of the electron density. Through Laplacian plots, the alternating shells of charge concentration and charge depletion can be revealed.[161] In the different planes of the molecules, the distribution of charge density, and the bonding features of the atoms are represented through the Laplacian maps for both the compounds from both theoretical as well as experimental multipolar modelling. The contours are drawn at logarithmic scale in $-\nabla^2\rho_b$ ($eÅ^{-5}$). For all the Laplacian plots, blue and red lines represent positive and negative contours respectively.

IQ1

Plane 1

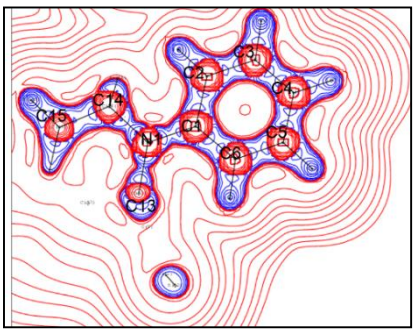

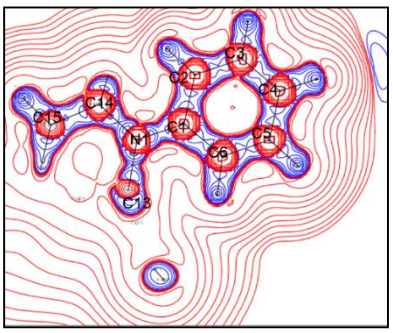

Plane 2

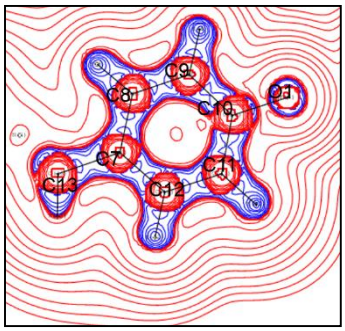

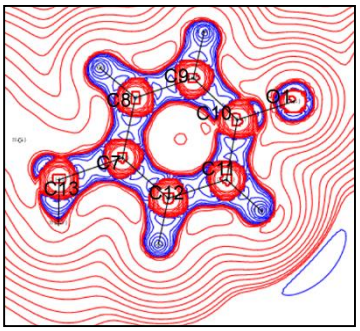

Plane 3

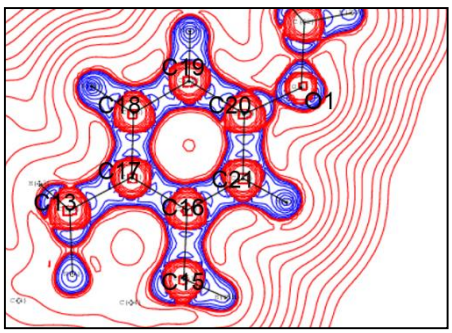

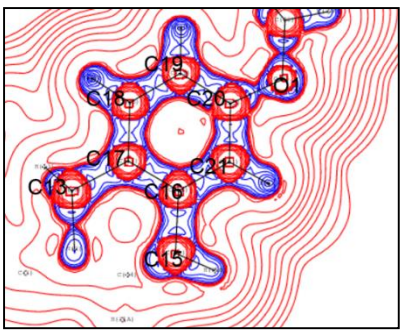

Plane 4

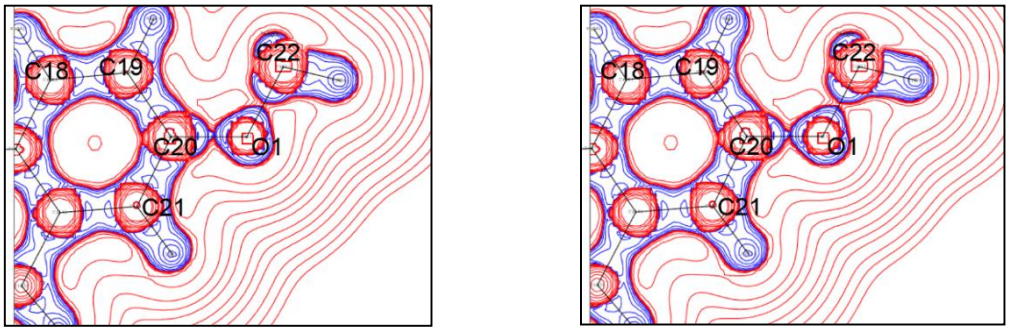

Figure 5.6a: Laplacian plots in different planes of the compound **IQ1** (Theoretical – Left; Experimental – Right).

IQ2

Plane 1

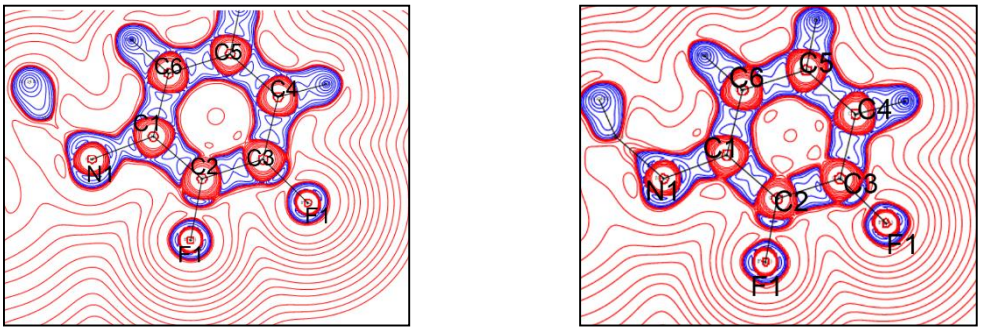

Plane 2

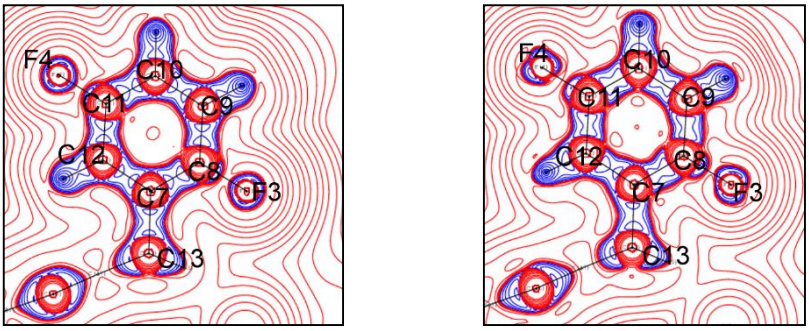

Plane 3

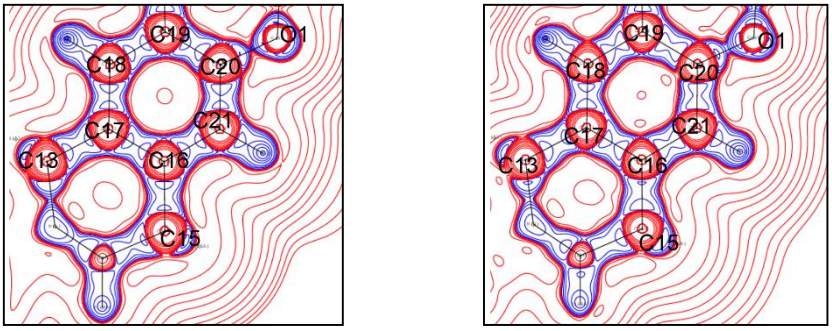

Plane 4

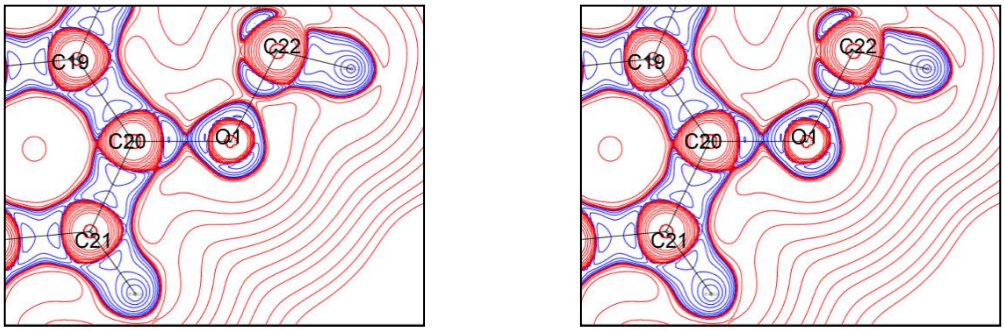

Figure 5.6b: Laplacian plots in different planes of the compound **IQ2** (Theoretical – Left, Experimental – Right).

5.11.3 Evaluation of C–H···F, C–H···O and C–F···F–C Interactions in IQ1 and IQ2

As discussed in the previous chapters, the role of intermolecular interactions such as C–H···F hydrogen bonds has been found to be substantial in the field of crystal engineering. Therefore, in the following section, an attempt has been made to carry out in-depth analyses of these interactions based on the results of charge density studies.

Mallinson *et al.*,[168] through their experimental charge density analysis on a series of ionic complexes have concluded that the nature of interactions can be estimated in terms of the first four of the K

och and Popelier (KP) criteria. It was also emphasized that the penetration criterion is a sufficient condition to predict the nature of an interaction (hydrogen bond type or van der Waals interaction). The rest of his four criteria involve integration over the atomic basin, which is computationally expensive. In this section, the nature of the C–H···F and C–H···O hydrogen bonds has been characterized in terms of first four of the KP criteria. The details of all the parameters describing the C–H···F, C–H···O and C–F···F–C interactions are given in table 5.6a, 5.6b and 5.6c respectively. The results of the evaluation of these interactions in terms of the four essential KP criteria are being described below.

Criterion 1 is the presence of a BCP between the two interacting atoms, which have been found in all interactions. It is also worth mentioning that, a critical point was not found between the C–H···F interaction, where the distance between the H and F was greater than 2.8 Å.

Criterion 2 emphasizes the existence of charge density at the BCP and its relationship with the R_{ij}. It is noteworthy that the in the structures of **IQ1** and **IQ2**, ρ_b values for the C–H···F

and C–H···O hydrogen bonds range from 0.03 to 0.07 eÅ^{-3} (experiment) and 0.03 to 0.05 eÅ^{-3} (theory), which is a sensible range. But, its relationship with R_{ij} and overall hydrogen bond energy could not established, which could be due to the lesser number of data points.

Criterion 3 stresses the positive value of Laplacian at the BCP and its sensible value. The values of the Laplacian ($\nabla^2\rho_b$) for both C–H···F and C–H···O hydrogen bonds are found to be positive. Moreover, these values range from 0.53 to 0.94 eÅ^{-5} (experiment) and 0.53 to 0.96 eÅ^{-5} (theory).

Criterion 4. In this criterion, difference between the non-bonded radii of the donor (r_D^o) and the acceptor (r_D^o) atoms with their corresponding bonding radii, is calculated to understand the interpenetration of the van der Waals spheres of the donor and acceptor atoms by evaluating the quantity, $\Delta r_D + \Delta r_A$. The negative values of this quantity represent the van der Waals type of the interaction while its positive values prove the interaction to be of hydrogen bond type.

Except for one interaction, all other interactions of the type of C–H···F and C–H···O has been found to satisfy this criterion. While, in one of the C–H···F interaction (involving H19 with F1) in the structure of **IQ1**, the fourth criterion was not satisfied. This could be due to the large distance between the concerned H and F (2.70 Å) and poor directionality of that particular interaction (121^o).

Table 5.6a: The parameters characterizing the C–H···F interactions in **IQ1** and **IQ2**. The values obtained from the periodic calculations are given in *italics*.

Code	C–H···F	ρ_b	$\nabla^2\rho_b$	d_1 (H−CP)	d_2 (CP−F)	$\Delta r_D + \Delta r_A$ $(1.2-d_1)+ (1.47-d_2)$
IQ1	C19–H19···F1	0.042	0.574	1.214	1.472	-0.016
		0.033	*0.571*	*1.187*	*1.490*	*-0.007*
	C5–H5···F1	0.034	0.473	1.062	1.511	0.097
		0.032	*0.532*	*1.110*	*1.469*	*0.009*
IQ2	C5–H5···F1	0.038	0.772	1.016	1.446	0.209
		0.044	*0.733*	*1.056*	*1.406*	*0.208*
	C15–H15A···F2	0.041	0.591	1.199	1.469	0.010
		0.033	*0.591*	*1.171*	*1.463*	*0.036*
	C19–H19···F1	0.043	0.595	0.954	1.450	0.267
		0.050	*0.738*	*1.007*	*1.397*	*0.266*
	C14–H14A···F3	0.054	0.939	0.994	1.403	0.273
		0.054	*0.964*	*1.007*	*1.378*	*0.285*

Table 5.6b: The parameters characterizing the C–H···O interactions in **IQ1** and **IQ2**. The values obtained from the periodic calculations are given in *italics*.

Code	C–H···O	ρ_b	$\nabla^2\rho_b$	d_1 (H–CP)	d_2 (CP–O)	$\Delta r_D + \Delta r_A$ $(1.2-d_1)+ (1.47-d_2)$
IQ1	C4–H4···O1	0.057	0.749	1.110	1.460	0.181
		0.044	*0.733*	*1.071*	*1.472*	*0.207*
	C11–H11···O1	0.052	0.802	1.083	1.446	0.221
		0.055	*0.868*	*1.063*	*1.434*	*0.253*
IQ2	C4–H4···O1	0.032	0.494	1.170	1.564	0.016
		0.035	*0.557*	*1.095*	*1.536*	*0.119*

Table 5.6c: The parameters characterizing the C–F···F–C interactions in **IQ1** and **IQ2**. The values obtained from the periodic calculations are given in *italics*.

Code	C–F···F–C	ρ_b	$\nabla^2\rho_b$	d_1 (F–CP)	d_2 (CP–F)
IQ1	C10–F1···F1–C10	0.072	1.482	1.322	1.322
		0.064	*1.363*	*1.322*	*1.322*
IQ2	C11–F4···F4–C11	0.046	0.935	1.438	1.438
		0.039	*0.810*	*1.435*	*1.434*

5.11.3.1 Laplacian Plots for the Intermolecular Interactions Observed in the Compounds IQ1 and IQ2

The crystal packing of the molecules in **IQ1** and **IQ2** is mainly controlled by weak intermolecular interactions such as C–H···F, C–H···O, C–F···F–C, and C–H···π (Cg), *etc*. Representative Laplacian maps from the experimental as well as theoretical analysis, in the intermolecular region having C–H···F, C–H···O and C–F···F–C type of interactions are shown in the following figures (5.7a and 5.7b):

Laplacian plots for IQ1

C10–F1···F1– C10

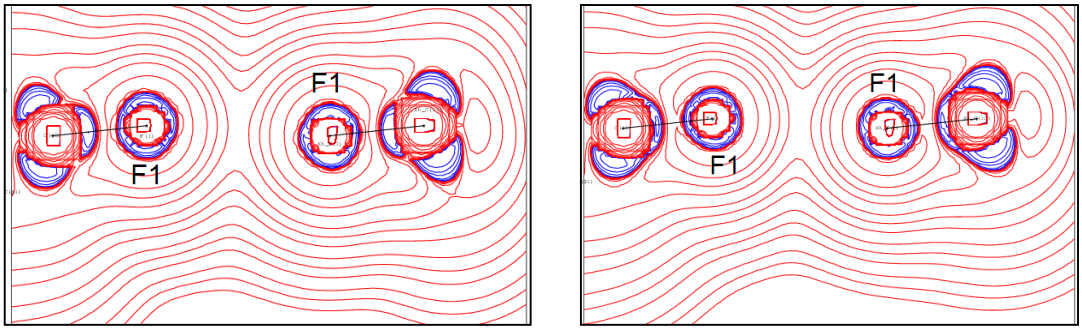

C5–H5···F1

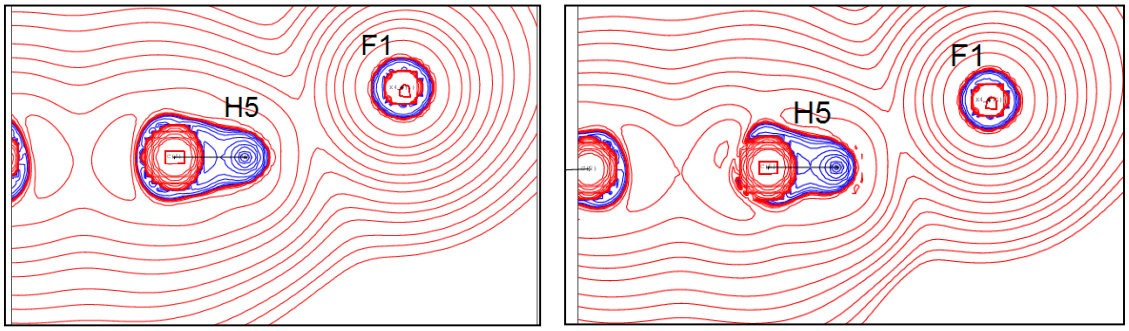

C19–H19···F1

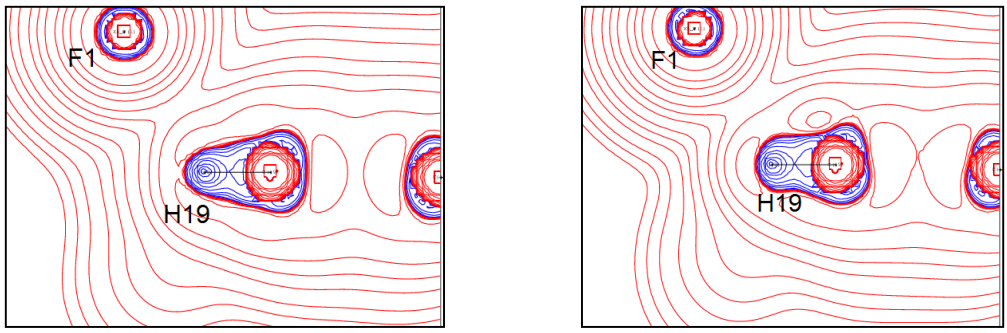

C4–H4···O1

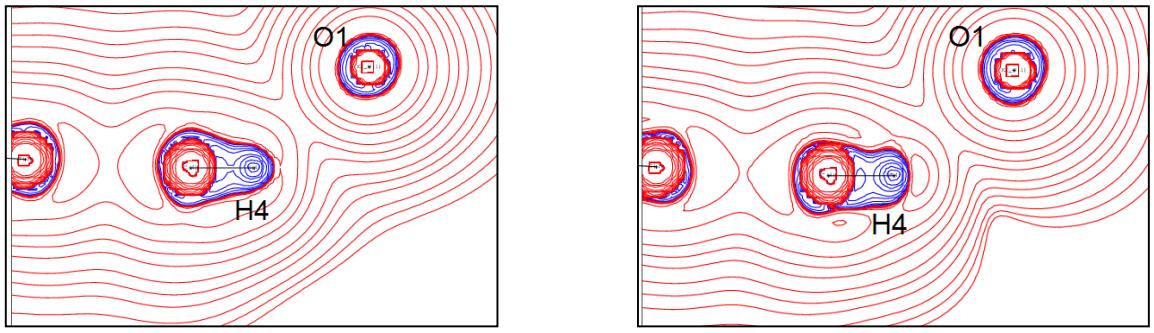

C11–H11···O1

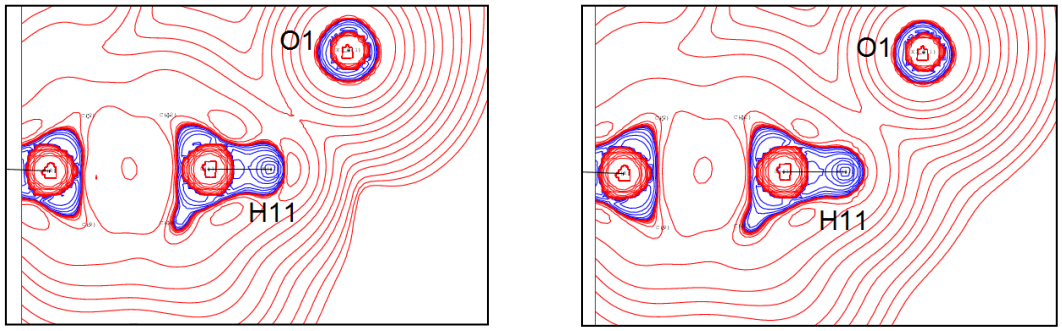

Figure 5.7a: Laplacian plots in different intermolecular regions of the compound **IQ1** (Theoretical – Left; Experimental – Right).

Laplacian plots for IQ2

C11–F4···F4– C11

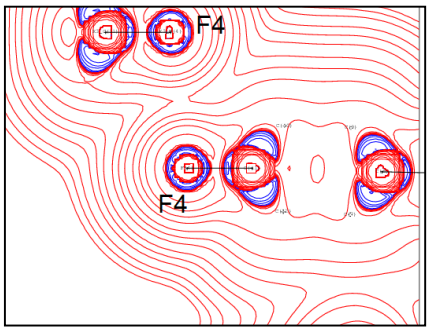

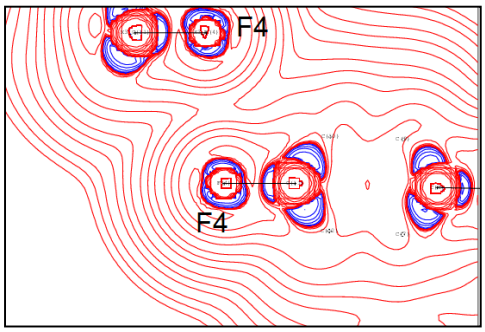

C4–H4···O1

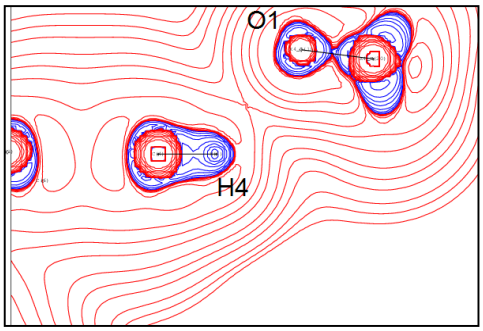

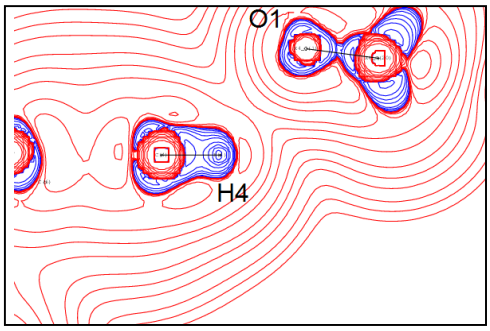

C5–H5···F1

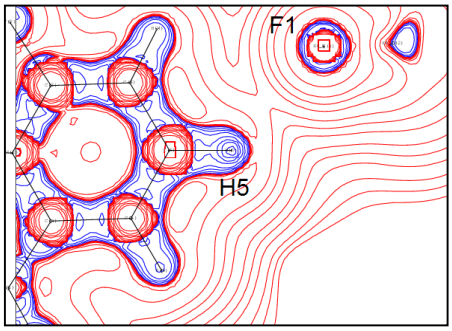

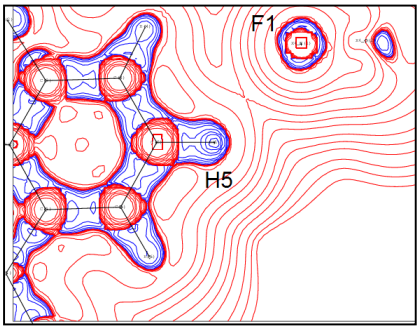

C19–H19···F1

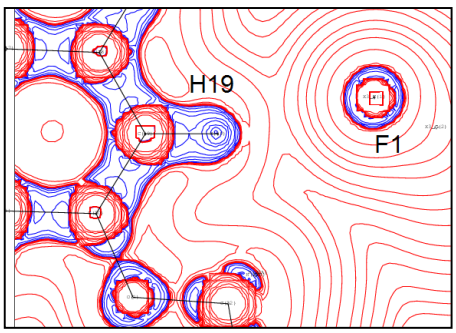

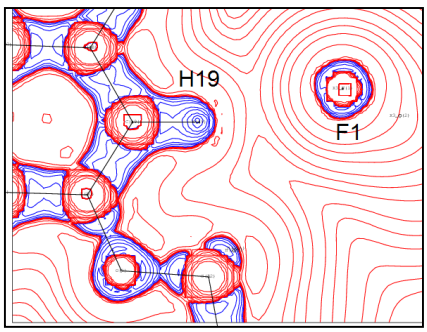

C14–H14A···F3

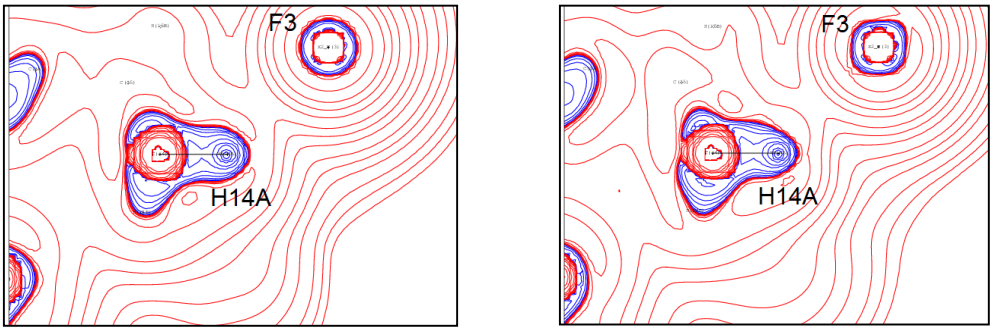

C15–H15A···F2

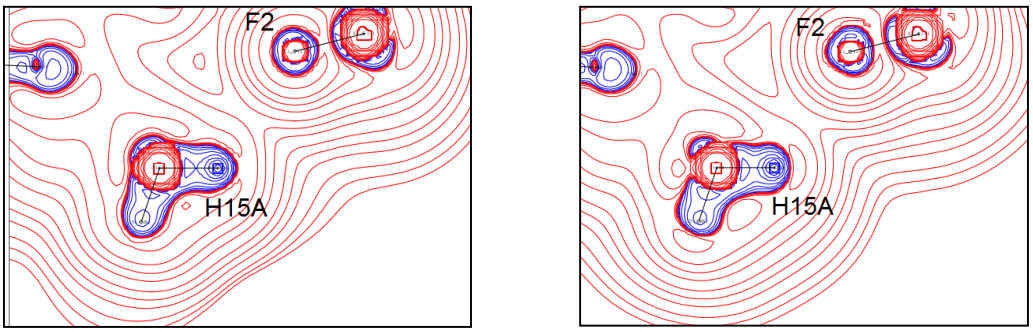

Figure 5.7b: Laplacian plots in different intermolecular regions of the compound **IQ2** (Theoretical – Left; Experimental – Right).

5.11.3.2 3D Deformation Density Plots for the Intermolecular Interactions present in the Compounds IQ1 and IQ2

3D static deformation density maps have been plotted in C–H···F, C–H···O and type I C–F···F–C intermolecular space. Though C–F···F–C interactions (2.65 Å, 171^{o} in **IQ1**; 2.87 Å, 97^{o} in **IQ2**) present in both the structures of **IQ1** and **IQ2** are of type I, yet these differ in their directionality. In the 3D deformation density maps of C–F···F–C intermolecular interactions, regions of same polarity of fluorine atoms have been found to face each other in **IQ1**, while in **IQ2**, in addition to the facing of similar polarity regions, electrophilic (δ+) region on one of F atom also interacts with the nucleophilic (δ−) region of the F atom. Therefore, the C–F···F–C interaction in **IQ2** is expected to be less repulsive than in **IQ1**. Moreover, in both the compounds the aspherical distribution of electron density around the F atom and the presence of sigma hole is evident (figure 5.8a and 5.8b). Furthermore, in C–H···F and C–H···O interactions, the electron deficient region over H

have been seen to point towards the electron rich region, present in the F and O atoms respectively (figure 5.8a and 5.8b) confirming the attractive nature of these interactions.

3D deformation density plots for IQ1

C10–F1···F1– C10

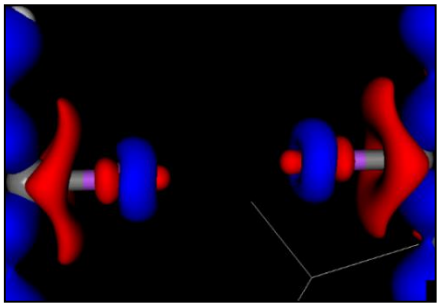
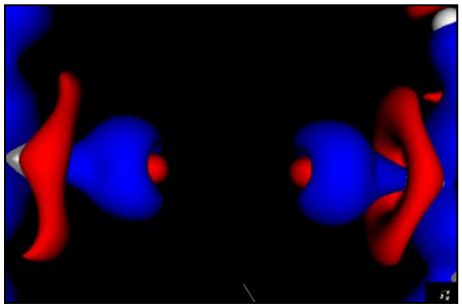

C5–H5···F1

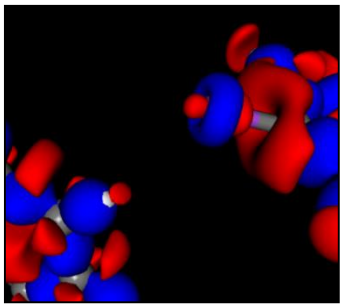
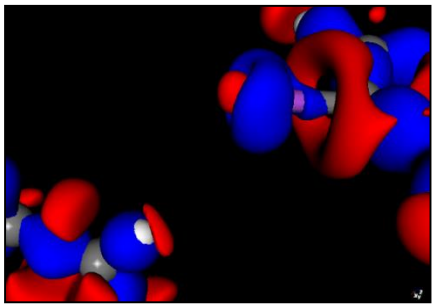

C19–H19···F1

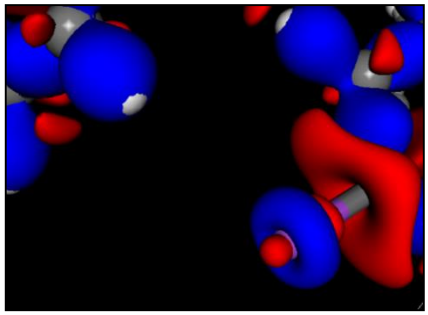
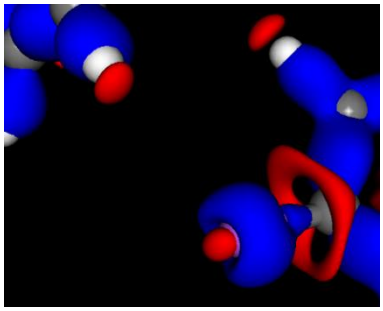

C4–H4···O1

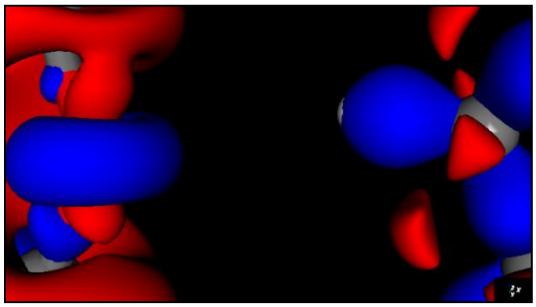
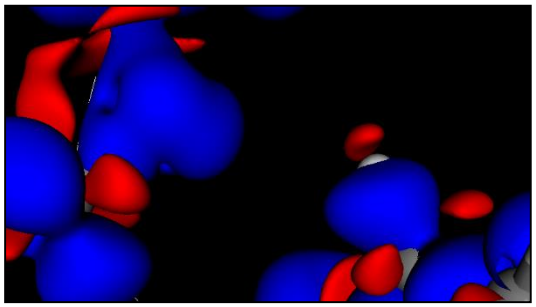

C11–H11···O1

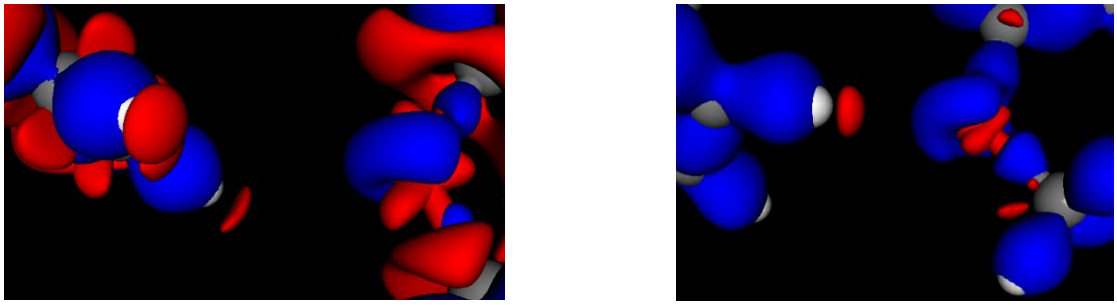

Figure 5.8a: 3D deformation density plots in the intermolecular regions of the compound **IQ1.**

3D deformation density plots for IQ2:

C11–F4···F4– C11

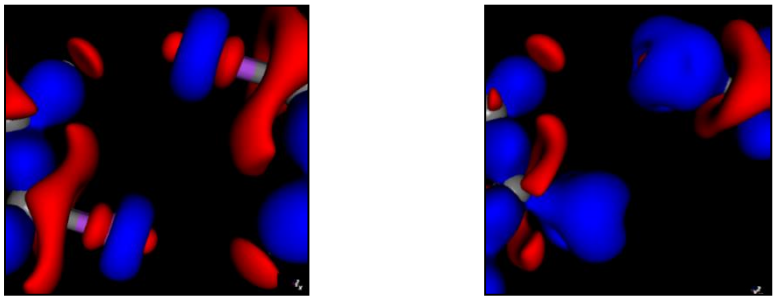

C4–H4···O1

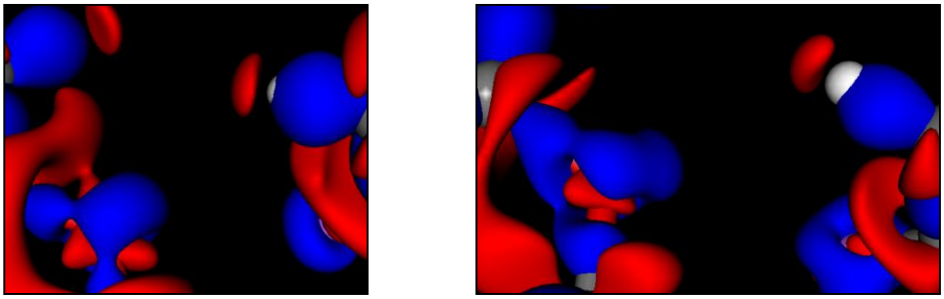

C5–H5···F1

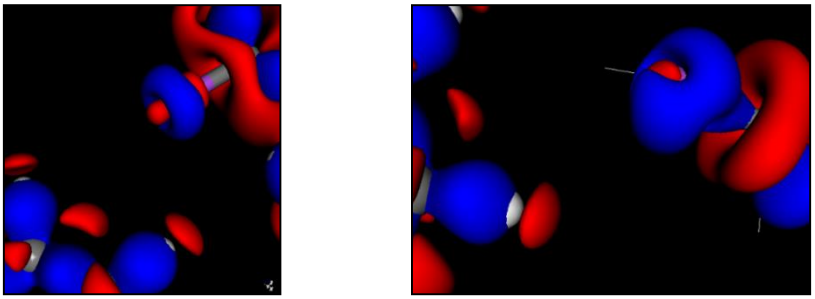

C19–H19···F1

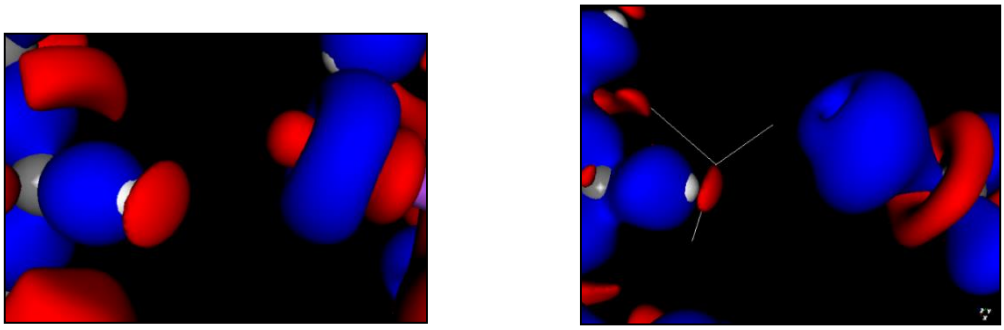

C14–H14A···F3

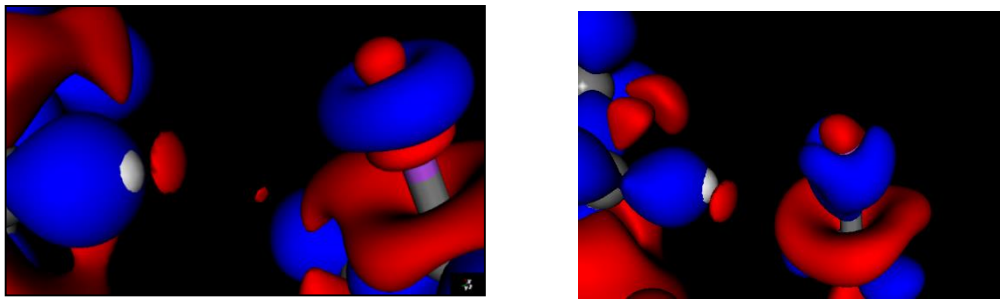

C15–H15A···F2

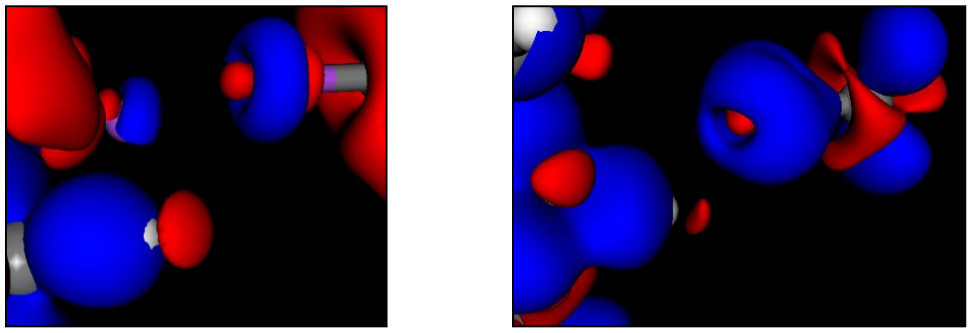

Figure 5.8b: 3D deformation density plots in the intermolecular regions of the compound **IQ2** (Theoretical – Left; Experimental – Right).

5.12 Conclusions

Experimental and theoretical charge density studies on two fluorinated compounds belonging to the class of isoquinolines have been done to gain insights of C–H···F, C–H···O and type I C–F···F–C interactions. Though, in the charge density analysis on **IQ1** had been reported in the literature,[166] no C–H···F hydrogen bonds were recognized in the earlier analyses. A better modelling of **IQ1** could be done as is evident from the table 5.2. Initially, the accuracy of the model was retrieved through featureless plots of residual densities, presence of electron density in the bonding regions in the deformation density maps and also

through Hirshfeld's rigid bond test. The static deformation density (figure 5.5a and 5.5b) and Laplacian (figure 5.6a and 5.6b) maps obtained from both experimental and theoretical multipole refinements are in agreement with each other. All the subtle bonding features like 'lone pair' on the methoxy oxygen and aspherical distribution of electron density on fluorine atoms can be visualized from the static deformation density maps. The presence of sigma hole over the F atoms is an indication of its polarizability, which induce directionality. Hence, directionality associated with the C–H···F hydrogen bonds guides the molecule in generating the stabilizing supramolecular motifs in the crystal engineering. The present work quantitatively evaluates the topological features associated with the C–H···F interactions and proves them to be of hydrogen bond type nature by satisfying the first four essential criteria of Koch and Popelier for hydrogen bond formation.

Concluding Remarks

The importance of weak intermolecular interactions involving organic fluorine has been analyzed and articulated in this thesis. Based on the molecular framework of *N*-benzylideneaniline, the structure directing ability of a C–F group has been studied in the absence of strong hydrogen bonds. In this thesis, efforts have been made to establish the role of fluorine mediated interactions in the formation of recurring supramolecular synthons even in the presence of other halogen atoms. The systematic analyses on halogenated *N*-benzylideneaniline revealed that the C–F group is capable of offering various structural motifs (like zigzag chains, molecular layers, ladders or sheets) involving C–H···F hydrogen bonds. The gas phase stabilization energy calculations done on the dimer formed through the weak C–H···F interactions have proven that the interactions with H···F distances in the range of 2.3-2.5 Å and with ∠C–H···F ~ 160^{o} are the most stabilizing in nature. Moreover, through topological analysis of these interactions, the electron density values were found to be highest among all other interactions. The positive values of the Laplacian further validate the closed shell type nature of these interactions.

The robustness of synthons found in the difluorinated *N*-benzylideneaniline (Chapter 2), was verified by replacing one of the two fluorine atoms by chlorine or bromine (Chapter 3). The outcome of this exercise has emphasized the robustness of the synthons involving fluorine in those structures, where the non-interacting fluorine (fluorine which does not participate in any interaction in the crystal lattice) was replaced by Cl or Br. Whereas, the replacement of interacting fluorine has resulted in entirely different structural features and altered supramolecular synthons. It was noteworthy that the *chloro* and *bromo* analogues were found to have the same structural pattern, but different from the corresponding fluorinated one. The unique nature of fluorine among the halogens has been emphasized.

Furthermore, to explore these interactions in more detail, structural investigations on the tetra fluorinated *N*-benzylideneanilines were conducted (Chapter 4). Herein, the effects of addition of more fluorine atoms to the structural motifs, seen in 2nd chapter were observed. This study has resulted in the observation of a vast variety of structural features in the crystal lattices. But, some of the recurring supramolecular synthons, which were seen to be robust in the earlier cases, remained unaltered in these cases as well. The formation

of a few robust supramolecular synthons has been found to be dependent on the position of fluorine atoms on the different aromatic rings. A correlation has been drawn between the positions of fluorine substituents and the occurrence of a particular supramolecular motif. Other than these, formation of some of the recurring synthons have also been highlighted, and CSD studies on those synthons were also performed. These studies correlate well with our observations.

The gas phase stabilization energy calculations for the dimers studied in this thesis, and the topological studies on them indicated that C–H···F interactions follow the same trend as followed by C–H···O hydrogen bonds in the literature, thus confirming their hydrogen bond type character. Most of the synthons involving fluorinated interactions were found to consist of C–H···F hydrogen bonds. Therefore, to quantify these interactions charge density studies were done. Due to the unavailability of a good quality single crystal for any of the fluorinated *N*-benzylideneanilines, evaluation of C–H···F and C–F···F interactions were conducted in fluorine substituted derivatives of isoquinolines through experimental and theoretical charge density analyses. Both experimental and theoretical charge density analyses on the two compounds have revealed the hydrogen bond type nature of C–H···F interactions by satisfying the first four essential criteria of Koch and Popelier for hydrogen bond formation. The presence of a sigma hole over the F atoms is an indication of its polarizability, which induce directionality. The directionality associated with the C–H···F hydrogen bonds guides the molecule in generating the stabilizing supramolecular motifs in crystal engineering. Additionally, type I C–F···F–C interactions were found to be repulsive, though, the interactions with ∠C–F···F = 97^{o} are less repulsive than those with ∠C–F···F = 170^{o}.

To conclude, it may be said that "organic fluorine" is capable of altering, controlling and directing the crystal packing through various supramolecular synthons formed by weak but directional C–H···F hydrogen bonds. The existence of type I C–F···F interaction leads to a certain amount of destabilization of the structure. But this destabilization being subtle, is easily overcome by other strong and weak interactions present in the structure.

References:

1. Desiraju, G. R.; Steiner, T. *The Weak Hydrogen Bond in Structural Chemistry and Biology*; Oxford University Press: Oxford, **1999**.
2. Desiraju, G. R. *J. Chem. Sci.* **2010**, *122*, 667–675.
3. Desiraju, G. R. *Angew. Chem. Int. Ed. Engl*. **1995**, *34*, 2311−2337.
4. (a) *Crystal engineering. Structure and function. Perspectives in supramolecular chemistry*; Desiraju, G. R., (Ed).; Wiley: Chichester, 2003. (b) *Frontiers in crystal engineering*; Tiekink, E. R., Vittal, J. J., Eds.; Wiley: Chichester, 2005. (c) *Crystal engineering. From molecules to crystals to materials*; Braga, D., Grepioni, F., Orpen, A. G., Eds.; Kluwer: Dordrecht, 1999**.**
5. Desiraju, G. R. *Angew. Chem. Int. Ed. Engl*. **2007**, *46*, 8342−8356.
6. Bragg, W. H. *Proc. Phys. Soc. London* **1921**, *34*, 33−49.
7. Robertson, J. M. *P. Roy. Soc. (London) Ser. A* **1951**, *207*, 101−110.
8. Desiraju, G. R.; Gavezzoti, A. *J. Chem. Soc., Chem. Commun*. **1989**, 621−623.
9. Pepinsky, R. *Phys. Rev*. **1955**, *100*, 971.
10. Schmidt, G. M. J. *Pure Appl. Chem.* **1971**, *27*, 647–678.
11. Cohen, M. D. *Tetrahedron* **1987**, *43*, 1211−1214.
12. Herbstein, F. H. *Crystalline molecular complexes and compounds*; OUP: Oxford 2005**.**
13. Addadi, L.; Lahav, M. *J. Am. Chem. Soc*. **1978**, *100*, 2838−2844.
14. Leiserowitz, L. *Acta Crystallogr. Sect. B* **1976**, *32*, 775−802.
15. (a) Desiraju, G. R. *Crystal Engineering: The Design of Organic Solids*; Elsevier: Amsterdam, 1989, 54. (b) Desiraju, G. R.; Vittal, J. J.; Ramanan. *Crystal Engineering A Textbook*, World Scientific Publishing Company: Singapore, 2011.
16. Lehn, J. -M. *Angew. Chem. Int. Ed. Engl*. **1988**, *27*, 89−112.
17. Dunitz, J. D. *Pure App. Chem*. **1991**, *63*, 177−185.
18. Corey, E. J. *Pure App. Chem*. **1967**, *14*, 30–37.
19. (a) Seto, C. T.; Whiteside, G. M. *J. Am. Chem. Soc.* **1993**, *115*, 905−916. (b) Zimmerman, S. C.; Corbin, P. S. *Struct. Bonding* **2000**, *96*, 63−94. (c) Prins, L. J.; Reinhoudt, D. N; Timmerman, P. *Angew. Chem. Int. Ed*. **2001**, *40*, 2382–2426. (d) Yamauchi, K.; Lizotte, J. R.; Long, T. E. *Macromolecules* **2002**, *35*, 8745−8750. (e) Park, P.; Zimmerman, S. C. *J. Am. Chem. Soc*. **2006**, *128*, 11582−11590. (f)

Bouteiller, L. *Adv. Polym. Sci*. **2007**, *27*, 79−112; (g) Wua, Y. -C.; Kuo, S. -W. *J. Mater. Chem.* **2012**, *22*, 2982−2991.

20. Metrangolo, P.; Neukirch, H.; Pilati, T.; Resnati, G. *Acc. Chem. Res.* **2005**, *38*, 386–395.
21. Nishio, M.; Umezawa, Y.; Suezawa, H.; Tsuboyama, S., The CH/π Hydrogen Bond: Implication in Crystal Engineering In *The Importance of Pi-Interactions in Crystal Engineering*; Tiekink, E. R. T., Zukerman-Schpector J., Eds.; John Wiley & Sons, Ltd: Chichester, UK, 2012; pp 1−39.
22. (a) Morokuma, K. *Acc. Chem. Res.* **1977**, *10*, 294–300; (b) Scheiner, S. *Hydrogen Bonding: A Theoretical Perspective*; Oxford University Press: Oxford, 1997.
23. Pauling, L. *The nature of the chemical bond and the structure of molecules and crystals: an introduction to modern structural chemistry*; Cornell University Press: Ithaca, NY, 1960, Vol. 18.
24. Pauling, L.; Delbrück, M. *Science* **1940**, *92*, 77−79.
25. Pauling, L. *The nature of the chemical bond and the structure of molecules and crystals*; Cornell University Press: Ithaca, NY, 1939.
26. (a) Jeffrey, G. A.; Saenger, W., *Hydrogen bonding in biological structures*; Springer−Verlag: Berlin, 1991. (b) Jeffrey, G. A. *An Introduction to Hydrogen Bonding*; Oxford University Press: Oxford, 1997.
27. Pimentel, G. C.; McClellan, A. L. *Hydrogen bonding*: *Annual Review of Physical Chemistry* **1971**, *22*, 347−385.
28. Steiner T. *Angew. Chem. Int. Ed. Engl*. **2002**, *41*, 48−76.
29. Steiner, T.; Saenger, W. *J. Am. Chem. Soc.* **1993**, *115*, 4540–4547.
30. (a) Arunan, E.; Desiraju, G. R.; Klein, R. A.; Sadlej, J.; Scheiner, S.; Alkorta, I.; Clary, D. C.; Crabtree, R. H.; Dannenberg, J. J.; Hobza, P.; Kjaergaard, H. G.; Legon, A. C.; Mennucci, B.; Nesbitt. D. *J. Pure Appl. Chem*. **2011**, *83*, 1637−1641. (b) Desiraju, G. R. *Angew. Chem., Int. Ed.* **2011**, *50*, 52−59.
31. (a) Atwood, J. L.; Steed, J. W. *Encyclopedia of Supramolecular Chemistry, Volume 1*; CRC Press: 2004; pp 357−363. (b) Hamilton, A. D. *Supramolecular control of structure and reactivity, Perspectives in supramolecular chemistry*; Wiley: Chichester, 1996, Vol. 3.
32. (a) Etter, M. C.; *Acc. Chem. Res*. **1990**, *23*, 120–126. (b) Etter, M. C.; Admond, D. A. *J. Chem. Soc. Chem. Commun.* **1990**, 589−591. (c) Ermer, O.; Eling, A. *J. Chem. Soc. Perkin Trans. 2.* **1994**, 925−944. (d) Aakeröy, C. B.; Desper, J.; Fasulo, M.;

Hussain, I.; Levin, B.; Schultheiss, N. *CrystEngComm* **2008**, *10*, 1816−1821. (e) Aakeröy, C. B.; Salmon, D. J.; *CrystEngComm* **2005**, *7*, 439–448.

33. Desiraju, G. R. *Acc. Chem. Res.* **2002**, *35*, 565–573.
34. Glasstone, S. *Trans. Faraday Soc.* **1937**, 200−214.
35. Gordy, W. J. *Chem. Phys.* **1939**, *7*, 163−166.
36. Dougill, M. W.; Jeffrey, G. A. *Acta Crystallogr.* **1953**, *6*, 831−837;
37. Jones, G. P.; Cornell, B. A.; Horn, E.; Tieklink, E. R. T. *J. Cryst. Spectrosc. Res.* **1989**, *19*, 715−723.
38. (a) Sutor, D. J. *Acta Crystallogr.* **1958**, *11*, 453–458. (b) Sutor, D. J. *Nature* **1962**, *195*, 68–69. (c) Sutor, D. J. *J. Chem. Soc.* **1963**, 1105−1110.
39. (a) Taylor, R.; Kennard, O. *J. Am. Chem. Soc.* **1982**, *104*, 5063−5070. (b) Allen, F. H.; Kennard, O.; Taylor, R. *Acc. Chem. Res.* **1983**, *16*, 146–153.
40. (a) Desiraju, G. R. *Acc. Chem. Res.* **1991**, *24*, 290−296. (b) Pedireddi, V. R. *Cryst. Growth Des.* **2001**, *1*, 383−385. (c) Boryczka, S.; Rozenberg, M. S.; Schreurs, A. M. M.; Kroon, J.; Starikov, E. B.; Steiner, T. *New J. Chem.* **2001**, *25*, 1111−1113. (d) Pedireddi, V. R. *CrystEngComm* **2002**, *4*, 315−317. (e) Steiner, T. *Angew. Chem. Int. Ed.* **2002**, *41*, 48−76. (f) Domagała, M.; Grabowski, S. J.; Urbaniak, K.; Mloston´, G. *J. Phys. Chem. A* **2003**, *107*, 2730−2736. (g) Steiner, T. *Crystallogr. Rev.* **2003**, *9*, 177−228.
41. (a) Sarma, J. A. R. P.; Desiraju, G. R. *Acc. Chem. Res.* **1986**, *19*, 222−228. (b) Desiraju, G. R. *Acc. Chem. Res.* **1996**, *29*, 441−449. (c) Langley, P. J.; Hulliger, J.; Thaimattam, R.; Desiraju, G. R. *New J. Chem.* **1998**, *22*, 1307−1309. (d) Foces-Foces, C.; Jagerovic, N.; Elguero, J. *Acta Crystallogr. Sect. C* **2000**, *56*, 215−218. (e) Wolstenholme, D. J.; Weigand, J. J.; Cameron, E. M.; Cameron, T. S. *Phys. Chem. Chem. Phys.* **2008**, *10*, 3569−3577.
42. (a) Etter, M. C. *Acc. Chem. Res.* **1990**, *23*, 120−126. (b) Aakeröy, C. B.; Evans, T. A.; Seddon, K. R.; Palink, I´. O´. *New J. Chem.* **1999**, *23*, 145−152. (c) Jeffrey, G. A. *Crystallogr. Rev.* **2003**, *9*, 135−176. (d) Steiner, T. *Crystallogr. Rev.* **2003**, *9*, 177−228. (e) Virdo, J. D.; Crandall, L.; Dang, J. D.; Fulford, M. V.; Lough, A. J.; Durfee, W. S.; Bender, T. P. *CrystEngComm* **2013**, ***15***, 8578−8586.
43. (a) Pascard, C. *Acta Cryst.* **1995**, *D51*, 407−417. (b) Glusker, J. P. *Acta Cryst.* **1995**, *D51*, 418−427. (c) Pierce, A. C.; Sandretto, K. L.; Bemis G. W. *Proteins Struct. Funct. Bioinf.* **2002**, *49*, 567−576. (d) Pierce, A. C.; Haar, E.; Binch, H. M. *J. Med. Chem.* **2005**, *48*, 1278−1281. (e) Nayak, S. K.; Mallik, S. B.; Kanaujia, S. P.; Sekar,

K.; Ranganathan, K. R.; Ananthalakshmi, V.; Jeyaraman, G.; Saralaya, S. S.; Rao, K. S.; Shridhara, K. *CrystEngComm* **2013**, *15*, 4871−4884.

44. Malone, J. F.; Murray, C. M.; Charlton, M. H.; Docherty, R.; Lavery, A. J. *J. Chem. Soc. Faraday Trans*. **1997**, *93*, 3429–3436. (b) Perutz, M. F. *Philos. Trans. Roy. Soc. London Ser. A* **1993**, *345*, 105–112.
45. (a) Nishio, M.; Hirota, M. *Tetrahedron* **1989**, *45*, 7201–7245. (b) Nishio, M.; Umezawa, Y.; Hirota, M.; Takeuchi, Y. *Tetrahedron* **1995**, *51*, 8665–8701.
46. Nishio, M.; Hirota, M.; Umezawa, Y. *The CH/πInteraction. Evidence, Nature, and Consequences*; Wiley-VCH: New York, USA, 1998.
47. Nishio, M. *CrystEngComm.* **2004**, *6*, 130–158.
48. Tatko, C. D.; Waters, M. L.; *J. Am. Chem. Soc*. **2004**, *126*, 2028−2034.
49. (a) Brandi, M.; Weiss, M. S.; Jabs, A.; Suhnel, J.; Hilgenfeld, R. *J. Mol. Biol.* **2001**, *307*, 357−377. (b) Steiner, T.; Koellner, G. *J. Mol. Biol.* **2001**, *305*, 535–557. (c) Bhattacharya, R.; Chakrabarti, P. *J. Mol. Biol*. **2003**, *331*, 925−940.
50. (a) Muller, K.; Wegner, G. *Electronic Materials: The Oligomer Approach*; Wiley-VCH: Weinheim, 1998. (b) Österbacka, R.; An, C. P.; Jiang, X. M.; Vardeny, Z. V. *Science* **2000**, *287*, 839–842.
51. (a) Liu, C. -S.; Sun, G. -H.; Li, M.; Guo, L. -Q.; Zhou, L. -M.; Fang, S. -M. *Open Crystallogr. J.* **2008**, *1*, 24−30. (b) Goel, M.; Jayakannan. M. *Chem. Eur. J.* **2012**, 1*8*, 11987–11993.
52. (a) Ozawa, T.; Tsuji, E.; Ozawa, M.; Handa, C.; Mukaiyama, H.; Nishimura, T.; Kobayashi, S.; Okazaki, K. *Bio. Med. Chem.* **2008**, *16*, 10311−10318. (b) Kumari, M.; Balaji, P. V.; Sunoj, R. B. *Phys. Chem. Chem. Phys*. **2011**, *13*, 6517−6530. (c) Sogawa, K.; Okuda, R.; In, Y.; Ishida, T.; Taniguchi, T.; Minoura, K.; Tomoo, K. *J. Biochem.* **2012**, *152*, 221−229.
53. Hassel, O.; Romming, C. *Quart. Rev. Chem. Soc*. **1962**, *16*, 1−18.
54. Auffinger, P.; Hays, F. A.; Westhof, E.; Shing Ho, P. *Proc. Natl. Acad. Sci. U. S. A.* **2004**, *101*, 16789−16794.
55. (a) Robinson, J. M. A.; Kariuki, B. M.; Harris, K. D. M.; Philip, D. *J. Chem. Soc., Perkin Trans. 2* **1998**, *11*, 2459−2470. (b) Moorthy, J. N.; Natarajan, R.; Mal, P.; Venugopalan, P. *J. Am. Chem. Soc*. **2002**, *124*, 6530−6531. (c) Gonnade, R. G.; Bhadbhade, M. M.; Shashidhar, M. S.; Sanki, A. K. *Chem. Commun*. **2005**, *47*, 5870−5872. (d) Reddy, C. M.; Kirchner, M. T.; Gundakaram, R. C.; Padmanabhan,

K. A.; Desiraju, G. R. *Chem. Eur. J.* **2006**, *12*, 2222−2234. (e) Gonnade, R. G.; Shashidhar, M. S.; Bhadbhade, M. M. *J. Indian Inst. Sci.* **2007**, *87*, 149−165.

56. (a) Aakeröy, C. B.; Evans, T. A.; Seddon, K. R.; Palink, I. *New J. Chem*. **1999**, *23*, 145−152. (b) Gibb, C. L. D.; Stevens, E. D.; Gibb, B. C. *J. Am. Chem. Soc*. **2001**, *123*, 5849−5850.
57. van den Berg, J. A.; Seddon, K. R. *Cryst. Growth Des*. **2003**, *3*, 643−661.
58. Sakurai, T.; Sundaralingam, M.; Jeffrey, G. A. *Acta Crystallogr.* **1963**, *16*, 354−363.
59. Ramasubbu, N.; Parthasarathy, R.; Murray-Rust, P. *J. Am. Chem. Soc*. **1986**, *108*, 4308−4314.
60. (a) Desiraju, G. R.; Partasarathy, R. *J. Am. Chem. Soc.* **1989**, *111*, 8725−8726; (b) Hathwar, V. R.; Roopan, S. M.; Subashini, R.; Khan, F. N.; Guru Row, T. N. *J. Chem. Sci*. **2010**, *122*, 677–685.
61. Tothadi, S.; Joseph, S.; Desiraju, G. R. *Cryst. Growth Des*. **2013**, *13*, 3242–3254.
62. (a) Navon, O.; Bernstein, J.; Khodorkovsky, V. *Angew. Chem. Int. Ed. Engl*. **1997**, *36*, 601−603. (b) Bosch, E.; Barnes, C. L.; *Cryst. Growth Des*. **2002**, *2*, 299−302. (c) Saha, B. K.; Jetti, R. K. R.; Reddy, L. S.; Aitipamula, S.; Nangia, A. *Cryst. Growth Des*. **2005**, *5*, 887−899. (d) Paulini, R.; Müller, K.; Diederich, F. *Angew. Chem. Int. Ed. Engl*. **2005**, *44*, 1788−1805. (e) Zordan, F.; Brammer, L.; Sherwood, P. *J. Am. Chem. Soc*. **2005**, *127*, 5979−5989.
63. Wulf, O. R.; Liddel, U.; Hendricks, S. B. *J. Am. Chem. Soc*. **1936**, *58*, 2287−2293.
64. Pedireddi, V. R.; Sarma, J. A. R. P.; Desiraju, G. R. *J. Chem. Soc. Perkin Trans. 2* **1992**, 311−312. (b) Desiraju, G. R.; Pedireddi, V. R.; Sarma, J. A. R. P.; Zacharias, D. E. *Acta Chim. Hung*. **1993**, *130*, 451−465.
65. Dumas, J. M.; Gomel, L.; Guerin, M. *Molecular Interactions Involving Organic Halides, The Chemistry of Functional Groups, Supplement D*; Wiley: New York, 1983; pp 985–1020.
66. (a) Blackstock, S. C.; Lorand, J. P.; Kochi, J. P. *J. Org. Chem*. **1987**, *52*, 1451−1460. (b) Metrangolo, P.; Resnati, G. *Chem. Eur. J*. **2001**, *7*, 2511−2519. (c) Mele, A.; Metrangolo, P.; Neukirch, H.; Pilati, T.; Resnati, G. *J. Am. Chem. Soc*. **2005**, *127*, 14972−14973. (d) Esrafili, M. D.; Shahabivand, S. *Struct. Chem.* **2014**, *25*, 403−408.
67. (a) Legon, A. C. *Angew. Chem. Int. Ed. Engl*. **1999**, *38*, 2686−2714. (b) Metrangolo, P.; Neukirch, H.; Pilati, T.; Resnati, G. *Acc. Chem. Res.* **2005**, *38*, 386–395. (c)

Awwadi, F. F.; Taher, D.; Haddad, S. F.; Turnbull, M. M. *Cryst. Growth Des*. **2014**, *14*, 1961−1971.

68. Muller. P. *Pure Appl. Chem*. **1994**, *66*, 1077−1184.
69. Desiraju, G. R.; Ho, P. S.; Kloo, L.; Legon, A. C.; Marquardt, R.; Metrangolo, P.; Politzer, P.; Resnati, G.; Rissanen, K. *Pure Appl. Chem*. **2013**, *85*, 1711–1713.
70. (a) Taylor, R.; Kennard, O. *J. Am. Chem. Soc.* **1982**, *104*, 5063−5070. (b) Han, Z.; Zhao, Y.; Peng, J.; Tian, A.; Liu, Q.; Ma, J.; Wang, E.; Hu, N. *CrystEngComm* **2005**, *7*, 380−387. (c) Wei, H. -Q.; Jin, W. -J. *Fenxi Huaxue* **2007**, *35*, 1381−1386. (c) Takemura, A.; McAllister, L. J.; Karadakov, P. B.; Pridmore, N. E.; Whitwood, A. C.; Bruce, D. W. *CrystEngComm* **2014**, *16*, 4254−4264. (d) Baldrighi, M.; Bartesaghi, D.; Cavallo, G.; Chierotti, M. R.; Gobetto, R.; Metrangolo, P.; Pilati, T.; Resnati, G.; Terraneo, G. *CrystEngComm* **2014**, *16*, 5897−5904.
71. (a) Erdélyi, M. *Chem. Soc. Rev*. **2012**, *41*, 3547−3557. (b) Beale, T. M.; Chudzinski, M. G.; Sarwar, M. G.; Taylor, M. S. *Chem. Soc. Rev*. **2013**, *42*, 1667–1680.
72. Wilcken, R.; Zimmermann, M. O.; Lange, A.; Joerger, A. C.; Boeckler, F. M. *J. Med. Chem.* **2013**, *56*, 1363−1388 and references therein.
73. (a) Thalladi, V. R.; Weiss, H. C.; Bla1ser, D.; Boese, R.; Nangia, A.; Desiraju, G. R. *J. Am. Chem. Soc.* **1998**, *120*, 8702−8710. (b) Politzer, P.; Lane, P.; Concha, M. C.; Ma, Y.; Murray, J. S. *J. Mol. Model*. **2007**, *13*, 305–311. (c) Clark, T.; Hennemann, M.; Murray, J. S.; Politzer, P. *J. Mol. Model*. **2007**, *13*, 291–296. (d) Herlitzke, B. J.; Ojala, W. H. Abstracts of Papers, *247th ACS National Meeting & Exposition*, Dallas, TX, United States, March 16−20, **2014** (2014), CHED−1113.
74. (a) Schlosser, M. *Angew. Chem. Int. Ed*. **1998**, *110*, 1496−1513 and references therein. (b) Smart, B. E. *J. Fluorine Chem*. **2001**, *109*, 3−11 and references therein.
75. (a) Dunitz, J. D.; Taylor, R. *Chem. Eur. J.* **1997,** *3*, 89–98. (b) Dunitz; J. D. *ChemBioChem* **2004**, *5*, 614–621.
76. Zhou, P.; Zou, J.; Tian, F.; Shang, Z. *J. Chem. Inf. Model*. **2009**, *49*, 2344–2355
77. O'Hagan, D.; Rzepa, H. S. *Chem. Commun*. **1997**, *7*, 645–52.
78. Smart, B. E. *J. Fluorine Chem*. **2001**, *109*, 3−11
79. Bondi, A. *J. Phys. Chem*. **1964**, *68*, 441−451.
80. Williams, D. E.; Houpt, D. J. *Acta Crystallogr*. **1986**, *B42*, 286−295.
81. Kim H. W.; Rossi, P.; Shoemaker, R. K.; Dimagno, S. G. *J. Am. Chem. Soc*. **1998**, *120*, 9082−9083

82. Moran, S.; Ren, R. X. −F.; Rumney S. IV.; Kool, E. T. *J. Am. Chem. Soc*. **1997**, *119*, 2056−2057.
83. Evans, T. A.; Seddon, K. R. *Chem. Commun*. **1997**, *21*, 2023−2024.
84. (a) Kool, E. T.; Morales, J. C.; Guckian, K. M. *Angew. Chem. Int. Ed*. **2000**, *39*, 990−1009. (b) Kool, E. T.; Sintim, H. O. *Chem. Commun*. **2006**, *35*, 3665−3675.
85. (a) Parsch, J.; Engels, J. W. *Helv. Chim. Acta* **2000**, *83*, 1791–1808. (b) Bats, J. W.; Parsch, J.; Engels, J. W. *Acta Crystallogr*. *Sect. C*, **2000**, *56*, 201–205. (c) Leist, R.; Frey, J. A.; Leutwyler, S. L. *J. Phys. Chem. A*, **2006**, *110*, 4180–4187. (d) Frey, J. A.; Leist, R.; Leutwyler, S. L. *J. Phys. Chem. A*, **2006**, *110*, 4188–4195.
86. Shimoni, L.; Glusker, J. P. *Struct. Chem.* **1994**, *5*, 383– 397.
87. Howard, J. A. K.; Hoy, V. J.; O'Hagan, D.; Smith, G. T. *Tetrahedron* **1996**, *52*, 12613–12622.
88. Thalladi, V. R.; Weiss, H. C.; Bläser, D.; Boese, R.; Nangia, A.; Desiraju, G. R. *J. Am. Chem. Soc.* **1998**, *120*, 8702–8710.
89. Choudhury, A. R.; Nagarajan, K.; Guru Row, T. N. *Acta Crystallogr. Sect. C: Cryst. Struct. Commun.* **2004**, *60*, o644−o647.
90. (a) Choudhury, A. R.; Urs, U. K.; Guru Row, T. N.; Nagarajan, K. *J. Mol. Struct.* **2002**, *605*, 71–77. (b) Choudhury, A. R.; Guru Row, T. N. *Cryst. Growth Des.* **2004**, *4*, 47–52. (c) Choudhury, A. R.; Nagarajan, K.; Guru Row, T. N. *Cryst. Eng.* **2003**, *6*, 43–55. (d) Choudhury, A. R.; Guru Row, T. N. *CrystEngComm* **2006**, *3*, 265–274.
91. (a) Chopra, D.; Guru Row, T. N. *CrystEngComm* **2008**, *10*, 54– 67. (b) Nayak, S. K.; Reddy, M. K.; Guru Row, T. N.; Chopra, D. *Cryst. Growth Des.* **2011**, *11*, 1578–1596.
92. Panini, P.; Chopra, D. *CrystEngComm* **2012**, *14*, 1972–1989.
93. Karanam, M.; Choudhury, A. R. *Cryst. Growth Des.* **2013**, *13*, 4803– 4814.
94. (a) Schwarzer, A.; Seichter, W.; Weber, E.; Stoeckli-Evans, H.; Losada, M.; Hulliger, J. *CrystEngComm*, **2004**, *6*, 567−572. (b) Schwarzer, A.; Weber, E. *Cryst. Growth Des*. **2008**, *8*, 2862−2874. (c) Asensio, G.; Medio-Simon, M.; Alema´n, P.; Arellano, C. R. de *Cryst. Growth Des*. **2006**, *6*, 2769−2778. (d) Schwarzer, A.; Bombicz, P.; Weber, E. *J. Fluorine Chem*. **2010**, *131*, 345−356;
95. Alkorta, I.; Elguero, J. *Struct. Chem*. **2004**, *15*, 117−120.
96. Bayo´n, R.; Coco, S.; Espinet, P. *Chem.–Eur. J*. **2005**, *11*, 1079−1085.

97. Mariaca, R.; Behrnd, N. -R.; Eggli, P.; Stoeckli-Evans, H.; Hulliger, J. *CrystEngComm* **2006**, *8*, 222−232.
98. Prasanna, M. D.; Guru Row, T. N. *Cryst. Eng*. **2000**, *3*, 135−154.
99. (a) Vangala, V. R.; Nangia, A.; Lynch, V. M. *Chem. Commun.* **2002**, *12*, 1304−1305. (b) Schwarzer, A.; Seichter, W.; Weber, E.; Stoeckli-Evans, H.; Losada, M.; Hulliger, J. *CrystEngComm* **2004**, *6*, 567−572. (c) Schwarzer, A.; Weber, E. *Cryst. Growth Des*. **2008**, *8*, 2862−2874.
100. Hayashi, N.; Mori, T.; Matsumoto, K. *Chem. Commun*. **1998**, *17*, 1905−1906.
101. Kawahara, S.; Tsuzuki, S.; Uchimaru, T. *J. Phys. Chem. A*, **2004**, *108*, 6744−6749.
102. (a) Prasanna, M. D.; Guru Row, T. N. *Cryst. Eng.* **2000**, *2*, 134−140. (b) Prasanna, M. D.; Guru Row, T. N. *J. Mol. Struct.* **2001**, *559*, 255−261. (c) Prasanna, M. D.; Guru Row, T. N. *J. Mol. Struct.* **2001**, *562*, 55−61. (d) Saraogi, I.; Vijay, V. G.; Das, S.; Sekar, K.; Guru Row, T. N. *Cryst. Engg.* **2003**, *6*, 69−77.
103. (a) Benitex, Y.; Baranger, A. M. *J. Am. Chem. Soc.* **2011**, *133*, 3687−3689. (b) Campbell, N. H.; Smith, D. L.; Reszka, A. P.; Neidle, S.; O'Hagan, D. *Org. Biomol. Chem.* **2011**, *9*, 1328−1331.
104. (a) Chopra, D.; Guru Row, T. N. *Cryst. Growth Des*. **2005**, *5*, 1679−1681. (b) Chopra, D.; Guru Row, T. N. *Cryst. Growth Des*. **2008**, *8*, 848−853.
105. (a) Gupta, K. C.; Sutar, A. K. *Coord. Chem. Rev*. **2008**, *252*, 1420–1450. (b) Aziz, A. A. A.; Salem, A. N. M.; Sayed, M. A.; Aboaly, M. M. *J. Mol. Struct.* **2011**, *1010*, 130−138. (c) Shi, L.; Fang, R. -Q.; Zhu, Z. -W.; Yang, Y.; Cheng, K.; Zhu, H. -L; Zhong, W. -Q. *Eur. J. Med. Chem.* **2010**, *45*, 4358−4364. (d) Shi, D. -H.; You, Z. -L.; Xu, C.; Zhang, Q.; Zhu, H. -L. *Inorg. Chem. Commun*. **2007**, *10*, 404–406. (e) Jr. Nuss, G. W.; Santora, N. J.; Douglas, G. H. United States Patent, **1980**, 4187317. (f) Jr. Nuss, G. W.; Santora, N. J.; Douglas, G. H. United States Patent, **1980**, 4198349.
106. (a) Burgi, H. B.; Dunitz, J. D.; Zust, C. *Acta Crystallogr*. **1968**, *B24*, 463−464. (b) Burgi, H. B.; Dunitz, J. D. *Chem. Comm.* **1969**, 472−473. (c) Robertson, J. M.; Woodward, I. *P. Roy. Soc.* **1937**, A, *162*, 568−583. (d) de Lange, J. J.; Robertson, J. M.; Woodward, I. *P. Roy. Soc.* **1939**, A, *171*, 398−410. (e) Brown, C. J. *Acta Crystallogr.* **1966**, *21*, 146−152.
107. (a) Bernstein, J.; Bar, I.; Christensen, A. *Acta Crystallogr.* **1976**, *B32*, 1609−1611. (b) Bar, I.; Bernstein, J. *Acta Crystallogr.* **1978**, *B33*, 1738−1744. (c) Bar, I.; Bernstein, J. *Acta Crystallogr.* **1982**, *B38*, 121−125.

108. (a) Choudhury, A. R.; Urs, U. K.; Smith, P. S.; Goddard, R.; Howard, J. A. K.; Guru Row, T. N. *J Mol. Struct.* **2002**, *641*, 225−232. (b) Nayak, S. K.; Reddy, M. K.; Chopra, D.; Guru Row, T. N. *CrystEngComm.* **2012**, *14*, 200−210.
109. (a) http://www.ohcd-system.com/infos/infos.htm. (b) Choudhury, A. R.; Winterton, N.; Steiner, A.; Cooper, A. I.; Johnson, K. A. *J. Am. Chem. Soc.* **2005**, *127*, 16792–16793. (c) Choudhury, A. R.; Islam, K.; Kirchner, M. T.; Mehta, G.; Guru Row, T. N. *J. Am. Chem. Soc.* **2004**, *126*, 12274–12275. (d)) Choudhury, A. R.; Yufit, D. S.; Howard, J. A. K. *Z. Kristallogr.* **2014**, *229*, 625–634.
110. Roisnel, T.; Rodriguez-Carvajal J. WinPLOTR: a Windows tool for powder diffraction patterns analysis Materials Science Forum, Proceedings of the Seventh European Powder Diffraction Conference (EPDIC 7), **2000**, 118−123.
111. Macrae, C. F.; Bruno, I. J.; Chisholm, J. A.; Edgington, P. R.; McCabe, P.; Pidcock, E.; Rodriguez-Monge, L.; Taylor, R.; Streek, J.; Wood, P. A *J. Appl. Crystallogr.* **2008**, *41*, 466–470.
112. APEX2, SADABS and SAINT; Bruker AXS Inc.: Madison, Wisconsin, USA, **2008**.
113. Dolomanov, O. V.; Bourhis, L. J.; Gildea, R. J.; Howard, J. A. K.; Puschmann, H. *J. Appl. Cryst.* **2009**, ***42***, 339–341.
114. Farrugia, L. J. WinGx, *J. Appl. Cryst.* **1999**, *32*, 837–838.
115. Sheldrick, G. M. *Acta Crystallogr.* **2008**, *A64*, 112–122.
116. Nardelli, M. *J. Appl. Crystallogr*. **1995**, *28*, 569.
117. Spek, A. L. *Acta Crystallogr.* **2009**, *D65*, 148–155.
118. Frisch, M. J.; Trucks, G. W.; Schlegel, H. B.; Scuseria, G. E.; Robb, M. A.; Cheeseman, J. R.; Scalmani, G.; Barone, V.; Mennucci, B.; Petersson, G. A.; Nakatsuji, H.; Caricato, M.; Li, X.; Hratchian, H. P.; Izmaylov, A. F.; Bloino, J.; Zheng, G.; Sonnenberg, J. L.; Hada, M.; Ehara, M.; Toyota, K.; Fukuda, R.; Hasegawa, J.; Ishida, M.; Nakajima, T.; Honda, Y.; Kitao, O.; Nakai, H.; Vreven, T.; Montgomery, J. A., Jr.; Peralta, J. E.; Ogliaro, F.; Bearpark, M.; Heyd, J. J.; Brothers, E.; Kudin, K. N.; Staroverov, V. N.; Kobayashi, R.; Normand, J.; Raghavachari, K.; Rendell, A.; Burant, J. C.; Iyengar, S. S.; Tomasi, J.; Cossi, M.; Rega, N.; Millam, J. M.; Klene, M.; Knox, J. E.; Cross, J. B.; Bakken, V.; Adamo, C.; Jaramillo, J.; Gomperts, R.; Stratmann, R. E.; Yazyev, O.; Austin, A. J.; Cammi, R.; Pomelli, C.; Ochterski, J. W.; Martin, R. L.; Morokuma, K.; Zakrzewski, V. G.; Voth, G. A.; Salvador, P.; Dannenberg, J. J.; Dapprich, S.; Daniels, A. D.; Farkas,

Ö.; Foresman, J. B.; Ortiz, J. V.; Cioslowski, J.; Fox, D. J. Gaussian 09, Revision A.1; Gaussian, Inc.: Wallingford, CT, 2009.

119. GaussView, Version 5, Dennington, R.; Keith, T.; Millam, J. Semichem Inc., Shawnee Mission KS, 2009.
120. Møller, C.; Plesset, M. S. *Phys. Rev*. **1934**, *46*, 618−622.
121. Boys, S. F.; Bernardi, F. *Mol. Phys*. **1970**, *19*, 553–566.
122. (a) Bader. R. F. W. *Atoms in Molecules–A Quantum Theory*, Clarendon: Oxford, 1990. (b) Bader. R. F. W.; *J. Phys. Chem*. **1998**, *A102*, 7314–7323.
123. (a) König, F. B.; Schönbohm, J.; Bayles, D. *J. Comput. Chem.* **2001**, 22, 545–559. (b) König, F. B.; Schönbohm, J.; Bayles, D. *J. Comput. Chem.* **2002**, 23, 1489–1494.
124. (a) Hathwar, V. R.; Guru Row, T. N. *Cryst. Growth Des*. **2011**, *11*, 1338−1346. (b) Hathwar, V. R.; Chopra, D.; Panini, P.; Guru Row, T. N. *Cryst. Growth Des*. **2014**, *14*, 5366−5369.
125. (a) Harada, J.; Harakawa, M.; Ogawa, K. *Acta Crystallogr*. **2004**, *B60*, 578−588. (b) Harada, J., Harakawa, M.; Ogawa, K. *Acta Crystallogr*. **2004**, *B60*, 589−597.
126. Kálmán, A.; Párnkányi, L.;Argay, G. *Acta Crystallogr*. **1993**, *B49*, 1039−1049.
127. Allen, F. H. *Acta Crystallogr*. **2002**, *B58*, 380−388.
128. **CSD version 5.33** (November 2011): The following constraints were applied: No REFCODE restrictions applied, 3D coordinates determined, R factor ≤ 0.1, No errors, Not polymeric, No ions, Only Organics.
129. (a) Bernstein, J.; Izak, I. *J. Chem. Cryst.* **1975**, *5*, 257−266. (b) Bernstein, J.; Schmidt, G. M. J. *J. Chem. Soc. Perkin Trans II.* **1972**, 951−955. (c) Bernstein, J.; Izak, I. *J. Chem. Soc. Perkin Trans II.* **1976**, 429−424. (d) Ojala, C. R.; Ojala, W. H.; Britton, D. *J. Chem. Cryst.* **2011**, *41*, 464−469. (e) Navon, O.; Bernstein, J. *Struct. Chem.* **1997**, *8*, 3−11. (f) Zamir, S.; Bernstein, J. *Acta Chim. Hung.* **1993**, *130*, 301−325. (e) Wang, C. *Acta Crystallogr.*, **2011**, *E67*, o2204.
130. Munshi, P.; Guru Row T. N. *J. Phys. Chem. A* **2005**, *109*, 659−672.
131. Vasylyeva, V.; Merz, K. *Cryst. Growth Des*. **2010**, *10*, 4250−4255.
132. SigmaPlot (Systat Software, San Jose, CA).
133. (a) Coppens, P.; Koritsanszky, T. S. *Chem. Rev*. **2001**, *101*, 1583–1627. (b) Spackman, M. A. *Annu. Rep. Prog. Chem., Sect. C: Phys. Chem*. **1997**, *94*, 177–207. (c) Spackman, M. A.; Brown, A. S. *Annu. Rep. Prog. Chem., Sect. C: Phys.*

Chem. **1994**, *91*, 175–212. (d) Spackman, M. A. *Chem. Rev*. **1992**, *92*, 1769–1797. (e) Hirshfeld, F. L. *Crystallogr. Rev*. **1991**, *2*, 169–204.

134. (a) Low, A. A.; Kunze, K. L.; MacDougall, P. J.; Hall, M. B. *Inorg. Chem*. **1991**, *30*, 1079-1086. (b) Coppens, P.; Guru Row, T. N.; Leung, P.; Stevens, E. D.; Becker, P. J.; Yang, Y. W. *Acta Crystallogr*. **1979**, *A35*, 63–72.
135. (a) Pavan, M. S.; Pal, R.; Nagarajan, K.; Guru Row, T. N. *Cryst. Growth Des.* **2014**, *14*, 5477–5485. (b) Hathwar, V. R.; Chopra, D.; Panini, P.; Guru Row, T. N. *Cryst. Growth Des.* **2014**, *14*, 5366–5369. (c) Thomas, S. P.; Pavan, M. S.; Guru Row, T. N. *Cryst. Growth Des.* **2012**, *12*, 6083–6091. (d) Hathwar, V. R.; Gonnade, R. G.; Munshi, P.; Bhadbhade, M. M.; Guru Row, T. N. *Cryst. Growth Des.* **2011**, *11*, 1855–1862. (e) Munshi, P.; Jelsch, C.; Hathwar, V. R.; Guru Row, T. N. *Cryst. Growth Des.* **2010**, *10*, 1516–1526. (f) Park, H.; Yoon, J.; Seok, C. *J. Phys. Chem. B* **2007**, *112*, 1041– 1048. (g) Munshi, P.; Guru Row, T. N. *J. Phys. Chem. A* **2005**, *109*, 659– 672. (h) Munshi, P. Intermolecular Interactions in Molecular Crystals: Quantitative Estimates from Experimental and Theoretical Charge Densities, Ph.D. Dissertation: Indian Institute Of Science, India, June 2005. (i) Espinosa, E.; Molins, E. *J. Chem. Phys*. **2000**, *113*, 5686– 5694.
136. Debye, P. *Ann. Phys*. **1915**, *46*, 809.
137. Coppens, P. *X-ray Charge Densities and Chemical Bonding*, Oxford University Press: Oxford, UK, 1997.
138. Coppens, P.; Guru Row, T. N.; Leung, P.; Stevens, E. D.; Becker, P. J.; Yang, Y. W. *Acta Crystallogr*. **1979**, *A35*, 63–72.
139. (a) Hirshfeld, F. L. *Acta Crystallogr.* **1971**, *B27*, 769–781. (b) Stewart, R. F. *Acta Crystallogr.* **1976**, *A32*, 565–574.
140. Hansen, N. K.; Coppens, P. *Acta Crystallogr.* **1978**, *A34*, 909–921.
141. Seiler, P. Accurate *Molecular Structures. Their Determination and Importance*, Domenicano, A., Hargittai, I., Eds.; Oxford University Press: Oxford, 1992; pp 170.
142. (a) Spackman, M. A. *Chem. Rev*. **1992**, *92*, 1769–1797. (b) Spackman, M. A.; Brown, A. S. *Annu. Rep. Prog. Chem., Sect. C: Phys. Chem*. **1994**, *91*, 175–212. (c) Spackman, M. A. *Annu. Rep. Prog. Chem., Sect. C: Phys. Chem*. **1997**, *94*, 177–207.
143. Koritsanszky, T. S.; Coppens, P. *Chem. Rev.* **2001**, *101(6)*, 1583–1621.
144. Blessing, R. H. *Crysallogrt. Rev.* **1987**, *1*, 3–58.

145. Blessing R. H. *Acta Crystallogr.* **1995**, *A51*, 33–38
146. Volkov, A.; Macchi, P.; Farrugia, L. J.; Gatti, C.; Mallinson, P.; Richter, T.; Koritsanszky, T. S. XD 2006, A Computer Program Package for Multipole Refinement, Topological Analysis of Charge Densities and Evaluation of Intermolecular Energies from Experimental and Theoretical Structure Factors.
147. Clementi, E.; Roetti, C. *Atomic Data and Nuclear Data Tables* **1974**, *14*, 177-478.
148. Allen, F. H. *Acta Crystallogr.* **1986**, *B42*, 515–522.
149. (a) Munshi, P.; Madsen, A. Ø.; Spackman, M. A.; Larsen, S.; Destro, R. *Acta Crystallographica Section A: Foundations of Crystallography*, **2008**, *64*, 465-475. (b) Madsen, A. Ø. *J. Appl. Cryst.* **2006**, *39*, 757–758.
150. (a) Abramov, Yu.; Volkov, A.; Coppens, P. *Chem. Phys. Lett*. **1999**, 311, 81–86. (b) Volkov, A.; Abramov, Y. A.; Coppens, P. *Acta Crystallogr*., *Sect A* **2001**, *57*, 272–282.
151. Hirshfeld, F. L. *Acta Crystallogr.* **1976**, *A32*, 239–244.
152. Dovesi, R.; Saunders, V. R.; Roetti, C.; Orlando, R.; Zicovich-Wilson, C. M.; Pascale, F.; Civalleri, B.; Doll, K.; Harrison, N. M.; Bush, I. J.; D'Arco, P.; Llunell, M.; Causá, M.; Nöel, Y. *CRYSTAL14 User's Manual*, University of Torino: Torino, 2014.
153. Becke, A. D. *J. Chem. Phys.* **1993**, *98*, 5648–5652.
154. (a) Fock, V. *Z. Physik.* **1930**, *61*, 126–148 (b) Hartree, D. R.; Hartree, W. *P. Roy. Soc*. **1935**, *9*, A150
155. Lee, C.; Yang, W.; Parr, R. G. *Phys. Rev.* **1988**, *B37*, 785–789.
156. Hariharan, P. C.; Pople, J. A. *Theor. Chim. Acta*. **1973**, *28*, 213–222.
157. Page, Y. L.; Gabe, E. J. *J. Appl. Cryst.* **1979**, *12*, 464–466.
158. Popelier, P. L. A. *Atoms in Molecules. An Introduction*: Prentice Hall, UK, 2000.
159. Koch, U.; Popelier, P. L. A. *J. Phys. Chem.* **1995**, *99*, 9747–9754.
160. (a) Abramov, Yu. A. *Acta Crystallogr*. **1997**, *A53*, 264–272. (b) Espinosa, E.; Molins, E.; Lecomte, C. *Chem. Phys. Lett*. **1998**, *285*, 170–173.
161. Nyburg, S. C.; Faerman, C. H. *Acta Crystallogr*. **1985**, *B41*, 274–279.
162. Chopra, D.; Cameron, T. S.; Ferrara, J. D.; Guru Row, T. N. *J. Phys. Chem. A* **2006**, *110*, 10465-10477.
163. Chan L. C.; Cox, B. G. *J. Org. Chem*. **2007**, *72*, 8863-8869.
164. Prasad, A. S. B.; Kanth, J. V. B.; Periasamy, M. *Tetrahedron*, **1992**, *48*, 4623-4628.
165. Lukanov, L. K.; Venkov, A. P.; Mollov, N. M. *Synthesis* **1987**, *11*, 1031-1032.

166. Nagarajan, K.; Talwalker, P. K.; Kulkarni, C. L.; Shah, R. K.; Shenoy, S. J.; Pravu, S. S. *Ind. J. Chem.* **1985**, *24B*, 83.
167. Agilent. CrysAlis PRO. Agilent Technologies, Yarnton, England, **2012**.
168. Mallinson, P. R.; Smith, G. T.; Wilson, C. C.; Grech, E.; Woz´niak, K. *J. Am. Chem. Soc*. **2003**, *125*, 4259–4270.

Appendix

Evaluation of the influence of C–H···F hydrogen bond in crystal engineering in the presence of O–H···N hydrogen bond

As the interactions offered by organic fluorine are generally weak in nature, their application in crystal engineering has mostly been studied in the absence of any strong hydrogen bond donor and acceptors group(s). We have been exploring the weak interactions offered by organic fluorine in a series of *N*-benzylideneaniline with various halogen substitutions (*difluoro*, *fluoro-bromo*, *fluoro-chloro* and *tetrafluoro*), but without any strong hydrogen bond donor or acceptor groups, which was the central theme of the work done in this thesis too. Further, to explore the role of fluorinated interactions in the same molecular scaffold, but in the presence of strong hydrogen bond donor and acceptor sites, studies have been carried out on *N*-benzylideneaniline with both fluorine and hydroxyl substitution in either ring. Our earlier studies indicate that organic fluorine plays an influential role in directing the packing of molecules through different robust supramolecular synthons formed *via* C–H···F hydrogen bond(s). We have attempted to evaluate the structure directing/controlling ability of organic fluorine in the presence of a hydroxyl group. Therefore, we have synthesized a series of *N*-benzylideneanilines with a hydroxyl group on one ring and a fluorine atom on the other ring. These compounds were characterized by single crystal X-ray diffraction technique supported by ^{1}H NMR, FTIR and PXRD. These molecules gave us an opportunity to perform systematic analysis on C–H···F interactions in the presence of hydrogen bonds (O–H···N and O–H···O). We have analysed these molecules in terms of the packing motifs offered by them in their respective crystal structures and those packing motifs have been studied computationally to understand the stabilization offered through them. The lattice energy calculations and energy decomposition analysis were done by PIXEL and gas phase stabilization energies were calculated using Gaussian09. The topological properties related to the interacting molecules have been determined through AIM calculation using AIM2000. Thorough analyses of the results obtained are in progress. It is observed that although all the structures contain strong O–H···N hydrogen bond, the wide variation in the crystal structure of the related compounds were observed as a result of differences in the supramolecular synthons governed by the weak C–H···F hydrogen bonds.

Publications from Thesis

1. **Kaur**, **G**.; Panini, P.; Chopra, D.; Choudhury, A. R. "*Structural investigation of weak intermolecular interactions in fluorine substituted isomeric N-benzylideneanilines*" – *Cryst. Growth Des*. **2012**, *12*, 5096−5110.
2. **Kaur**, **G**.; Choudhury, A. R. "*Understanding of the weak intermolecular interactions involving halogens in substituted N-Benzylideneanilines: Insights from structural and computational perspectives*" – *Cryst. Growth Des*. **2014**, *14*, 1600−1616.
3. **Kaur**, **G**.; Choudhury, A. R., "*A comprehensive understanding of the synthons involving C–H···F–C hydrogen bond(s) from structural and computational analyses*" – (*CrystEngComm*, **2015**, *17*, 2949-2963).
4. **Kaur**, **G**.; Munshi, P. P.; Choudhury, A. R., "*Quantitative evaluation of weak interactions involving organic fluorine: Insights from experimental and theoretical charge density studies on fluorinated isoquinolines*" – (manuscript in preparation)
5. **Kaur**, **G**.; Singh, S.; Srikumar, A.; Choudhury, A. R. "*Evaluation of the influence of C–H···F hydrogen bond in crystal engineering in the presence of O–H···N hydrogen bond*" – (manuscript in preparation).
6. **Kaur**, **G**.; Choudhury, A. R., "*Structural analysis of weak intermolecular interactions in chloro-bromo substituted isomeric N-benzylideneanilines*" – (manuscript in preparation).

Other Publications

1. Dudi, S.; Sharma, N.; **Kaur**, **G**.; Choudhury, A. R. – C*rystengcomm, 2015, under review.*
2. Laskar, I. R.; Alam, P.; **Kaur**, **G**.; Choudhury, A. R.; Gupta, A.; Kachawal, V. *J. Mater. Chem. C* **2015** (Just Accepted).
3. Alam, P.; **Kaur**, **G**.; Chakraborty, S.; Choudhury, A. R.; Laskar, I. R. *Dalton Trans*. **2015**, *44*, 6581-6592.
4. Mal, S. K.; Mitra, M.; Biswas, B.; **Kaur**, **G**.; Bag, P. P.; Reddy, C. M.; Choudhury, A. R.; Aliaga-Alcalde, N.; Ghosh, R. *Inorg. Chim. Acta* **2015**, *425*, 61–66.

5. Mal, S. K.; Mitra, M.; Biswas, B.; **Kaur**, **G**.; Manikandamathavan, V. M.; Kiran, M. S.; Choudhury, A. R.; Nair, B. N. *RSC Adv.* **2014**, *4*, 61337–61342.
6. Dey, D.; **Kaur**, **G**.; Ranjani, A.; Gayathri, L.; Chakraborty, P.; Adhikary, J.; Pasan, J.; Dhanasekaran, D.; Choudhury, A. R.; Akbarsha, M. A.; Kole, N.; Biswas, B. *Eur. J. Inorg. Chem.* **2014**, *21*, 3350–3358.
7. Dey, D.; **Kaur**, **G**.; Patra, M.; Choudhury, A. R.; Kole, N.; Biswas, B. *Inorg. Chim. Acta* **2014**, *421*, 335–341.
8. Laskar, I. R.; Alam, P.; **Kaur**, **G**.; Choudhury, A. R.; Alemany, P.; Pasha, S.; Climent, C.; Casanova, D. *RSC Adv.* **2014**, *4*, 50549–50553.
9. Laskar, I. R.; Alam, P.; **Kaur**, **G**.; Choudhury, A. R.; Alemany, P.; Pasha, S.; Climent, C.; Casanova, D. *Dalton Trans.* **2014**, *43*, 16431–16440.
10. Mitra, M.; Maji, A. M.; Ghosh, B. K.; **Kaur**, **G**.; Choudhury, A. R.; Lin, C. –H.; Ribas, J.; Ghosh, R. *Polyhedron*, **2013**, *61*, 15–19.
11. Naveen, **Kaur**, **G**.; Srinivasarao, A.; Aslam, N. A.; Karanam, M. *RSC Adv.* **2014**, *4*, 18904–18916.
12. Mahesh, S.; Pareek, M.; Ramanjaneyulu, B. T.; **Kaur**, **G**.; Anand, R. V. *Ind. J. Chem. Sec. A* **2013**, *52A*, 1086–1092.

Publications from MS Project, NIT Jalandhar

1. **Kaur**, **G**.; Kumar, H.; Gaba, R. *J. Mol. Liq*. **2010**, 157, 151–157.
2. Singh, T.; Kumar, A.; Kaur, M.; **Kaur**, **G**.; Kumar, H. *J. Chem. Thermodyn*. **2009**, 41, 717–723.

****